WESTERN SYDNEY UNIVERSITY

Flood Frequency Analysis: A Case Study for the Brisbane River Catchment

By

S M Anwar Hossain, B.Sc. Eng. (BUET), M. Eng. (AIT)

(SID:18916573)

Principal Supervisor: Professor Ataur Rahman

Co-supervisor: Associate Professor Surendra Shrestha

School of Engineering

Western Sydney University

Master of Philosophy

June 2020

STATEMENT OF AUTHENTICATION

I declare that this thesis is written by me and all works within this thesis is from my own original research. I also acknowledge that to the best of my knowledge this research is my own work except where otherwise referenced to the others. This thesis or any part of this thesis has not been submitted previously to any other intuitions for any degree.

Signature…….. Date ……/……/……

ACKNOWLEDGEMENTS

I gratefully acknowledge:

- My Principal Supervisor of this research study Professor Ataur Rahman, for his brilliant guidance, encouragement, valuable suggestions, inspirational advice and his eagerness to assist any time during this study.
- My Associate Supervisor of this research Associate Professor Surendra Shrestha for his constructive comments, encouragement and advice.
- The Queensland Government's Water Monitoring Information Service and Bureau of Meteorology for their online streamflow data.
- My family members for their encouragement in continuing this research.

ABSTRACT

Flood is the most common natural hazards around the globe that has notable negative effects on humans and environment. One of the examples is Queensland 2010-2011 flood, which is considered as one of the severest floods in recent history of Australia that claimed 31 human lives and caused direct damage costing over $5 billion. To reduce the flood damage, it is vital to understand properly the causes of major floods, their magnitudes and frequencies. Estimation of the magnitude of possible future floods (also called design floods) is an important task in hydrology. Most of the hydraulic structures and flood management tasks require an accurate estimation of design floods. For this reason, estimation of design flood is still an area of great interest in flood hydrology and is being researched worldwide. Frequent devastating floods in Australia have drawn attention at the state and national levels for more accurate flood estimation with reduced uncertainty. Many design floods estimation methods are being practiced around the world. This study focuses on the widely used design flood estimate techniques called “flood frequency analysis (FFA)”. The main objective of FFA is to find probability distribution model that best fits the measured flood data series at a given site. Although Australian Rainfall and Runoff ARR (Australian Rainfall and Runoff), 1987 recommended Log Pearson type III probability distribution to use for FFA in Australia, in ARR 2019, no specific probability distribution is recommended. There has been limited guideline in Australia to select probability distribution models for flood frequency analysis. Also, many users have limited understanding on the uncertainties involved in design flood estimates based on a given probability distribution. This study is devoted to fill this research gap and examines the selection of the most appropriate probability distributions and associated uncertainty in FFA.

This study focuses on the Brisbane River catchment of Queensland, one of the worst flood-prone areas in Australia. In this research, a total of 26 streamflow gauging stations are selected from the Brisbane River catchment, with the lengths of recorded annual maximum flood (AMF) data series in the range of 20 years to 91 years.

The goodness-of-fit tests and visual assessment by graphical methods are used to compare the candidate distributions and to find the best-fit probability distribution model for a given station. Five probability distribution models i.e. Lognormal, Log Pearson type 3 (LP3), Gumbel, Generalised Extreme Value and Generalised Pareto are selected as the candidate

distributions to select a suitable probability distribution at each of the 26 stations. The available AMF data for each of the selected stations are examined for outliers, and the identified outliers in the AMF data series are censored in FFA in quantile estimation by the log-Normal and LP3 distributions. To identify the most appropriate probability distribution that would minimise the influence of high and low floods on flood quantile estimation, FFA are carried out twice i.e. the high and low flood values are (i) included in the data and (ii) excluded from the data. The investigation shows that flood quantiles magnitude reduces notably when low floods are available in the data set. Sensitivity of flood quantile estimation on maximum recorded flow in the data series is carried out by removing the highest recorded flood data point from the data series in carrying out FFA.

Uncertainty analysis in quantile estimation is carried out by bootstrapping and Monte Carlo simulation techniques. Trend analysis on the AMF data is conducted to identify any trend, abrupt change or shift in the AMF data.

Software packages FLIKE (recommended in ARR 2019) and EasyFit are used to fit and compare the selected five probability distributions. Three well known goodness-of-fit statistical hypothesis tests (Chi-Squared, Anderson-Darling and Kolmogorov-Smirnov) are adopted via EasyFit software to assess how well the selected probability distributions fit the AMF data. The results of EasyFit software are also compared with the results of FLIKE where possible. Finally, FLIKE software is used for quantile estimation.

It is found that, overall LP3 is the best-fit probability distribution model, followed by Generalised Pareto for the Brisbane River catchment. The analysis shows that quantile estimation is highly sensitive to the maximum recorded flood data point at most of the stations. Uncertainty analysis shows that the estimated flood quantiles have significant uncertainty, in particular, for the 100-year floods. It is found that the AMF data series at many selected gauging stations have linear trends, but these are generally statistically insignificant.

PUBLICATION FROM THIS STUDY

Hossain, S. M. A., Rahman, M. M. and Rahman, A. (2017): Queensland Flood in 2010-11: Will This Type of Flood Occur Soon? In: *Proceedings of the 1st International Conference on Engineering Research and Practice*, 4-5 February 2017, Dhaka, Bangladesh, pp. 102-108.

Hossain, S. M. A. and Rahman, A. (2018). Flood Frequency Analysis for the Brisbane River Catchment, *38th Hydrology and Water Resources Symposium*, 3-6 Dec 2018, Melbourne, Australia, pp. 340-350.

Hossain, S. M. A. and Rahman, A. (2019). Trend Analysis in Flood Data in the Brisbane River Catchment, Australia, *2nd International Conference on Water and Environmental Engineering* (iCWEE-2019), 19-22 January 2019, Dhaka, Bangladesh, pp. 199-209.

Hossain, S. M. A. (2019). Selection of the best-fit probability distribution for Brisbane River Catchment. *International Journal of Engineering, Construction and Computing (IJECC) Volume 1 Issue 1, 2019*, Sydney, Australia, pp. 90-103.

TABLE OF CONTENTS

LIST OF FIGURES

LIST OF TABLES

ABBREVIATIONS

A-D	Anderson Darling Statistic
AUD	Australian Dollar
AEP	Annual Exceedance Probability
AM	Annual Maximum
AMF	Annual Maximum Flood
Aust.	Australia
ARR	Australian Rainfall and Runoff
ARI	Average Recurrence Interval
BOM	Bureau of Meteorology
CDF	Cumulative Distribution Function
C-S	Chi Squared Statistic
DF	Design Flood
FFA	Flood Frequency Analysis
GEV	Generalised Extreme Value distribution
GoF	Goodness-of-fit test
GP	Generalised Pareto distribution
GLS	Generalised Least Squares
IID	Independent and identically distributed
IFM	Integrated Flood Management
IPCC	Intergovernmental Panel on Climate Change
K-S	Kolmogorov Smirnov Statistic
LP3	Log Pearson type III distribution
LN	Lognormal distribution
MLE	Maximum Likelihood Estimator
NERC	Natural Environment Research Council (UK)
NSW	New South Wales
PD	Probability Distribution
PDF	Probability Density Function
PILF	Potentially Influential Low Flow
POT	Peaks Over Threshold
QLD	Queensland

RFFA	Regional Flood Frequency Analysis
SD	Standard Deviation
TS	Time Series
T	Return Period
VIC	Victoria
WLS	Weighted Least Squares

CHAPTER 1 : INTRODUCTION

1.1. Background to the Proposed Research

Among the environmental hazards, flooding is the world's most destructive environmental hazard. Floods cause social, economic, and environmental impact on both individuals and on urban, suburban and rural communities (OQCS, 2016). Among all-natural hazards in the world during 1963-1992, percentage of death due to flood ranks the highest with 26% (Cunderlik and Burn, 2003; Thompson and Perry, 1998). Percentage of significant damage caused by flood in total number of affected people is 32%, which ranks second highest after draughts (Cunderlik and Burn, 2003). Therefore, among all natural hazards, flood is one of the most ubiquitous natural hazards that causes negative impact on humans, and that requires several mitigation measures including building of flood embankment and flood defence structures, flood forecasting and evacuation, and land-use management.

Statistics show that in recent era, the frequency and effect of extreme flood events have become more frequent around the globe (Van Herk, 2014; Bouwer et al., 2007; Zevenbergen et al., 2013). Many extreme floods in recent time including floods in the United Kingdom (2019, 2003, 2000), United States of America (2011, 1993), Europe (2010, 1995), China (2017, 1998), Pakistan (2010), Thailand (2011) and Australia (2011) stressed the need for better understanding of the global hydro-meteorological phenomenon accountable for these extreme floods (CWC, 2018).

Many major floods have occurred over Australia over the last 150 years. In Australia, six major floods occurred during the first decade of the 21st century, seventy-seven major floods are recorded within the last 35 years of the 20th century and eight major floods are recorded in 19th century (OQCS, 2016). The 2010-11 flood is one of the worst ones in the Australia's history which affected three eastern Australian states. This dangerous flooding began in December 2010, hit hard the north-eastern state Queensland (Figure 1.1) and then by early 2011 it moved towards south, which flooded part of New South Wales and Victoria (Hossain et al., 2017). During this period, about 75% of Queensland (QLD) was declared disaster zone, loss of 35 human lives, and more than 200,000 people were directly affected (Boon et al, 2016).

Flood is the costliest natural disaster in Australia and year 1974 was one of the most expensive years for flood in Australia amounting a total cost of AU$2.9 billion when Victoria (VIC), NSW and QLD were affected by floods (Hossain et al., 2017; OQCS, 2016).

Figure 1.1: Location of Queensland (QLD) and Brisbane (https://australia-map.blogspot.com/2012/05/australia-political-map-pictures.html**)**

Floods cause significant damage in different sectors including infrastructure, services agriculture, animal lives, and loss of valuable human lives. Australia spends around $1 billion annually on building infrastructure that requires design flood estimation (Hossain et al., 2017; OQCS, 2016). In Australia, the estimated average annual direct cost due to flood is AU$448 million (2016 Australian dollars price) for period 1967-2005 (OQCS, 2016). During 2011 flood, the estimated cost of infrastructure damage to the local government in Queensland is AU$2 billion and estimated total cost of damage on public infrastructure is AU$5 to AU$6 billion (OQCS, 2016).

Amongst various natural disasters on earth, floods contribute maximum in terms of economic damage. Throughout the ages human beings are facing challenge from different natural

disasters such as flood, draught, tsunami and earthquake. Despite the amazing advancements of technology and science in this century, drought and flood continue to affect human beings resulting loss of human lives and injuries, sufferings, and material losses (Guru and Jha, 2015). Although it is not possible to prevent floods, we can develop new strategies and protective measures that minimise loss of lives, major financial losses, environmental damage and social vulnerability (Platt, 1995, IFMRC, 1994). More accurate estimation of the risk of flooding is required for development of financially viable, economically efficient and environmentally sustainable plans (IFMRC, 1994). Advancement in predicting climates and weather conditions and availability of climatological satellites and development of early flood warning systems are an aid to flood forecasting. However, it is still not possible to forecast accurately the time of future occurrence of severe flood events and their magnitudes accurately. Therefore, to reduce the vulnerability and heavy loss due to flood, it is very important to look for improvement in hydrological flood estimation and forecasting. Estimation of the risk of flooding or risk of flood hazard is function of estimated flood discharge or stage, and flood frequency analysis (FFA) is generally used for this flood estimation (Kidson and Richards, 2005; Dunne and Leopold, 1978). Design of large hydraulic structures such as bridges, dams and flood embankments require flood estimation using FFA and for this reason the accuracy of FFA methods has notable impact on economic investment (Kidson and Richards, 2005; Bao et al., 1987). For design of such major engineering hydraulic structures, a specific design flood event for a particular return period such as the 50-year flood or the 100-year flood is considered. Since the measured flood discharge data period available for most catchments are significantly less than 50 or 100 years, extrapolation is required to estimate design flood discharge or design flood stage (water level) for 50- or 100-year flood event and this extrapolation is done through different curve-fitting techniques using the recorded flood data, thus bringing uncertainty in flood estimates (Kidson and Richards, 2005).

1.2. The Need for This Research

Severity of flood is usually described in terms of magnitude of flood (such as discharge, extent, depth and duration of flood). In order to minimise expected future flood damage, it is necessary to estimate with sufficient accuracy the magnitude and depth of flood that is likely to be exceeded any time within the design life of a structure. Expected future flood is usually

termed as a “design flood (DF)”. The DF is a flood magnitude, which is associated with a given average recurrence interval (ARI) or an annual exceedance probability (AEP). Depending on the type of flood control measures, estimation of different types of flood magnitude is required including peak flood volume, depth of flood, duration of flood flow, flow rate and its velocity and time to peak flow (Rahman et al., 2012). Application of peak flow estimation is widely practiced for design of hydraulic structures within 25 km^2 to 500 km^2 rural catchments (I. E. Aust., 2014). As flood causes huge financial, economic and environmental damage; DF estimation has still been widely researched with great importance (Haddad, 2008; IFMRC, 1994).

Rainfall based methods and streamflow based methods are two commonly used DF estimation methods. The runoff routing and unit hydrograph methods are generally used for design flood hydrograph (DFH) estimation. Design event approach is one of the runoff routing DF estimation methods. The design event approach model uses rainfall as input and it assumes that frequency of input rainfall is equal to the frequency of output DF (Benjamin, 2008; Caballero and Rahman, 2014). All DF estimation techniques are based on some types of frequency analysis of observed flows. FFA is a well-known method for estimating DF and it is convenient both economically and politically (Haktanir, 1992). Among various flood estimation methods, most direct method is at-site FFA (Rahman et al., 2013). The DF estimation with at-site FFA can be used as a yardstick to compare estimation of design floods using other methods including rainfall based modelling and regional flood estimation methods. For at-site FFA, relatively long-period of observed flood data is required. It is a fact that the record lengths of streamflow data at many streamflow measuring stations in Australia and in different parts of the world are much shorter than the return periods used for DF estimation. Therefore, the DF estimation requires extrapolation in the form of curve fitting beyond available record length. If adequate and quality data are available, at-site FFA is recommended to use in the ARR guidelines (Ball et al., 2019) for estimation of DF.

The current methods for undertaking FFA assume that the observed peak flow data are stationary (Gilroy and McCuen, 2012) i.e. measured streamflow events are independent and identically distributed (IID). However, changing environment such as climate change and land use change may influence recorded hydrological data. Stationarity assumption means that the probability of occurrence of flood events for any return period such as 50- or 100-years will remain same over time. This stationary assumption is still applied to estimate DF

using FFA. However, statistics such the mean, standard deviation or skewness of hydrological data may change due to climate change. Hydraulic design of new infrastructure is generally carried out using historical information on hydrometrological extremes. As the record lengths of existing hydrometrological data are generally relatively short compared to the required design life of infrastructure, extreme value theory is used to the historical observations of hydrometrological extremes to estimate DF magnitude without considering effect of climate change (Data, 2009). It is apparent from recent studies that in near future global climate change will increase the frequency of flood events and their magnitude resulting in significant increase of flood damage in Australia (Muzik, 2002; Ball et al., 2019).

Independence and stationarity are two fundamental assumptions of present FFA methods. However, as the climate change may influence the design flood, it is possible that in future these assumptions may not be valid. Under such circumstances, it is important to investigate different approaches taking into account non-stationarity and non-independence nature of hydro-meteorological extremes (Khaliq et al., 2006). Upward or downward trends or step jump in long term hydrological time series data are the first step to proceed with non-stationary FFA.

Many probability distributions are available for FFA. However, finding the most appropriate probability distribution (PD) for FFA is it is still a question. Until recently several research studies have been conducted on the comparison of different PDs for at-site FFA. As the length of available data is relatively small in comparison with the required return period, this remains a difficult task (Rahman et al., 2013; Bobee et al., 1993). Repetitive floods in Queensland, including the devastating 2011 flood, raised the immediate need for accurate design flood estimation for the Brisbane River catchment in Queensland for better flood management in future. Moreover, not many in-depth flood estimations studies were carried out in the past within the Brisbane River catchment.

Therefore, this study is focused on finding a method for more appropriate DF estimation by FFA. The study is carried out with annual flood peaks data from the Brisbane River catchment in Queensland, Australia. This study aims to carry out at-site FFA by selecting the best-fit PD using different goodness-of-fit (GoF) tests and use the identified PD to estimate DFs. This study also aims to conduct trend analysis to examine the presence of any trend or

step jump in annual maximum flood (AMF) data. It also investigates the uncertainty in FFA by boot strapping and Monte Carlo simulation.

1.3. Research Questions

This research uses at-site FFA techniques with an aim to select the best-fit PD and estimate uncertainty associated with the selected PD. This study uses data from the Brisbane River catchment, Queensland, Australia.

This study examines the following research questions:

- How to select best-fit PD in the selected study region?
- Is there any trend in observed AMF data within the study region?
- Is there any impact of outliers in data on estimation of design flood and on selection of best-fit PD?
- What is the level of uncertainty in the estimated flood quantiles?

1.4. Overview of Methodology

FFA establishes relationship between flood event magnitude and its frequency of exceedance. The approach of finding relationship can be applied locally using at-site FFA or regionally using regional flood frequency analysis (RFFA). In this study, the at-site FFA approach has been implemented. The research methodology is summarised into the following steps:

a) Selection of study region and preparation of data;
b) Selection of best-fit PD (using EasyFit);
c) Quantile estimation by stationary approach (using FLIKE);
d) Uncertainty analysis applying bootstrapping and Monte Carlo simulation techniques; and
e) Trend analysis on the AMF data series.

Twenty-six stream gauging stations from the Brisbane River catchment are selected. The best-fit PD is selected using EasyFit software (Mathwave, 2017; Drokin, 2018). Five widely used PDs and three GoF statistical tests are adopted in this study. Visual observation of the

fitted distributions is carried out using plots produced by FLIKE (Kuczera and Franks, 2016; Kuczera, 1999) and comparing with EasyFit results. FLIKE software is also used for quantile estimation. The sensitivity or impact of first, second and third highest AMF records on the best-fit PD is examined. Uncertainty analysis is carried out using bootstrapping and Monte Carlo simulation. Trend analysis is conducted by TREND software (Chiew, 2005) developed by eWater (eWater, 2018) using twelve different trend tests one each of the selected station's AMF data set.

1.5. Outline of the Thesis

This thesis is composed of six chapters. Chapter 1 presents background, the need for this research, summary of methodology and research questions.

A review of various DF estimation techniques is presented in Chapter 2. The review particularly focuses on at-site FFA, trend analysis, the non-stationary approach to FFA and a review of recent studies on different PDs, associated parameter estimation and GoF tests to choose the best-fit PDs for DF estimation.

Chapter 3 discusses selection of study catchment, selection of streamflow gauging stations, streamflow data collation and preparation of streamflow data. Filling of gaps for missing data in the AMF data series is also discussed. The list of streamflow gauging stations selected for this study is also presented.

Chapter 4 outlines the proposed research methodology. This includes methods and mathematical functions for PDs, parameter estimation, GoF tests, quantile estimation, trend analysis, sensitivity analysis and uncertainty analysis. This chapter also discusses the non-stationary approach of FFA.

Chapter 5 presents the results and discussion, including the selected best-fit PD. Visual assessment and numerical assessment using GoF tests are discussed. This chapter also covers quantile estimation, sensitivity analysis and trend analysis. Five different PDs have been tested. The results from sensitivity analysis with bootstrapping are discussed. The sensitivity on selection of the best-fit PD is presented. Impact of the presence of outliers in data series is

discussed. The results of uncertainty analysis using bootstrapping and Monte Carlo simulation approaches are presented. This chapter also contains the results of trend analysis. Twelve different trend tests, including Spearman's Rho and Mann-Kendall, are used to test the AMF data for presence of any trends.

Chapter 6 presents summary and conclusions of this study. This chapter finally presents the recommendations for future research.

CHAPTER 2 : FLOOD ESTIMATION AND FREQUENCY ANALYSIS METHODS

2.1 General

This chapter contains review of previous studies on estimation of design flood (DF) with a focus on at-site flood frequency analysis (FFA). Firstly, various methods used in FFA are discussed. A review of FFA methods is then presented. The assumptions, advantages, and limitations of FFA are also discussed. Stationary and non-stationary FFA are then discussed. Trend analysis methods are also reviewed. An overall summary of literature review on DF estimation and FFA methods is presented at the end of this chapter.

2.2 Design Flood (DF) Estimation Techniques

Design flood (DF) is the expected peak flood discharge at a given location associated with an AEP. DF is used in various infrastructure planning and development projects such as bridges and flood control and drainage structures.

Many DF estimation techniques are used around the world. The DF estimation methods can be classified on the basis of flood frequency methods used, empirical formula developed from analysis of observed flood data and envelop curves (Cordery and Pilgrim, 2000). In general, methods involve in DF estimation are grouped into two broad categories, i.e. the rainfall-based methods (rainfall-runoff simulation) and the streamflow-based methods (statistical analysis of recorded streamflow) (Haddad, 2008; I. E. Aust., 1987; James and Robinson, 1986; Lumb and James, 1976; Feldman, 1979). Each of these methods has advantages and disadvantages. The choice of a method for a given purpose constitutes a significant aspect of the design process (I. E. Aust., 1987). Different DF estimation methods are illustrated in Figure 2.1.

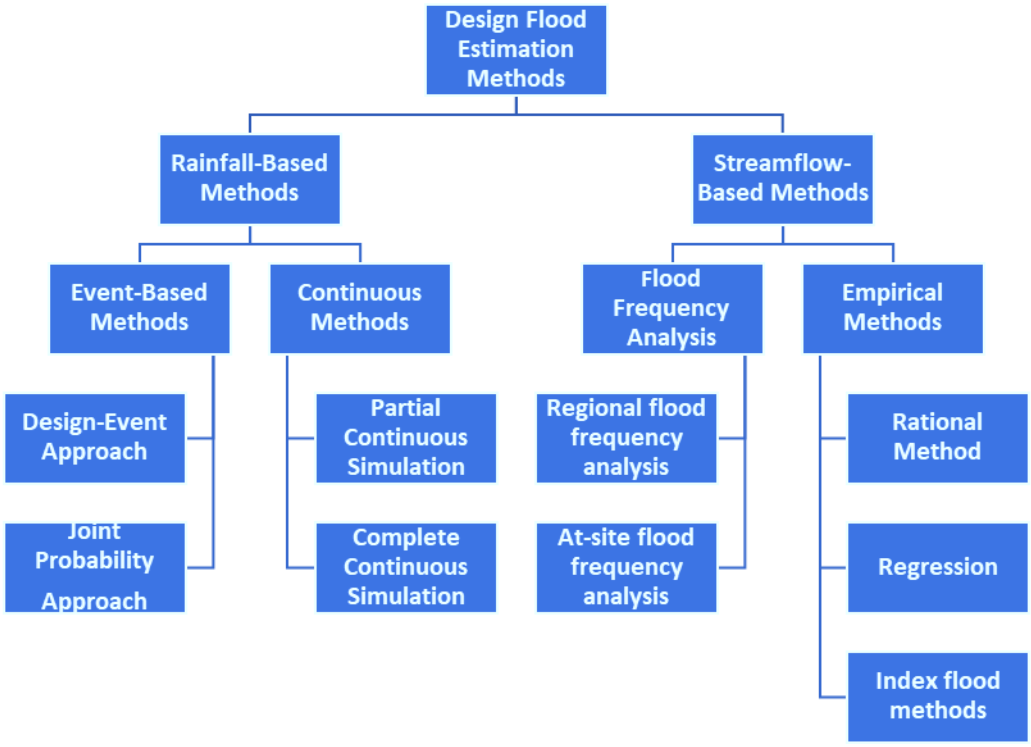

Figure 2.1: Different design flood (DF) estimation methods

When adequate data on observed streamflow are available, the basic approach to estimating flood-frequency relationship involves statistically analysing observed streamflow. If the available streamflow record length is relatively short, a regional relationship with flows from nearby stations may potentially be used to estimate DF. At-site FFA is only applicable to gauged catchments, and for ungauged sites RFFA is used for estimating DF. If the observed flow data is missing or insufficient, using a rainfall-runoff model to obtain DF could be a possible solution. This is especially used to produce detailed simulations for a given catchment.

Rainfall-runoff models typically estimate flood hydrographs using given rainfall inputs. Based on the storm rainfall input, there can be two approaches of rainfall-runoff modelling. In the design storm approach, a design storm rainfall serves as the input to the rainfall-runoff model, and the output is a design flow. Design storms are obtained by statistically analysing rainfall observations. In this approach, the frequency of design flow is assumed equivalent to that of design storm, which may not always be valid, as the rainfall-runoff relationship is not linear.

The observed storm approach applies a rainfall-runoff model to rainfall data to obtain simulated flows. These are then used instead of observed flows. A flood-frequency relationship is found by statistically analysing the simulated flows. The observed storm approach may be event-based, or continuous. In the former, separate storms are used as inputs to rainfall-runoff models. In the latter, the complete rainfall record is used to model runoff continuously; however, this necessitates initial condition at the start of every event being estimated and can be demanding in terms of the required data and model calibration (IFM, 2018). The approach to be chosen for flood analysis and estimation depends on consideration of the nature of the project, and resource and data availability.

If the flood frequency relationship needs to be extended beyond the range of observations, and is based on a very short flow record, FFA is deemed unreliable. Without sufficient detailed information on the land cover or geology of a catchment, complex rainfall-runoff models cannot be built. Reliable flood estimates are needed for more important projects as it is thought that methods that are more sophisticated and comprehensive produce more reliable results. However, the models used in these methods are not easy to calibrate and can be sensitive to input and parameter changes. Consequently, financial resources and the available time and expertise are also considered when choosing a method for flood estimation (IFM, 2018).

At-site FFA is the most direct DF estimation method. This method is also used as a base or standard for other DF estimation methods, such as rainfall-runoff modelling method and regional DF estimation methods (Rahman et al., 2013).

2.2.1 Streamflow Based Methods

Streamflow based methods are suitable for a catchment if relatively long record of streamflow data is available. In these methods, estimates of DF are made by analysing streamflow data. Both at-site FFA and RFFA are streamflow based methods, which are widely used DF estimation methods. Streamflow-based methods are mostly based on streamflow data analysis and involve empirical equations in RFFA and at-site FFA (Mishra et al., 2010).

2.2.1.1 Flood Frequency Analysis (FFA)

FFA is a technique for estimation of DF that corresponds to particular AEP or return period. Statistical frequency curves were first applied to flood data as a method by Gumbel. Analysing recorded annual maximum (AM) flow data for relatively large number of years (preferably > 20 years), FFA method calculates sample (or population) parameters (e.g. standard deviation, mean and skewness) of probability distribution (PD) which are finally used to define PD for estimation of DF. FFA can be made either using observed flood data for DF estimation or using flood depth data for DF depth estimation. For design flow estimation using these methods, peak flow magnitudes of varying AEP or average recurrence intervals (ARI) are computed. FFA is performed using one of two models: the annual series and partial series. Generally, the annual series is used to estimate design flows less frequent than the 10-year ARI, whereas the partial series is used for estimating more frequent flows.

The AM flow series is the record of each year's peak flow. Each year's annual peak flow is assumed independent of other year's annual peak flow. In reality time intervals between two peak floods are different and also the time and magnitude of occurrence of these peak floods do not follow any regular pattern. The return period or ARI is the estimated average time (year) interval for a flood event expected to exceed. Although occurrence of one flood event is independent of other event, it is expected that the return periods for larger floods are longer and vice versa. Return period is inversely proportional to AEP. If a given flood magnitude q equals or exceeds certain flow once in T years (return period) then for flood quantile QT it can be written as (Haddad, 2008):

$$F(Q_T) = P(Q_T \leq q) = 1 - P(Q_T > q) = 1 - \frac{1}{T} \tag{2.1}$$

Probability plot requires estimating chance or probability of non-exceedance of individual event and this is known as plotting position (points) formula. There are many plotting position formula available and one commonly used one is:

$$F = \frac{i - 0.4}{N + 0.2} \tag{2.2}$$

Where *i* is rank in ascending order of observed sample values and *N* is sample size. Rao and Hamed (2000) documents many commonly used plotting position formula.

It is not unlikely that at a stream gauging location, second and third highest flood values in a given year are higher than the highest flood values in some other years. As the AM series contains only the highest flow of a given year, DF estimation using AM series may miss some useful flood information (Rao and Hamed, 2000). However, this limitation can be avoided if partial duration flow or peak over a threshold (POT) model is used, where all independent flow peaks above a threshold value are included in DF estimation. The selected threshold value should be low enough so that for each year at least one event is selected (Rao and Hamed, 2000). Nonetheless, the POT model also involves some limitations as some peak observations may have influence from the previous peak flow event.

To describe probability of flood events, Australia Rainfall and Runoff ARR 2019 Book-1 (Ball et al., 2019) recommends to use term AEP, ARI and EY and not the return period (*T*) where EY stands for number of exceedances per year and AEP stands for annual exceedance probability.

The most important advantage of FFA is that FFA approach provides independent estimation of design flow for a given AEP as it assumes that all events are independent. As FFA method uses only direct flood data, factors affecting flood magnitudes has no impact. This approach is easily applicable and computes confidence limits that can indicate the relative accuracy of the results.

2.2.1.1.1 At-Site Flood Frequency Analysis (FFA)

At-site FFA is the most direct DF estimation method (Haddad, 2008). This method needs a relatively longer period of observed data at the stream gauging site of interest. In this method, it is required to select a suitable PD and procedure for associated parameter (θ) estimation. Generally, PDs are chosen arbitrarily as there is no specific guideline to choose a PD for a given site. At-site FFA is useful for flood estimation involving smaller AEP. Moreover, at-site FFA can be used as a base to assess the accuracy of estimation of DF using other

methods, including RFFA and rainfall-runoff modelling. At-site FFA is recommended to estimate design peak floods, if enough streamflow data of acceptable quality is available (Ball et al., 2016).

In at-site FFA, a relationship is established between peak flood discharge and ARI for a gauged catchment. To establish this relationship recorded streamflow data is used. Three different types of recorded stream flow data may be used for establishing this relationship (Haddad, 2008): (1) AM flow series, (2) POT series, and (3) full recorded time series (TS) (Haddad, 2008). In this study, univariate at-site FFA approach is adopted using AM flow series. Univariate FFA is based on peak data either derived from AM or PD series as this is considered representative of flood characteristics at a given site.

2.2.1.1.2 Regional Flood Frequency Analysis (RFFA)

Many catchments have limited observed streamflow data or sometimes data may not be available at all for a specific site where DF estimation is required. If the observed flood data is limited or unavailable for a catchment for FFA then observed flood data from similar catchments or neighbouring catchments can be used for FFA (Haddad, 2008). This method is named as "Regional Flood Frequency Analysis (RFFA)". In RFFA, DF at an ungauged site may be estimated using observed flood data from a group of sites within the selected region (Haddad, 2008). RFFA assumes that the distribution of the standardised variate is same for all the sites of the selected region within a margin of sampling variability. In index flood method (a type of RFFA method), a single regional flood frequency curve is derived by combining all available observed data within the region and it is assumed that this curve can be used with appropriate site-specific scaling factor anywhere within the selected region (Haddad, 2008; Gabriele and Arnell, 1991).

RFFA is useful where availability of streamflow data is limited. Physically unrealistic parameter estimates may be derived by statistical estimation from too small a sample, especially if PD of three or more parameters is involved. RFFA uses information from gauged sites and transforms it for use in ungauged sites. RFFA has two uses. If data is not available for a site, RFFA makes use of regional flood data (Haddad, 2008; Cunnane, 1989). When recorded data is limited for a site, combination of available data at that site and data

from nearby stations within the region are used to produce enough information to increase confidence and reliability in parameter estimation of selected PD. Combining data from various locations within the region for a single site is achieved by substituting time in place of space (Haddad, 2008; Stedinger et al., 1993; NRC, 1988). As an example, in South Africa, Nortje (2010) estimated extreme flood peaks for a site from regional data by developing and applying REFSSA (Extreme Flood Peaks by Selective Statistical Analyses) procedure (Smithers, 2012), and the author applied the REFSSA method and found that it was suitable to estimate DF with 1,000 to 10,000 ARIs for 100-7000 km^2 catchment areas (Smithers, 2012).

2.2.1.2 Empirical Methods

Empirical flood estimation method uses empirical formula for DF estimation. All empirical formula establish relationship among flood statistics, size of catchments, climate and physiographical characteristics. Empirical methods are less accurate and use of this method should be avoided if empirical formula is not calibrated using data from the selected catchments (Smithers, 2012; Cordery and Pilgrim, 2000). These methods are used mainly for ungauged catchments where very limited or no record of peak flood discharge data is available. The most common empirical flood estimation method is the Probabilistic Rational Method, which was presented in ARR 1987 (I. E. Aust., 1987). If catchment area is A in km^2 then peak discharge (Q_T) in m^3/s for T years ARI by this method is given by (Pilgrim and McDermott, 1982; Haddad, 2008):

$$Q_T = 0.278\, C_T\, T_{tc,T}\, A \qquad (2.6)$$

Where C_T is runoff coefficient (dimensionless) for T years ARI; $I_{t_c,T}$ (mm/hour) is average rainfall intensity for t_c (hours) design duration and T years ARI *(*Haddad, 2008*)*. For short duration rainfall intensity estimates, there are notable uncertainties as noted by Green et al. (2011) which can affect DF estimates obtained by the Probabilistic Rational Method.

2.2.2 Rainfall Based Methods

As the observed rainfall data are readily available and physical characteristics of catchments can be used in the model easily, rainfall-based flood estimation techniques are widely used for DF estimation (El-Kafagee and Rahman, 2011). Rainfall-runoff models (flood routing or unit hydrograph techniques) used for flood estimation usually convert rainfall data into runoff (flood discharge). The rainfall-runoff model used in this method is calibrated using available observed rainfall and flood data. Limitation in rainfall based DF estimation method includes finding appropriate deterministic models to convert input rainfall into flood discharge as outputs and to preserve the important probability characteristics involved in this process (Rahman et al., 1998).

Event-based approach and continuous simulation approach are two main approaches in rainfall-based methods. Some of the rainfall-based methods are discussed below.

2.2.2.1 Event-Based Methods

To estimate DF, design rainfall or intensity-frequency duration (IFD) data is used in the event-based method. The IFD data for different durations at any location within Australia are available in the ARR 2019 (Ball et al., 2019) via Australian Bureau of Meteorology (BOM, 2019) website. In ARR, IFD data is derived using rainfall data from the BOM rain gauges and rain gauges those are managed by other organisations across Australia and this rainfall data was prepared through rigorous quality control procedures (Ball et al., 2019). Event-based methods are probabilistic, and they require calibrated rainfall-runoff-model for the catchment of interest.

The event-based method involves few concepts and assumptions, the impacts of which are difficult to quantify. For example, the assumption of same return period for rainfall and flood events and simplified hyetograph shape can affect flood estimation from an event-based method (Grimaldi et al., 2012).

2.2.2.1..1 Design Event Approach

The design event approach can be used to estimate DF (Mirfenderesk et al., 2013). This approach estimates DFs for selected ARIs using IFD data at the catchment of interest (Viglione et al., 2009). This approach is relatively easy to apply and allows catchment processes to be considered in modelling (Rogger et al., 2012). Event-based rainfall-runoff model transforms probabilistic behaviour of input rainfall to corresponding DF (Ball et al., 2019). Although this method takes into account the probabilistic behaviour of rainfall depth, this does not consider probabilistic nature of other input variables (e.g. initial loss and temporal pattern of rainfall) in the rainfall-runoff modelling. This method is basically based on three major assumptions, i.e. (a) choice of design rainfall hyetograph i.e. duration and shape can preserve ARI; (b) input rainfall and output flood discharge ARI is equivalent; and (c) use of chosen initial soil moisture condition can preserve ARI (Camici et al., 2011). The process for estimating DF for a specified AEP using this method is shown in Figure 2.2 (Rahman et al., 2002).

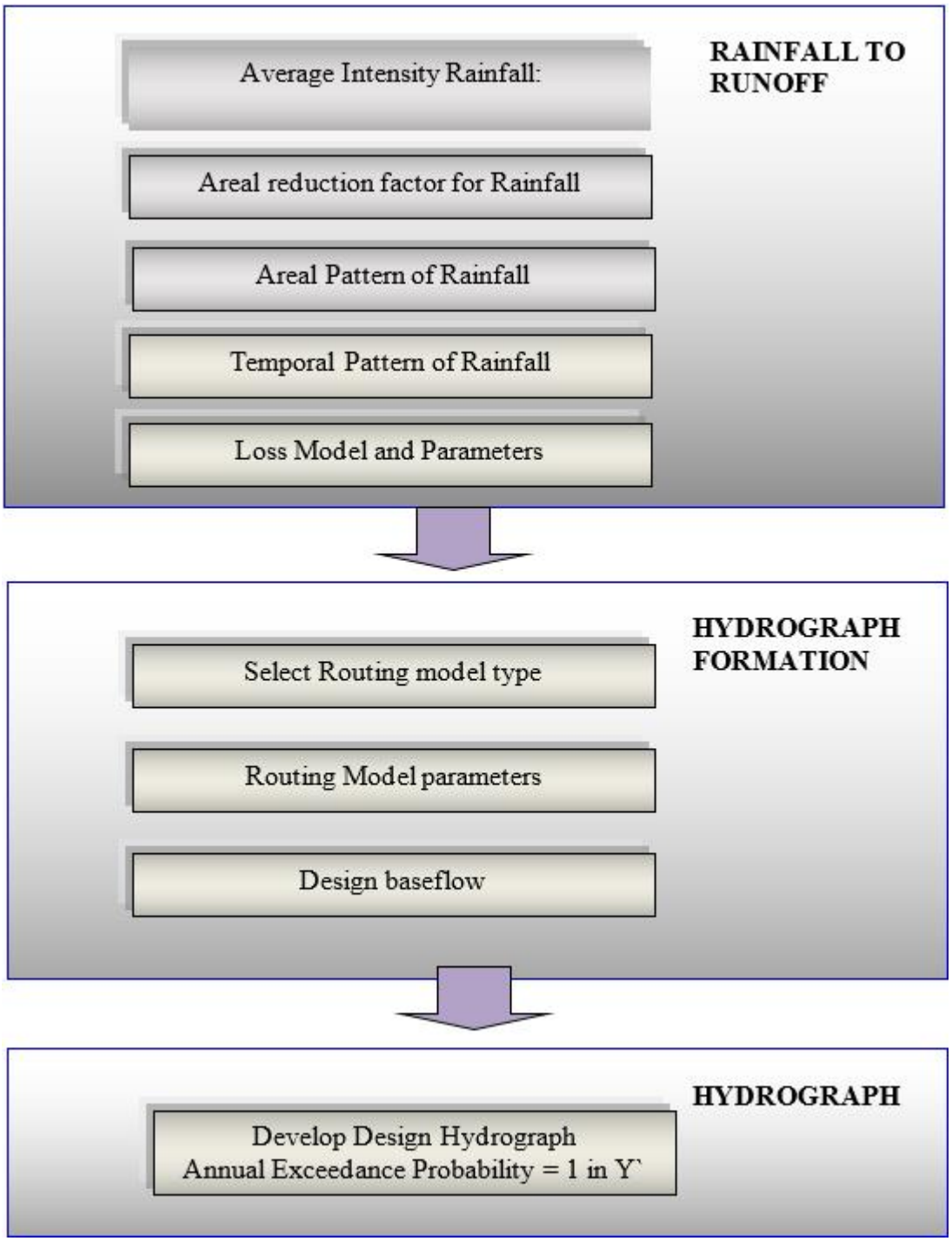

Figure 2.2: **Estimation of design flood with design event method (**Rahman et al., 2002**)**

2.2.2.1.2 Continuous Simulation Approach

The continuous simulation flood estimation method is an alternative approach to direct statistical flood estimation specially for catchments when historical flood peaks data are limited (Blazkova and Beven, 2009). Continuous simulation type DF estimation approach

may be preferred over the event based approach as this may overcome some of the probabilistic limitations of the event based approach of flood estimation. Continuous simulation models use rainfall time series as input and transform rainfall series into probabilistic estimated flood series as outlined in ARR 2019 (Ball et al., 2019). In this method catchment flow is generated taking rainfall time series data as input using hydrologic model and then discharge time series (continuous flood hydrograph) is generated. Several studies are reported in the literature for DF estimation using this approach such as Grimaldi et al. (2012) and Blazkova and Beven (2009).

2.2.2.1.3 Joint Probability Approach

The Joint Probability Approach (JPA) is a type of holistic approach for estimation of DFs that takes into account the probabilistic nature of important input variables such as temporal pattern, intensity and duration of rainfall, initial loss into model more clearly (Charalambous et al., 2005). Joint probability and continuous simulation methods of flood estimation use similar techniques in hydrograph generation phase of the modelling, but basic inputs to model and process of using these inputs to develop runoff generation model are different (Rahman et al., 1998). In JPA, consideration of randomness in input variables helps to eliminate biasness in the input values. JPA is also known as derived distribution approach as probability distributed or random inputs are combined to produce probability distributed outputs (Mazumder, 2005). The procedure by which a flood frequency distribution is determined for a given a catchment combines deterministic and stochastic hydrologic modelling (Charalambous, 2004). Many studies have been found in literature using JPA for DF estimation. All these studies indicate that the JPA may be applied for more accurate DF estimation than flood estimation by design event approach.

2.3 Basics of Flood Frequency Analysis (FFA)

As the most common natural hazard in the world, we cannot avoid but to live with floods. We can minimise the negative impacts of floods taking structural (e.g. building flood embankment and dam) and non-structural measures (e.g. land use management and flood forecasting and warning system). All of these necessitate hazard or risk assessment through

FFA, to some degree (Dunne and Leopold, 1978). The FFA aims to estimate DF magnitudes corresponding to a given AEP (Stedinger et al., 1993).

FFA is a statistical technique that selects and fits a PD model using historical streamflow data (Haddad and Rahman, 2008). It is a procedure for estimating the AEP of extreme events, in which extreme event's magnitude and its frequency of occurrence are inversely proportional. The magnitude and frequency of occurrence of future/extreme floods are estimated using probability concepts. Hydrologists use FFA to estimate flow magnitude corresponding to a particular AEP. Thus, FFA has a significant role in water engineering practice. FFA establishes relationship between magnitude of a flood event (e.g. peak discharge) and its frequency of occurrence by applying probability models.

The design of infrastructure such as dams, spillways, bridges and flood defence structures make use of knowledge of flood magnitude-frequency relationships. It is crucial to apply appropriate statistical tools to carry out FFA so that optimum design specification for hydraulic structures is facilitated and over-designing or under-designing is minimised. FFA provides measurement parameters to analyse the damage associated with specific flows during floods and it is applicable to planning, design and operation of different hydraulic structures (Haddad and Rahman, 2012). FFA is useful for flood zoning, flood insurance activities and also is used for flood hazard or flood risk mapping for the region (Karmakar et al., 2010). Not only are engineers able to better design safe structures given accurate estimates of flood frequency, but economic losses from structural maintenance can be minimised. Thus, FFA continues to be relevant and important, as it has large economic and environmental impact. Research to improve methods for deriving more accurate flood estimation is continuing, but with new emphasis (Bobee and Rasmussen, 1995).

To understand FFA, understanding on the concept of ARI or return period and AEP is essential. Return period or ARI is the estimated average time (year) interval for an event expected to occur. Return period estimates the likelihood of any flood event in any given year. It is inversely proportional to the AEP and AEP is the probability of occurrence of event of same size or larger in any year. Statistical FFA is still considered as the most relevant means of estimating design floods systematically (Haktanir, 1992).

2.4 Assumptions of Flood Frequency Analysis

All methods of FFA involve a degree of extrapolation. The ARI for estimation of design discharge is usually much larger than the discharge data record length for most catchments used for FFA. Therefore, the estimation of the design discharge requires, to some extent, extrapolation, which finally needs curve-fitting to the observed flood data. The fitting of any probabilistic model requires assumption regarding the PD that is used to generate flood events (Klemes, 1988). Through the history of FFA, sophisticated statistical techniques have been used for rigorous PD curve fitting. Although this has improved the accuracy of flood estimates and way to treat uncertainty in estimate; all these techniques are embedded within the broader model assumptions (Kidson and Richards, 2005). The flood data are stochastic in nature. For FFA, flood data are assumed random i.e. independent of time and space and independent of any impact due to anthropogenic or natural changes in the hydrological system (Haddad and Rahman, 2011).

The basic assumption in empirical FFA is that flood data are independently and identically distributed. The implication is that the climate is assumed static at all time. Therefore, irrespective of climate mechanisms, the chance of occurrence of flood of certain magnitude is assumed to be the same for any year. Whilst this assumption may be satisfied in many locations, it may also produce substantially biased estimates of both long-and short-term flood risk if the assumption is violated (Franks et al., 2015).

Basic assumptions of FFA include:

1. Observed flood data are from same population;
2. Flood data represent the population; and
3. Process responsible for generating these events is static over time.

FFA assumes that no errors of measurement or computation are made. Hydrological data are assumed independent, i.e. selected events are not correlated with one another; rather the flood data are random being generated from a stationary platform. The first assumption is that the hydrologic system is stochastic and independent over time. Usually the individual AM flow occurs relatively after long interval of time and for this reason AM events are more likely to be independent. However, it is important to check the date of occurrence of successive AM

events. The use of AM series used for FFA to satisfy this assumption has been described in ARR 2019 (Ball et al., 2019, Book3, Sections 2.3.3 and 2.3.4).

The second assumption is called the assumption of homogeneity. This means that the observed flood data are identically distributed, i.e. all data are derived from same population and have same statistical properties because all data are based on same hydrological processes. This assumption is satisfied by choosing observations from the same population (meaning no changes in the watershed and recording gauges are made). If the recorded floods come from different processes (for example, due to storm or snow melt), this assumption may be violated. Another aspect of homogeneity is that the flood regime is assumed to be time-independent; this may be violated by changes in the catchment over time caused by natural factors or human activities.

2.5 Selection of Probability Distributions (PDs) in Flood Frequency Analysis

The usefulness of FFA depends on the level of accuracy in estimating the frequency of occurrence of extreme events and its magnitude. Of primary importance in at-site FFA and RFFA is the choice of a proper PD model and related parameter estimation techniques (Rahman et al., 2018). This has been widely researched (Cunnane, 1989). Choice of appropriate PD for FFA cannot be made on a physical basis (Rahman et al., 2014a). In FFA, graphical methods or statistical tests are used to select appropriate probability model. Major consideration to choose PD is given on convenience (Bobee et al., 1993). More weight is given on empirical suitability than a priori reasoning while choosing a PD in FFA (Cunnane, 1989; Cunnane, 1985).

The distribution of annual maximum flood (AMF) values at a particular site can be described using several probability models. Until recently different studies around the globe recommend several suitable probability models for FFA. As there is no consensus on which PD(s) should be used for FFA, the selection of a suitable PD still remains problematic. Selection depends mostly on the properties of the available data. Hence, a suit of alternative distributions must be evaluated so as to find an appropriate distribution model that could estimate design floods with acceptable accuracy (Tao et al., 2002).

Inappropriate selection of a PD model could produce biasness and substantial error in estimated DF values, especially when ARI is high leading underestimated or overestimated DFs that might have dire consequences in practice (Rahman et al., 2013). As there is no universal guide available to adopt, PD is usually chosen arbitrarily (Rahman et al., 2013).

Haddad and Rahman (2008) analysed AMF data from 18 gauged sites throughout south-east Australia to evaluate relative suitability of the currently recommended methods of at-site FFA in Australia. To compare the performances of various FFA methods with ARIs from 2-year to 100-year, they applied a number of approaches, including statistical hypothesis testing and comparison of the quantile estimates found through fitted distributions with graphical estimates. Laio et al. (2009) evaluated capability of different performance criteria to find suitable PD for the available AMF series of 1000 catchments in the United Kingdom (UK). They inferred that, where two criteria yielded similar results, the model could be selected safely.

2.5.1 Probability Distributions (PDs) and Parameter (θ) Estimation Methods for FFA

The PDs commonly used can be conventionally divided into four groups: (1) a group of transformed gamma distributions, including Pearson type III and Kritskii-Menkel distributions; (2) a group of Lognormal distributions, including Lognormal, a family of functionally normal curves of Yu. B. Vinogradov; (3) distributions derived by generalization of the theory of extreme values, Generalised extreme value (GEV) distribution combining Gumbel or extreme value type I (EV1) distribution, Freshet or extreme value type II (EV2) and Weibull or extreme value type III (EV3) distribution; and (4) a group of power distributions, including Generalised Pareto distribution and Pearson type V distribution (Gubareva, 2011).

Usually, a smaller number of PD models have been used in FFA for DF estimation. However, available PD models are of many different types, e.g. two-parameter models and three-parameter models. The two-parameter probability models are simpler models that are based on scale and location parameters and that can be fitted analytically, e.g. Lognormal (LN) and

Gumbel (EV1) double-exponential models. The mean and variance of the sample (AMF data) required for these models can be calculated using Method of Moments. The three-parameter models such as GEV and Log Pearson type III (LP3) cannot be fitted analytically. The widely used LP3 model is a generalised gamma distribution. The location, scale and shape are the three parameters in these three-parameter models. These models depend on the variance, mean and skewness of the sample data when Method of Moments may be used (Kidson and Richards, 2005). The two-parameter models are advantageous as they are simple and can be fitted easily with sample data; however, the three-parameter models with an extra shape parameter, have the advantage of fitting a catchments' AMF data with longer record length (Kidson and Richards, 2005; NERC, 1999).

A list of PDs commonly used in FFA has been documented by Cunnane (1989). FFA can make use of both AMF and POT flood data; however, the former is more commonly used as POT data does not fully meets the assumption of independence of data for FFA (Rahman et al., 2013). As AMF data are frequently skewed, many skewed distributions have been developed and used in FFA.

Cunnane (1989) mentioned that EV1 distribution has been recommended to use for FFA in 10 countries, GEV distribution for 2 countries and LP3 distribution for 7 countries. Lim and Lye (2003) in their study found that GEV and Generalised Logistic distribution could well approximate the observed extreme floods in Sarawak, Malaysia. In ARR 1987, similar to the United States (USWRC, 1967), LP3 distribution was suggested for general use in combination with Method of Moments (Hossain, 2019). However, in ARR 2019, no specific distribution is recommended (Ball et al., 2019) for FFA. Rahman et al. (2013) researched the suitability of using 15 different PDs for FFA in eastern Australia i.e. Five-parameter Wakeby (WAK5), Three-parameter Lognormal (LN3), Four-parameter Wakeby (WAK4), LP3, Pearson type 3, GEV, Generalised Pareto (GP), EV1, Normal, Two-parameter Gamma (G2), Weibull, Logistic, Generalised Logistic (GL), Two-parameter Lognormal (LN2) and Exponential distributions. Most of these PD models are recommended to use for at-site FFA in different countries around the globe (Rahman et al., 2013; Cunnane, 1989).

Different countries adopt different approach to FFA. A potential reason for this is to make an effort to minimise legal liability. Since 1967, LP3 distribution for FFA is the official model in the United States (NRC, 1988). By contrast, up until 1999, the GEV distribution was

endorsed in the UK (NERC, 1999), and currently the official distribution is the Generalised Logistic. In some cases, more than one probability models have been favoured in a country (Kidson and Richards, 2005) such as LP3, GEV, GPA for Australia (Rahman et al., 2013), GEV and Wakeby for Turkey (Seckin et al., 2011) and GEV, LN and LP3 for Bangladesh (Karim and Chowdhury, 1995).

Many countries adopt standard methods for government and private use on the basis of large-scale studies of the country's flood data in an effort to achieve uniformity in FFA. LP3 was recommended as standard for the United States (US) by the Water Resources Council of US (Abida and Ellouze, 2008; Benson, 1968) and GEV distribution was recommended for the United Kingdom (UK) (Abida and Ellouze, 2008; NERC, 1975). In the then former USSR, the Generalised Gamma distribution was recommended (Abida and Ellouze, 2008) while in West Germany, LP3 distribution and Pearson 3 distributions were proposed (Abida and Ellouze, 2008). The Institution of Engineers in Australia also advocated for the LP3 method (I. E. Aust., 1987). In 1984, the World Meteorological Organization (WMO) prepared a global survey of flood frequency methods and found that GEV, EV1, LN2, Pearson 3, LP3 and EV2 are widely used distributions (Abida and Ellouze, 2008).

The appropriateness of a PD model to explain the nature of distribution of a given AMF data series can be evaluated using various criteria. Statistical (i.e. goodness-of-fit (GoF) tests) tests can be applied to evaluate whether a given PD can be used for observed AMF data. GoF tests together with graphical probability plots are useful methods to evaluate the suitability of a PD for observed AMF data (Stedinger et al., 1993). Graphical probability display methods show how accurate the assumed distribution is in fitting the observed AMF data. Quantile-quantile (Q-Q) plot and probability-probability (P-P) plot compare the observed sample to a probability model. Table 2.1 outlines a few most commonly applied PDs recommended by various countries for at-site FFA.

Table 2.1: Some most commonly used probability distributions for FFA

Distribution	First Applied by	Country/Region of application
Pearson Type 1 and 3	Foster, 1924	West Germany
Log-Pearson Type III	Beard, 1962 Benson, 1968 USWRC, 1967	USA (NRC, 1988), West Germany and Australia
Generalised Extreme Value	Jenkinson, 1955	UK (NERC, 1999) until 1999, Bangladesh (Karim and Chowdhury, 1995)
Extreme Value Type 1	Gumbel, 1941	Italy (Rossi et al., 1984)
Lognormal	Hazen, 1914	New York, USA (Stedinger and Cohn, 1986)
Wakeby	Houghton,1977; Houghton,1978	Eastern Australia (Rahman et al., 2015)
Log-logistic	Ahmad et al., 1988	The Netherlands (Ahmad et al., 1988)

In FFA, various methods are used for estimating parameters of a PD based on the methods of probability theory and mathematical statistics. In the past, many such methods were thoroughly studied. Many of these methods are now widely used in practice in many countries. Numerous methodological recommendations and scientific publications on probabilistic estimation are available in the literature (Kuczera, 1983; Cunnane, 1989; Rahman et al., 2018). However, there is no universal recommendation which ensures reliable estimation of DF with smaller AEPs (Gubareva, 2011).

For a selected PD, it is important that the parameters needed to fit the theoretical distribution to the relevant data are identified. This is done by estimating statistical moments/ parameters (e.g. variance, mean and skewness) of observed data using parameter estimation methods such as MoM, L-moments method and maximum likelihood estimation (MLE) method. Rahman et al. (2013) used L-moments, MoM and MLE in their at-site FFA study for Australia. Statistically, the MLE is considered a better parameter estimation technique as compared to the MoM (Bickel and Doksum, 1977). The effect of extreme values in the observed data series is less in estimating parameters using L-moments method and this is able to model many distributions (Rahman et al., 2013). MLE method is especially advantageous in that they can be used to multimodal PDFs (Kidson and Richards, 2005). MLE is also applicable for data series that does not follow normality assumption. As most hydrological

data does not follow normality assumption, MLE can be a better parameter estimation technique for hydrological data (Kidson and Richards, 2005). MLE method helps to define the confidence limits on DF estimation; however, a numerical solution may not be found for all cases (Kidson and Richards, 2005).

MLE is more preferable for parameter estimation for long time series having possibility of climate change impact in data as the MLE method can be adapted to account for the non-stationarity (Data, 2009). When samples are small, the method of L-moments is preferred, as with a small sample size the estimation of parameters with MLE may not be successful in many cases for GEV distribution (Data, 2009).

Zaman et al. (2012) investigated the suitability of fifteen different PDs with MLE, L-moments and MoM parameter estimation procedures for Australian AMF data. Haddad and Rahman (2011) evaluated MoM, MLE and Bayesian Markov Chain Monte Carlo (BAY) methods for the Lognormal distribution in Tasmania and found that the BAY procedure produces better estimates with Lognormal model, for which quantile estimation became less bias than parameter estimation with MoM and MLE. Rahman et al. (2019) adopted a regional LP3 distribution for RFFA in Australia (Ball et al., 2019). Kuczera et al. (2005) and Kuczera (1983; 1999) uses Bayesian parameter estimation procedure for FFA. Viglione et al. (2013) used Bayesian method for FFA. Bayesian approach provides a general inference procedure for at-site FFA. Viglione et al. (2013) found that the estimated uncertainty is reduced significantly if more information is used through Bayesian analysis. According to study of Haddad and Rahman (2012), the model errors can be handled better with the Bayesian estimator.

2.5.2 Selection of Distributions: Graphical Methods and Goodness-of-Fit Tests

Three major steps are involved in FFA modelling: data choice, selection of probability model and selection of a parameter estimation method (Bobee, 1999). The results from FFA are influenced by model choice, and hence comparing several PDs is the best option to quantify this (Haktanir and Horlacher, 1993). Choice of suitable PD model is the most important task in FFA. The choice of PD for FFA depends on many factors such as availability of long time-series flood data, and the method for estimation of parameters.

An inappropriate choice of PD for FFA could produce large error and bias on estimated DFs, especially if ARI is very high, which will result in under estimated or overestimated flood quantiles (Rahman et al., 2013). Rahman et al. (2013) documented numerous recent studies on selection of suitable PDs and related parameter estimation procedures.

LP3 distribution was recommended for FFA at coastal streams of NSW (Rahman et al., 2014b). FFA study in Queensland concluded that LP3 as the most appropriate PD (Kopittke et al., 1976). FFA study on 172 catchments in Australia used moment ratio diagrams to compare different distributions and this concluded that LP3 was the best suited PD in Australia (Srikanthan and McMahon, 1981). Conversely, the FFA study of Rahman et al. (2013) on FFA in Australia was unable to identify one single distribution for all Australian states.

Laio et al. (2009) in their study assessed the capability of different performance criteria to recognise the suitable PD for the available AMF peak series collected from 1000 catchments in the UK. They inferred that, where two criteria yielded similar result, the model could be selected safely; otherwise two different models for FFA could be employed and one of the results to be selected to satisfy design criteria. Haddad and Rahman (2008) in their study used AMF data from 18 gauged sites throughout south-east Australia to evaluate relative capabilities of the most popular PDs for at-site FFA. Using several measures including statistical hypothesis testing and the comparison of quantile estimates taken from the fitted distributions with graphical estimates, they compared the capabilities of various FFA methods with ARIs ranging from 2 years to 100 years. They found that the GP-L moments and GEV-LH2 moments methods provided the best fit, followed by the LP3-BML method, whereas the ARR-recommended method (LP3-MoM) did not provide a good fit. Haddad and Rahman (2011) examined seven probability models for FFA in Tasmania and they concluded that Lognormal was the best choice.

The accuracy of a PD in fitting a given data set can be assessed through statistical GoF tests. As different GoF tests may favour different probability models, the same test cannot be used to assess all the candidate probability models (Kidson and Richards, 2005). A number of factors including parameter estimation procedures, availability of flood data and probability model comparison procedures can influence the choice of a PD. Using a data set from 127

gauging stations across Australia, Zaman et al. (2012) conducted at-site FFA study with Anderson-Darling (A-D) and Kolmogorov-Smirnov (K-S) statistical GoF tests and also used Bayesian information criterion (BIC) and Akaike information criterion (AIC) to identify most appropriate probability models and concluded that the LP3 and GEV distributions were the best fit probability models for most cases. Rahman et al. (2013) in their FFA study for Australia identified LP3, GEV, and GP distributions as the best-fit distributions.

The K-S GoF test assesses whether the observed data come from selected theoretical distribution or not. The A-D test shows better result with highly asymmetric distributions, which are very common in many hydrological applications (Zaman et al., 2012). Discrepancies between the population model and the sample model can be measured using AIC test. The BIC test relies on Bayesian framework and the most suitable PD model is the one that have the least AIC or BIC value (Zaman et al., 2012).

2.6 Sensitivity of Quantile Estimation on Maximum Recorded Flow Event

The maximum observed flow event at a flow gauging site may influence estimation of flood quantiles notably. Haddad et al. (2010) in their study found that quantile estimation might be seriously affected by maximum rating ratio (largest estimated quantile and maximum recorded flow ratio) in a gauging location. Viglione et al. (2013) found that extreme outliers (recorded flow) in flood time series significantly affect the flood frequency estimates. Rahman et al. (2015) examined how sampling variability may affect flood quantile estimates where they removed part of the AMF data to examine its effects on flood quantile estimates. In another study, Rahman et al. (2013) examined how rating curve extrapolation error could affect the highest AMF data, and how this could affect flood quantile estimates. Therefore, it is important to carry out sensitivity analysis of quantile estimation on maximum recorded flow event of each station's AMF data series.

2.7 Uncertainty in Flood Quantile Estimation Using Monte Carlo Simulation and Bootstrapping Techniques

Due to the limitations of sufficient data length, a high degree of uncertainty is involved in flood quantile estimation for smaller AEPs since FFA needs extrapolating theoretical curve

beyond the available data period. Al Mamoon and Rahman (2014) listed a number of studies proposing different techniques to quantify uncertainties in frequency analysis (Al Mamoon and Rahman, 2014). Haddad et al. (2010) proposed a rating ratio approach to estimate uncertainty in FFA. A Bayesian Monte Carlo simulation technique was adopted by Kuczera (1999) to assess uncertainty in FFA.

With current FFA methods, finding the best-fit PD and associated parameter estimation technique from many possible approaches appears to be difficult (Haddad and Rahman, 2011). The difficulty is posed by the existence of uncertainties resulting from both the model selection and parameter estimation. Merz and Thieken (2005) classified uncertainty in parametric estimation as epistemic or natural uncertainty where epistemic uncertainty is related with the lack of enough knowledge about the process and natural uncertainty comes from changing underlying process. Merz and Thieken (2005) in their study separated natural and epistemic uncertainties in FFA and found that while the former cannot be reduced, the latter can be through increased knowledge. Xu et al. (2010) studied other types of uncertainty for modelling of extreme events. Liang et al. (2012) adopted the Markov Chain Monte Carlo method to overcome difficulties in computing the integrals when estimating the sampling distribution. Li et al. (2010) applied bootstrapping techniques to calculate parameter uncertainty in SWAT (Soil and Water Assessment Tool) model. Baltussen et al. (2002) proposed an uncertainty analysis method using Monte Carlo simulations alongside non-parametric bootstrapping techniques. Al Mamoon and Rahman (2014) reviewed several sources of uncertainties in estimation of design rainfall and suggested that uncertainties could be analysed using Monte Carlo simulation and bootstrapping techniques.

2.8 Trend Analysis

According to Intergovernmental Panel on Climate Change (IPCC) (2007, 2014), global average surface air temperature is increasing. This may cause abnormalities in climatic events (e.g. precipitation and evapotranspiration); which in turn affect rainfall runoff process and streamflow regimes. Numerous studies around the globe have examined the presence of trends in hydrological variables (Khaliq et al., 2009). It is reported in many studies that due to climate change there exists systematic trends in many critical climate data (Rahman et al., 2012). Around the globe, different researchers reported temporal and spatial variability in

flood discharge data due to climate change. These changes can impact the rainfall runoff relationship (Villarini et al., 2009). Presence of trends in peak streamflow and rainfall data globally is the evidence of these changes (O'Brien and Burn, 2014; Hajani et al., 2017; Hajani and Rahman, 2018). Pekarova et al. (2003) highlighted the availability of high natural variation in streamflow around the globe might include strong periodic behaviour in streamflow, Therefore, if one or more cycles of such behaviour exist, trend analysis on the available streamflow data series for periods covering cyclic behaviour should be carried out (Pekarova et al., 2003).

As concerns regarding the impacts of climate change escalate (IPCC, 2007; IPCC, 2014), researchers around the world have been analysing hydrological data series using different statistical methods to determine trends, sharp drop or shifts in observed time series (Hossain and Rahman, 2019). Trends in data series can dramatically affect the results of FFA, which ultimately raise question on the concept of AEP used in FFA (Petrow and Merz, 2009). Therefore, DF estimation with data having varying flow regimes should be carried out assuming that the parameters of PD are variable over time (i.e. nonstationary FFA) (Petrow and Merz, 2009).

2.9 Stationary and Nonstationary Flood Frequency Analysis

The basic assumption in traditional FFA is that the flood data is stationary, homogenous (observed data is identically distributed), does not show any periodic pattern or any trends or any shifts (Machiwal and Jha, 2009). Stationarity means that hydrological data is random and independent over time and estimated parameters from any samples of same population will be the same within a margin of sampling variability. When statistical properties of a time series data do not change over time, this data series is called stationary time series data (Machiwal and Jha, 2009).

A time series data is considered nonstationary if distributional parameters of this data series changes with time (Cunderlik and Burn, 2003). Such changes in hydro-meteorological data series can be gradual (i.e. trend) or sudden (i.e. step change) or can be complex type of changes. These changes in data series may be due to natural causes (shifts in weather patterns/climate change) or due to human causes, including change of land use type (e.g. rural

to urban), shifting of gauging locations, flow extraction for irrigation and diversion of flow. If time series data have significant correlation (either positive or negative) between observed values and corresponding time, this series is considered to have trend (Machiwal and Jha, 2009).

One of the most direct techniques of detecting changes in hydrological time series is to test the recorded time series data for trends or step jumps by applying statistical tests. If no trend, step jump or periodicity is found in time series data, the data series is assumed stationary. Parametric and nonparametric are two common statistical tests that can be used to examine trends (Machiwal and Jha, 2009). Mann-Kendall (MK) test and Spearman's Rho (SR) test are two well-known nonparametric tests used to identify trends in hydrological time series (Sadeghi and Hazbavi, 2015; Laz et al., 2014; Liu et al., 2012). Three parametric tests i.e. Student's t, Autocorrelation and Linear Regression are used for identifying trends in data (eWater, 2018; Chiew, 2005). Parametric tests are reported to be more efficient than nonparametric ones. In general, nonparametric tests require 5 to 35% more data to achieve similar result at same confidence level of parametric test (Bethea and Rhinehart, 1991). To study trend on hydrological data series selected for non-stationarity frequency analysis, parametric tests are generally preferred over nonparametric test (Khaliq et al., 2009). However, trend analysis using parametric processes requires many assumptions about the trend behaviour, whereas nonparametric tests are more reliable in terms of non-normality, non-linearity, seasonality, missing records, serial dependence and sensitivity to outliers in data (Ishak et al., 2010).

Hossain and Rahman (2019) documented list of researches around the globe to investigate the presence of trend in hydrological time series data. Ishak et al. (2010), in their trend analysis study of 491 stream gauging stations across Australia, found that AMF data around 30% gauging stations showed trends. Rahman et al. (2012) concluded in their study that further investigation was necessary before any decisive conclusion could be made on possibility of trends in Australian flood data and whether the reason of these trends was the effect of the climate change or the climate variability.

Result of investigation on the presence of trends in AMF data series from 491 stations across Australia showed that numbers of stations with downward trends (21-33%) were substantially more compared to the numbers of stations with upward trends (1-6%) (Ishak et al., 2013).

Hajani and Rahman (2017) found mixed trends in annual rainfall data in their analysis of trends with 60 rainfall gauging stations across NSW. A trend analysis on annual rainfall data across Yarra River catchment showed decreasing trends (Hossain and Rahman, 2019; Barua et al., 2013). Trends have been found in Australian rainfall data series by many other researchers (Hossain and Rahman, 2019; Laz et al., 2014). Across Iran, Javari (2016) found seasonal variation in rainfall series.

Roughly speaking, a random process that does not change over time or that has statistical measures which remain constant over time is considered stationary. Presence of significant trends in time series records is the first step in non-stationarity FFA. Several parametric and nonparametric tests are available to identify trends in flood data series. In this study, twelve statistical tests i.e. MK nonparametric test, SR nonparametric test, Linear Regression parametric test, and Cumulative Deviation test, Cusum test, Rank Sum, test, Rank Difference, Worsley Likelihood, Autocorrelation, Student's t, Turning Point and Median Crossing test, are adopted to assess trends. These nonparametric methods have an advantage is that these tests are less sensitive to data gaps which may exist in AMF data series. World Meteorological Organization recommends SR and MK tests for identifying trends in the hydrological data (Chebana et al., 2013).

2.10 Climate Change and Flood Frequency Analysis

The Fourth Assessment Report of Intergovernmental Panel for Climate Change (IPCC) found that average surface air temperature is rising globally (IPCC, 2007). The expectation that these predicted temperature changes will cause the hydrological cycle to intensify at the global and regional levels is widely recognised (Huntington, 2006). The possibility that climate change will trigger increase in the average global temperature alongside global population growth has also been confirmed by many other studies, as the magnitude and timing of flood events can be changed. These changes can alter earth’s hydrometeorological systems and influence on the rainfall runoff process, and impact on the risk of flooding around the world (O’Brien and Burn, 2014).

It is reported that in near future, climate change will influence the magnitude and frequency of floods across Australia and as the rainfall runoff relationship will be affected by the future

climate change, assumption of stationary in hydrological data may not be valid (Hossain et al., 2017). Consequently, regional flood estimations, which use past flood data series, will not be representative for the future flood. Failing to take into consideration of climate change can raise question on the concept of AEP, leading to error and bias in DF estimation, which will bring large consequences on planning, design and operation of hydraulic infrastructures (Rahman et al., 2010).

In adopting most of the existing FFA methods, assumption of independence and stationarity is needed. In the context of global warming, water vapor in the atmosphere will increase; causing more intense and frequent heavy rainfall events (Kunkel, 2003). If the evidences of trends are found in hydrological data, then the IID assumption will not be valid on that data series and DFs estimated using current FFA method will be underestimated or over estimated. The PD and its parameters for non-stationary time series data change over time. In such situation alternate FFA method that use time-dependent distributional parameters (location, scale and shape) should be adopted for DF estimation, which is named as non-stationary FFA.

Several studies have been carried out to address non-stationarity in hydrological data series. For example, a second-order non-stationary techniques to pooled FFA was introduced by Cunderlik and Burn (2003) assuming non-stationarity in mean and variance where non-stationary pooled quantile function was a combination of regional time-dependent and local time-dependent component of scale and location parameters (Khaliq et al., 2006). To identify and assess local significance and to estimate changes in time-dependent components the author used trend analysis tools. A regional trend analysis was then carried out to assess changes at regional scale. The application of the model to a homogeneous catchment showed that quantile estimation for 20-year ARI could be heavily biased even if very insignificant non-stationarity in data series is ignored (Cunderlik and Burn, 2003).

To assess the suitability of non-stationary FFA to DF estimation and to examine the possible changes during extreme floods, Hounkpe et al. (2015) used an extreme-value non-stationary probabilistic model in the Oueme River Basin. Their study showed that use of non-stationarity in extreme FFA by connecting climate variables or time with the distributional parameters is necessary to produce better estimates.

Debele et al. (2017) evaluated GAMLSS, maximum likelihood (ML) and two-stage weighted least squares (WLS/TS) nonstationary FFA techniques using recorded seasonal maximum flow data to investigate the influence of nonstationarity on estimation of time-dependent parameters and flow quantile and found that GAMLSS produced the best results to estimate trends in standard deviation and WLS/TS provides better accuracy in estimating trends in time series data at mean value.

2.11 Summary

Globally, more people are affected by floods each year than any other natural disaster. Flood in Australia during 2010-2019 caused loss of many human lives, huge damage worth billions of Australian dollars and brought sufferings and hardship to millions of urban and rural Australians. As floods are a natural part of the hydrological cycle, they cannot be prevented through human intervention. However, losses can be minimised by reducing flood risk. In order to carry out flood risk analysis, it is required to estimate DF discharges for various AEPs. Several methods exist for estimation of design floods; among these, at-site FFA is the simplest and most direct. FFA serves as a standard for the accuracy of other DF estimation methods, including rainfall runoff based flood estimation and regional flood estimation methods.

FFA method uses flood time series data to fit probability distributions and establish relationship between flood magnitude and their AEPs. A relatively long-period of observed flood data is required for at-site FFA. Lengths of data period in most of flow gauging stations are much shorter than ARIs being investigated. For this reason, DF estimation often necessitates extrapolation beyond the limit of observed flood data.

In FFA, it is assumed that hydrologic data series are IID. It is also assumed that hydrologic system is space and time-independent and is stochastic (Pandey et al., 2018). In order to satisfy these assumptions, the streamflow data must be appropriately chosen. Selecting observations from the same population satisfies the assumption of identical distribution or homogeneity (i.e., no changes in the watershed and recording gauges are made). Selecting annual maximum value of flow data generally satisfies the assumption of independence, as the successive yearly observations are likely to be independent. However, recent evidences of

the effects of ongoing forms of regional climate variability, alongside intensified human activity, have prompted hydrologists to study flood regimes outside of the hypothesis of stationarity.

Some countries generally adopt a uniform PD to model floods (e.g. LP3 in in USA). The ARR 2019 guidelines in Australia do not recommend any specific distribution. However, selection of single probability model for all gauging stations in a country is not driven by specific theoretical considerations. Different statistical GoF tests can be adopted to select the most suitable probability model.

There are many studies available for at-site FFA, which have adopted many PDs. Attempts have been made to obtain best-fit PD model for a country or for a region. It is observed that a single PD model may not be suitable as the most appropriate PD model for a region or for the whole country. The PD that best fits the data at a given location should be adopted for flood quantile estimates at the location; however, its suitability at other locations in the region cannot be guaranteed.

As concerns regarding the effects of climate change escalate, various statistical and stochastic methods have been proposed by researchers to identify existence of trends and shifts in hydrological data. The existence of trends in data series can profoundly impact the results of FFA and compromise the practicality of the idea of AEP used in designing hydraulic structures. If trends exist, flood estimation procedures must account for varying flood regimes, e.g., assume that the parameters of the PD model are time dependent. Therefore, trend analysis should be carried out for hydrological time series data. One of the simplest techniques of detecting changes in hydrological time series is to examine this time-series data for presence of trends using different statistical tests. Two tests commonly used to this end are the SR tests and MK tests.

A number of literatures are available on FFA for Queensland (Weeks, 1991; Rahman et al., 2008; Palmen and Weeks, 2011; McMahon and Kiem, 2018; Ayre et al., 2015; Frisby et al., 2018). However, literatures on FFA for Brisbane River catchment in Queensland are limited. Previous FFA studies for Australia are found more for Victoria and for New South Wales as compared to that of Queensland. Since Queensland has different climate regime, the PD recommended for FFA in other Australian states may not be applicable to Brisbane River

catchment in Queensland. Hence, this study focuses on FFA using data from Brisbane River catchment, situated in Queensland.

The next chapter discusses the study catchment and details of collation and preparation of streamflow data for this study.

CHAPTER 3 : SELECTION OF STUDY AREA AND PREPARATION OF STREAM FLOW DATA

3.1 General

Streamflow data plays a vital role in FFA. The collection of streamflow data from different gauging stations of the selected catchment and preparation of the data for FFA is very crucial in any FFA study. This chapter covers different aspects of peak flow data collation for FFA. These include selection of the study area (which is the Brisbane River catchment in Queensland), selection of stream gauging stations, checking quality of peak flow data series, filling gaps in the data, checking for any outliers in the data, and testing selected AMF data series for any significant trends.

3.2 Selection of Study Catchments

The following factors are considered in selecting the study catchments for this study.

3.2.1 Catchment Area

The flood frequency behaviour of a catchment may vary with catchment size. The behaviour of flood and their frequencies of occurrence in large catchments is found notably different than that of smaller catchments (Haddad, 2013). ARR 2019 Book 3 (Ball et al., 2019) recommended to select small to medium sized stream gauging catchments with a maximum catchment area of 1 000 km^2 for RFFA; however, for at-site FFA, there is no such limit.

In the present study, the Brisbane River catchment in Queensland has been selected as the study area since it is one of the most flood affected areas in Australia.

The Brisbane River catchment is situated in the southeast corner of Queensland. It extends from Great Dividing Range at upstream up to Moreton Bay at downstream. The catchment area, including the Brisbane River and its tributaries, the Lockyer Creek and the Bremer River is 13,570 km^2 of which major percentage of area is rural (van den Honert and

McAneney, 2011). Its climate is sub-tropical, with average annual rainfall being 1500 mm (Weber, 2018), mostly as a result of intense summer storms.

The Brisbane River catchment has different types of land uses. The upstream part of the catchment is mainly rural and downstream is urban. Majority of catchment is rural with forest and grazing land. Urban area of catchment has number of towns including Brisbane city, Toogoolawah, Ipswich, Crows Nest, Rosewood, Forest Hill, Blackbutt, Laidley, Gatton and Woodford. Brisbane city is the largest town and is situated on the Brisbane River floodplain. Brisbane city has population more than two million and it is experiencing a fast population growth.

The Brisbane River catchment drains to Moreton Bay. The economy of the region and the lifestyle of its population revolve greatly around the Bay. Brisbane is the only major city in the world within sight of which 700-900 dugong graze on seagrasses. Internationally acknowledged sites for migratory birds are also found on the Bay (Weber, 2018).

The Brisbane River catchment has number of sub-catchments including Stanly River catchment, Upper Brisbane River sub-catchment, Lockyer Creek sub-catchment, Bremer River sub-catchment, Purge Creek sub-catchment, Warril Creek sub-catchment and Lower Brisbane River sub-catchment. Among these, the Upper Brisbane River sub-catchment is the largest sub-catchment with an area of 5,645 km^2. One of the major waterway related problems in this catchment is flooding, as 80 km of the river's lower ranges are prone to flooding, and since 1840 Brisbane experienced 11 major floods. The study area along with the seven main Brisbane River sub-catchments is shown in Figure 3.1. Table 3.1 shows the area of these sub-catchments.

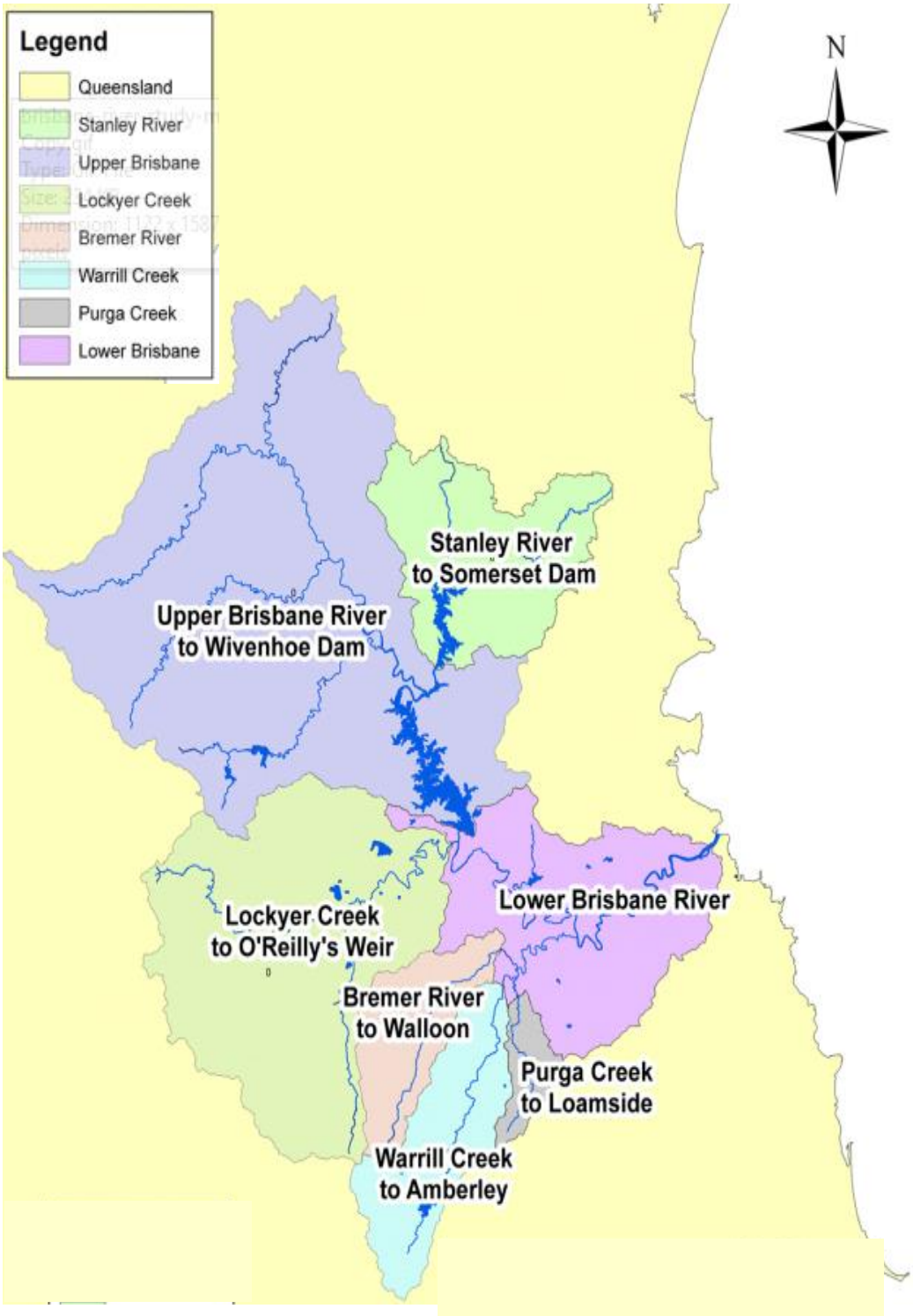

Figure 3.1: Brisbane River catchment (study area) (Jordan et al., 2014; Seqwater, 2013)

Table 3.1: Area of elected catchments

Catchment	Area (km^2)
Stanley River to Somerset Dam	1,324
Upper Brisbane river to Wivenhoe Dam	5,645
Lockyer Creek to O'Reilly's Weir	2,964
Bremer River to Walloon	634
Warrill Creek to Amberley	902
Purga Creek to Loamside	209
Lower Brisbane River	1,855

The Brisbane River has a long history of flooding. The 1974 and 2011 flood events of this River system caused extensive damage (Hossain, 2019). The main tributaries of the upper Brisbane River are Emu Creek, Cressbrook and Cooyar Creek, and have headwaters in the Great Dividing Range. The Cooyar Creek is the most northerly of the upper Brisbane River tributaries and tends to have the lowest annual rainfalls recorded within the catchment. The Stanley River is the major tributary of the Brisbane River that flows westwards. Warrill Creek is main tributary of the Bremer River. The lower reaches of the Bremer River flow through the City of Ipswich. With a total area of 2 600 km^2, Lockyer Creek is the largest tributary of the Brisbane River. Figure 3.2 shows major rivers/creeks within Brisbane River catchment.

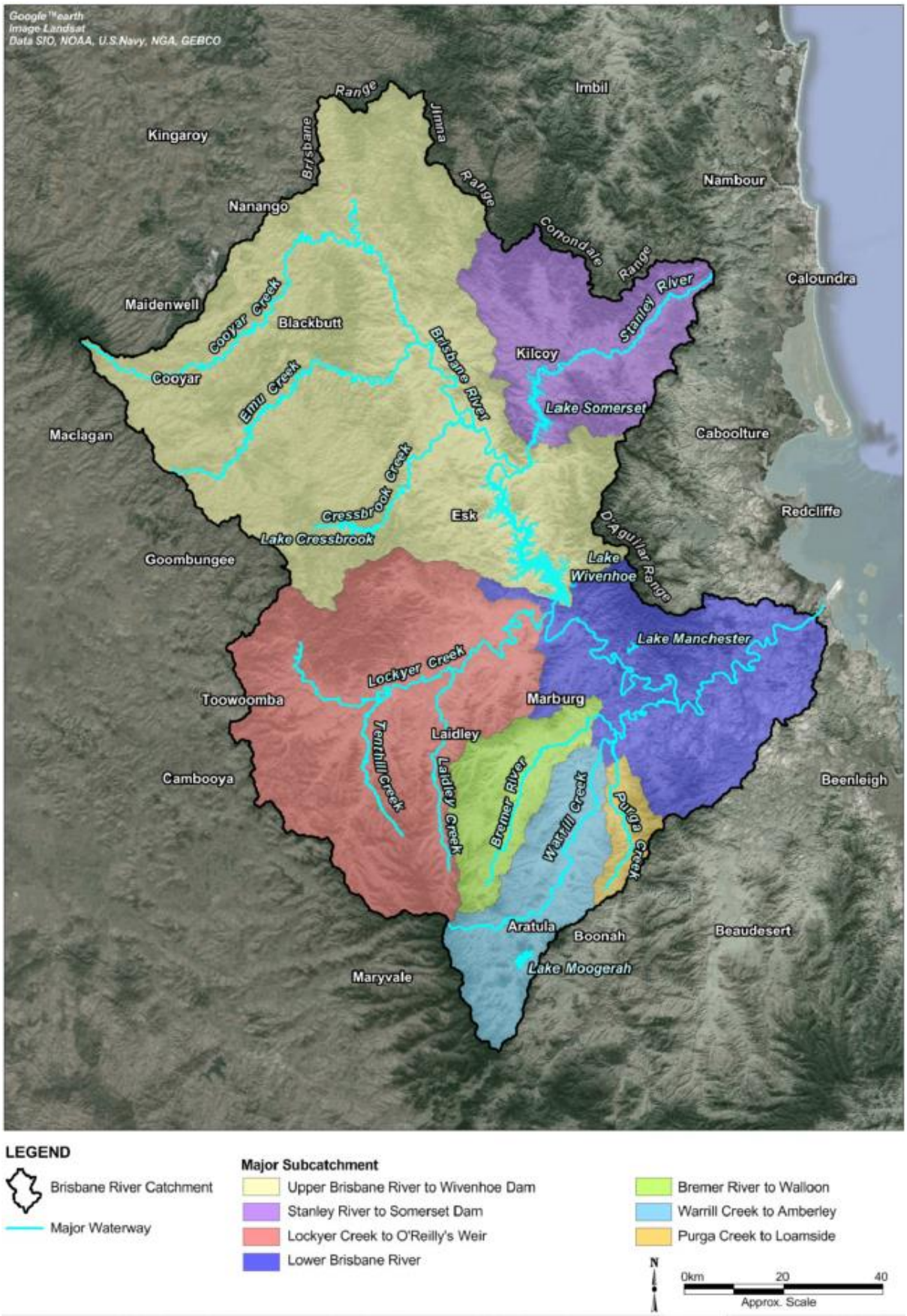

Figure 3.2: Brisbane River catchment and its major river system (SoQ, 2017**;** QLD Gov., 2017**)**

The stream gauging network used in the study is shown in Figure 3.3 and detailed in Table 3.2. Some stream gauges have historical records extending over a period of more than ninety years. The majority of gauge records cover the post-1960 period. All gauges with 2011 flow data and a record length of at least 20 years are considered in this study. Latest continuous gauge recordings are collected from the Department of Natural Resources and Mines (DNRM) website that includes daily maximum flow and annual maximum flow time series.

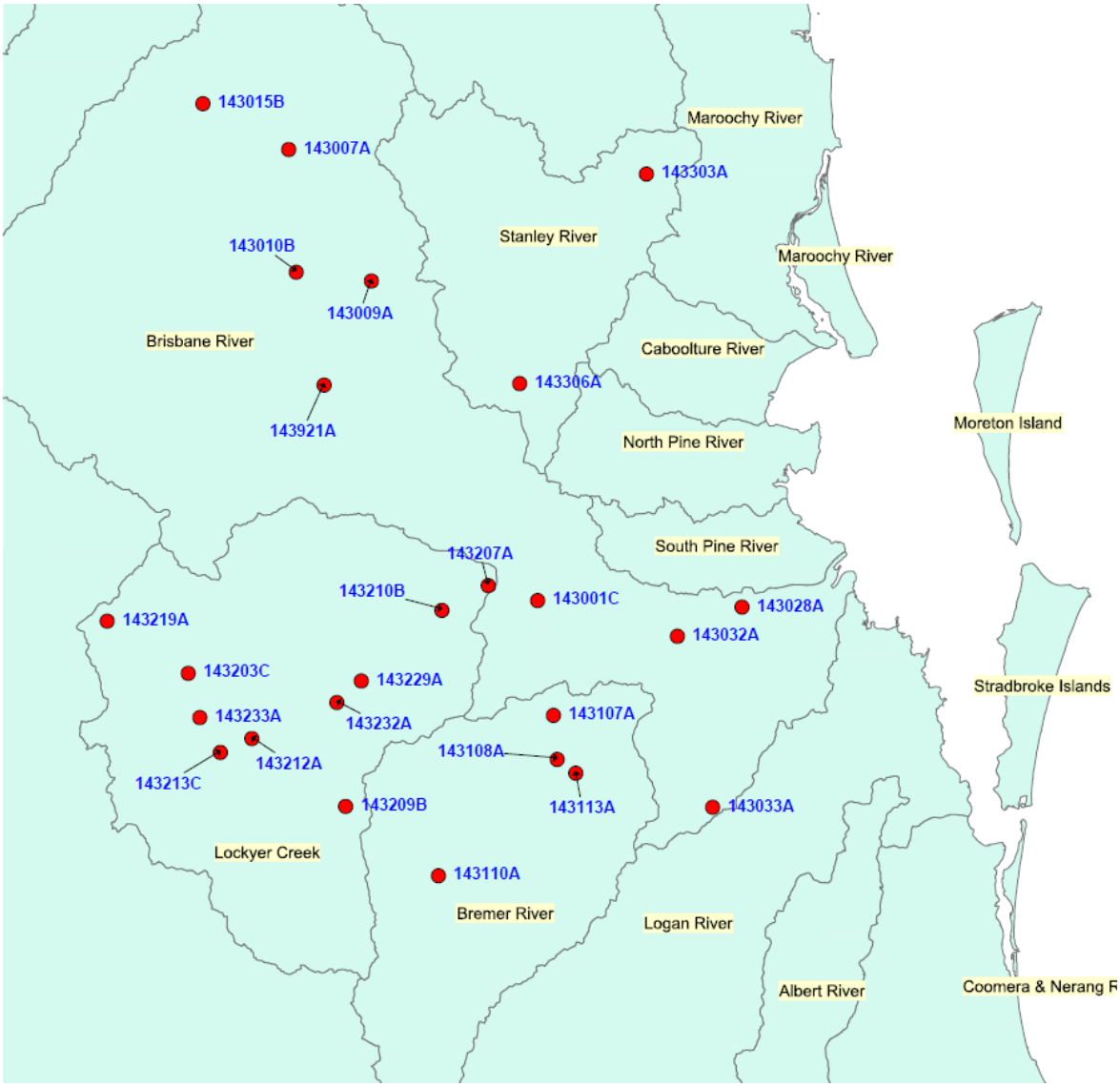

Figure 3.3: Selected stream gauging locations

Table 3.2: Selected catchments with annual maximum flood record lengths

Station ID	Description	Record Length (Year)
143001C	Brisbane River at Savages Crossing	60
143007A	Brisbane River at Linville	54
143009A	Brisbane River at Gregors Creek	56
143010B	Emu Creek at Boat Mountain	51
143015B	Cooyar Creek at Taromeo Creek	49
143028A	Ithaca Creek at Jason Street	46
143032A	Moggill Creek at Upper Brookfield	42
143033A	Oxley Creek at New Beith	42
143107A	Bremer River at Walloon	57
143108A	Warrill Creek at Amberley	57
143110A	Bremer River at Adams Bridge	54
143113A	Purga Creek at Loamside	45
143203C	Lockyer Creek at Helidon Number 3	91
143207A	Lockyer Creek at O'Reillys Weir	67
143209B	Laidley Creek at Mulgowie	50
143210B	Lockyer Creek at Rifle Range Road	30
143212A	Tenthill Creek at Tenthill	50
143213C	Ma Ma Creek at Harms	23
143219A	Murphys Creek at Spring Bluff	39
143229A	Laidley Creek at Warrego Highway	28
143232A	Sandy Creek at Forest Hill	20
143233A	Flagstone Creek at Brown-Zirbels Road	23
143303A	Stanley R at Peachester	87
143306A	Reedy Creek at Upstream Byron Creek Junction	37
143921A	Cressbrook Creek at Rosentretters Crossing	30
143307A	Byron Creek at Causeway	36

3.2.2 Record Length

In at-site FFA, for the underlying probability distribution to have acceptable fit, the streamflow gauging data record length should be relatively long (Haddad, 2008). Design flow estimation in FFA using streamflow data with long record length has less uncertainties and standard errors compared to that of with shorter length (Griffis and Stedinger, 2007). Streamflow record length at many gauging stations is in fact not long enough for FFA. To compensate for this, number of gauging stations are selected in this study by compromising between the available number of stream gauging sites (to capture better spatial information) and relatively longer record length (to enhance accuracy of at-site FFA). It is not feasible to select only stations those have long record length, as this criterion reduces the number of stations greatly. For this study, all the stations within the Brisbane River catchment with a minimum record length of 20 years of AMF data are chosen initially. All the selected gauges have record of 2011 severe flood event. Altogether 26 stations are selected. The range of the AMF series record lengths for the chosen 26 stations is 20 to 91 years and mean of record length is 47 years. The flood record of the stations shows that 2011 flood event is the highest peak of most of the stations during the recorded data period (Hossain, 2019). Figure 3.4 shows that AMF in year 2011 is the highest, followed by year 1974 for stations 143001C and AMF of other years are much less compared to the 2011 AMF.

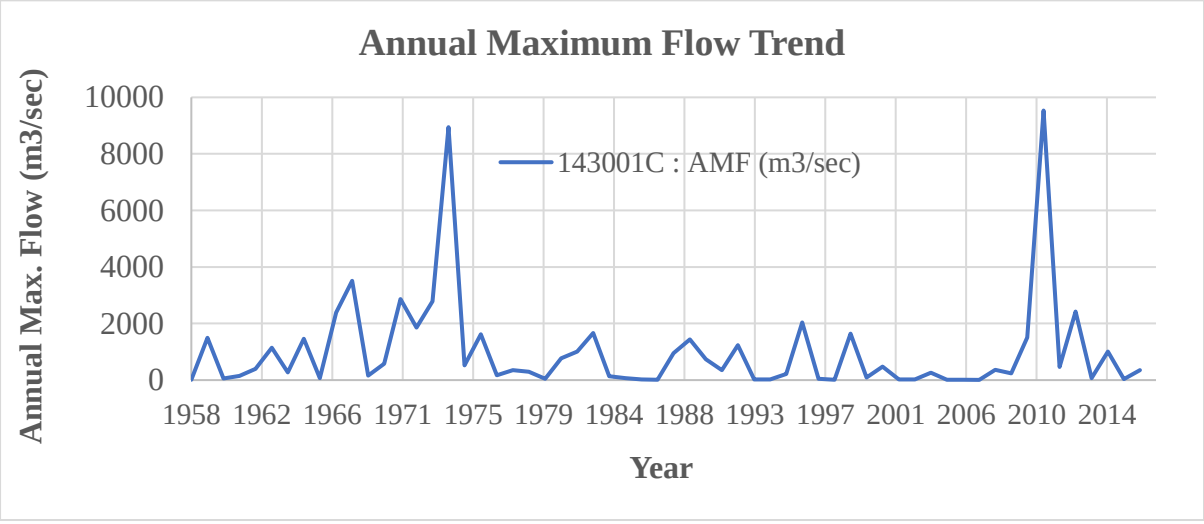

Figure 3.4: Annual Maximum Flow at station 143001C

3.2.3 Regulation

Ideally, the selected gauging stations for FFA should not have any major flow control or regulation, as major flow regulation may change flow storage upstream of gauging stations. The presence of major flow regulation in the stream may influence the rainfall runoff relationship greatly. Consequently, the assumption of independence of measured flow at gauging stations may be violated. However, gauging stations with minor flow regulation including small dams for farm irrigation in their watercourses, can be chosen as this type of flow regulation is unlikely to have any significant impacts on higher flows at a station.

3.2.4 Quality of Data

In any FFA, the quality of AMF data plays a significant role in determining the accuracy of estimated flood quantiles. AMF series needs to be checked to ensure they are appropriate for FFA. This involves filling in missing data, detection of trends and shifts in data (Salas, 1993). All AMF data should be quality-checked before commencing FFA.

The FFA assumes that the AMF events are independent. Therefore, it is important to check whether the successive AMF events are independent or not. This is done by checking the date of occurrence of successive AMF events using guideline form ARR 2019 Book 3, section 2.3.3 (Ball et al., 2019). If the date of occurrence of an AMF event at the end of a year is close to the date of occurrence of next AMF event at the beginning of next year then only one of these two is selected.

Most FFA assumes that the selected data are free from any error. Usually streamflow gauging authority audits quality of recorded data and assigns quality code at every station. If any station's data is marked as 'poor quality' or any other comments related to poor data quality, then that station's data need to be checked properly before selecting for FFA. After detail assessment, if the data are considered to be of low quality then that station is excluded from present FFA study.

3.3 Filling Missing Records

Flood events may damage streamflow measurement stations. Sometimes data recording device may have mechanical or electrical failure during storm events. For these or for other reasons, it is usual that some gauging stations may have missing records in streamflow data series. One of the preliminary steps when preparing data for FFA is dealing with this issue. Although streamflow time series records for FFA are assumed to be independent events, however missing records can cause loss of significant information in data series and can bring unreliability in data series and ultimately increase uncertainties in FFA. Filling up gaps in AMF series appropriately provides more accurate information of AMF data series at a given site. Filling missing records is one of the elementary steps in any FFA. Infilling of missing flow data can be accomplished through a range of techniques. This includes different interpolations techniques or some types of statistical analysis. The types of appropriate method to be used for filling record in streamflow time series data depend on many factors including season of missing data period, length of missing data period, regional climate condition of the catchment, characteristics of available data and availability of data in nearby stations (Gyau-Boakye and Schultz, 1994).

If nearby other stations have data during the missing period of concerned station, the missing data can be filled up using weighted average approach (Wallis et al., 1991; Hirsch, 1979).
One of the weighted average approach is to find the ratio of average flow of neighbouring stations and average flow of stations having missing records or to use the ratio of drainage area of neighbouring station and the stations having the missing record (Tencaliec et al., 2015).

Woodhouse et al. (2006) and Rahman et al. (1997) recommended regression analysis to reconstruct missing data. The study on filling missing time series data records found that usage of simple models like regression is sufficient (Gyau-Boakye and Schultz, 1994). One of the commonly adopted methods of filling missing records is by correlating available records of common period between a neighbouring station and the target gauging station through linear regression method. Relatively more complex method is correlating available records of common period among number of neighbouring gauging stations and the target station through multiple regression techniques. These methods can be utilised to fill a few missing records, which increases the number of data records for a station having missing

records and can provide better estimates of means and variances (Stedinger et al., 1993). In this study, a correlation is established between available records covering a common period of one or more neighbouring stations to estimate the missing data points.

3.4 Checking for Outliers in the Data

Outliers may be present in any AMF data series. An outlier is an observation/record in a data series that deviates considerably from the majority of the data in the series. There are several reasons of presence of outliers in time series data. These may include error in recording data due to malfunction or damage of recording instruments, error in calibration or installation of recording equipment, or error in data collection process. Outliers in data series cause problems to fit probability distribution model to that data series (Haddad, 2008). Identification of low outlier and their treatment are important issues in FFA, as the estimate of extreme flood quantiles can be heavily affected by such observations. Outliers can be low outliers or high outliers. Therefore, it is very important to identify and treat low outliers in hydrological time series data before using for FFA (Lamontagne et al., 2013). Identifying potentially influential low flows (PILFs)/outliers becomes a large concern when the flow data series is used to fit the probability model in FFA (Rahman et al., 2014b). In the analysis, if a data point is detected as a possible outlier, it should be checked whether there is an error with the data.

There are no specific criteria to detect and treat outliers in flow data series (Jackson, 1981). Most of the methods available for detecting and treating outliers are statistical and they require hydrological and mathematical judgement for sensible application (Haddad, 2008). Various methods are used in past to detect and treat outliers in AMF flood data series. The potentially influential low flows (PILFs) in data series can be detected by Grubbs-Beck test with one sided 10% significance level (Grubbs and Beck, 1972). A sequential two-sided outlier test formulated from generalisation of Grubbs (1969) test for outliers was proposed by Rosner (1975, 1983). ARR 1987 (I. E. Aust., 1987) suggests a method that requires an adjustment for skew. The FFA method in Bulletin 17B (USDIGS, 1981; IACWD, 1982) is widely used as well. Rao and Hamed (2000) suggest using the G-B (Grubbs and Becks, 1972) method to detect outliers.

If $\bar{x}$ is mean and s is SD of the natural logarithms of AMF data then x_H and x_L are calculated as follows (Haddad, 2008):

$$x_H = e^{(\bar{x} + k_N S)} \quad (3.1)$$

$$x_L = e^{(\bar{x} - k_N S)} \quad (3.2)$$

Where, k_N is the G-B test statistic, its value depends on sample size and significance levels used. If observed sample data magnitude is higher than x_H then it is considered high outliers, and if it is lower than x_L then it is considered low outliers (Haddad, 2008).

The multiple Grubbs-Beck (MGB) test was recommended in the updated version of Bulletin 17B, also known as "Bulletin 17C" (Rahman et al., 2014b). The basic relationships required to develop an acceptable MGB test are provided by Cohn et al. (2013).

FLIKE software has implemented the MGB test to detect outliers in AMF data series. This MGB test in FLIKE software has been used in this study for identification of outliers.

The outlier detection results are stated below:

- The maximum percentage of low outliers found in the AMF data at a single station is 41%.
- Maximum low outliers were detected during dry years, especially years with severe drought. During droughts, the maximum flows occurring in many rivers are actually base flow, which in unrelated to flood event. Rahman et al. (1997) found similar results.

The identified outliers in AMF data are marked as censored flows in FFA in FLIKE.

In summary, the AMF data of the 35 stations were collected; these data were checked for data quality, gaps were filled, outlier points were censored, and trends and shifts in the AMF data series were tested. Finally, twenty-six (26) stream gauge stations are selected for this study where each station has at least 20 years of AMF data.

3.5 Trend in Annual Maximum Flood (AMF) Data

The presence of significant positive or negative trends in the observed AMF data makes the data non-stationary.

AMF data for FFA is generally assumed to be stationary, consistent and homogeneous i.e. records follow IID assumption. AMF data should be screened by testing for decreasing or increasing trends, and for presence of a shift series. The method of trend analysis adopted in this study is discussed in Chapter 4.

3.8 Chapter Summary

The Brisbane River catchment is selected for this study. The AMF data as well as daily maximum flow data from the stream gauging stations within this catchment are obtained from the DNRM website. The gaps in the data are filled and outliers are identified. Stations with poor data quality are excluded. Altogether 26 stations are finally identified to use for FFA in this study.

The next chapter discusses the methodology adopted in this study.

CHAPTER 4 : METHODS ADOPTED IN THIS STUDY

4.1 General

Methodology used in this study is discussed in this chapter. Most AMF data series generally show skewness. Therefore, many skewed distributions are used in FFA. A suit of statistical approaches is adopted in this study. It is also possible to transform the skewed data so that the skew was approximately zero. This approach has been explored by Kuczera (1983); however, this approach is not adopted in this study.

4.2 Methodology

The initial step involved collection and review of available flow data from all the sources as presented in Chapter 3. According to Department of State Development, Infrastructure and Planning/Department of Natural Resources and Mines, Queensland (DSDIP/DNRM, 2015), for FFA, gauge data should meet following conditions:

- Each gauging site should have reasonable long period of continuous record. The minimum record length for each gauging site considered in this study is 20 years.
- The recorded data should be homogeneous i.e. data should reliably indicate all floods within the period of record.
- The flood flow estimates method (rating curve or other method) should be reliable.

To identify the best-fit PD for the Brisbane River catchment, AMF data series is used instead of POT series.

Following steps are considered in the methodology:

a. selection of candidate PDs;
b. selection of suitable parameter estimation methods;
c. use of statistical hypothesis test to assess goodness-of-fit (GoF) of the hypothesised PDs to the AMF data at a selected site;

d. evaluation of the selected probability distributions with respect to right tail behavior

e. graphical analysis i.e. visual plots of selected PD and AMF data series. The flowchart in Figure 4.1 depicts the main procedure carried out for at-site FFA and evaluating flood quantiles.

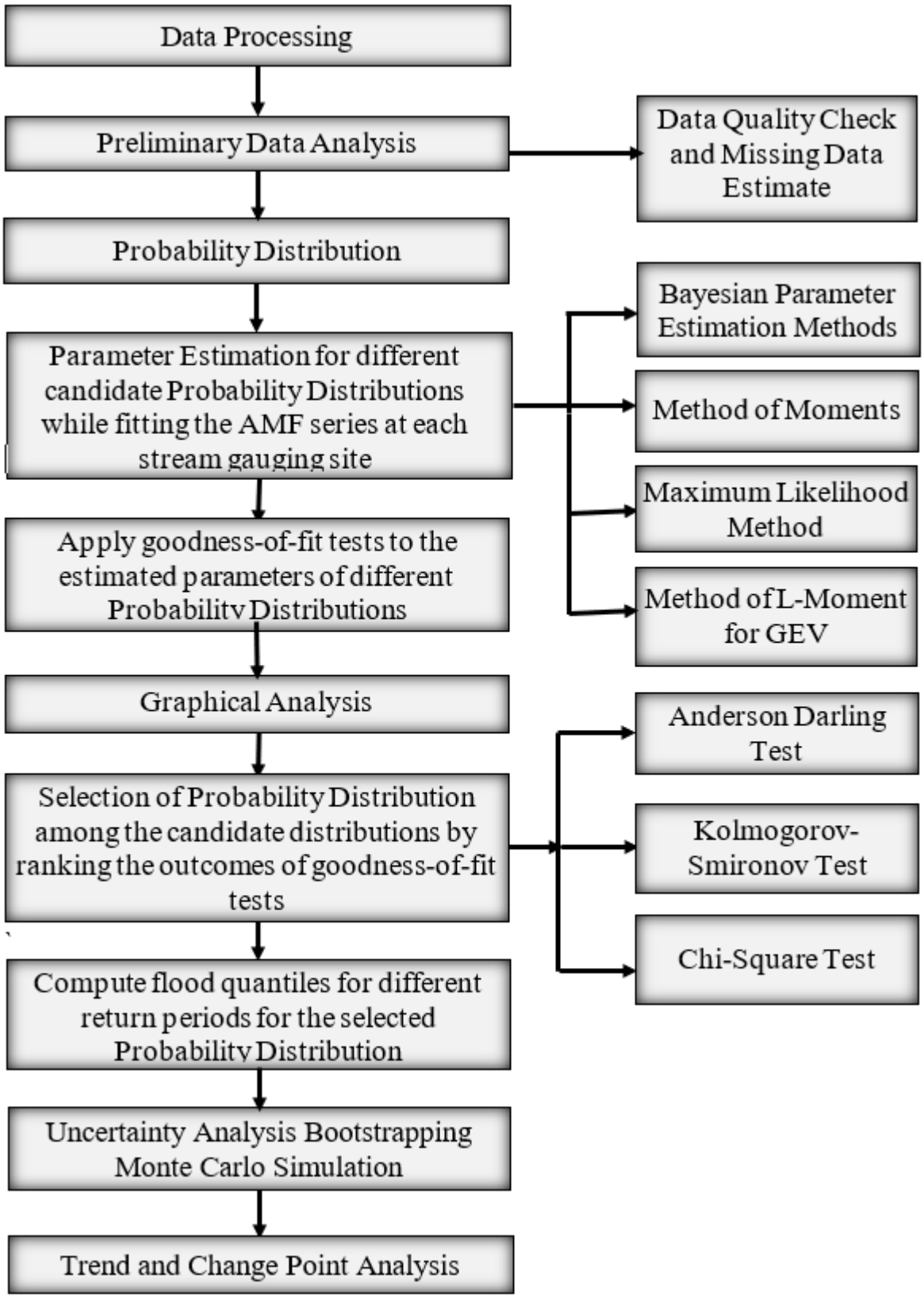

Figure 4.1: Flood frequency analysis (FFA) method adopted in this study.

The techniques for evaluating the suitability of distributions can be divided into two groups (Cunnane, 1989): (a) tests of descriptive ability, which seeks from some known PDs one which fits the observed data, judged best from graphical analysis, GoF (GoF) tests, and tests based on skewness, and (b) tests of predictive ability, which examines the statistical behaviour of candidate distributions, especially the sampling distribution of coefficient of variation and skewness, and standardised largest sample values, to determine their capability to generate random samples with same statistical characteristics as the AMF data series, and this is done by methods such as split sample and robustness tests (Haddad and Rahman, 2008).

To assess the suitability of selected distributions, three different statistical GoF tests are applied in this study to assess how good the AMF data fit to a given distribution and then compared with the graphical method.

In the graphical method, distribution graphs with result from GoF tests help to identify best fit PD. The graphical approach is subjective and depends on user. This approach uses various graphs to visualise data and decide the best fitting model. On the other hand, the GoF tests are outcome of statistical calculation and the results are independent of the user (assuming the tests are carried out correctly).

All commonly available GoF tests tell mathematically whether a particular PD fits well for a given data set or not. The results of these tests differ depending on the formulation and how they are performed. Different GoF test results sometimes differ among themselves. For example, the Anderson-Darling GoF test find that the LP3 distribution can be the best-fit for a particular AMF series, but the Kolmogorov-Smirnov test may show that LP3 is the second best-fit for the same data series. In such a situation, visual inspection of graphs may help to decide on the best-fit PD.

This study used FLIKE and EasyFit, two well-known statistical software for FFA (Kuczera and Franks, 2016). The FLIKE software was developed by Professor George Kuczera, University of Newcastle and has been recommended in the ARR 2019 guidelines. FLIKE has the advantage of using automated Bayesian fitting techniques. In Bayesian techniques, properties of population or PD are obtained from sample data using Bayes' theorem. The mathematical formulations of the Bayesian procedure are available in Kuczera (1999).

Bayesian statistics use prior information for model parameters with a PD and then update this prior information with current recorded data to obtain posterior PD. Bayesian approach of PD is more useful when observed data length is smaller.

FLIKE supports five commonly adopted PDs, i.e. LP3, LN, Gumbel, GP, GEV and a number of parameter estimation methods. FLIKE has the capability to incorporate prior or regional information and to address uncertainty in stage-discharge and to evaluate parameter uncertainty found from regional information (Rahman et al., 2014a). This software also has the option to select threshold values for censoring. However, FLIKE does not have any GoF test. In this study updated version of FLIKE (2017) is used. Identification of PILFs was done manually using GB test in the older version of FLIKE. The new version of FLIKE has built in MGB test that can recognise multiple PILFs in the AMF series (Rahman et al., 2014a).

EasyFit is statistical data analysis and simulation tools that enable fitting and simulation of statistical PDs with sample data, choosing of the most appropriate PD, and use of the obtained result of the analysis to make a better decision. The EasyFit has number of parameter estimation methods such as MLE for LN, MoM for Gumbel and LP3 distribution and for GP and GEV distributions Method of L-moments is used for estimation of the distributional parameters. EasyFit has three GoF tests which help to select the best-fit distribution at a given station.

A number of FFA studies have been completed using EasyFit software. For example, Singo et al. (2012), Atroosh and Moustafa (2012), Kamal et al. (2017), and Sarauskiene and Kriauciuniene (2011). Singo et al. (2012) applied this software for FFA in South Africa. Kamal et al. (2017) used this software for FFA of the Ganga River at Haridwar and Garhmukteshwar in India.

It should be noted that FLIKE does not have any GoF test. Hence, the alternative software EasyFit, which has three GoF tests, has been adopted in this study to assist in selecting the appropriate PD for a given catchment.

4.3 Probability Distributions Used in This Study

In this study; based on a broad literature survey, five candidate PDs are selected i.e., LN, Gumbel, LP3, GEV and GP. Details of these statistical distributions are available in EasyFit and FLIKE Manual (Drokin, 2018; Mathwave, 2017; FLIKE, 2017). Both FLIKE and EasyFit software are used in this study. Both the software includes the selected five PDs.

The probability density functions (PDF) for the selected PDs are described below (FLIKE, 2017).

4.3.1 Lognormal (LN) Distribution

The LN PD assumes that the logarithm of random sample is normally distributed. Since the logarithm of any variable exists only when the variable itself is a real positive number, therefore, to apply LN distribution, the quantity of interest must be real positive value. It is a special case of the LP3 model as described below.

This distribution is generally well-behaved for a wide range of flood data. FLIKE software uses MoM for estimation of most probable parameter to the selected AMF data for this distribution. EasyFit software uses the MLE for parameter estimation of the LN PD.

LN probability model has the PDF:

$$f(\log_e x \,|\mu, \sigma) = \frac{1}{\sigma\sqrt{2\pi}} \exp\left(-\frac{(\log_e x-\mu)^2}{2\sigma^2}\right), -\infty < \log_e x < \infty \quad (4.1)$$

where x is the random variable (AMF in this study), μ and σ represents location and scale parameters respectively (FLIKE, 2017).

The first three moments i.e. mean, variance and skewness of $\log_e$ x are given by (FLIKE, 2017):

$$\text{Mean } (\log_e x) = \mu \quad (4.2)$$

Variance ($\log_e x$) = σ^2 (4.3)

Skew ($\log_e x$) = 0 (4.4)

Skew of LN distribution is zero. When skew become non-zero then it becomes LP3 distribution. Detail explanation of LN distribution is available in FLIKE manual (FLIKE, 2017).

4.3.2 Log Pearson Type III (LP3) Distribution

LP3 is widely used PD for FFA. In many studies around the world it was found that this distribution fits observed flood data relatively better than many other distributions. If the skew of the logarithm of variable ($\log_e x$) become zero, the distribution becomes LN distribution. LP3 is a three-parameter distribution, i.e. location (μ), scale (σ) and shape (γ). EasyFit software uses the MoM for parameter estimation of LP3 distribution.

The PDF of LP3 distribution is given by (FLIKE, 2017):

$$f(\log_e x\,|\alpha,\beta,\tau) = \frac{|\beta|}{\tau(\alpha)}[\beta(\log_e x - \tau)]^{x-1}\exp[-\beta(\log_e x - \tau)]$$

$$\text{for } \beta > 0, x > \tau;\ \beta < 0, x < \tau \quad (4.5)$$

Where, x is random variable and $\Gamma(\alpha)$ is the gamma function.

The mean, variance and skewness moments of $\log_e x$ are estimated as (FLIKE, 2017):

First moment, Mean ($\log_e x$) = $\tau + \frac{\alpha}{\beta}$ (4.6)

Second moment, Variance ($\log_e x$) = $\frac{\alpha}{\beta^2}$ (4.7)

$$\text{Third moment, Skew } (\log_e x) = \begin{cases} \frac{2}{\sqrt{\alpha}}, & \text{if } \beta > 0 \\ -\frac{2}{\sqrt{\alpha}}, & \text{if } \beta < 0 \end{cases} \quad (4.8)$$

Further explanation on LP3 distribution can be found in FLIKE manual (FLIKE, 2017).

4.3.3 Gumbel Distribution

The Gumbel PD is two-parameter extreme value type I (EV1) distribution. This distribution can have two forms i.e. highest or maximum extremes and smallest or minimum extremes. For FFA, Gumbel maximum is used. The location and scale parameters of this distribution are the mean and the standard deviation respectively. The Gumbel PD is a special type of GEV distribution. The Gumbel distribution has fixed shape, skewed to the left. EasyFit software uses MoM for estimation of its location and scale parameters. The PDF and CDF of Gumbel probability model are (FLIKE, 2017):

$$\text{PDF: } f(x|\tau,\alpha) = \frac{1}{\alpha}\exp\left[-\frac{(x-\tau)}{\alpha}\right]\ \exp\left\{-\exp\left[-\frac{(x-\tau)}{\alpha}\right]\right\} \tag{4.9}$$

where *x* is the random variable, α and τ are location and scale parameters respectively.

$$\text{CDF: } f(x|\tau,\alpha) = \exp\left\{-\exp\left[-\frac{(x-\tau)}{\alpha}\right]\right\} \tag{4.10}$$

Mean, Variance and Skew are:

$$\text{Parameter Mean (x)} = \tau + 0.5772\alpha \tag{4.11}$$

$$\text{Parameter Variance (x)} = \frac{\pi^2\alpha^2}{6} \tag{4.12}$$

$$\text{Fixed Skew (x)} = 1.1396 \tag{4.13}$$

EasyFit allows automatic or manual fitting of the Gumbel maximum distribution, including other distributions. FLIKE software uses MoM method for estimation of most probable location (τ) and scale (α) parameters, fitted to the selected AMF data for this distribution. Experience indicates that the Gumbel is a well-behaved distribution in most FFA studies (FLIKE, 2017). Detail explanation of Gumbel distribution is given in FLIKE manual (FLIKE, 2017).

4.3.4 Generalised Pareto (GP) Distribution

The GP distribution is a 3-parameter (location, scale, and shape) extreme value continuous probability model with fat tails.

The PDF of GP distribution is:

$$f(x|\alpha,\kappa)=\begin{cases}\frac{1}{\alpha}\left[1-\kappa\frac{x}{\alpha}\right]^{\frac{1}{\kappa}-1}, & \text{if } \kappa<0 \text{ and } x\geq 0 \text{ or } \kappa>0 \text{ and } 0\leq x\leq \frac{\alpha}{\kappa}\\ \frac{1}{\alpha}\exp\left(-\frac{x}{\alpha}\right), & \text{if } \kappa=0 \text{ and } x\geq 0\end{cases} \quad (4.14)$$

Where, x is the random sample variable, α is scale, and κ is shape parameter. The CDF of GP distribution is:

$$f(x|\alpha,\kappa)=\begin{cases}\left[1-\kappa\frac{x}{\alpha}\right]^{\frac{1}{\kappa}-1}, & \text{if } \kappa<0 \text{ and } x\geq 0 \text{ or } \kappa>0 \text{ and } 0\leq x\leq \frac{\alpha}{\kappa}\\ 1-\exp\left(-\frac{x}{\alpha}\right), & \text{if } \kappa=0 \text{ and } x\geq 0\end{cases} \quad (4.15)$$

Its first three moments mean, variance and skew are:

$$\text{Mean}(x)=\frac{\alpha}{1+\kappa},\ \kappa>-1 \quad (4,16)$$

$$\text{Variance }(x)=\frac{\alpha^2}{(1+\kappa)^2(1+2\kappa)},\qquad \kappa>-\frac{1}{2} \quad (4.17)$$

$$\text{Skew }(x)=\frac{2(1-\kappa)\sqrt{(1+2\kappa)}}{(1+3\kappa)},\qquad \kappa>-\frac{1}{3} \quad (4.18)$$

The GP PD becomes two-parameter exponential distribution if shape parameter κ is zero and κ has an upper bound when it is positive.

EasyFit allows automatically or manually fitting the GP distribution, including other distributions. FLIKE use MoM for estimation of scale parameter α fitted to the gauged data

with the shape parameter κ fixed at zero. This strategy is robust with the flow's upper bound pushed to infinity. Experience indicates the GP distribution is well-behaved in FFA studies (FLIKE, 2017). Detail explanation of GP is given in FLIKE manual (FLIKE, 2017).

4.3.5 Generalised Extreme Value (GEV) Distribution

The GEV distribution is an extreme value probability model. In this distribution, three different extreme value distributions, i.e. EV1, EV2 (Frechet) and EV3 (Weibull) are combined to a single function. The location, scale and shape are 3 parameters of GEV distribution. The location parameter explains the left or right shift/movement of the distribution on horizontal axis relative to the standard normal distribution. For standard normal distribution the location parameter is zero. The scale parameter shrinks or stretches out the PD function. For standard normal distribution scale parameter is one standard deviation. The more the value of scale parameter the flatter is the distribution curve. The shape parameter defines the general shape of the distribution. This shape does not change with the change of location or scale parameter. The shape parameter describes the tail behaviour of the distribution.

The GEV probability model has the PDF:

$$f(x|\tau,\alpha,\kappa) = \begin{cases} \exp\left\{-\left[1-\frac{\kappa(x-\tau)}{\alpha}\right]^{\frac{1}{\kappa}}\right\}\left[1-\frac{\kappa(x-\tau)}{\alpha}\right]^{\frac{1}{\kappa}-1}, & \text{when } \kappa>0, x<\tau+\frac{\alpha}{\kappa}; \text{when } \kappa<0, x>\tau+\frac{\alpha}{\kappa} \\ \frac{1}{\alpha}\exp\left[-\frac{(x-\tau)}{\alpha}\right]\exp\left\{-\exp\left[-\frac{(x-\tau)}{\alpha}\right]\right\}, & \text{if } \kappa=0 \end{cases} \quad (4.19)$$

where α, τ and κ are scale, location and shape parameters, respectively. It's CDF is:

$$f(x|\tau,\alpha,\kappa) = \begin{cases} \exp\left\{-\left[1-\frac{\kappa(x-\tau)}{\alpha}\right]^{\frac{1}{\kappa}}\right\}, & \text{when } \kappa>0, x<\tau+\frac{\alpha}{\kappa}; \text{when } \kappa<0, x>\tau+\frac{\alpha}{\kappa} \\ \exp\left[-\frac{(x-\tau)}{\alpha}\right], & \text{if } \kappa=0 \end{cases} \quad (4.20)$$

Its mean and variance are respectively:

$$\text{Mean}\ (x) = \tau+\frac{\alpha}{\kappa}[1-\Gamma(1+\kappa)],\ \ \kappa>-1 \quad (4.21)$$

$$\text{Variance}\ (x) = \frac{\alpha^2}{\kappa}[\Gamma(1+2\kappa)-[\Gamma(1+\kappa)]^2],\ \ \kappa>-\frac{1}{2} \quad (4.22)$$

With different value of shape parameter, GEV distribution becomes three different type of distributions. When no shape is considered i.e. when κ = 0, it becomes extreme value type1 (EV1: Gumbel), when κ > 0, it becomes extreme value type 2 (EV2: Frechet) and when κ < 0, it becomes extreme value type 3 (EV3: Weibull) distribution (Millington et al., 2011).

FLIKE starts the search for the most probable parameters by setting the shape parameter κ to zero and using the Gumbel MoM estimates of location (τ) and scale (α) parameters, fitted to observed data series. This approach is very sound with the flow's upper bound pushed to infinity. Experience indicates the GEV is well-behaved in FFA (FLIKE, 2017).

In the present study, every candidate distribution is fitted to at-site AMF data of all the selected stations. Using FLIKE, for each of the distributions, flood quantiles (Q_{ARI}) are obtained for ARIs of 2, 5, 10, 20, 50, 100 and 200 years. These estimates are referred to as "distributional estimates".

4.4 Parameter Estimation

After selection of PD, parameters estimation for each selected PD is the next step in FFA. Various parameter estimation methods are available to fit a PD to AMF data. As mentioned

earlier, both EasyFit and FLIKE software are used in this study. This software uses different parameter estimation methods.

The parameter estimation using EasyFit software (Mathwave, 2017; Drokin, 2018) is carried out with MoM for Gumbel and LP3 distributions, MLE for LN distribution and for GP and GEV distributions Method of L-moments is used. Table 4.1 summarises the PDs, parameters and parameter estimation methods adopted in this study.

Table 4.1: Probability distributions, parameters and parameter estimation methods

Distribution	Parameters	Parameter estimation method
Lognormal (LN)	location (μ) and scale (σ),	MLE
Log Pearson type III (LP3)	location (γ), shape (α) and scale (β)	MoM
Gumbel	location (μ) and scale (σ)	MoM
Generalised Pareto (GP)	location (μ), shape (k) and Scale (σ)	Method of L-moments
Generalised Extreme Value (GEV)	location (μ), shape (k) and scale (σ)	Method of L-moments

FLIKE software uses Bayesian inference for parameter estimation. This method can be viewed as a generalisation of Maximum Likelihood (ML). The likelihood function is the main component in Bayesian analysis. It is to be mentioned that likelihoods are attached to hypotheses and probabilities are attached to results. Likelihood function tells about the parameters and the prior distribution. This prior distribution and likelihood are coupled to find posterior distribution. FLIKE software also uses the LH moment. In this study, LP3 and LN and Gumbel distributions are fitted using the Bayesian inference method, whereas GEV and GP distributions are fitted using the LH moment (with H = 1) method. When H = 0, the LH moment becomes L moment. When H > 1 is used, higher floods are given more importance in distributional fitting. Hence, for the LH moment, censoring of data may not be necessary.

4.5 Selection of Best-fit Probability Distribution (PD) and Goodness-of-Fit (GoF) Tests

Statistical hypothesis tests are used to evaluate statistical GoF of hypothesised PDs to AMF data series. Most of the available statistical hypothesis tests are formulated on normality assumption. The normality tests assume that the observed sample data follow normal distribution and the populations from where data sample comes are also assumed to follow normal distribution. Test of normality along with different probability plots are used to verify these important assumptions of sample distribution (Ghasemi and Zahediasl, 2012).

The GoF tests for normality are statistical hypothesis tests and they are applied to explain how good the random sample data represents a probability model with normally distributed population. This GoF test clarifies whether the distribution of random variable of sample fits a selected distribution in the population or not. Alternatively, GoF test shows how much is random sample data is compatible to the PD function. If the observed random data match properly along with the fitted probability functions, then it can be expected that a good fit is achieved between random sample and selected distribution.

The GoF test calculates the difference between recorded random data and selected PD. This is called test statistics which is the function of fitted cumulative distribution function (CDF) and the observed sample data (Mathwave, 2017; Drokin, 2018). If this test statistic is lesser compared to the critical value (threshold) then the fit between measured data and PD is considered acceptable. The critical values are function of the observed data size and the significance level considered for the test. The significance level is the probability of rejecting the fitted distribution (null hypothesis) when the distribution is actually fits (when it is true) (Mathwave, 2017; Drokin, 2018). Significance levels 0.05 and 0.01 are commonly used in the GoF test.

Different types of GoF tests are available to assess assumption of normality such as Anderson-Darling (A-D) test, Chi-Squared (C-S) test, and Kolmogorov–Smirnov (K-S) test (Ghasemi and Zahediasl, 2012). The fundamental approach of GoF tests are similar, i.e. these tests compare test statistics with the critical values, however each test differs from the other in calculating test statistic and critical value. The A-D, C-S and K-S tests are widely used GoF tests, either based on PDF (f(x)) or cumulative distribution functions (CDF) (F(x)), to identify best-fit distribution for sample.

The A-D test uses more weight at the distribution tails than that of K-S test. In cases with relatively large extremes, the A-D test is more preferable test for selection of the best fit PD model (Alam et al., 2018). The A-D test is refinements of the K-S test. The test is not calculated when a frequency variable is specified. The K-S test compares the maximum distance between the observed CDF value and the expected /theoretical CDF value. This test can be used to decide whether an observed data come from a population with a completely specified continuous distribution or not (Baghban et al., 2013). The advantage of the C-S test is that it is relatively easy to use, but it is not a very strong test.

Different GoF tests may produce different outcomes, and hence more than one test should be adopted. In this study three different tests are adopted following the approach of Mamoon and Rahman (2017).

EasyFit, software from Mathwave (Drokin, 2018) is used to perform GoF tests. It should be noted that FLIKE does not have any GoF test. Hence, the alternative software EasyFit, which has three of GoF tests, has been adopted in this study to assist in selecting the appropriate PD for a given catchment. The three GoF tests in EasyFit software are the A-D test, K-S test and C-S test. Once random data is loaded to the software, EasyFit fits the distributions and it provides tables of the test statistics and critical values at various significance levels (Mathwave, 2017; Drokin, 2018). The test statistics are described in Table 4.2.

Table 4.2: Details of Goodness-of-fit (GoF) tests

GoF test	Test Statistic	Interpretation
Kolmogorov-Smirnov (K-S) test	The K-S test uses empirical CDF and theoretical CDF to calculate test statistics. This test can be used to evaluate level of difference between theoretical continuous distribution being specified and observed distribution from sample data. The K-S test is nonparametric test and no assumption is required regrading distribution of sample data. Candidate distribution is needed to be fully specified for K-S test. The K-S test statistic (D) is the maximum vertical difference between empirical CDF ($P(X\text{n})$) and theoretical CDF ($F(X\text{n})$) and is expressed as: $D=max\|P(X\text{n})-F(X\text{n})\|$ with, $P(Xn)$ is empirical CDF of observed random sample of n ordered observations., and $F(Xn)$ is the theoretical CDF for each of the ordered observations (Sharma et al., 2016).	When test statistics D becomes smaller than the critical value, then observed data is considered having a good fit with the assumed distribution.
Anderson-Darling (A-D) test	The Anderson-Darling (A-D) test is a distribution free or nonparametric test. The A-D test compares expected (theoretical) CDF to an observed CDF. Compared to K-S test, A-D test provides higher weight to the tails of distribution to be fitted. The A-D test statistic (A^2) is (Solaiman, 2011): $A^2 = -n - S$ Where, $$S = \sum_{k=1}^{n} \frac{2k-1}{n} [\ln F(Y_k) + \ln\{1 - F(Y_{n+1-k})\}]$$ Where, n = sample size, Y_1, Y_2, Y_3, Y_4, …, Y_n are sample data and F = CDF (Solaiman, 2011).	If test statistics (A^2) is higher than critical value, the null hypothesis is rejected.

Chi-Squared (C-S), ($\chi 2$) test	The C-S test is a nonparametric test. In this test observed data are grouped into number of bins (k). Based on the size of sample data, the number of bins can be calculated using empirical expression where $$k = 1 + \log_2 N$$ N is the size of sample. The C-S test statistic is: $$\chi^2 = \sum_{i=1}^{k} \frac{(O_i - E_i)^2}{E_i}$$ $$E_i = F(x_2) - F(x_1)$$ where, E_i *is* expected frequency for bin i, O_i *is* observed frequency for bin i (Sharma et al., 2016). where, x_1, x_2 are the limits for bin i, F is CDF of expected distribution.	The null hypothesis is rejected when test statistics is higher than the critical value i.e. statistically significant difference exists between observed and expected value.

4.6 Graphical Method of Selecting the Best-fit Probability Distribution

The graphical method is a simple technique that can be used to select the best-fit PD. The distribution graph is a visual way to identify PD that fits AMF data. Graphical test or a visual inspection method assesses how well the PD fit the observed sample visually. This method plots histogram, probability and quantiles from observed sample with those against theoretical (fitted) distribution. This method is generally not reliable, and this method should not be used alone to conclude that the expected PD fits the observed sample data since conclusion from visual plots is more subjective. Graphical methods are typically more useful when the observed sample size is very large. When observed sample size is large, interpretation from graphical plots including histogram (frequency distribution graph), quantile-quantile (Q-Q) plot, probability-probability (P-P) plot, PDF graph, CDF graph, stem-and-leaf plot, box plots and FLIKE probability plot are useful in selecting the best-fit PD.

The Q-Q plot is the plot of observed sample quantile in one-axis and calculated theoretical distribution quantile (inverse of CDF) in another axis. The Q-Q plots are used to compare the selected distribution to sample data which helps to assess level of GoF to the model. Actually, Q-Q plot compares sample quantiles with the quantile function for the distribution at the plotting positions. Commonly used plotting position formula is:

$$p_{i;n} = \frac{n-a}{N+1-2a} \tag{4.23}$$

Where N is observed sample size, n is rank of the sample data (n = 1, 2, 3, …., N) and a is a constant.

When a = 3/8 this formula is called Blom's plotting position, when a =0.44 this is called Gringorten's plotting position and when a = 0.40 this is called Cunnane's plotting position. Blom's plotting position is suitable for Normal, Gamma, 2-parameters LN, 3-parameter LN and LP3 distributions, and for Gumbel and Weibull distributions, Gringorten's plotting position and Cunnane's plotting position are suitable for GEV and Log-Gumbel distributions (Kim et al., 2008, Vogel and Kroll, 1989; Cunnane, 1978).

In P-P plot, theoretical CDF values are plotted against cumulative probability of observed sample i.e. empirical CDF values. This plot displays how good a candidate distribution fits the sample data. The PDF graph plots histogram (frequency distribution plot) of sample data and theoretical PDF of the candidate distribution. The shape of the sample data can be clearly visualised from PDF graph. The histogram is the plot of the observed sample data and their frequency of occurrence and this provides a visual judgment on location, scale and shape of distribution (Ghasemi and Zahediasl, 2012). The CDF graph plots empirical CDF (derived from sample data) and theoretical CDF of the candidate distribution. The plot of CDF graph is helpful to decide how well the sample data fit a distribution.

In EasyFit, the P-P, Q-Q, PDF, CDF and probability difference plots are used to assess visually how well a candidate PD fits the AMF data at a given station. FLIKE probability plot shows observed AMF data and fitted PD, which helps to assess visually how well a PD fits the observed AMF data at a given station (Hossain, 2019). The procedure is repeated for each of the candidate PDs for each of the selected stations using EasyFit and FLIKE.

4.7 Flood Quantile Estimation

In this study, flood quantiles are estimated for each of the sites using each of the five PDs. Flood quantiles are estimated using FLIKE software for different ARIs (2, 5, 10, 20, 50, 100 and 200 years) along with 90% confidence limits.

4.8 Sensitivity of Quantile Estimation on Maximum Recorded Flow

The record length of AMF data and maximum value of the AMF data series can influence the selection of the best-fit PD. In general, the record length of flood data is relatively small compared to the required average recurrence intervals (ARIs) in practice. For this reason, uncertainties are introduced in quantile estimation when the fitted PD is used to extrapolate to large ARIs (e.g. ARIs of 100-year). The fitted PD with small record length of flood data can have a large effect on quantile estimates especially when ARIs are greater than 50 years. When the observed data length is increased by few more years at a given location, the fitted PD with few more flood data can be different than the fitted PD with smaller record length (Boughton and Hill, 1997). The sensitivity of the selection of the best-fit PD and the flood quantile estimation is tested in three different ways, i.e. (a) remove the highest flow record from each of the site's AMF data series, (b) remove the first and second highest flow records and (c) remove the first, second and third highest records. For each of above scenarios; parameter estimation, GoF tests, selection of the best-fit PD, and quantile estimation are conducted.

4.9 Uncertainty Analysis using Bootstrapping and Monte Carlo Simulation Methods

Flood quantile estimation using by FFA or RFFA is subject to uncertainties that should be estimated (Arnaud et al., 2017). Uncertainties in flood quantile estimation may exist due to error in input data, due to inability of mathematical model to represent physical hydrological process accurately (i.e. modelling error), sampling error comes from accuracy of sample to represent population, and error due to change in climate that affect hydrological process. Uncertainty in estimation is usually expressed in terms of confidence level. The

hydrological process is not linear and extreme flow events from this nonlinear hydrological process show higher uncertainties and use of these flow events for estimation of flood quantile increases uncertainties on estimated flood quantiles (Arnaud et al., 2017).

Uncertainty in flood quantile estimates may arise due to the following issues:

- Record length of observed flood data.
- Error form instrument used to measure flood data.
- Gaps in observed flood data.
- Human error while entering and processing flood data.
- Insufficient number of stream gauging stations within the region.
- Choosing of AMF or PDS data series in modelling.
- Serial and interstation correlations of the flood data.

Uncertainty in flood quantile estimates using non-stationary FFA may result from:

- Trend analysis methods.
- Data length.

Different methods are used for uncertainty analysis including statistical and simulation methods based on resampling processes (Arnaud et al., 2017). A detailed review on uncertainty analysis was done by Melching (1995). Some approaches used to understand and quantify uncertainties are:

- Bootstrapping that allows resampling of dataset (Efron and Tibshirani, 1993; Efron and Tibshirani, 1994);
- Bayesian approaches that continuously updates the probability of a hypothesis as new information becomes available (Renard et al., 2010);
- Monte Carlo simulation (Baltussen et al., 2002); and
- Cross validation techniques (Mamoon and Rahman, 2019; Haddad et al., 2013).

4.9 1 Monte Carlo Simulation

Analysis of probabilistic uncertainty using Monte Carlo simulation has been well explained in Baltussen et al. (2002). Sensitivity of any hydrological model is commonly assessed using Monte Carlo simulation techniques. This technique performs repeated simulations using randomly generated parameter combinations (Harlin and Kung, 1992). Monte Carlo simulation uses random samples in groups as inputs and evaluates deterministic model through iteration. This technique is suitable to assess model impacts and evaluate uncertainty in parameter estimation which is generally expressed as confidence limits on estimates (Al Mamoon and Rahman, 2014). Random data generated from probability distribution may be used as inputs in Monte Carlo simulation. The Monte Carlo simulation results can be plotted as a histogram or error bars or as confidence limits (Al Mamoon and Rahman, 2014).

Steps in a typical Monte Carlo simulation technique for assessing uncertainty are presented below (Al Mamoon and Rahman, 2014):

- Select PD for each of the input variables and estimate distributional parameters and correlation structure among the input variables;
- Generate 10,000 values of the input variables from the specified PDs and correlation structure;
- Select model to convert each of the sets of the input variables to output;
- Create 10,000 model outputs and save model outputs for further analysis;
- Repeat the above procedures many times until the total number of simulations is completed or the convergence criterion is met; and
- Analyse the results to derive expected value of the output and confidence limits.

4.9 2 Bootstrapping

Bootstrapping is a resampling technique that uses an observed sample to create many simulated samples. Nonparametric bootstrapping can be used to compute standard error, build confidence intervals, and perform hypothesis testing for different types of sample statistics (Efron and Tibshirani, 1993). Bootstrapping does not require normality assumption to be satisfied like many traditional statistical methods (Tung and Wong, 2014).

The following basic steps may be used for bootstrapping (Al Mamoon and Rahman, 2014):

- Generate numerous (~10,000) samples by randomly drawing samples with replacement from the AMF data set at a station;
- Calculate statistics of interest from the generated samples;
- Create sampling distribution of the statistic; and
- Find standard deviation of the statistic.

In FFA, flood quantiles can be estimated from the selected PD using mean, standard deviation and skewness of the AMF data. If a range of mean, standard deviation and skewness values is generated, a range of flood quantiles for a given ARI can be estimated. With a range of quantile values, the uncertainty in the estimated quantiles can be understood.

For this study, five (5) stations where LP3 is found as the best-fit PD are selected for uncertainty analysis. Standard error of mean, standard deviation, skewness and correlations of the sample are estimated using the bootstrapping method. Then, uncertainty is examined using Monte Carlo simulation techniques. The procedure is explained below:

- From the AMF data of a station, 10,000 samples (Q) are generated by bootstrapping. For each of these samples, the mean, standard deviation and skewness of the log(Q) values are noted.
- The mean and SD values of the above 10,000 means are estimated.
- The mean and SD values of the above 10,000 standard deviations are estimated.
- The mean and SD values of the above 10,000 skewnesses are estimated.
- The correlations of the above mean, standard deviation and skewness values are estimated.
- The above values are used to fit a multivariate normal distribution to the mean, standard deviation and skewness values. A Monte Carlo simulation is then conducted to generate 10,000 sets of LP3 distributional parameters and used to estimate flood quantiles. These flood quantiles are arranged in ascending order and 5% and 95% limits are noted to obtain the 90% confidence limits for a given ARI.

4.10 Trend Analysis

Inconsistency and non-homogeneity may exist in hydrological time series data (Yevjevich and Jeng, 1969) which can be viewed as trends and jumps in time series data. Inconsistency in data may come from systematic error while recording hydrological data at a station. This error may come from the instrument used for recording data or the method used for recording data. If there exist changes in statistical properties in the hydrological time series data, non-homogeneity in time series is assumed to exist. Non-homogeneity in time series may arise preliminary from natural causes, e.g. due to climate change that alters existing weather patterns over time or man-made causes, e.g. land use, urbanisation, flow diversion and construction of dams. (Wijesekera and Perera, 2012). The presence of non-homogeneities and inconsistencies in data series is identified by using specific statistical tests and the result of these statistical tests is used to confirm the presence of trend and change points in data (Wijesekera and Perera, 2012).

Hydro-metrological processes (also called probabilistic or stochastic process) are random process as the variables in hydro-metrological process (flood, rain, temperature, etc.) are random in nature. Hydrological variables are probabilistic as these cannot be predicted with certainty. A hydrological process can be considered as stationary if this process does not change over a period of time or if the statistical properties e.g. mean and variance of the hydrological data series do not change over time period. Presence of trend in hydrological time series is an indication that the data series may not be stationary.

Many statistical tests are available to find whether a time series show significant trend and is non-stationary. Most of these tests usually check for the trend in statistics (e.g. mean or median) of the data series or check the sudden change in mean or median in the data series. A simple quick way to check the presence of trend in data is to divide the data series into two time spans and then compare the mean and variance of each time span. If these statistics (mean, variance) of these two sub-data series differ significantly then there may exist trend in the data series and the time series is likely to be non-stationary.

This study considers 12 statistical tests for detecting trend, randomness or sudden change in the AMF data. Trend tests are conducted using the TREND software developed by eWater, CRC (eWater, 2018; Chiew, 2005). These statistical tests basically compare null hypothesis

(i.e. there is no trend in the time series data) and alternative hypothesis (i.e. there is trend in the time series data) (eWater, 2018; Chiew, 2005) for specified levels of error. The accepted level of error in a statistical test is expressed as significance level. The statistical tests within TREND software use 1%, 5% and 10% significance levels. It is a way of expressing change of difference of test statistics under alternative hypothesis with those of null hypothesis (eWater, 2018; Chiew, 2005). A 5% significance level means that there is a chance/probability that a test statistic has 5% chance of becoming not true.

This study adopts non-parametric and parametric tests for detection of trend and step jumps in the AMF data. In parametric tests, shape (generally Normal Distribution) and parameters (mean and standard deviation) of the population distribution are assumed from the sample distribution. When all assumptions of parametric tests are met, these tests are considered more powerful tests to analyse the data than non-parametric tests (eWater, 2018; Chiew, 2005). Non-parametric statistical tests do not require assumptions for the shape or parameters of population distribution. The Non-parametric test is distribution free test and does not require to use null hypothesis on population parameters (eWater, 2018; Chiew, 2005). Non-parametric test does not quantify the trend/change, although it detects the presence of trend/change in time series data (eWater, 2018; Chiew, 2005). As hydrometrological time series data generally do not follow normal distribution, non-parametric tests are preferred for detection of trend or change in time series. (eWater, 2018; Chiew, 2005).

This study use Spearman's Rho (SR), Mann-Kendall (MK), Rank-Sum, Rank Difference, Turning Point, Distribution-Free CUSUM and Median Crossing non-parametric tests and Linear Regression, Autocorrelation, Student's t, Worsley Likelihood Ratio and Cumulative Deviation parametric tests for trend analysis (Hossain and Rahman, 2019). Trends in the data, step jumps in the data, difference in the mean or median from two selected data periods and randomness in the data are evaluated through these tests (Hossain and Rahman, 2019). The presence of trend in data is evaluated using the Linear Regression parametric tests, MK non-parametric and Spearman's Rho non-parametric tests (Hossain and Rahman, 2019).

Critical test statistics for null hypothesis under different significance levels are valid as long as the test assumptions are satisfied. Resampling analysis can be used when test assumptions are violated. As there are chances of violation of test assumptions in hydrological data, resampling technique has been adopted in this research using TREND to estimate

significance level of test statistics (eWater, 2018; Chiew, 2005). TREND provides tabular output at three significance level, α = 0.01, α = 0.05 and α = 0.1 of test statistic and critical values of test statistic and write notes on test result (eWater, 2018; Chiew, 2005).

TREND resamples data using bootstrapping method. The details of trend test with resampling are available in TREND user guide (eWater, 2018; Chiew, 2005).

The details of tests mentioned below are available in TREND user guide (eWater, 2018; Chiew, 2005).

4.10.1 Mann-Kendall (MK) Test

This non-parametric test is used to detect the existence of monotonic trend in AMF data. The null hypothesis and alternative hypothesis are compared in MK statistical test. In null hypothesis it is assumed that the sample data are IID random variables from population i.e. no trend exists in the AMF data series and the alternative hypothesis assumes that trend exists in the data (eWater, 2018; Chiew, 2005). The test statistic (*S*) in the MK test is expressed as:

$$S = \sum_{j=1}^{n-1} \sum_{k=j+1}^{n} sign(Y_j - Y_i) \tag{4.24}$$

where *n* is sample data length, *Y* is the sample data ranked in order 1, 2, 3, …, *n*, and $sign$ can be obtained by:

$$\begin{aligned} sign(Y_j\text{-}Y_k) &= \ \ 1 \quad && \text{when } (Y_j\text{-}Y_k) \text{ is positive} \\ sign(Y_j\text{-}Y_k) &= \ \ 0 \quad && \text{when } (Y_j\text{-}Y_k) \text{ is zero} \\ sign(Y_j\text{-}Y_k) &= -1 \quad && \text{when } (Y_j\text{-}Y_k) \text{ is negative} \end{aligned} \tag{4.25}$$

According to Kendall (1975) and Mann (1945), the statistic *S* can be expressed by using normal distribution approximately when sample data (*n*) is greater than or equal to 10 (Null Hypothesis H_0 is true), with values of mean and variance are (Ahmad et al., 2015):

Mean of S; $E(S) = 0$ (4.26)

$$Variance\ (S) = \sigma^2 = \frac{1}{18}\left[n \cdot (n-1) \cdot (2n+5) - \sum_{j=1}^{p} t_j(t_j-1)(2t_j+5)\right]` \quad (4.27)$$

where, t_j is ties for j_{th} and p is the number groups forming ties. Assuming S follow normal distribution, critical test statistic Z at different significance levels is given by (Ahmad et al., 2015):

$$Z = \begin{cases} \frac{S-1}{\sigma}, & S > 0 \\ \frac{S+1}{\sigma}, & S < 0 \\ 0, & S = 0 \end{cases} \quad (4.28)$$

Statically significant trend in time series can be exist if the null hypothesis is rejected at specified significance level, when $|Z| > Z_{\frac{\alpha}{2}}$ where, $Z_{\frac{\alpha}{2}}$ is the standard normal variate having exceedance probability equal to $\frac{\alpha}{2}$ (Ishak et al., 2013; Ahmad et al., 2015). Time series has statistically upward trend if $Z > 0$ and vice versa.

4.10.2 Spearman's Rho (SR) Test

The SR test is used to test presence of positive or negative trends in a time series. This non-parametric test assesses the presence of significant correlation between the ranking of two variables (year/time and corresponding flow) in AMF data series. The test statistics ρ_s is given below by (eWater, 2018; Chiew, 2005):

$$\rho_s = \frac{\sum_{i=1}^{n}(x_i-\bar{x})\cdot(y_i-\bar{y})}{(\sum_{i=1}^{n}(x_i-\bar{x})^2 \cdot \sum_{i=1}^{n}(y_i-\bar{y})^2)^{\frac{1}{2}}} \quad (4.29)$$

Where x_i and y_i is the year of AMF and AMF values respectively in AMF data series, $\overline{X}$ and $\overline{Y}$ is the ranks.

Detailed procedures of SR test are available at TREND user guide (eWater, 2018; Chiew, 2005).

4.10.3 Linear Regression Test

This parametric test is based on the assumption that sample data series are normally distributed IID random variables (eWater, 2018; Chiew, 2005). Linear regression test assesses the relationship between time (*x*) and the corresponding AMF (*y*) in AMF time series data for the possibility of trend in the data.

The linear regression test statistics is given by:

$$S = \frac{\frac{\sum_{i=1}^{n}(x_i-\bar{x})\cdot(y_i-\bar{y})}{\sum_{i=1}^{n}(x_i-\bar{x})^2}}{\sqrt{\frac{12\sum_{i=1}^{n}(y_i-a-bx_i)}{n(n-2)(n^2-1)}}} \tag{4.30}$$

Where

a is *y* intercept of regression line, b is regression line slope and *n* is record length.

$$a = \bar{y} - b\bar{x} \tag{4.31}$$

$$b = \frac{\sum_{i=1}^{n}(x_i-\bar{x})(y_i-\bar{y})}{\sum_{i=1}^{n}(x_i-\bar{x})^2} \tag{4.32}$$

The detailed description of this test is available at TREND user guide (eWater, 2018; Chiew, 2005).

4.10.4 Distribution Free CUSUM Test

In this test, data series is divided into two groups and then compare the means of these two groups to find whether they are significantly different (eWater, 2018; Chiew, 2005). This non-parametric test does not use any assumption of distribution for sample data. The distribution free CUSUM test is expressed as:

$$V_k = \sum_{i=1}^{k} \mathrm{sgn}(x_i - x_{median}), \;\; k = 1, 2, 3, \ldots, n \tag{4.33}$$

Where

Sample time series; $X_i = x_i, x_2, x_3, \ldots x_n$

Sample time series median = X_{median}

$\text{sgn}(x) = 1, \text{for } x > 0$
$\text{sgn}(x) = 0, \text{for } x = 0$
$\text{sgn}(x) = -1, \text{for } x < 0$

The detailed description of this test is available at TREND user guide (eWater, 2018; Chiew, 2005).

4.10.5 Cumulative Deviation Test

This parametric test identifies the possible change point of the mean by comparing the means in the two parts of time series data (eWater, 2018; Chiew, 2005). According to Buishand (1982) this test calculates cumulative deviations and adjusted partial sums from the mean.

The cumulative deviations are:

$$S_k * = \sum_{i=1}^{k} (x_i - \bar{x}), \quad k = 1, 2, 3, \ldots, n \tag{4.34}$$

X_i is the observed sample data, n is total number of sample data and $\overline{X}$ is the mean.

The adjusted partial sums are:

$$S_k{}^{**} = \frac{S_k{}^{*}}{D_x} \tag{4.35}$$

Where Dx is the standard deviation.

$$D_x{}^2 = \sum_{i=1}^{n} \frac{(x_i - \bar{x})^2}{n} \tag{4.36}$$

The test statistic Q in Cumulative Deviation Test is given by:

$$Q = \max \left| \frac{S_k^{**}}{D_x} \right| \quad (4.37)$$

The detailed description of this test including critical value is available at TREND user guide (eWater, 2018; Chiew, 2005).

4.10.6 Worsley Likelihood Ratio Test

In this method, time series data is divided into two periods and this test finds difference in means by comparing the two means of two sets of data (eWater, 2018). This test is based on the assumption of normality of sample data and is an extension of Cumulative Deviation Test. The weighted cumulative deviations (Z_k*) and adjusted partial sum are:

$$Z_k^{*} = [k(n-k)] - 0.5[\sum_{i=1}^{k}(x_i - \bar{x})],\ k = 1, 2, 3, \dots, n \quad (4.38)$$

$$Z_k^{**} = \frac{Z_k^{*}}{D_x} \quad (4.39)$$

X_i is the observed sample data, n is total number of sample data and $\overline{X}$ is the mean.
The test statistic W is given by:

$$W = \frac{(n-2)^{0.5} V}{(1-V^2)^{0.5}} \quad (4.40)$$

Where V = max | Z_k**|

The detailed description of this test including Critical value of W is available at TREND user guide (eWater, 2018; Chiew, 2005).

4.10.7 Rank-Sum Test

This non-parametric test is similar to the 2-sample *t*-test. This test divides the sample time series data into two sub-groups (two sub time-periods) and compares the medians of these two groups. In this test sample time series data is first sorted in ascending order (1, 2, 3,…, K). If the values of two records in the sample are same, then average of ranks of two records is used as the rank of these two records. If T is sum of ranks of smaller sub-group, and j and k

are the number of records of two sub-groups respectively, then the mean (μ_T) and standard deviation (σ_T) of T are:

$$\mu_T = k * (K + 1) / 2 \quad (4.41)$$

$$\sigma_T = [k * j * (K + 1) / 12]^{0.5} \quad (4.42)$$

and the test statistic Z is:

$$Z = (T - 0.5 - \mu_T) / \sigma_T \quad \text{for } T > \mu_T \quad (4.43)$$

$$Z_{rs} = 0 \text{ for } T = \mu_T \quad (4.44)$$

$$Z_{rs} = |T + 0.5 - \mu_T| / \sigma_T \quad \text{for } T < \mu_T \quad (4.45)$$

The detailed description of this test including critical test statistics at different confidence levels is available at TREND user guide (eWater, 2018; Chiew, 2005).

4.10.8 Student's *t* Test

This statistical test is used to detect whether two groups of sample data differ significantly by calculating the mean of sample data of two data periods. Like some other test, this test is based on the normality assumptions. The Student's *t* test statistic is calculated as:

$$t = \frac{(\bar{x} - \bar{y})}{T\sqrt{\frac{1}{n} + \frac{1}{m}}} \quad (4.46)$$

where

$\overline{x}$ is the mean of one sub-group of sample data and $\overline{y}$ the mean of another sub-group of sample data respectively, m and n are record number of two sub-group data sets respectively and standard deviation of sample data is T (eWater, 2018; Chiew, 2005). The detailed description of this test is available at TREND user guide (eWater, 2018; Chiew, 2005).

4.10.9 Median Crossing Test

In median crossing normality test, each time series data is assigned zero if median of sample data is greater than the particular data value and one if median of sample data is less than the particular data value. The mean (μ) and SD (σ) of data set with 0 and 1 value are (eWater, 2018; Chiew, 2005):

$$\mu = (k - 1) / 2 \quad (4.47)$$

$$\sigma = (k - 1) / 4 \quad (4.48)$$

here, k is the sample size.

The median crossing test statistic (z) is calculated as with median (m) (eWater, 2018; Chiew, 2005):

$$z = \frac{|m-\mu|}{\sigma^{\frac{1}{2}}} \quad (4.49)$$

The detailed description of this test is available at TREND user guide (eWater, 2018; Chiew, 2005).

4.10.10 Turning Points Test

It is a non-parametric test for randomness and is based on assumption of normality. In this test, each record of time series data is assigned a value of 1 or 0. If the value (a) of data of a particular time step is greater than the value of data of immediately before or immediately after that time step i.e. if $a_i\text{-}1 < a_i > a_i\text{+}1$, then 1 otherwise 0. The mean and SD of the data series with 0 or 1 are calculated as (eWater, 2018; Chiew, 2005):

$$\mu = 2\ (k - 2) / 3 \quad (4.50)$$

$$\sigma = (16k - 29) / 90 \quad (4.51)$$

The turning point test statistic (Z) is calculated as (eWater, 2018; Chiew, 2005):

$$z = \frac{|m* - \mu|}{\sigma^{\frac{1}{2}}} \quad (4.52)$$

The detailed description of this test is available at TREND user guide (eWater, 2018; Chiew, 2005).

4.10.11 Rank Difference Test

Rank Difference non-parametric test assigns rank in ascending order to the time series data. Assume a large data set (n > 10), the statistics U is calculated as (eWater, 2018; Chiew, 2005):

$$U = \sum_{i=2}^{n} |R_i - R_{i-1}| \quad (4.53)$$

Where, absolute rank differences sum between consecutive ranks is (R_i -- R_{i-1})
The mean and SD of rank sample are (eWater, 2018; Chiew, 2005):

$$\text{Mean; } \mu = (k + 1)\,(k - 1) / 3 \quad (4.54)$$

$$\text{SD; } \sigma = (k - 2)\,(k + 1)\,(4k - 7) / 90 \quad (4.55)$$

The rank difference test z-statistic is computed as (eWater, 2018; Chiew, 2005):

$$z = |\, U - \mu \,| \,/\, \sigma^{0.5} \quad (4.56)$$

The detailed description of this test is available at TREND user guide (eWater, 2018; Chiew, 2005).

4.10.12 Autocorrelation Test

`In this test one autocorrelation coefficient between value at r_{th} time step and value at one time step before (r_{th}-1) i.e. lag-1 autocorrelation (i.e. the correlation between time series sample values that are separated by 1 time period) coefficient is expressed as (eWater, 2018; Chiew, 2005):

$$r_1 = \frac{[\sum_{i=1}^{k-1}(x_i - \bar{x})(x_{i+1} - \bar{x})]}{\sum_{i=1}^{k}(x_i - \bar{x})^2} \quad (4.57)$$

The expected value and variance of r_1 are (eWater, 2018; Chiew, 2005):

$$E(r_1) = -1 / k \quad (4.58)$$

$$Var(r_1) = (k^3 - 3k^2 + 4) / [k^2 (k^2 - 1)] \quad (4.59)$$

The autocorrelation test statistic (z) is given by (eWater, 2018; Chiew, 2005):

$$z = | r_1 - E(r_1) | / Var(r_1)^{0.5} \quad (4.60)$$

The detailed description of this test is available at TREND user guide (eWater, 2018; Chiew, 2005).

4.11 Summary

This chapter presents methods adopted in this study covering mathematical formulation of selected PDs and parameter estimation methods. Three GoF tests are also described. Bootstrapping and Monte Carlo simulation techniques are also presented. Different tests for trend analysis are also outlined.

The next chapter presents results and discussion.

CHAPTER 5 : RESULTS AND DISCUSSION

This chapter presents statistical characteristics of AMF data, outcomes of selection of the best-fit probability distribution (PD) for FFA using GoF tests and visual assessment, and results of trend, sensitivity and uncertainty analysis.

5.1 Statistical Characteristics of AMF Data

For better understanding of the statistical properties of AMF data, basic statistics are computed. A total of 26 streamflow measuring stations are selected as mentioned in Chapter 3. All the AMF data was screened, and outliers were identified. Table 5.1 lists the descriptive statistics such as mean, maximum, minimum, SD, range, skewness, variance, coefficient of variation, excess kurtosis and standard error of the AMF data for each of the 26 stations.

From Table 5.1 it is seen that station 143001C shows the highest AMF value of 9533 m^3/s. This flow was recorded in 2011, which was one of the worst flooding years in the study area. This station also shows the highest AMF mean (1425 m^3/s). The skewness is positive with a value of 3.176. The minimum and maximum skewness vales are 0.27 and 6.10 for station 143209B and 143203C, respectively. In regard to excess kurtosis, station 143203C shows the highest value of 43.01. The lowest value is -1.32 at station 143209B. It is seen that for station 143203C, skewness and excess kurtosis values are the highest among all the 26 stations. Standard deviation and excess kurtosis of 6.10 and 43.01 respectively at station 143203C are very high compared to the minimum value 0.27 and -1.32, respectively at station 143209B. Station 143203C is an upstream station where mean flow is 264 m^3/s and maximum flow is 3643 m^3/s in 2011. There is a very high difference between mean flow and maximum flow. The maximum flow for this station is 1380% larger than its mean flow. These statistics indicate that AMF data at this station follows relatively peaky positively skewed distribution.

On the other hand, station 143209B has a mean flow of 250 m^3/s and maximum flow of 349 m^3/s. The maximum flow for this station is only 140% higher than its mean AMF. It is seen in Table 5.1 that skewness is positive for all the stations, although excess kurtosis is negative for three stations. Maximum SD and coefficient of variation values are found to be 1968.58 m^3/s and 9.45 at station 143001C and 143232A, respectively. Although station 143219A

shows the lowest mean of 21.06 m^3/s, the skewness (5.51) and excess kurtosis (32.38) for this station are very high. The percentile estimates of the AMF data are shown in Table 5.2 for all the 26 stations.

Table 5.1: Descriptive Statistics of the AMF data for all the 26 stations

Station ID	Range m^3/s	Mean m^3/s	Variance m^3/s	Std. Deviation m^3/s	Coef. Of Variation	Std. Error m^3/s	Skewness	Excess Kurtosis
143001C	9439.3	1425.9	3875300	1968.60	1.381	303.76	3.176	11.014
143007A	4402.8	525.98	805880	897.71	1.707	122.16	2.472	6.410
143009A	6969.5	1045.4	3235500	1798.70	1.721	240.37	2.210	3.801
143010B	2025.6	270.24	173100	416.05	1.540	64.98	2.774	8.274
143015B	2324.5	297.51	194880	441.46	1.484	68.94	2.953	10.875
143028A	126.72	35.41	804	28.36	0.801	4.43	1.764	3.140
143032A	271.81	85.207	5404	73.51	0.863	14.15	1.971	3.515
143033A	353.37	140.11	10186	100.92	0.720	20.19	1.017	0.128
143107A	1884	513.89	132170	363.55	0.707	60.59	2.463	8.410
143108A	1939	490.2	173170	416.14	0.849	75.98	2.507	7.340
143110A	290.18	178.09	7651	87.47	0.491	13.34	1.072	-0.215
143113A	373.86	126.72	6040	77.72	0.613	14.96	1.896	5.756
143203C	3610	263.83	212100	460.54	1.746	55.05	6.061	43.132
143207A	2950	627.43	557960	746.96	1.191	99.82	1.671	1.884
143209B	250.51	203.56	6849	82.76	0.407	15.64	0.270	-1.322
143210B	1361.8	321.06	100780	317.45	0.989	64.80	2.049	4.941
143212A	1358.2	225.41	123350	351.21	1.558	51.23	1.962	2.872
143213C	509.63	101.88	23122	152.06	1.493	36.88	1.880	2.751
143219A	361.43	21.062	3412	58.41	2.773	9.35	5.507	32.380
143229A	1379.3	239.4	123860	351.93	1.470	76.80	2.532	6.248
143232A	33.43	22.884	89	9.45	0.413	2.44	0.997	0.254
143233A	501.51	105.38	17035	130.52	1.239	32.63	2.379	6.361
143303A	531.77	351.64	16523	128.54	0.366	19.60	0.983	0.628
143306A	154.84	79.301	2510	50.10	0.632	10.93	0.640	-0.769
143921A	589.5	71.022	21634	147.09	2.071	27.31	3.089	9.130
143307A	433.64	144.54	14978	122.38	0.847	24.98	1.314	0.994

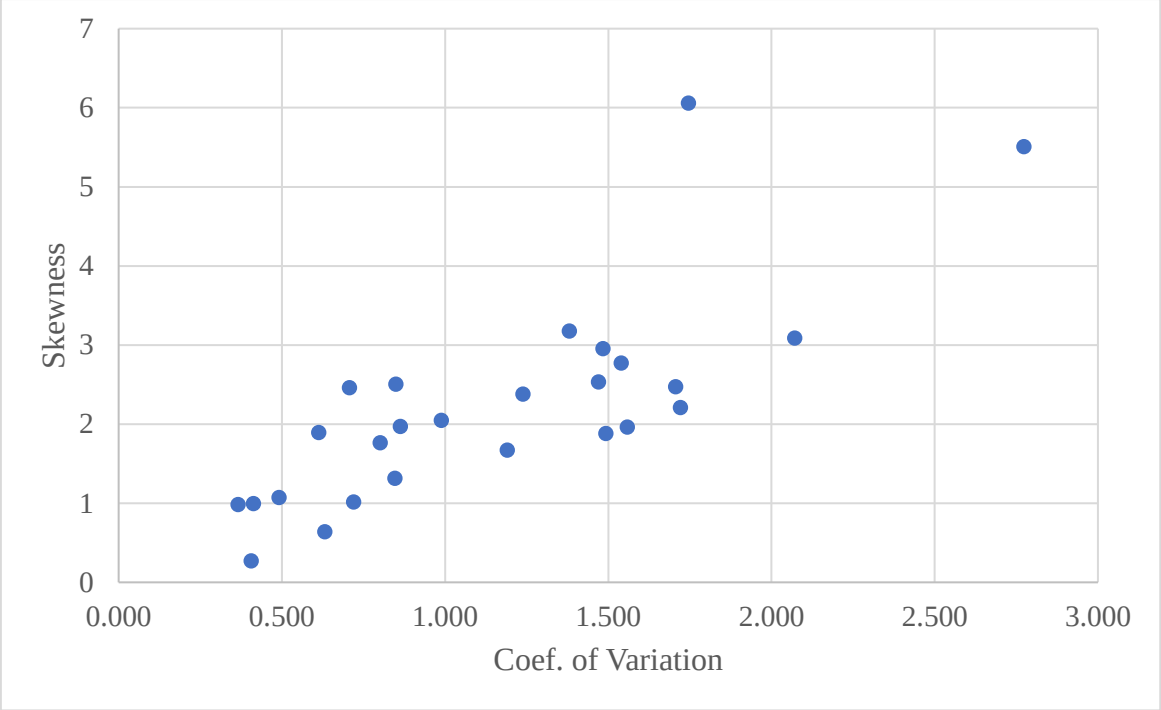

Figure 5:1: Variation of absolute skewness in the AMF data for 26 stations

Table 5.2: Percentile estimates of AMF data for all the 26 stations

Station ID	05 % Percentile (m^3/s)	10 % Percentile (m^3/s)	25% (Q1) Percentile (m^3/s)	50% (Median) Percentile (m^3/s)	75% (Q3) Percentile (m^3/s)	90% Percentile (m^3/s)	95% Percentile (m^3/s)	Max. Percentile (m^3/s)
143001C	136.81	162.64	337.07	857.11	1648.80	2838.4	8130.0	9533.0
143007A	6.58	8.89	29.03	143.09	391.45	2104.3	2559.8	4404.0
143009A	12.81	18.53	83.71	322.63	785.85	4462.3	5938.9	6975.8
143010B	19.34	22.50	38.66	128.90	255.99	989.5	1288.8	2035.7
143015B	12.09	19.74	43.39	110.69	383.19	915.1	1142.9	2335.3
143028A	8.05	13.64	16.61	24.09	45.77	66.9	105.8	133.4
143032A	26.50	28.27	35.22	55.97	107.12	206.8	296.1	297.1
143033A	35.18	46.71	54.48	96.50	203.58	312.0	373.0	385.4
143107A	177.55	194.82	291.02	408.47	612.51	936.4	1275.6	2057.0
143108A	174.75	196.74	229.92	337.71	569.62	1127.4	1657.3	2107.5
143110A	86.82	95.48	117.05	146.03	212.95	338.0	353.7	370.0
143113A	40.38	51.66	70.15	111.30	164.56	203.6	328.3	410.8
143203C	41.47	50.66	65.47	140.56	341.93	484.8	676.7	3643.0
143207A	37.46	51.85	133.36	284.13	850.35	2067.7	2489.9	2976.6
143209B	99.59	104.08	122.79	204.24	277.60	327.7	348.3	349.0
143210B	40.67	48.42	104.55	209.57	417.06	801.6	1258.3	1400.6
143212A	1.61	3.87	12.20	58.71	215.37	908.5	1145.3	1359.4
143213C	0.93	3.00	7.00	33.03	147.18	426.9	510.6	510.6
143219A	0.27	0.34	2.20	4.93	16.02	47.2	78.2	361.6
143229A	15.68	17.56	55.17	105.09	252.27	932.5	1359.4	1394.7
143232A	11.51	14.38	16.32	17.00	32.14	37.5	44.9	44.9
143233A	14.87	16.26	27.92	45.09	165.83	325.0	516.4	516.4
143303A	186.56	194.75	271.48	312.70	423.73	549.9	638.5	710.3
143306A	19.78	20.62	34.25	67.31	125.65	167.7	174.4	174.6
143921A	0.23	0.72	2.48	15.43	66.46	176.8	576.9	589.6
143307A	28.72	29.26	53.71	88.28	201.99	377.6	445.2	462.2

5.2 Parameter estimation and selection of the best-fit probability distribution (PD)

In FLIKE, the parameters are estimated by the in-built modules in the FLIKE which vary from distribution to distribution. In using FLIKE, these in-built parameter estimation methods are used. Since FLIKE does not have any GoF test, EasyFit is used to carry out the GoF test.

It should be noted that PILFs are only censored for LN and LP3 distributions as per FLIKE guide, these are not censored for the other three distributions (EV1, GEV and GP). PILFs were not removed in EasyFit as it compares many distributions and most of them are not affected by the presence of PILFs.

In using EasyFit software, the parameter estimation methods in-built with this software is applied. EasyFit software provides distribution graph of the candidate PDs, which provides a clear visual fitting of the distributions in relation to the observed AMF. The estimated parameters for candidate PDs for stations 143001C, 143007A and 143009A are given in Table 5.3, Table 5.4 and Table 5.5, respectively. The estimated parameters for other stations are provided in Appendix-A

Table 5.3: Estimated parameters for Station 143001C

Distribution	Parameters	Parameters Estimation method
Lognormal	σ = 1.1018, μ = 6.6497	Maximum Likelihood Method (MLE)
Log Pearson type III	α = 129.87, β = 0.09786, γ = -6.0592	Method of Moments
Gumbel	σ = 1534.9, μ = 539.89	Method of Moments
Generalised Pareto	K = 0.33611, σ = 906.41, μ = 60.561	Method of L-moments
Generalised Extreme Value	K = 0.45938, σ = 611.88, μ = 569.44	Method of L-moments

Table 5.4: Estimated parameters for Station 143007A

Distribution	Parameters	Parameters Estimation method
Lognormal	$\sigma = 1.8747$, $\mu = 4.8721$	Maximum Likelihood Method (MLE)
Log Pearson type III	$\alpha = 135.02$, $\beta = -0.16285$, $\gamma = 26.86$	Method of Moments
Gumbel	$\sigma = 699.94$, $\mu = 121.97$	Method of Moments
Generalised Pareto	$K = 0.49192$, $\sigma = 293.06$, $\mu = -50.824$	Method of L-moments
Generalised Extreme Value	$K = 0.57188$, $\sigma = 217.25$, $\mu = 119.61$	Method of L-moments

Table 5.5: Estimated parameters for Station 143009A

Distribution	Parameters	Parameters Estimation method
Lognormal	$\sigma = 1.809$, $\mu = 5.5886$	Maximum Likelihood Method (MLE)
Log Pearson type III	$\alpha = 916.39$, $\beta = -0.0603$, $\gamma = 60.845$	Method of Moments
Gumbel	$\sigma = 1402.5$, $\mu = 235.84$	Method of Moments
General Pareto	$K = 0.50966$, $\sigma = 557.23$, $\mu = -91.044$	Method of L-moments
Generalised Extreme Value	$K = 0.58517$, $\sigma = 417.39$, $\mu = 234.27$	Method of L-moments

To identify the best-fit PD (s) for the station; three GoF tests i.e. K-S, C-S and A-D are applied via EasyFit software. Test results showed that for some station's AMF data series, best-fit distribution types are same for all the three GoF tests, which is regarded as the best outcome. However, for majority of the stations, the best-fit PD types varied. Therefore, a scoring technique is applied to rank and select the best-fit PD for each station. The best-fit PD of a station (where distribution type is not common across the three GoF tests) is the one that has the minimum sum of the rank scores. The results of the A-D, K-S and C-S tests for stations 143009A, 143007A and 143015B are summarised in Table 5.6, Table 5.7 and Table 5.8, respectively. The test statistics for the remaining stations are shown in Appendix-B.

The test statistics of A-D, K-S and C-S test for each station are computed and based on the lowest values of each of the test statistics, initially selected five PDs are ranked. It is clear from Tables 5.6, 5.7 and 5.8 that Log Pearson type III (LP3) distribution best fits the AMF data for Stations 143009A 143007A and 143015B based on the ranks of GoF tests.

Table 5.6: GoF test statistics for five candidate distributions used to fit AMF data for Station 143009A

Distribution	Kolmogorov Smirnov (K-S)		Anderson Darling (A-D)		Chi-Squared (C-S)		Avg. Rank
	Statistic	Rank	Statistic	Rank	Statistic	Rank	
Log Pearson type III	**0.07086**	**1**	**0.40106**	**1**	**0.86208**	**1**	**1.0**
Lognormal	0.07529	2	0.42323	2	1.12460	2	2.0
Generalised Pareto	0.15407	4	1.52180	3	3.54490	3	3.3
Gen. Extreme Value	0.14498	3	1.72000	4	3.60290	4	3.7
Gumbel	0.30794	5	7.16980	5	14.5870	5	5.0

Note: Bold value test statistics *is the best-fit PD according to GoF tests.*

Table 5.7: GoF test statistics for five candidate distributions used to fit AMF data for Station 143007A

Distribution	Kolmogorov Smirnov (K-S)		Anderson Darling (A-D)		Chi-Squared (C-S)		Avg. Rank
	Statistic	Rank	Statistic	Rank	Statistic	Rank	
Log Pearson type III	**0.06307**	**1**	**0.34135**	**1**	**3.14190**	**3**	**1.7**
Lognormal	0.07397	2	0.37311	2	3.38340	4	2.7
Generalised Pareto	0.15655	4	1.54220	3	2.50460	2	3.0
Gen. Extreme Value	0.1464	3	1.79270	4	2.32360	1	2.7
Gumbel	0.30474	5	6.31300	5	14.6900	5	5.0

Note: Bold value test statistics *is the best-fit PD according to GoF tests.*

Table 5.8: GoF test statistics for five candidate distributions used to fit AMF data for Station143015B

Distribution	Kolmogorov Smirnov (K-S)		Anderson Darling (A-D)		Chi-Squared (C-S)		Avg. Rank
	Statistic	Rank	Statistic	Rank	Statistic	Rank	
Log Pearson type III	**0.07531**	**1**	**0.28157**	**1**	**0.62942**	**2**	1.3
Lognormal	0.08028	2	0.30072	2	0.62255	1	1.7
Generalised Pareto	0.11182	3	0.54279	3	3.66680	4	3.3
Gen. Extreme Value	0.13335	4	0.76419	4	1.78780	3	3.7
Gumbel	0.27494	5	3.26390	5	3.99200	5	5.0

Note: Bold value test statistics *is the best-fit PD according to GoF tests.*

A comparative assessment of five candidate PDs for each station is performed to select the best-fit PD. Figure 5.2 shows a GoF test results summary with GoF test rank 1 for all the stations. In carrying out the GoF tests in EasyFit, no outlier/PILF is removed as this outlier/PILF is more important for flood quantile estimation using only LN and LP3 distribution, which has been undertaken using FLIKE. It is seen from this figure that according to A-D test, 18 stations show LP3 as rank 1, while 11 stations show GP as rank 1 and 6 station show GEV as rank 1. Whereas according to K-S test, 7 stations shows rank 1

with LP3, 11 stations rank 1 with GP and 6 stations rank 1with GEV. Table 5.9, Table 5.10 and Table 5.11 show the selected PDs of the 26 stations based on the A-D, K-S and C-S test statistics of rank 1, rank 2 and rank 3, respectively.

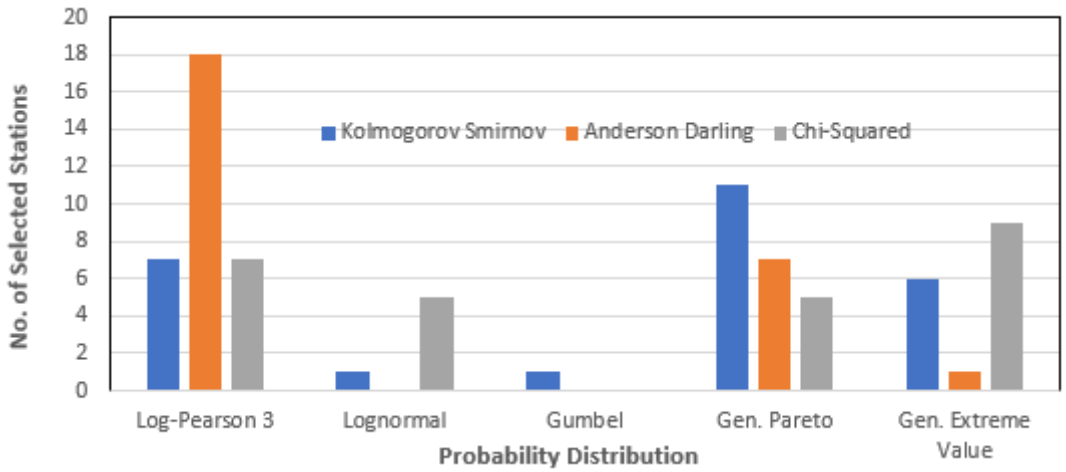

Figure 5.2: GoF tests summary for all selected stations

It is seen from Table 5.9, Table 5.10 and Table 5.11 that LP3 is the rank 1 distribution for 18 out of 26 stations (i.e. 69% of the cases) with A-D GoF test, for 7 out of 26 stations (23%) with K-S GoF test and for 7 out of 26 stations (23%) with C-S GoF test. Generalised Pareto (GP) distribution is ranked second: for 7 out of 26 stations (23%) with A-D GoF test, for 11 out of 26 stations (43%) with K-S GoF test, and for 5 out of 26 stations (19%) with C-S GoF test.

Table 5.9: Rankings of probability distributions for 26 stations based on A-D GoF test

Station	Probability distribution corresponding to ranks of A-D GoF test		
	I	II	III
143001C	GP	LP3	Lognormal
143007A	LP3	Lognormal	GP
143009A	LP3	Lognormal	GP
143010B	LP3	Lognormal	GP
143015B	LP3	Lognormal	GP
143028A	LP3	GEV	Lognormal
143032A	GP	LP3	GEV
143033A	GP	LP3	Lognormal
143107A	LP3	GEV	Lognormal
143108A	LP3	GEV	Lognormal
143110A	LP3	GEV	Lognormal
143113A	LP3	Lognormal	GEV
143203C	LP3	GEV	Lognormal
143207A	LP3	Lognormal	GP
143209B	GP	GEV	LP3
143212A	LP3	Lognormal	GP
143219A	LP3	Lognormal	GP
143229A	LP3	Lognormal	GP
143303A	GEV	LP3	Gumbel
143921A	LP3	Lognormal	GP
143210B	GP	GEV	LP3
143306A	GP	LP3	GEV
143213C	LP3	Lognormal	GP
143232A	LP3	GEV	Gumbel
143233A	LP3	GP	GEV
143307A	GP	LP3	Lognormal

Table 5.10: **Rankings of probability distributions for 26 stations based on K-S test**

Station	Probability distribution corresponding to ranks of K-S GoF test		
	I	II	III
143001C	GP	Lognormal	LP3
143007A	LP3	Lognormal	GEV
143009A	LP3	Lognormal	GEV
143010B	GP	LP3	GEV
143015B	LP3	Lognormal	GP
143028A	LP3	GEV	Lognormal
143032A	GEV	LP3	GP
143033A	GP	LP3	Lognormal
143107A	GEV	LP3	GP
143108A	GEV	LP3	GP
143110A	GP	LP3	GEV
143113A	Gumbel	GP	GEV
143203C	GP	LP3	GEV
143207A	LP3	Lognormal	GP
143209B	GP	LP3	Lognormal
143212A	LP3	Lognormal	GEV
143219A	GP	LP3	Lognormal
143229A	GEV	GP	LP3
143303A	GEV	LP3	Gumbel
143921A	LP3	Lognormal	GEV
143210B	GEV	Gumbel	LP3
143306A	GP	LP3	GEV
143213C	Lognormal	LP3	GP
143232A	GP	GEV	LP3
143233A	GP	LP3	GEV
143307A	GP	LP3	Lognormal

Table 5.11: **Rankings of probability distributions for 26 stations based on C-S test**

Station	Probability distribution corresponding to ranks of C-S GoF test		
	I	II	III
143001C	Lognormal	GP	LP3
143007A	GEV	GP	LP3
143009A	LP3	Lognormal	GP
143010B	GEV	LP3	GP
143015B	Lognormal	LP3	GEV
143028A	LP3	GEV	Lognormal
143032A	GP	GEV	LP3
143033A	GP	Lognormal	LP3
143107A	GEV	LP3	Lognormal
143108A	GEV	LP3	Lognormal
143110A	LP3	GEV	Lognormal
143113A	GEV	Gumbel	LP3
143203C	LP3	Lognormal	GEV
143207A	GEV	GP	LP3
143209B	GP	GEV	LP3
143212A	Lognormal	LP3	GP
143219A	LP3	GP	GEV
143229A	Lognormal	LP3	GP
143303A	LP3	GEV	Gumbel
143921A	GP	GEV	Lognormal
143210B	GEV	LP3	Lognormal
143306A	GEV	Gumbel	LP3
143213C	Lognormal	LP3	GP
143232A	LP3	GEV	Gumbel
143233A	GEV	GP	LP3
143307A	GP	Gumbel	LP3

The average of three GoF test results for rank 1, rank 2 and rank 3 are computed to find the most preferred PD for each station. Table 5.12 shows the average of three GoF test results with rank 1. The average of three GoF test results with rank 2 and rank 3 are given in Appendix-B (Table B.24 and Table B.25). It is seen that according to the average of three different GoF tests with rank 1, LP3 is the most preferred distribution for 11 stations, followed by GP with 8 stations. Gumbel is the lowest, with no station's AMF data fit this distribution. In Table 5.13, a station with rank 1 best-fit distribution is multiplied by weight of 3, rank 2 best-fit distribution is multiplied by weight of 2, and rank 3 best-fit distribution is multiplied by weight of 1. The average of the GoF test results in Table 5.13 shows that for 10 out of 26 stations, LP3 distribution is the most preferred PD, followed by GP. It is also seen

that Gumbel distribution is the least preferred PD as only the K-S GoF test selects this for only one station as rank 1.

Table 5.12: GoF test summary (number distributions with rank 1, for all the stations)

Probability Distribution	K-S test	A-D test	C-S test	Avg. no. of stations
	Number of stations with GoF test, Rank 1			
Log Pearson type III	7	18	7	11
Lognormal	1	0	5	2
Gumbel	1	0	0	0
Generalised Pareto	11	7	5	8
Gen. Extreme Value	6	1	9	5

Table 5.13: GoF test summary (number of distributions with ranks 1, 2, and rank 3 for all stations with weights for rank 1, rank 2 and rank 3)

Probability Distribution	K-S test	A-D test	C-S test	K-S test	A-D test	C-S test	K-S test	A-D test	C-S test	Avg. no. of stations
	Number of stations with GoF test Rank 1			Number of stations with GoF test Rank 2			Number of stations with GoF test Rank 3			
	Weight = 3			Weight = 2			Weight = 1			
Log Pearson type III	21	54	21	28	12	16	4	2	10	11
Lognormal	3	0	15	14	22	6	5	8	6	2
Gumbel	3	0	0	2	0	6	1	2	2	0
Generalised Pareto	33	21	15	4	2	10	6	10	5	8
Gen. Extreme Value	18	3	27	4	16	14	10	4	3	5

Figure 5.3 shows the location of stations with the best-fit PDs based on the A-D GoF test. It is seen that LP3 is the best-fit distribution model for majority of the gauging sites at upper part of the catchment i.e. LP3 is the most suited PD for mountainous area of the catchment ((within red and green circle) of Figure 5.3) and GP distribution appears to be most appropriate PD for downstream catchments. However, LP3 distribution is dominating over most of the Brisbane River catchment, which is an important finding.

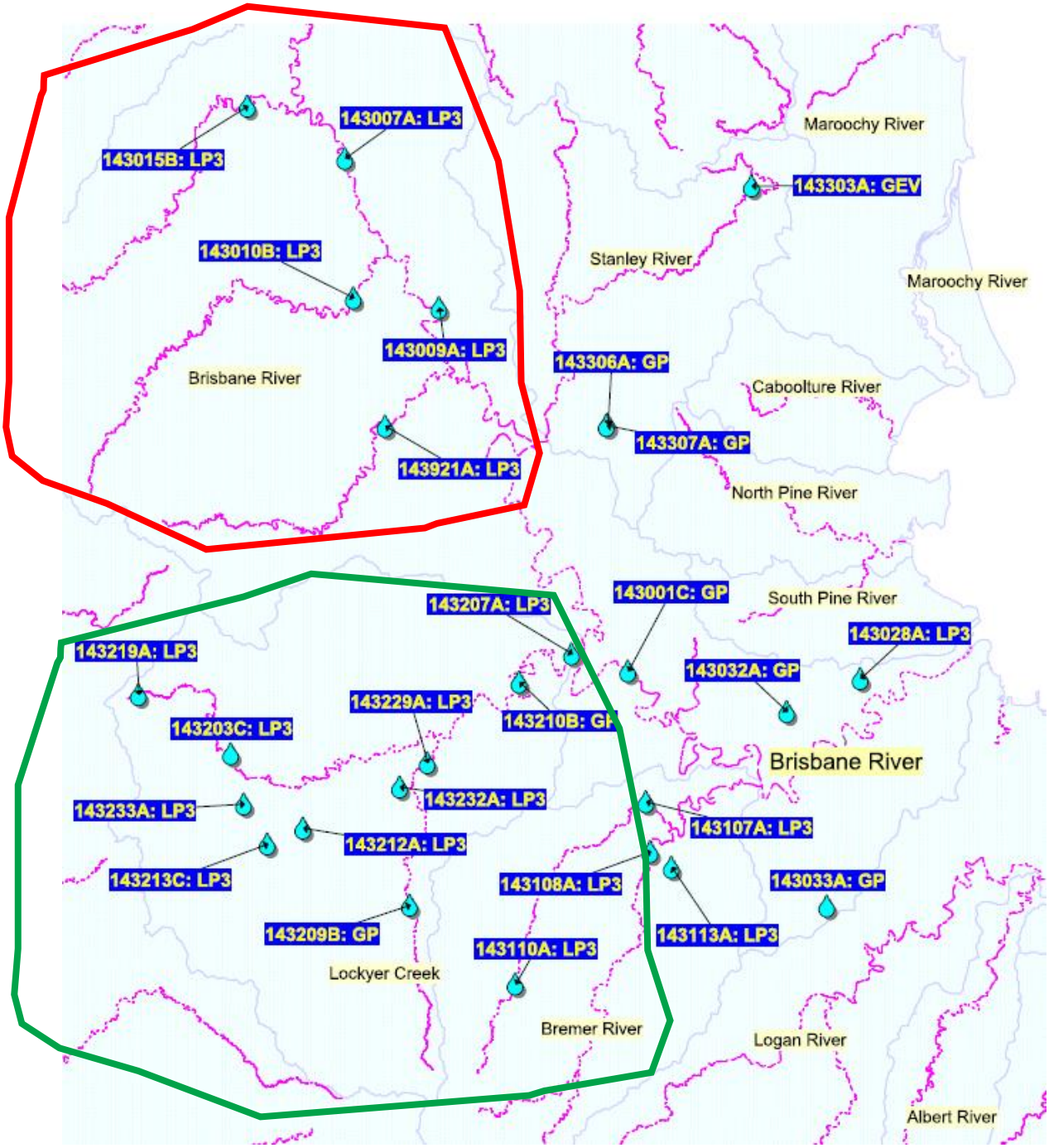

Figure 5.3: Geographical presentation of the best-fit distributions based on A-D test

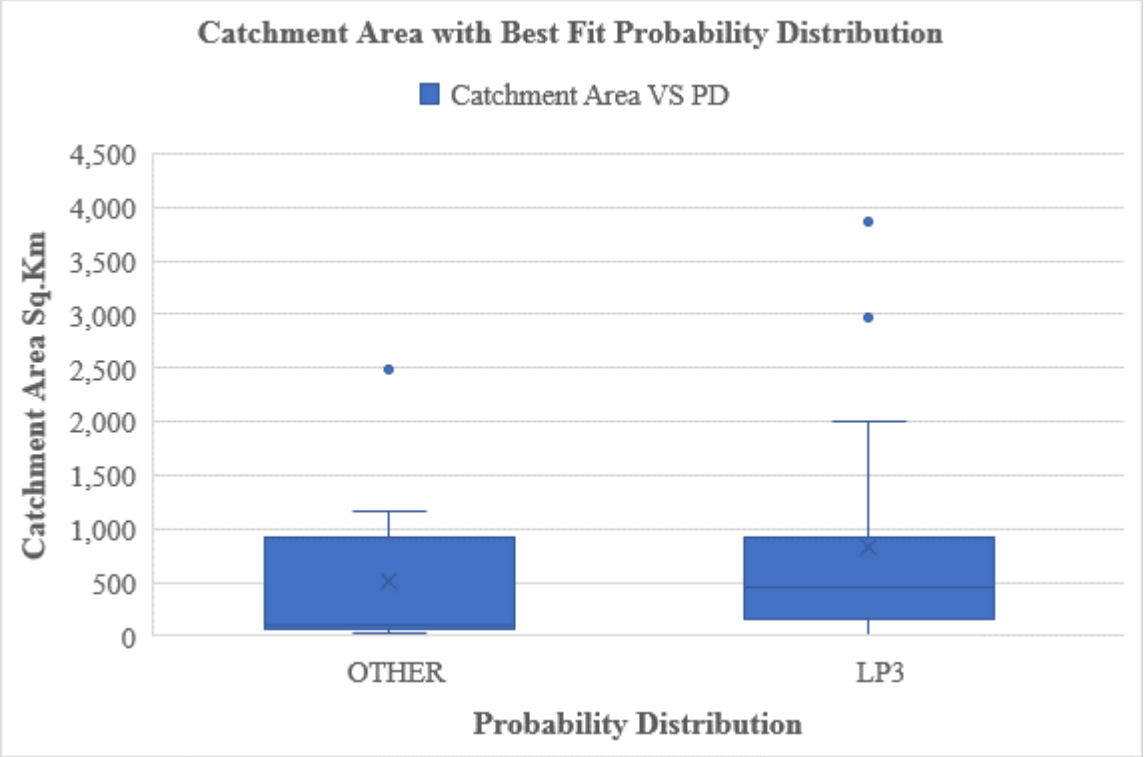

Figure 5:4: Box plot of the best-fit distributions with catchment area

It is seen from box plot of catchment area and best-fit distribution (Figure 5.4) of the selected stations that there is no relationship between catchment area and the best-fit PD.

The distribution plots are used to visually identify probability distribution that fits AMF data. The best-fit PD from the GoF tests for each station is compared with graphical fitting method using EasyFit generated graphs (Q-Q plot, PDF Graph, CDF Graph, P-P plot, Probability Difference graph) and FLIKE generated graphs. The PDF for the candidate PDs (Figure 5.5) at site 143028A shows that GEV, LP3, and LN distributions fit AMF series better than other two PDs. The histogram (Figure 5.5a) of AMF series indicates a positive skewed unimodal distribution skewed to the right. The PDF plots (Figure 5.5a) of all the five distributions are used to fit the empirical histograms of AMF data. It is seen form the PDF graph (Figure 5.5a) that the LN and LP3 distributions exhibit similar probability densities and their probability densities are very different than the probability densities of Gumbel and GP distributions. The CDF graph (Figure 5.5b) shows CDF of five theoretical distributions and empirical CDF from AMF data. The probability-probability (P-P) plot (Figure 5.5c) shows that CDF of LP3 is relatively closer to empirical CDF. The AMF magnitude and theoretical quantiles (Q-Q

plot) graph (Figure 5.5d) shows that quantiles form Lognormal and LP3 distributions are closer to sample quantiles.

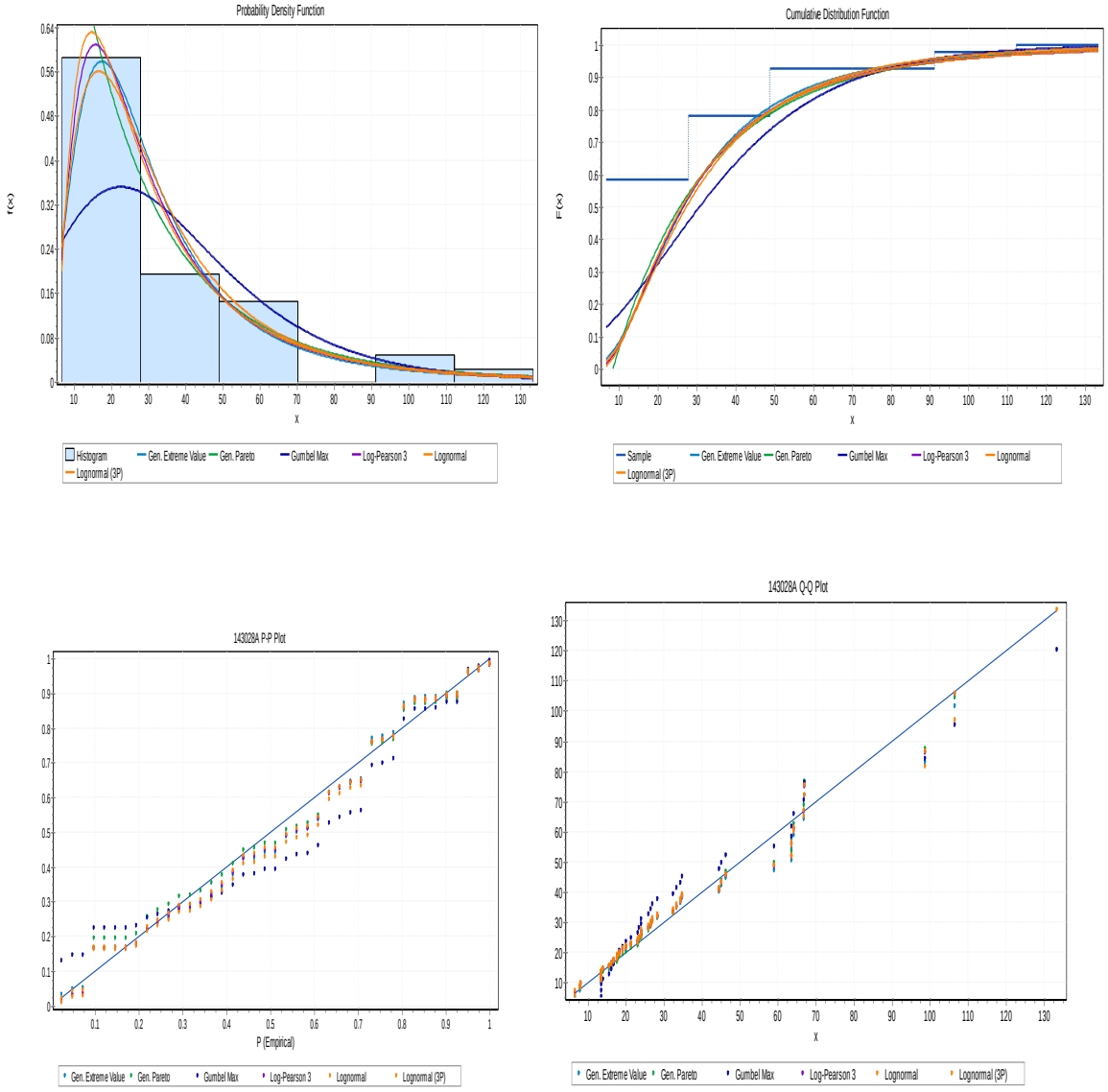

Figure 5:5: (a) PDF graph (b) CDF graph (c) P-P plot and (d) Q-Q plot for Station 143028A (obtained from EasyFit)

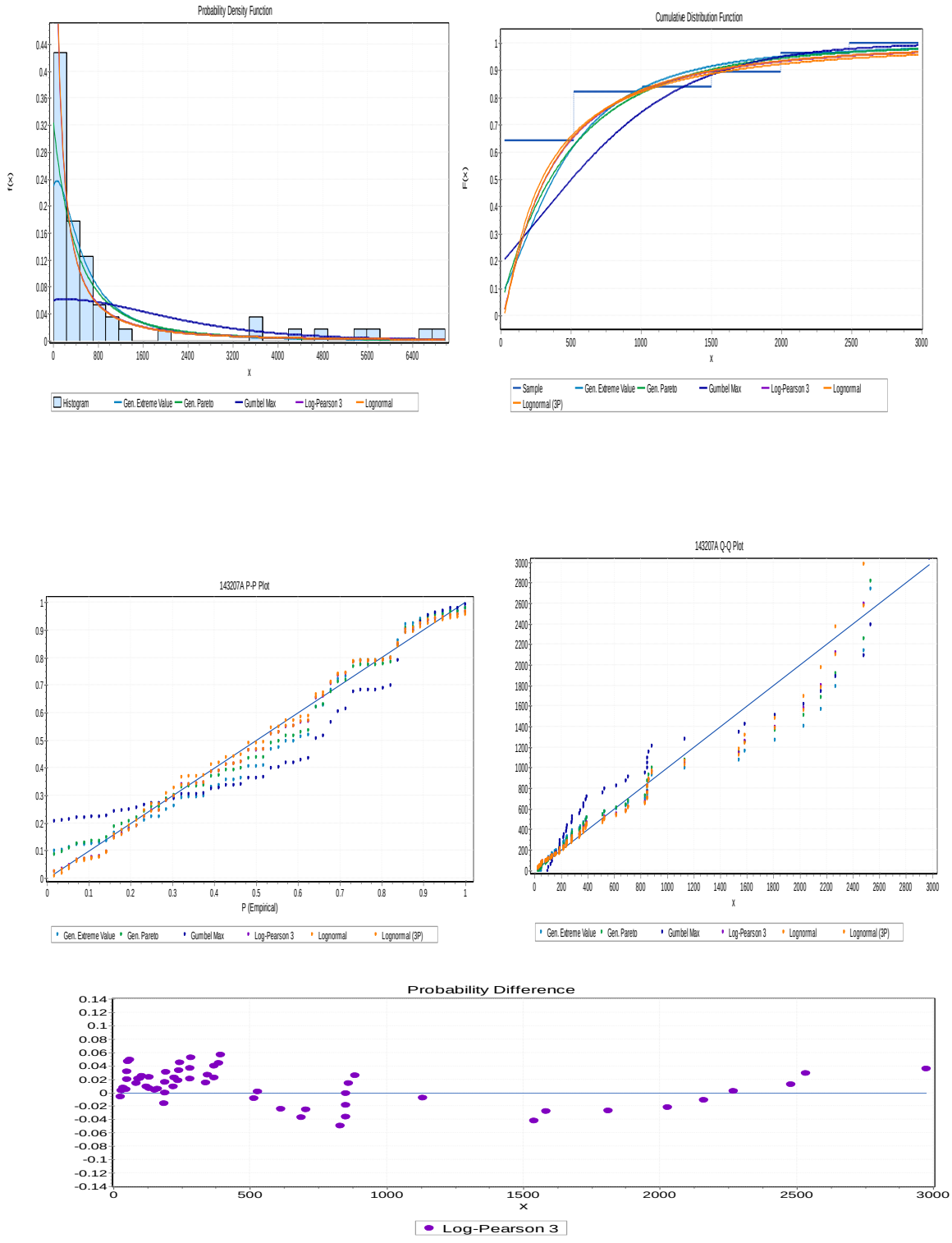

Figure 5.6: (a) PDF graph (b) CDF graph (c) P-P plot (d) Q-Q plot and (e) Probability Differences graph for Station 143207A (obtained from EasyFit)

Figure 5.6 shows PDF graph, CDF graph, Q-Q plot, P-P plot and Probability Difference graph of the five candidate PDs for Station 143207A. The PDF (Figure 5.6a) graph shows

GEV and LP3 as the better fit, the CDF graph (Figure 5.6b) shows LP3 and LN as better fit at high flow events compared to other candidate distributions. The P-P plot (Figure 5.6c) and Q-Q plot (Figure 5.6d) show LN and LP3 fit better towards highest flood events. The probability difference graph (Figure 5.6e) shows LP3 and LN fit better to AMF data. It is seen that that LP3 and Lognormal show the best fit than the other three distributions. The Gumbel distribution generally shows a poor fit. The histogram of AMF data (Figure 5.6a) shows recorded AMF frequency distribution is skewed to the right with single peak. From the PDF diagram, we can see that AMF data is skewed to the right. The probability difference graph also shows that LP3 is a relatively better fit distribution. The test statistics show that skewness of the AMF data of this station is below 0.6. The candidate distribution can be assessed as 'good fit' with AMF data if maximum absolute difference becomes lower than 5% (Singo et al., 2012). For LP3 distribution, the difference is within 5% (Fig. 5.6e) indicating an acceptable fit. The distribution plots for other stations are shown in Appendix-C.

FLIKE Probability Plots display estimated quantile line form candidate distributions, the AMF data and the confidence limit. The Y-axis of FLIKE probability plot is estimated quantile and observed AMF and the x-axis is AEP 1 in Y (ARI). FLIKE graphs for visual assessment in Figures 5.7 to 5.18 show fitting, estimated quantile as well as confidence limits. The result from graphical plots and that from GoF tests show that the best-fit distribution based on the statistical hypothesis GoF test result does not fully agree with the graphical observation for several stations. As discussed in the earlier part of this chapter that according to the GoF test results, LP3 distribution is the most preferred PD for many stations, followed by GP distribution. However, graphical assessment indicates for only 9 stations, LP3 is the best-fit PD.

The visual assessment of probability graphs of the AMF records and the distribution models for Station 143001C are shown in Figure 5.7 for LP3, Figure 5.8 for LN and Figure 5.9 for all the distributions. The visual graphs for Station 143028A are shown in Figure 5.10 for LP3, Figure 5.11 for GEV and Figure 5.12 for all the distributions. The visual graphs for station 143007A are shown in Figure 5.13 for LP3, Figure 5.14 for LN and Figure 5.15 for all distributions and visual graph for station 143032A are in Figure 5.16 (GP), Figure 5.17 (LP3), and Figure 5.18 (all distributions).

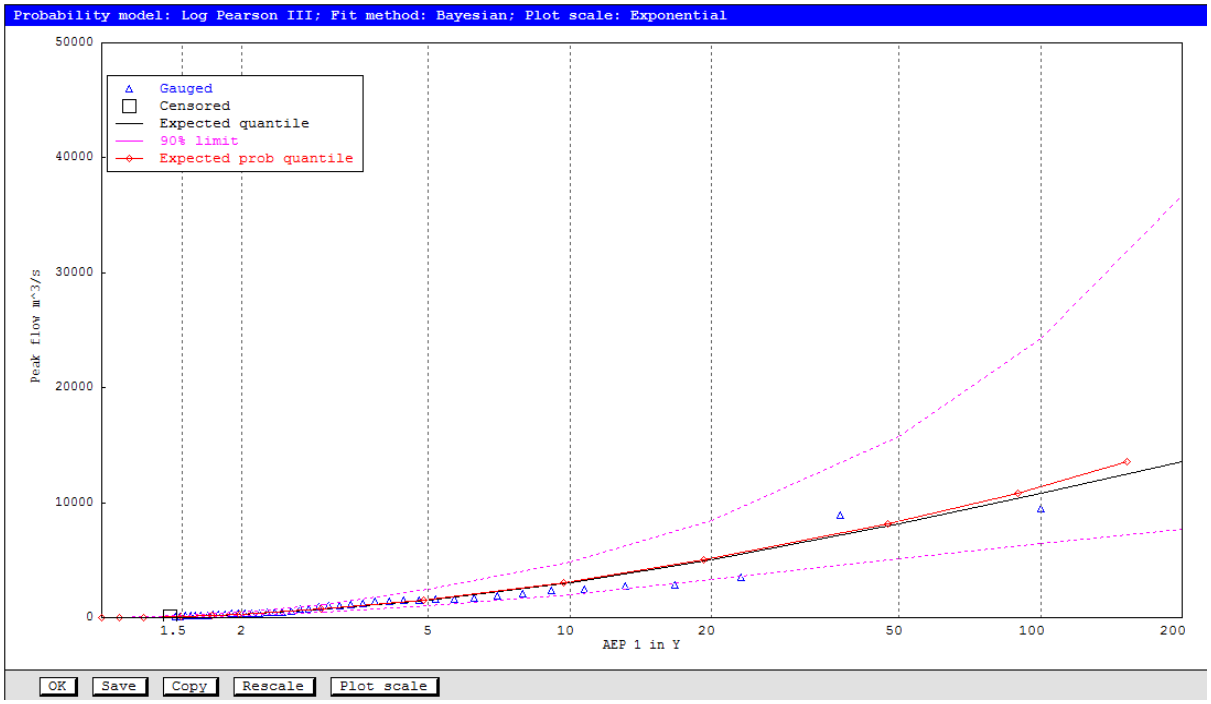

Figure 5.7: Estimated Quantile and AMF data vs ARI (AEP 1 in Y) plot for LP3 probability model for Station 143001C

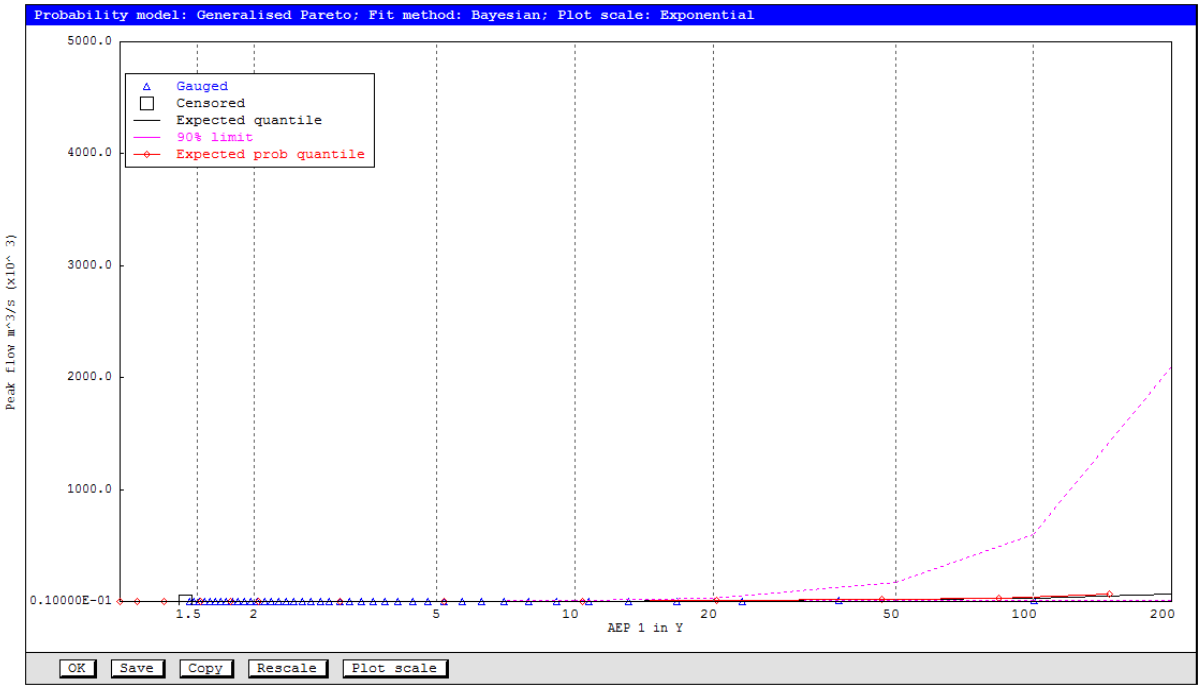

Figure 5.8: Estimated Quantile and AMF data vs ARI (AEP 1 in Y) plot for GP probability model for Station 143001C

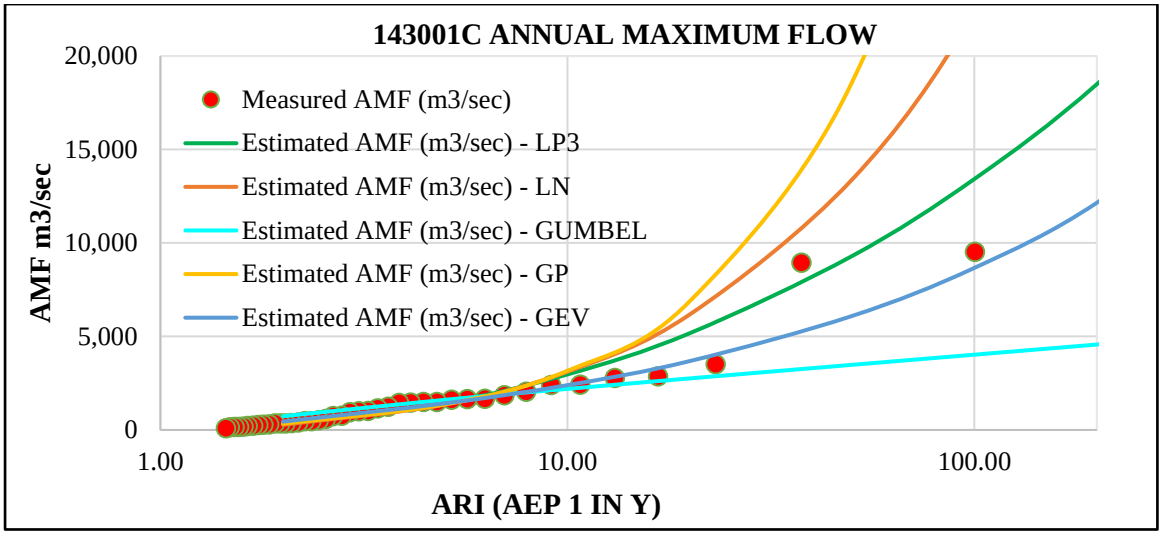

Figure 5.9: Estimated Quantile and AMF data vs ARI (AEP 1 in Y) plot for 5 probability models for Station 143001C

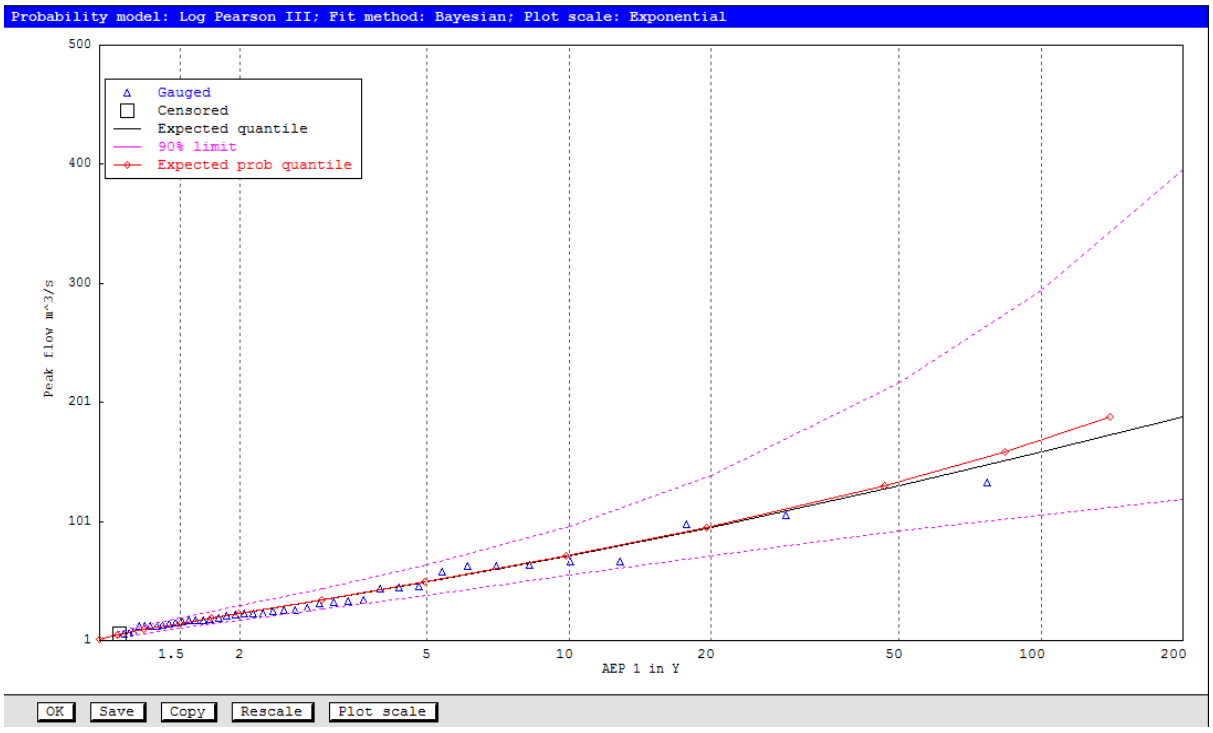

Figure 5.10: Estimated Quantile and AMF data vs ARI (AEP 1 in Y) plot for LP3 probability model for Station 143028A

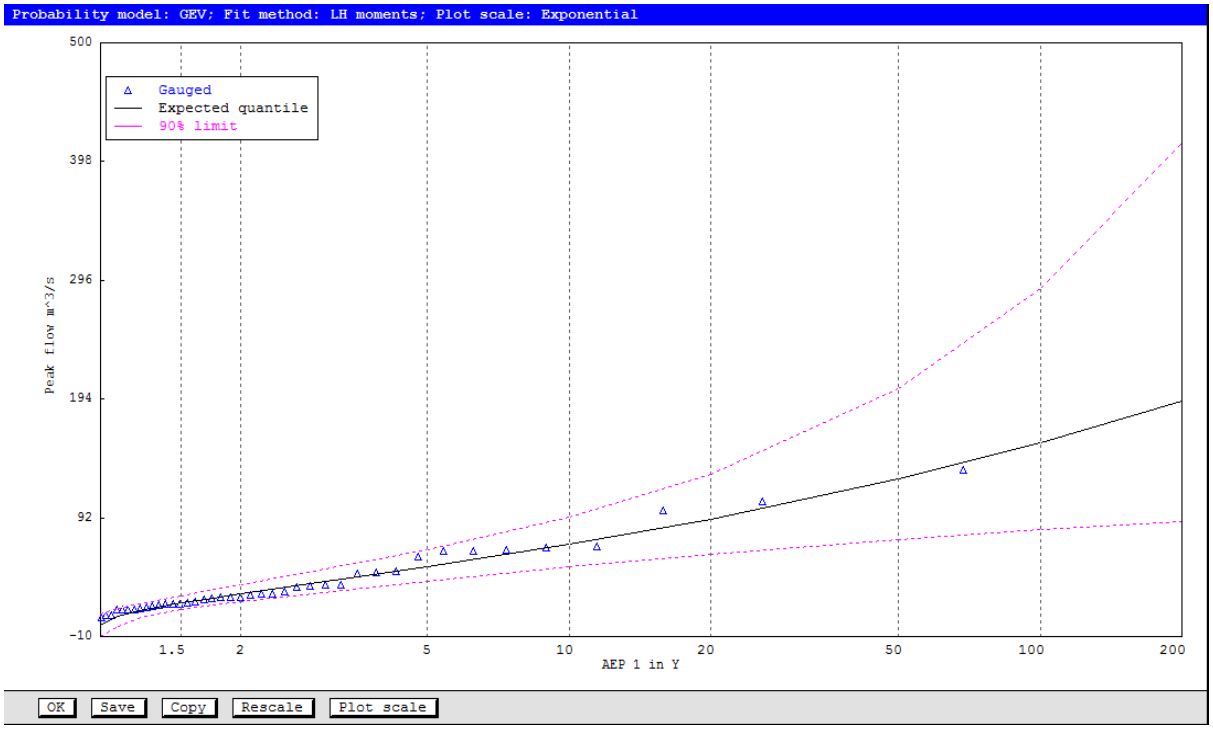

Figure 5.11: Estimated Quantile and AMF data vs ARI (AEP 1 in Y) plot for GEV probability model for Station 143028A

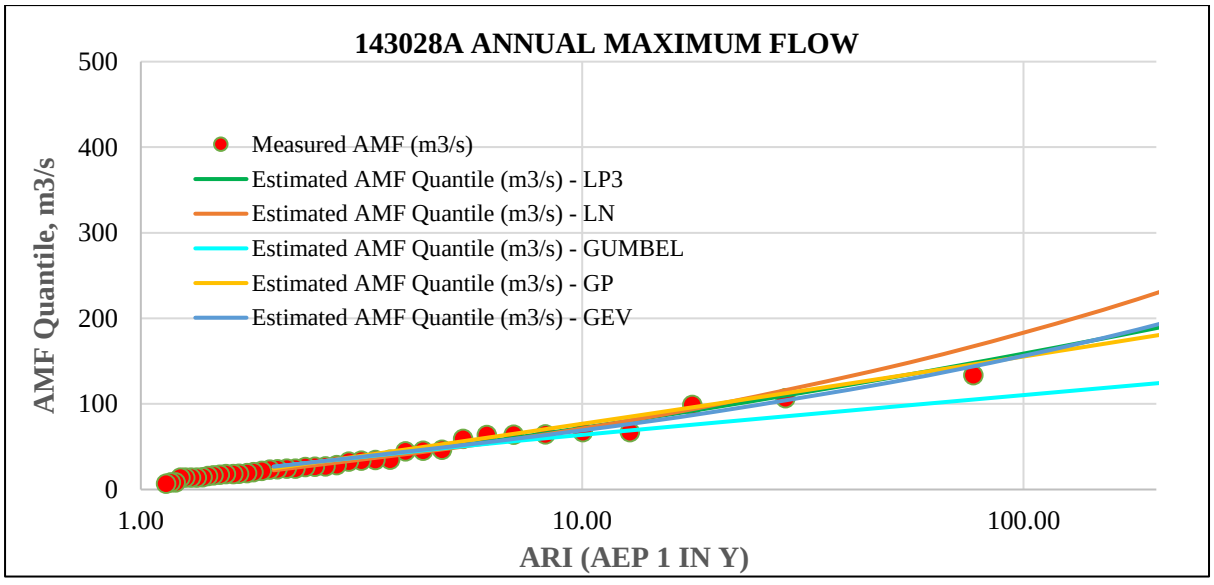

Figure 5.12: Estimated Quantile and AMF data vs ARI (AEP 1 in Y) plot for 5 probability models for Station 143028A

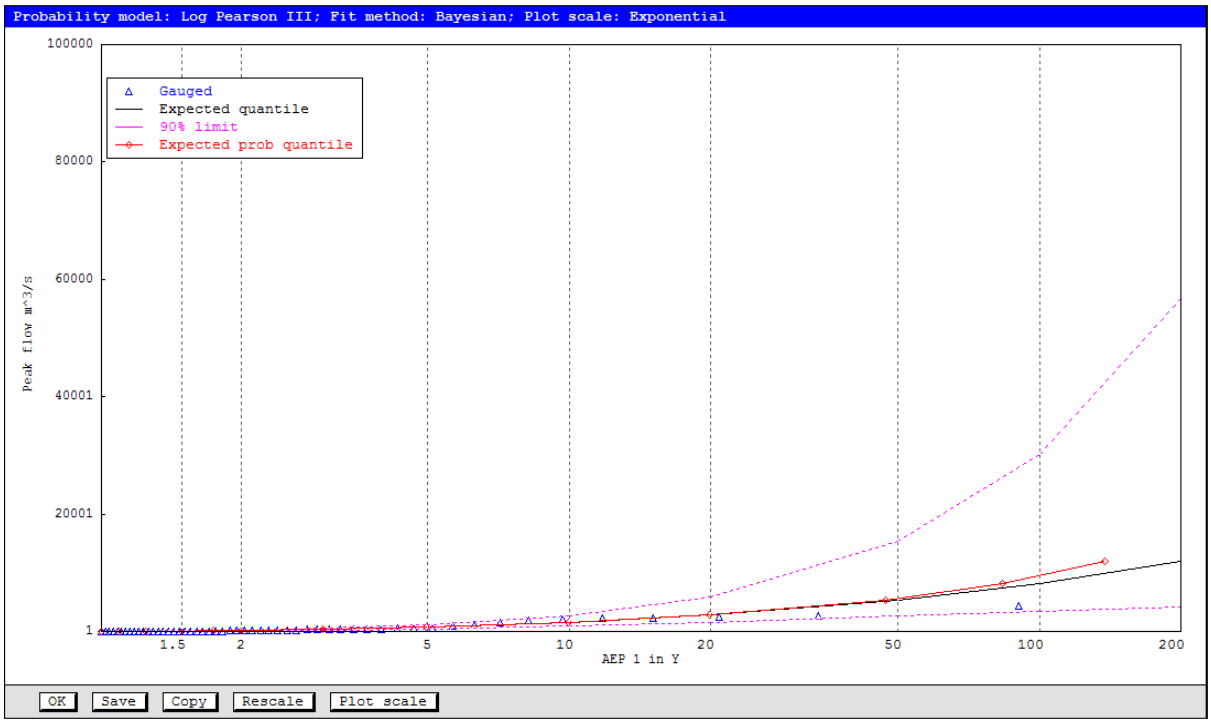

Figure 5:13: Estimated Quantile and AMF data vs ARI (AEP 1 in Y) plot for LP3 probability model for Station 143007A

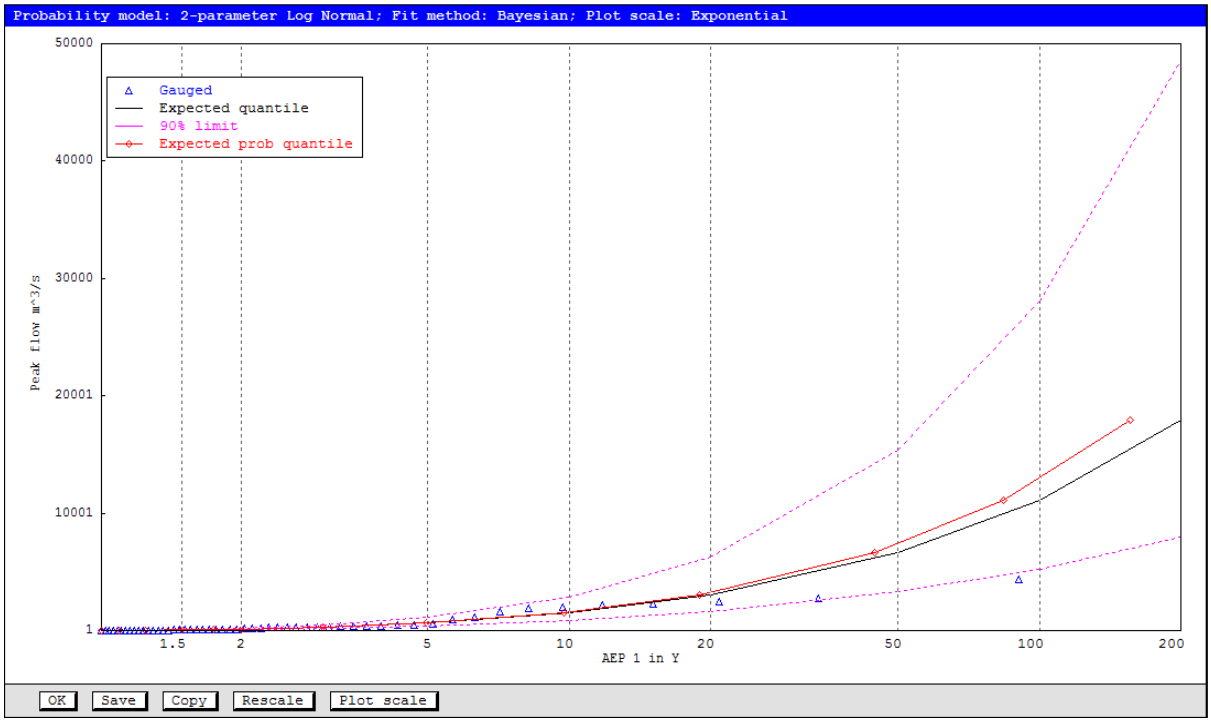

Figure 5:14: Estimated Quantile and AMF data vs ARI (AEP 1 in Y) plot for LN probability model for Station 143007A

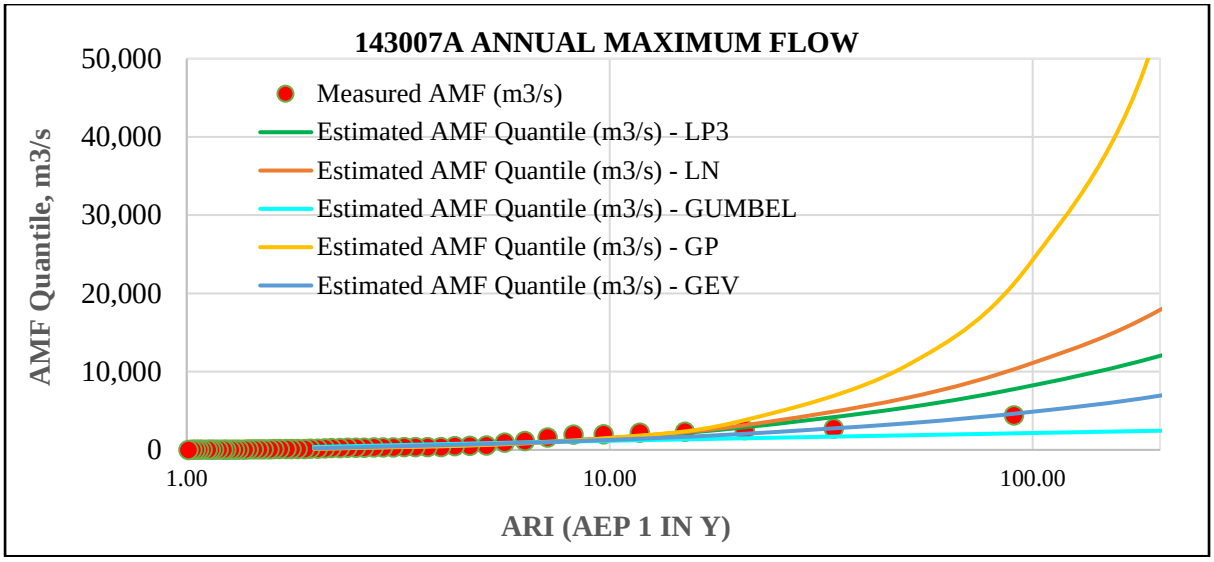

Figure 5:15: Estimated Quantile and AMF data vs ARI (AEP 1 in Y) plot for 5 probability models for Station 143007A

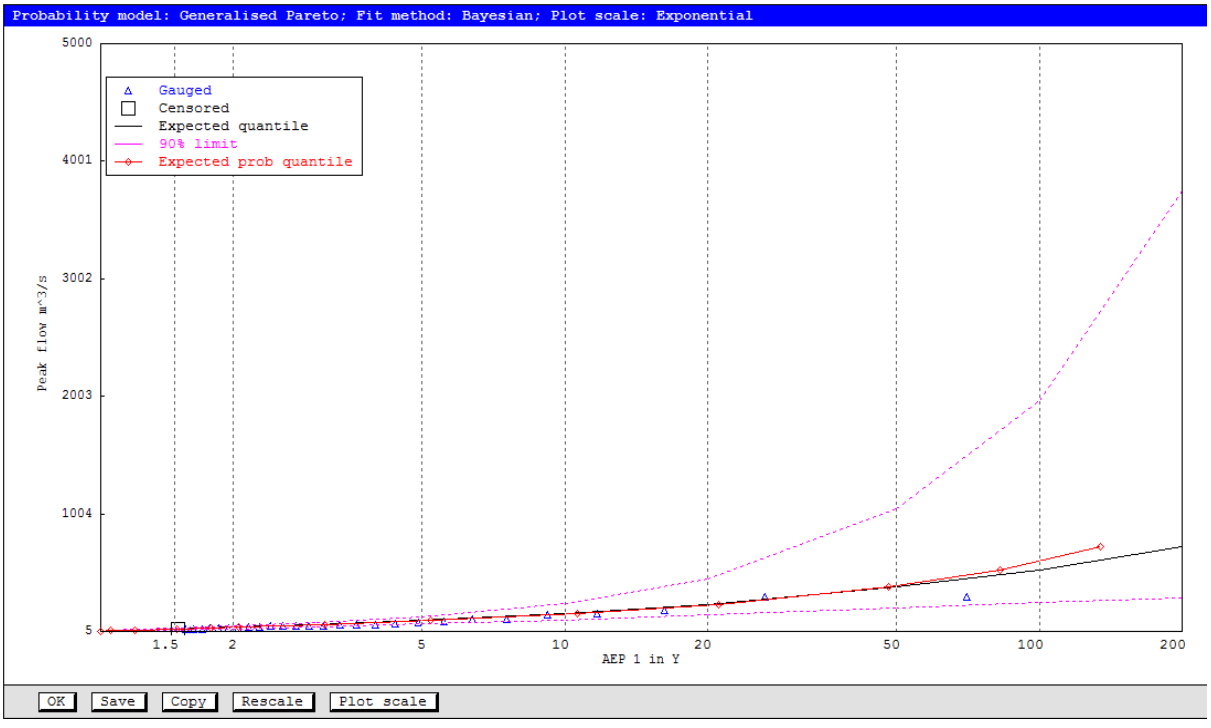

Figure 5.16: Estimated Quantile and AMF data vs ARI (AEP 1 in Y) plot for GP probability model for Station 143032A

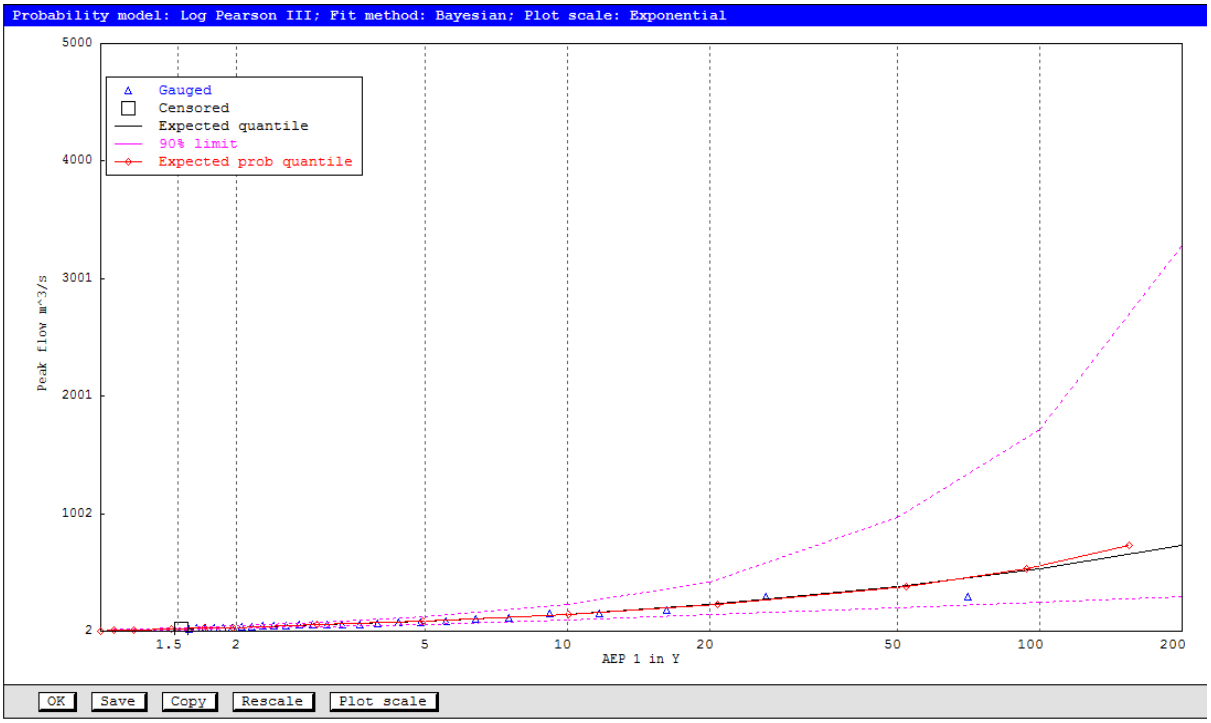

Figure 5.17: Estimated Quantile and AMF data vs ARI (AEP 1 in Y) plot for LP3 probability model for Station 143032A

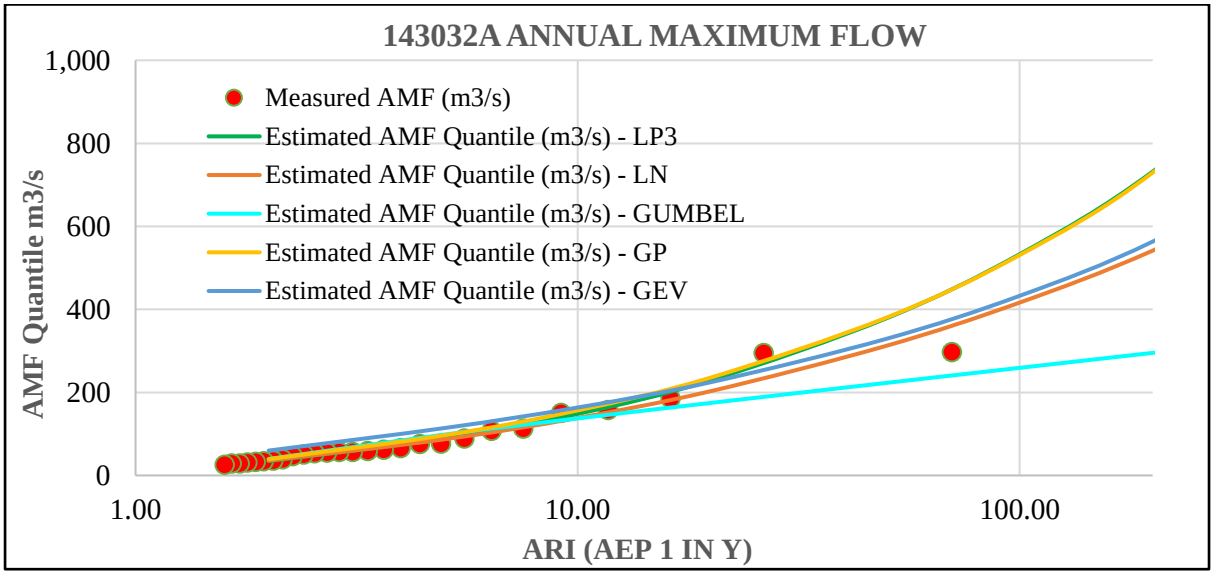

Figure 5.18: Estimated Quantile and AMF data vs ARI (AEP 1 in Y) plot for 5 probability models for Station 143032A

The visual observation from Figures 5.7, 5.8 and 5.9 for Station 143001C show that LP3 is the most closely fitted PD for flood quantile estimation. Although the A-D and K-S test show that the best-fit PD is GP (followed by LP3/LN). For station 143028A (Figure 5.10 to 5.12), LP3, GEV and GP appear to be representative PD for quantile estimation. For this station, GoF test results demonstrate that LP3 (followed by GEV) is the best-fit PD. For station 143007A (Figure 5.13 to 5.15), the most representative PD from visual assessment is GEV (followed by LP3). The GoF test result for this station shows that LP3 (followed by LN) is the best-fit PD. For station 143032A (Figure 5.16 to 5.18), GP is the best-fit PD as per A-D test and with visual fit. However, the K-S test indicates GEV as the best-fit PD. The comparison between visual and statistical GoF test for all the stations are summarised in Table-5.14. From this table, it is observed that out of 26 stations, 10 stations show LP3 as the most appropriate PD using both the A-D and GoF test and visual assessment. That is, for only 38% cases, GoF test results agree with visual assessment. Therefore, it is more appropriate to select a best-fit distribution model using both GoF tests and visual assessment. If both the methods do not agree, a decision should be made based on regional analysis and hydrological judgement by experts.

The above results show that GoF test results may not agree with the visual assessment, although visual assessment in FFA is widely practiced. Another important issue is that most of the high AMF data values suffer from very high rating curve extrapolation error (Rahman et al., 2019) and hence their relative locations in the FFA plot is tentative, and hence visual assessment has little validity in the region of high flows.

From both the GoF test results and graphical assessment, it can be concluded that LP3 is the most favourable PD for FFA in the Brisbane River catchment. It should be noted that LP3 was also found as the most appropriate PD by Rahman et al. (2013) in their investigation for at-site FFA based on larger number of data set from Australia. They recommended that LP3 is one of the top three best-fit distributions. LP3 distribution was recommended as the most favourable PD in Australia in the ARR 1987. However, the latest ARR 2019 does not specify any particular PD as the best model for flood estimation. Zaman et al. (2012) in their study for at-site FFA (using data across Australia) recommended LP3 and GEV distributions as the best-fit PD for flood estimation for majority of the stations.

Table 5.14: Best-fit probability distribution: comparing GoF test result and visual assessment

Station	Anderson Darling Rank 1	FLIKE Visual Rank 1	Agree (Yes/No)
143015B	LP3	LP3	Yes
143207A	LP3	LP3	Yes
143921A	LP3	LP3	Yes
143213C	LP3	LP3	Yes
143113A	LP3	LP3	Yes
143010B	LP3	LP3	Yes
143110A	LP3	LP3	Yes
143232A	LP3	LP3	Yes
143233A	LP3	LP3	Yes
143107A	LP3	LP3	Yes
143203C	LP3	GP	No
143007A	LP3	GEV	No
143009A	LP3	GEV	No
143028A	LP3	GEV	No
143212A	LP3	GEV	No
143219A	LP3	GP	No
143108A	LP3	GP	No
143229A	LP3	GP	No
143001C	GP	LP3	No
143032A	GP	GP	Yes
143033A	GP	GEV	No
143209B	GP	GEV	No
143306A	GP	GEV	No
143307A	GP	GEV	No
143210B	GP	GEV	No
143303A	GEV	GP	No

5.3 Quantile estimation

FLIKE software is used for estimation of flood quantile for different ARIs (*T*). Figures 5.19 to 5.23 and Figures 5.24 to 5.28 show the flood quantile estimation plots for Stations 143007A and 143028A, respectively. All other stations' probability plots of estimated quantile with LP3 model are provided in Appendix-D. It is seen from probability plots (Figures 5.19 to 5.23) that GEV appears to be the most favourable PD at 143007A. From probability plots (Figures 5.24 to 5.28), it appears that LP3 is the best-fit probability model at

143028A. From GoF tests, LP3 is found to be the most appropriate probability model for both 143007A and 143028A. From analysis it is evident that the best-fit distribution from visual observation and that from GoF test results do not agree for all the stations. Therefore, it is important to check both visual observation and GoF test results to decide the best-fit PD for a given station. Tables 5.15 and 5.16 show the estimated flood quantiles and Monte Carlo 90% quantile probability limits, with LP3 PD for Stations 143007A and for station 143028A, respectively. The flood quantile estimates for other stations are provided in Appendix-E.

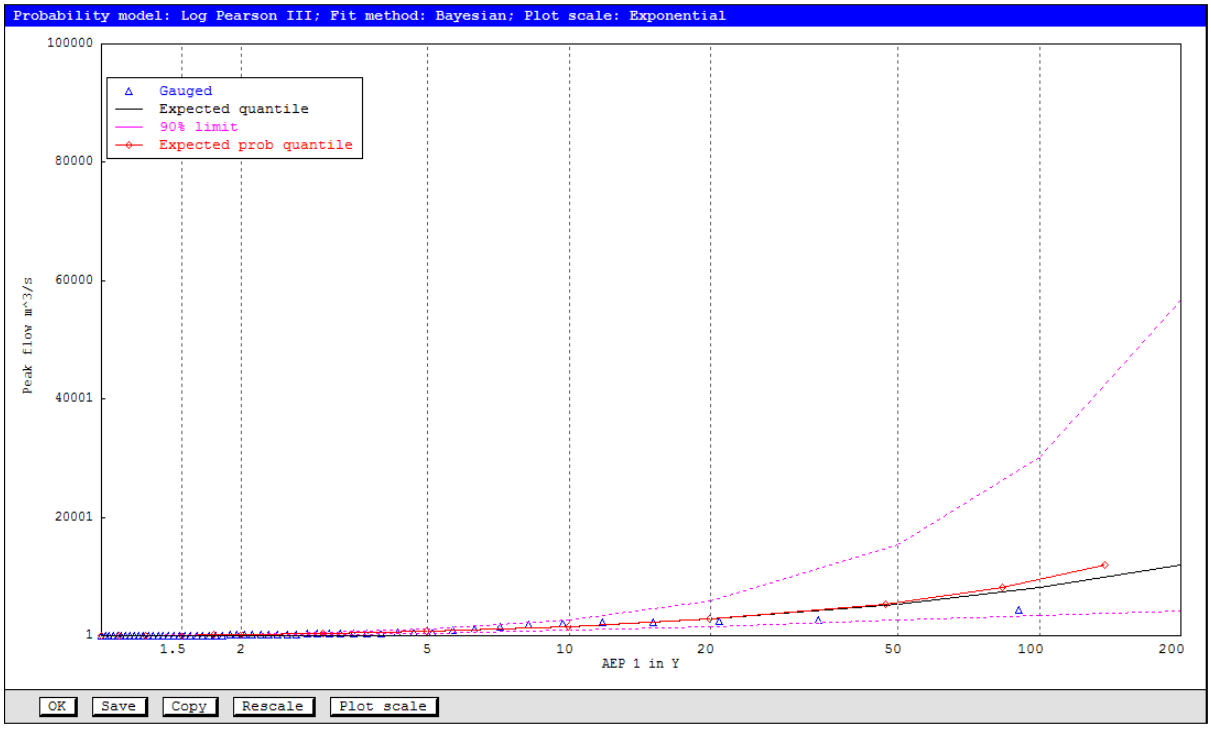

Log Pearson type III

Figure 5:19: Estimated quantile with LP3 probability distributions for 143007A using FLIKE

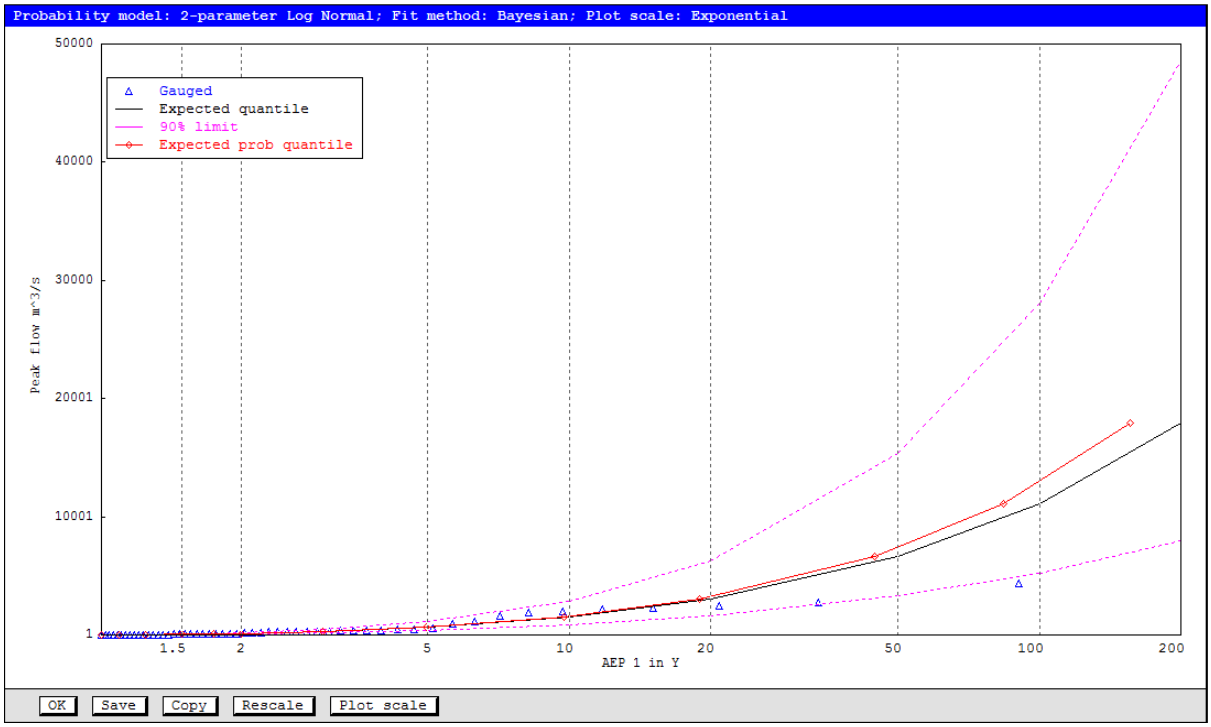

Lognormal

Figure 5:20: Estimated quantile with LN probability distributions for 143007A, using FLIKE

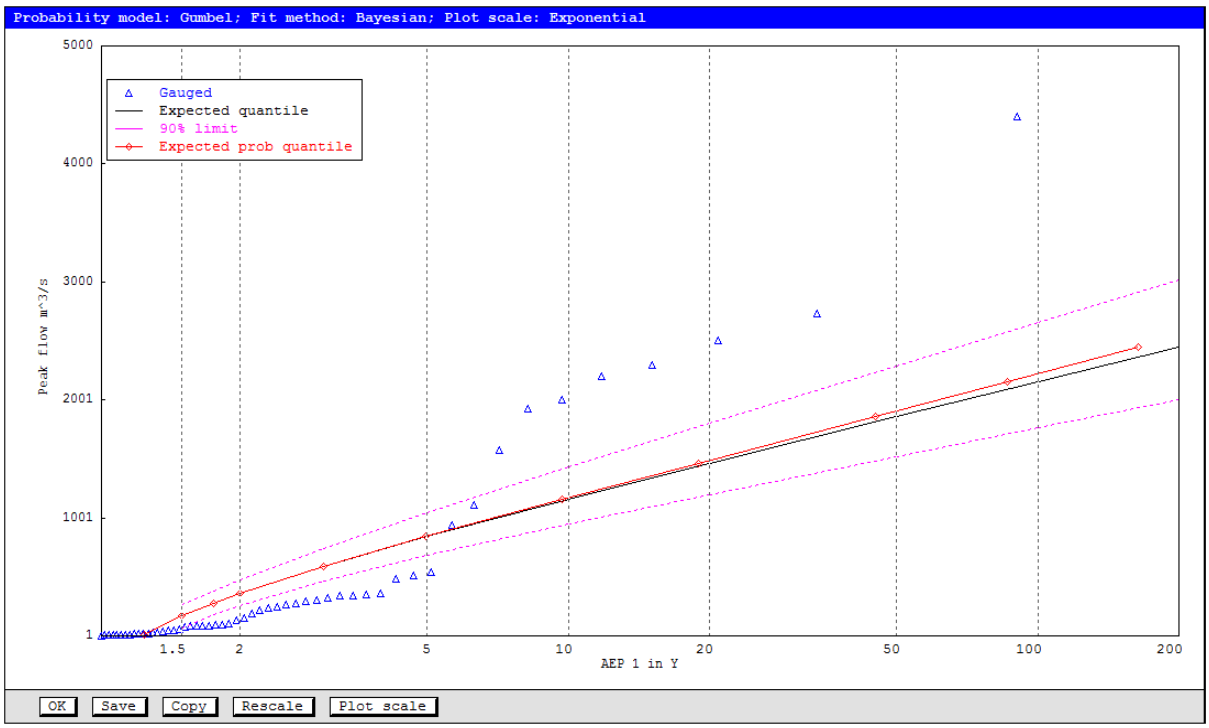

Gumbel

Figure 5:21: Estimated quantile with Gumbel probability distributions for 143007A, using FLIKE

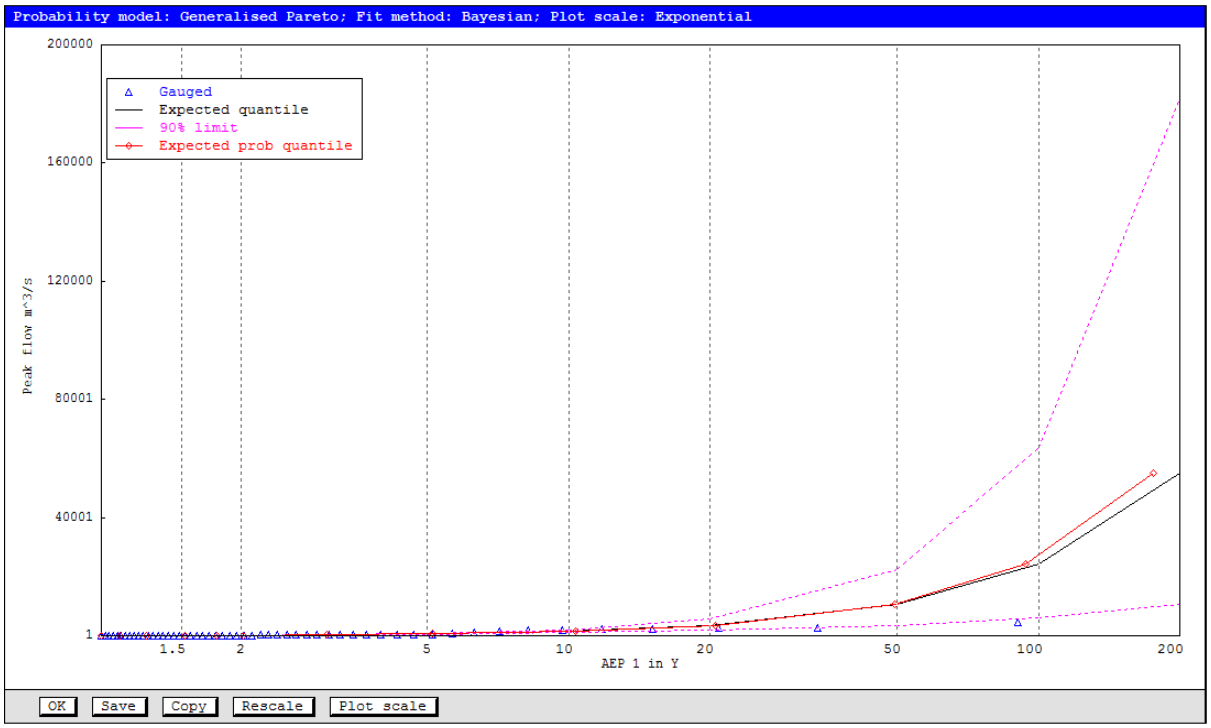

Generalised Pareto

Figure 5:22: Estimated Quantile with GP probability distributions for 143007A, using FLIKE

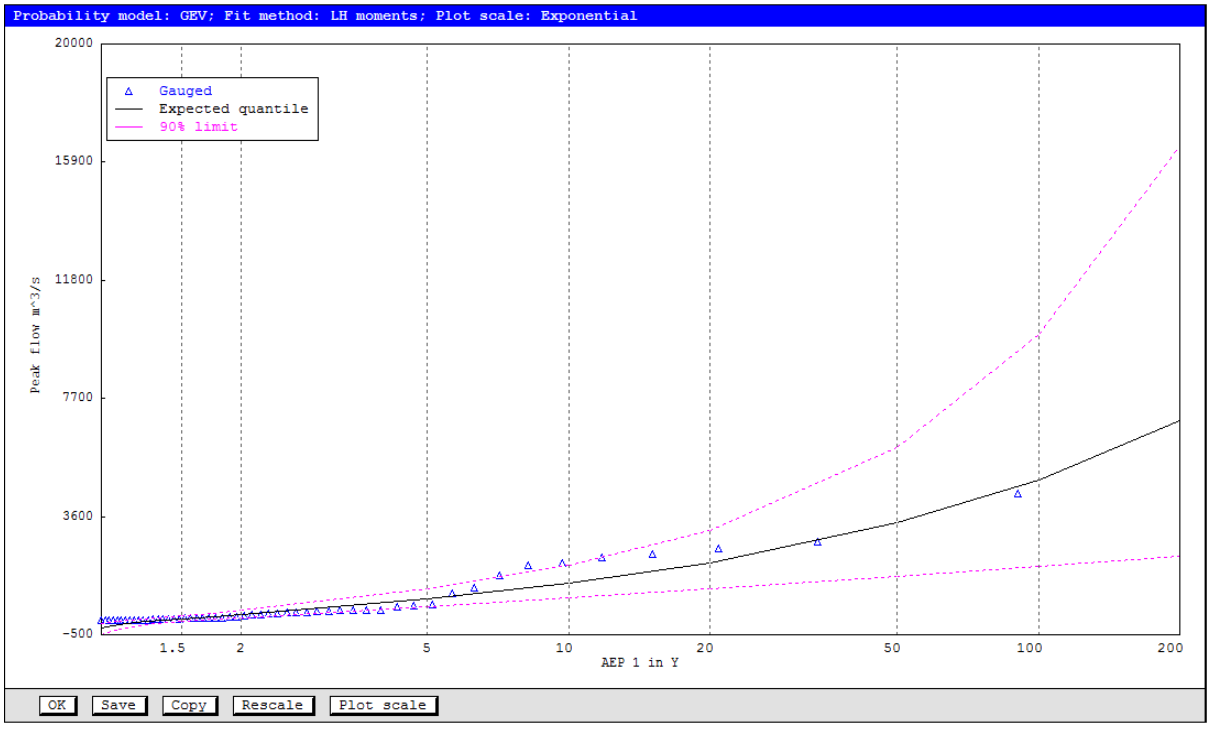

Generalised Extreme Value

Figure 5:23: Estimated Quantile with GEV probability distributions for 143007A, using FLIKE

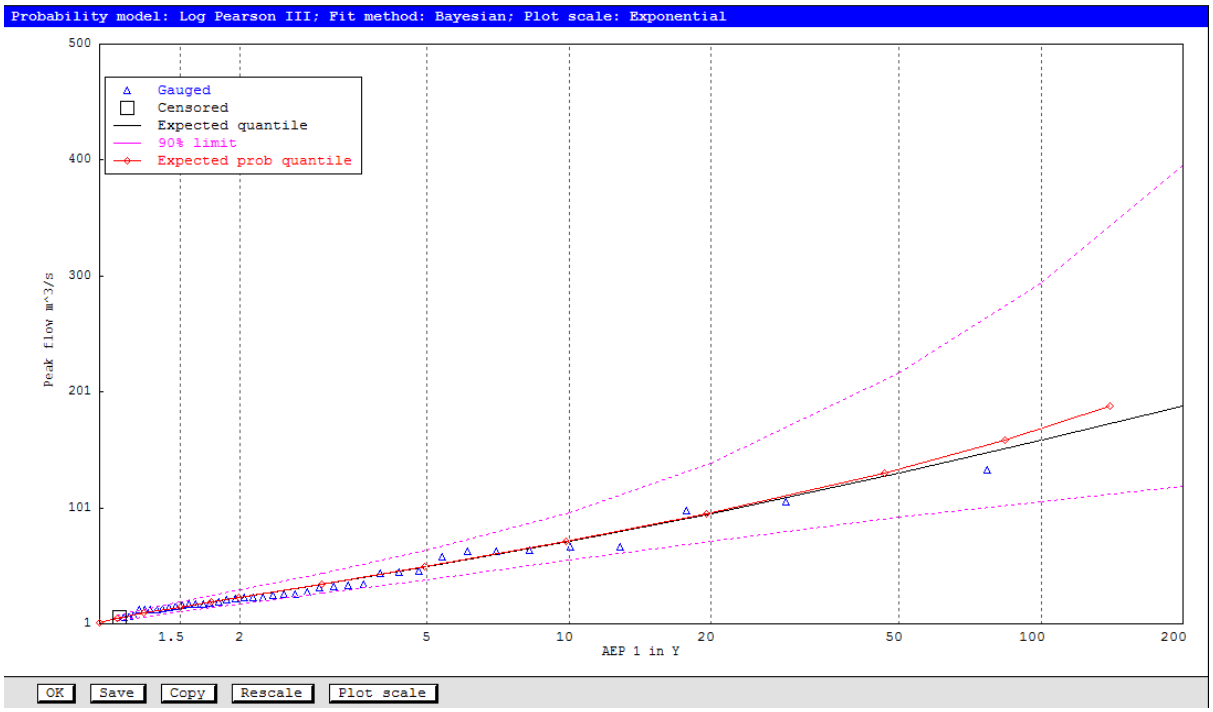

Log Pearson type III

Figure 5:24: Estimated Quantile with LP3 probability distributions for 143028A, using FLIKE

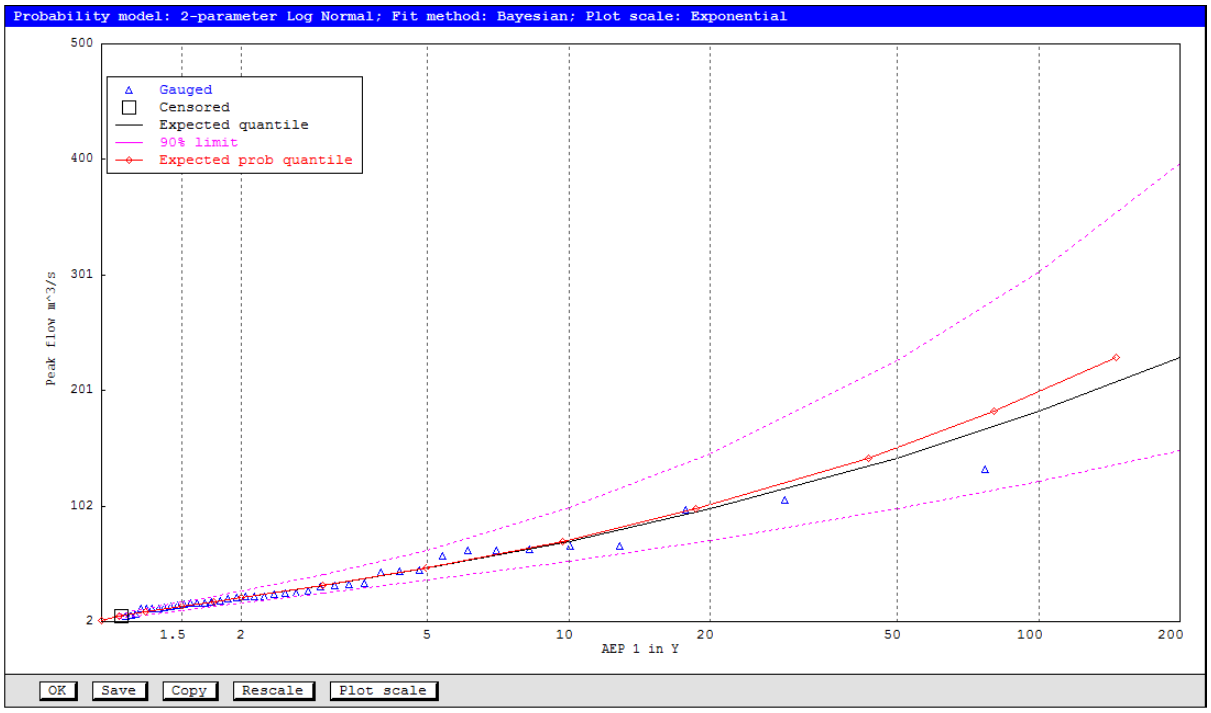

Lognormal

Figure 5:25: Estimated Quantile with LN probability distributions for 143028A, using FLIKE

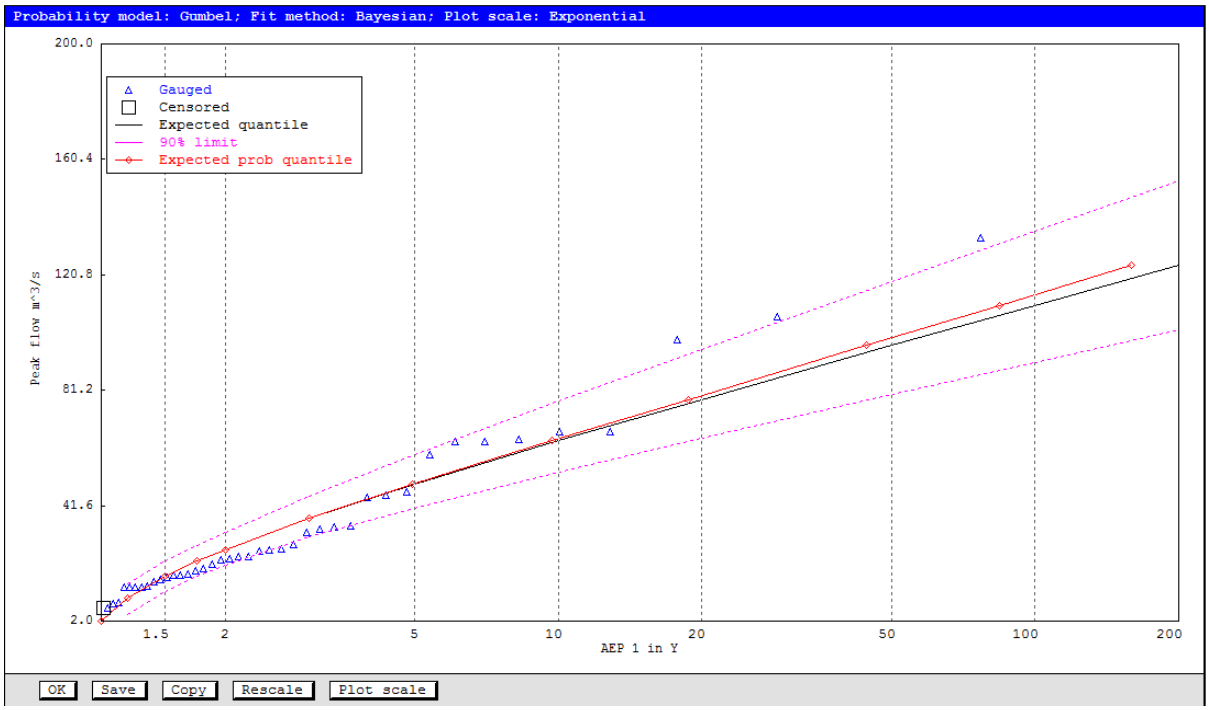

Gumbel

Figure 5:26: Estimated Quantile with Gumbel probability distributions for 143028A, using FLIKE

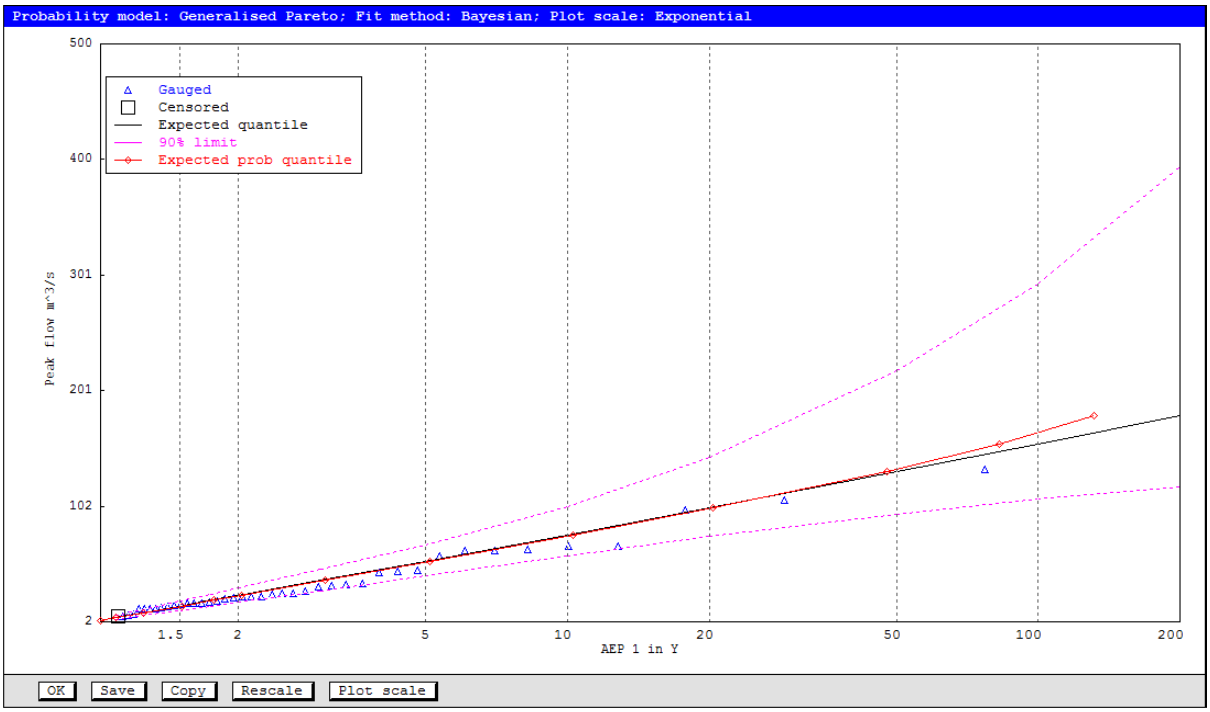

Generalised Pareto

Figure 5:27: Estimated Quantile with GP probability distributions for 143028A, using FLIKE

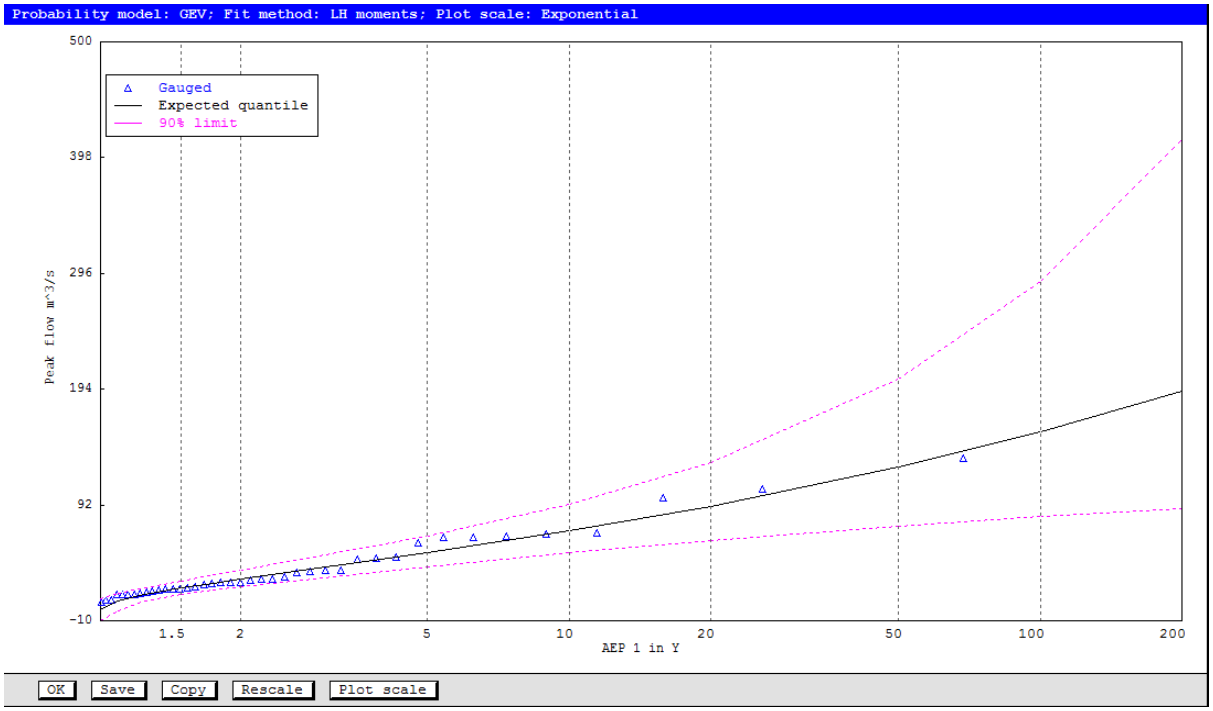

Generalised Extreme Value

Figure 5:28: Estimated Quantile with GEV probability distributions for 143028A, using FLIKE

Table 5.15: Quantile with 90% Monte Carlo probability limits for 143007A

Quantile with 90% Probability Limit for 143007A with LP3 Distribution			
	Estimated Annual Max Flow Quantile	90 % Monte Carlo probability limits	
ARI (AEP 1 in Y)	Estimated Quantile by LP3 (m^3/s)	Lower Bound (m^3/s)	Upper Bound (m^3/s)
2	142	88	232
5	694	433	1126
10	1506	916	2677
20	2781	1567	5951
50	5389	2597	15413
100	8240	3390	30195
200	12014	4166	56789
500	18704	5138	127248

Table 5.16: Quantile with 90% Monte Carlo probability limits for 143028A

Quantile with 90% Probability Limit for 143028A with LP3 Distribution			
	Estimated Annual Max Flow Quantile	Monte Carlo 90% probability limits	
ARI (AEP 1 in Y)	Estimated Quantile by LP3 (m^3/s)	Lower Bound (m^3/s)	Estimated Quantile by LP3 (m^3/s)
2	23	18	30
5	50	39	64
10	72	56	97
20	96	72	140
50	131	93	217
100	159	107	295
200	189	119	396
500	230	133	567

Table 5.17: Quantile estimates by 5 different probability distributions for station 143001C and % difference with LP3 distribution

ARI (Year)	Quantile Estimate AMF (m^3/s) (LP3)	Quantile Estimate AMF (m^3/s) (LN)	Quantile Estimate AMF (m^3/s) (Gumbel)	Quantile Estimate AMF (m^3/s) (GP)	Quantile Estimate AMF (m^3/s) (GEV)
2	315	291 (92%)	545 (173%)	366 (116%)	811 (257%)
5	1549	1379 (89%)	1800 (116%)	1412 (91%)	1953 (126%)
10	3067	3113 (102%)	2632 (86%)	3119 (102%)	3074 (100%)
20	5020	6097 (121%)	3429 (68%)	6469 (129%)	4540 (90%)
50	8134	12991 (160%)	4461 (55%)	16297 (200%)	7238 (89%)
100	10784	21512 (199%)	5235 (49%)	32337 (300%)	10084 (94%)
200	13598	34131 (251%)	6005 (44%)	63821 (469%)	13892 (102%)
500	17451	59714 (342%)	7022 (40%)	156166 (895%)	20976 (120%)

Table 5.17 shows estimated flood quantiles for 5 different PDs at station 143001C. This table displays that estimated flood quantiles using Gumbel and Lognormal PDs are notably different than those using LP3, GP and GEV distributions. Estimated flood quantiles for 143010B with 5 different PDs are shown in Table 5.18. It is visible from this table that 100-year flood quantiles at station 143010B are quite different with different distributions and this is found for all the selected stations. This study shows that the quantile estimates using Gumbel and Lognormal in most of the stations are notably different than that of using LP3, GEV and GP distributions.

Table 5.18: Quantile estimates with 5 different probability distributions for station 143010B and % difference with LP3 distribution

ARI (Years)	Quantile Estimate AMF (m^3/s) (LP3)	Quantile Estimate AMF (m^3/s) (LN)	Quantile Estimate AMF (m^3/s) (Gumbel)	Quantile Estimate AMF (m^3/s) (GP)	Quantile Estimate AMF (m^3/s) (GEV)
2	67	61 (91%)	133 (197%)	74 (111%)	124 (185%)
5	321	290 (90%)	374 (117%)	290 (90%)	352 (110%)
10	649	655 (101%)	534 (82%)	643 (99%)	590 (91%)
20	1099	1283 (117%)	687 (63%)	1341 (122%)	918 (84%)
50	1878	2738 (146%)	886 (47%)	3397 (181%)	1560 (83%)
100	2600	4537 (175%)	1035 (40%)	6771 (260%)	2277 (88%)
200	3427	7204 (210%)	1183 (35%)	13425 (392%)	3286 (96%)
500	4665	12615 (270%)	1379 (30%)	33052 (709%)	5277 (113%)

LP3 flood quantile plots (Figures 5.19 and 5.24) display good match at low ARI among recorded AMF and the estimated quantile values. However, when ARI is very high i.e. 100-year or more, choice of the preferred distribution is relatively difficult. The quantile estimation with all the 5 PDs show LP3 distribution fits relatively better to the recorded AMF data for majority of the stations.

The comparison of observed 2011 AMF (Q_{2011}) (one of the most devastating flood in recent time) and 100-year ARI flood quantile in Table 5.1 shows that Q_{2011} values are higher than estimated 100-year quantiles for 2 stations and they are similar to Q_{2011} for 3 stations. However, for remaining 21 stations, 100-year flood quantiles are higher than the Q_{2011} observed value.

Table 5.19: Comparison of recorded 2011 AMF and 100 ARI flood quantile (Q_{100}) using LP3 distributions for 26 stations

Station	Observed Q_{max} / Q_{2011} (m^3/s)	Estimated Quantile with T=100; Q_{100} (m^3/s)	% Difference (Quantile/Observed)
143203C	3643	1989	55
143219A	362	348	96
143108A	2108	2117	100
143303A	710	721	102
143107A	2057	2107	102
143113A	411	434	106
143001C	9533	10784	113
143028A	133	159	119
143209B	349	416	119
143207A	2977	3582	120
143033A	385	469	122
143010B	2036	2600	128
143015B	2335	3080	132
143306A	175	231	132
143307A	462	624	135
143210B	1401	1958	140
143110A	370	520	141
143232A	45	63	141
143212A	1359	2213	163
143032A	297	533	179
143921A	590	1058	179
143213C	511	927	182
143007A	4404	8240	187
143229A	1395	3606	259

5.4 Impact of outliers in AMF data on best-fit probability distribution (PD) and quantile estimation

The AMF data of all the 26 stations are analysed for the presence of outliers and outliers in data series are identified and removed from the AMF data to evaluate how this removal affects distributional fitting and parameter estimation. Each station's AMF data is checked

for the presence of outlier using the inbuilt tool of FLIKE software. The details of outlier test in FLIKE are highlighted by Kuczera et al. (2005) and discussed in Chapters 3 and 4.

Table 5.20 shows that generally LP3 is more suitable PD followed by GP for the Brisbane River catchments. The GoF test results with and without outliers differ for 12 stations out of 26 stations. Table 5.21 provides quantile estimates with and without outliers in AMF data for Station 143229A. The quantile estimation with and without outliers in AMF data varies up to a maximum of 47%. Rahman et al. (2014b) in their study for eastern Australia also found a high difference of up to 60% in quantile estimates due the presence of outliers.

Table 5.20: GoF test results summary for 26 stations including outliers in data

Probability Distribution Method	Kolmogorov Smirnov Rank 1	Anderson Darling Rank 1	Average Rank 1
Log-Pearson 3	11	14	13
Lognormal	1	1	1
Gumbel	0	0	0
Generalised Pareto	7	7	7
Gen. Extreme Value	7	4	5

Table 5.21: Comparison of quantile estimation for Station 143229A with and without outliers (% value indicates the increase in flood quantiles if the outliers are removed as compared to the quantiles if outliers are not removed)

	Quantile Estimation Including Outliers for 143229A with LP3 Distribution			Quantile Estimation Excluding Outliers for 143229A with LP3 Distribution		
ARI (AEP 1 in Y)	**Estimated AMF Quantile**	**Monte Carlo 90% Quantile probability limits**		**Estimated AMF Quantile**	**Monte Carlo 90% Quantile probability limits**	
	Estimated AMF (m^3/s) LP3	**Lower Limit (m^3/s)**	**Upper Limit (m^3/s)**	**Estimated AMF (m^3/s) LP3**	**Lower Limit (m^3/s)**	**Upper Limit (m^3/s)**
20	880	448	1844	1149 (131%)	500 (10.4%) (112%)	4252 (56.63%) (231%)
50	1506	764	4074	2305 (153%)	826 (7.51%) (108%)	16902 (75.90%) (415%)
100	2015	974	6270	3606 (179%)	1080 (9.81%) (111%)	50133 (87.49%) (799%)
200	2521	1232	8624	5368 (213%)	1306 (5.67%) (106%)	144555 (94.03%) (1676%)

5.5 Sensitivity on selected best-fit probability distribution (PD) and quantile estimation with respect to maximum recorded flow

The sensitivity analysis is carried to investigate the influence of very high values on the selection of the best-fit PD and on the quantile estimation using 3 different scenarios: (a) excluding the highest record from the AMF series; (b) excluding the two highest records from the AMF series; and (c) excluding the three highest records from the AMF series.

Table 5.22 shows the number of stations with best-fit distribution (Rank 1) when highest flood event from all station's AMF data is removed.

Table 5.22: Best-fit distributions with 3 different GoF tests when the highest ranked flood event is excluded from AMF data

Probability Distribution	Kolmogorov Smirnov No. of Stations Rank 1	Anderson Darling No. of Stations Rank 1	Chi-Squared No. of Stations Rank 1	Average No. of Stations Rank 1
Log Pearson type III	9	13	5	9.00
Lognormal	1	0	6	2.33
Gumbel	1	0	2	1.00
Generalised. Pareto	12	11	9	10.67
Gen. Extreme Value	3	2	4	3.00

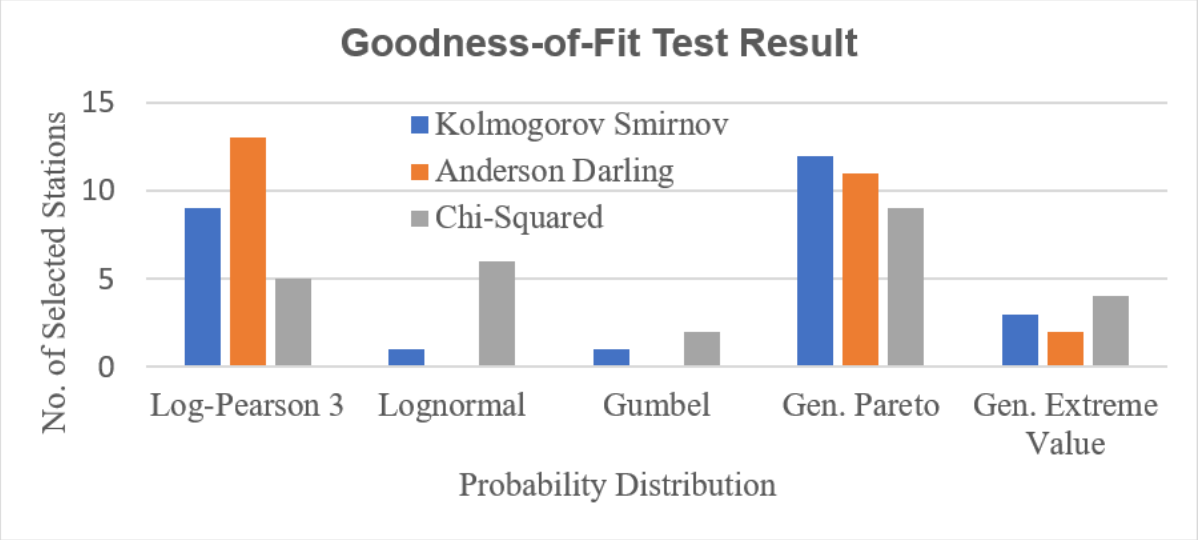

Figure 5:29: GoF tests summary for all selected stations excluding the highest ranked data point from AMF series

From Table 5.22 and Figure 5.29, it is seen that removal of the highest AMF data point affects overall GoF test results, e.g. GP becomes the most preferred distribution, followed by LP3. However, if the maximum observed data point is retained in the AMF series, LP3 is the preferred distribution (as found before in this chapter).

Table 5.23 shows the best-fit PD from 3 different GoF tests by excluding the highest and the 2nd highest flow records from the AMF data. Figure 5.30 shows GoF test summary with rank 1 for selected stations without the highest and 2nd highest AMF records in the data. From

Table 5.24 and Figure 5.31 it is seen that removal of the highest, 2nd highest and 3rd highest AMF data points results in GP being the preferred distribution in more cases, followed by the LP3 distribution.

Table 5.23: Best-fit distributions with 3 different GoF tests when the highest ranked and second highest ranked flood events are excluded from AMF data

Probability Distribution	Kolmogorov Smirnov No. of Stations Rank 1	Anderson Darling No. of Stations Rank 1	Chi-Squared No. of Stations Rank 1	Average No. of Stations Rank 1
Log Pearson type III	9	12	7	9.33
Lognormal	1	0	2	1.00
Gumbel	1	0	1	0.67
Generalised. Pareto	10	12	8	10.00
Gen. Extreme Value	5	2	7	4.67

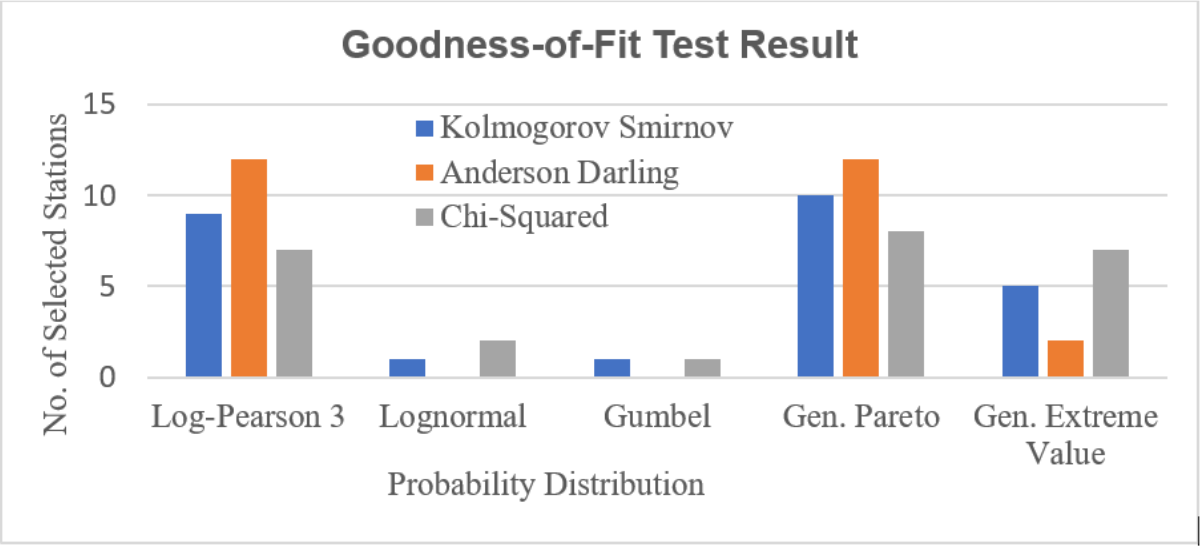

Figure 5:30: GoF tests summary for all selected stations excluding the highest and the second highest ranked data point from AMF series

Table 5.24 shows the best-fit distribution from three different GoF tests by removing three highest AMF records from data. Figure 5.31 shows summary of GoF test results where the highest, second highest and third highest AMF records are excluded from the data.

Table 5.24: Best-fit distributions with 3 different GoF tests when the highest ranked, second highest ranked and third highest ranked flood events are excluded from AMF data

Probability Distribution	Kolmogorov Smirnov No. of Stations Rank 1	Anderson Darling No. of Stations Rank 1	Chi-Squared No. of Stations Rank 1	Average No. of Stations Rank 1
Log Pearson type III	9	12	3	8.00
Lognormal	1	0	3	1.33
Gumbel	2	0	5	2.33
Generalised. Pareto	8	12	9	9.67
Gen. Extreme Value	6	2	5	4.33

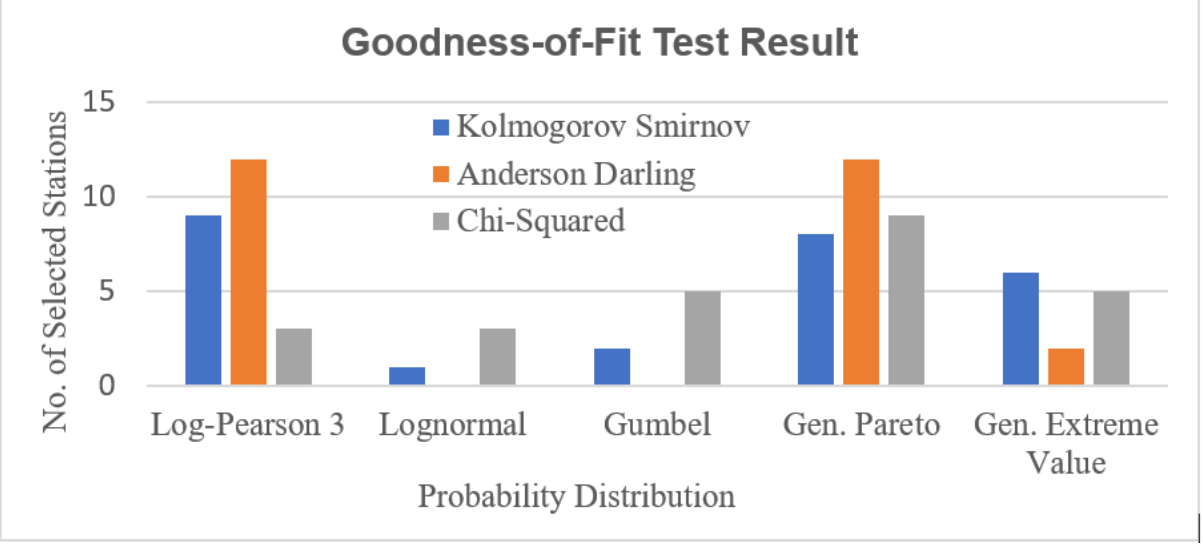

Figure 5:31: GoF tests summary for all selected stations excluding the highest, the second highest and the highest ranked data point from AMF series

It is understood from Table 5.24 and from Figure 5.31 that by excluding the 3 highest records, more stations show GP as the best-fit-distribution, followed by LP3.

Investigation for impacts of extreme events on flood quantiles is made by (a) removing the highest AMF data point; (b) two highest AMF data points; and (c) three highest AMF data points. Table 5.25 shows the comparison of estimated quantiles considering these three cases.

It is seen from Table 5.25 that the quantile estimation is greatly affected by the highest AMF data point in the series. The differences for Q_{100} range 9% to 86% (with a mean difference of 48 %). This in essence indicates that if a very high flood occurs in future, the Q_{100} estimate (which is widely used in practice) will be much different than that obtained from the current AMF data series. Hence, FFA should be carried out after each big flood event to ensure that the existing hydraulic structures designed with the old AMF data does not put significant risk to the infrastructure and the community.

Table 5.25: Estimated Q_{50} and Q_{100} flood quantiles using full AMF data and excluding the first, the second and the third highest AMF data points

Station	Full AMF Data	Full AMF Data	3 Highest AMF Records Removed	3 Highest AMF Records Removed	2 Highest AMF Records Removed	2 Highest AMF Records Removed	1 Highest AMF Record Removed	1 Highest AMF Record Removed
	Q_{50} (m^3/s)	Q_{100} (m^3/s)	Q_{50} (m^3/s)	Q_{100} (m^3/s)	Q_{50} (m^3/s)	Q_{100} (m^3/s)	Q_{50} (m^3/s)	Q_{100} (m^3/s)
143001C	8134	10784	6766	9090	4033	4033	3410	3410
143007A	5389	8240	4252	6228	5408	5408	4704	4704
143009A	11842	19085	9982	15796	12930	12930	10607	10607
143010B	1878	2600	1353	1760	1761	1761	1313	1313
143015B	2205	3080	1280	1581	1493	1493	1217	1217
143028A	131	159	109	129	113	113	85	85
143032A	379	533	308	422	270	270	227	227
143033A	415	469	370	417	370	370	331	331
143107A	1671	2107	1123	1271	1164	1164	937	937
143108A	1622	2117	1292	1642	1385	1385	1083	1083
143110A	447	520	429	499	475	475	455	455
143113A	369	434	224	235	238	238	243	243
143203C	1395	1989	946	1231	745	745	678	678
143207A	3009	3582	2700	3173	3037	3037	2743	2743
143209B	387	416	394	426	398	398	379	379
143210B	1558	1958	1488	2385	1660	1660	1108	1108
143212A	1696	2213	1486	1939	1758	1758	1639	1639
143213C	772	927	551	740	416	416	302	302
143219A	212	348	91	123	92	92	78	78
143229A	2305	3606	1134	1372	932	932	493	493
143232A	55	63	43	47	49	49	47	47
143233A	993	1645	344	449	478	478	432	432
143303A	658	721	585	625	658	658	605	605
143306A	208	231	214	238	186	186	605	605
143307A	517	624	446	533	450	450	356	356
143921A	758	1058	641	1000	239	239	199	199

5.6 Uncertainty Analysis using Bootstrapping and Monte Carlo Simulation Techniques

Six stations (143028A, 143009A, 143207A, 143015B, 143212A and 143007A) out of the 26 are selected for uncertainty analysis. From FFA as discussed in Section 5.2, LP3 is found to be the best-fit PD for these selected gauging sites. Table 5.26 to 5.31 show estimated flood quantiles with 5% and with 95% confidence levels for 143028A, 143009A, 143207A, 143015B, 143212A and 143007A, respectively. Tables 5-32 to 5-37 show moments and correlations for 143028A, 143009A, 143207A, 143015B, 143212A and 143007A, respectively. These moments and correlations were estimated by boot strapping.

The computed 5% and 95% confidence intervals for these six stations are compared with those obtained from the FLIKE. It is found that in few cases, the width of the confidence intervals is quite high indicating that the associated uncertainty level in FFA is quite high. This implies that design of hydraulic structures based on the expected quantiles may not be able to provide adequate protection in high floods, and hence necessary measures need to be planned e.g. emergency evacuation of the people, erosion control and ecological impacts.

It is found that out of these six stations, our Monte Carlo simulation provides narrower confidence limits for 4 cases. This shows that uncertainty analysis in FLIKE is not absolute uncertainty; it only provides an indication of possible uncertainty.

It should be noted that in FLIKE, a Bayesian method is used in carrying out the uncertainty analysis, but in this study a non-Bayesian Mote Carlo simulation is adopted where a multivariate normal distribution is used to generate correlated parameters of the LP3 distribution. The correlation was estimated by the boot-strapping of the AMF data. Since, there is a difference in the adopted Mote Carlo simulation methods in FLIKE and this study the observed differences in the confidence limits are not unexpected.

Table 5.26: Flood quantiles for 143028A by Monte Carlo simulation

AEP (1 in Y)	Expected Quantile (m^3/s)	5% Confidence Level (m^3/s)	95% Confidence Level (m^3/s)
2	23.37	18.31	30.10
5	49.96	37.63	66.47
10	70.60	50.91	98.53
20	91.55	63.35	134.63
50	119.54	78.12	188.49
100	140.68	87.78	235.90

Table 5.27: Flood quantiles for 143009A by Monte Carlo simulation

AEP (1 in Y)	Expected Quantile (m^3/s)	5% Confident Level (m^3/s)	95% Confident Level (m^3/s)
2	272.65	182.55	414.72
5	1249.15	801.72	1965.22
10	2740.02	1670.94	4520.97
20	5205.87	2966.17	9266.27
50	10664.01	5532.03	21286.26
100	17119.51	8201.78	37446.60

Table 5.28: Annual Maximum Flood Quantiles for 143207A

AEP (1 in Y)	Expected Quantile (m^3/s)	5% Confidence Level (m^3/s)	95% Confidence Level (m^3/s)
2	205.06	128.13	332.21
5	928.10	536.58	1618.37
10	1691.64	904.42	3207.62
20	2544.28	1263.24	5304.00
50	3702.27	1681.78	8752.15
100	4541.46	1916.06	11806.05

Table 5.29: Annual Maximum Flood Quantiles for 143015B

AEP (1 in Y)	Expected Quantile (m^3/s)	5% Confidence Level (m^3/s)	95% Confidence Level (m^3/s)
2	80.42	44.81	146.78
5	405.69	204.11	805.41
10	778.25	349.27	1772.43
20	1217.14	489.99	3205.23
50	1844.36	639.84	6006.72
100	2319.31	715.89	8694.48

Table 5.30: Annual Maximum Flood Quantiles for 143212A

AEP (1 in Y)	Expected Quantile (m^3/s)	5% Confidence Level (m^3/s)	95% Confidence Level (m^3/s)
2	72.50	34.31	153.70
5	346.04	135.20	870.00
10	572.81	190.53	1829.10
20	762.50	216.31	3226.24
50	939.12	228.44	5709.63
100	1022.36	234.10	7875.08

Table 5.31: Annual Maximum Flood Quantiles for 143212A

AEP (1 in Y)	Expected Quantile (m^3/s)	5% Confidence Level (m^3/s)	95% Confidence Level (m^3/s)
2	137.66	89.48	215.07
5	650.55	405.59	1048.25
10	1424.13	834.88	2444.06
20	2676.50	1453.68	5041.12
50	5363.09	2583.08	11603.18
100	8436.26	3630.89	20789.02

Table 5.32: Moments and Correlation Coefficient for 143028A obtained by bootstrapping

Most Probable	Standard Deviation	Correlation		
5.589	0.244	1.000		
1.825	0.139	-0.010	1.000	
-0.064	0.176	0.009	-0.006	1.000

Table 5.33: Moments and Correlations Coefficient for 143009A obtained by bootstrapping

Most Probable	Standard Deviation	Correlation		
3.053	0.145	1.000		
1.003	0.108	0.012	1.000	
-0.597	0.223	0.007	0.004	1.000

Table 5.34: Moments and Correlations Coefficient for 143207A obtained by bootstrapping

Most Probable	Standard Deviation	Correlation		
4.937	0.273	1.000		
2.242	0.225	0.008	1.000	
-1.068	0.216	-0.012	-0.009	1.000

Table 5.35: Moments and Correlations Coefficient for 143015B obtained by bootstrapping

Most Probable	Standard Deviation	Correlation		
3.992	0.337	1.000		
2.377	0.292	-0.006	1.000	
-1.029	0.305	0.005	0.001	1.000

Table 5.36: Moments and Correlations Coefficient for 143212A obtained by bootstrapping

Most Probable	Standard Deviation	Correlation		
3.581	0.391	1.000		
2.793	0.478	0.001	1.000	
-1.625	0.505	-0.014	0.010	1.000

Table 5.37: Moments and Correlations for 143212A obtained by bootstrapping

Most Probable	Standard Deviation	Correlation		
4.872	0.257	1.000		
1.892	0.155	-0.014	1.000	
-0.167	0.223	0.008	0.002	1.000

5.7 Trends Analysis and Change Point Test

Existence of trends or abrupt change in the AMF data for all the 26 stations is evaluated in this section. Twelve different statistical tests are used for this analysis at different significance levels (α) (10%, 5% and 1%). Trends in the data, step jumps in the mean of data, differences in the median from two data periods and randomness in data are evaluated through these tests. The possibility of trend in the AMF data is assessed through Spearman's Rho (SR) nonparametric test, Mann-Kendall (MK) nonparametric test and Linear Regression tests. In addition to trend analysis, trend analysis with data resampling is carried out in this study so that greater accuracy is achieved to estimate the significance level of a test statistic, especially if the null hypothesis is rejected (i.e. assumptions of test are violated). The summary of the 12 statistical tests (test statistic's magnitude, test statistic's critical values and re-sampling test statistic's critical values) at 1%, at 5% and at 10% significance levels for sites 143001C, 143015B, 143028A and 143033A, respectively are presented in Tables 5.38 to 5.41. The statistical trend test summary at 1%, 5% and 10% significance levels for all other stations are given in Appendix-F.

Table 5.38: Trend Analysis Result of AMF series at 143001C

Test Name	Test Statistic for Each Test	Critical Values of Trend test statistics for Significance Levels at			Critical Values of Trend test Re-Sampling statistics fo Significance Levels at			Result
		α=0.1	α=0.05	α=0.01	α=0.1	α=0.05	α=0.01	
Mann-Kendall	-1.512	1.645	1.960	2.576	1.652	1.939	2.570	NS
Spearman's Rho	-1.446	1.645	1.960	2.576	1.598	1.996	2.535	NS
Linear Regression	-0.419	1.673	2.002	2.664	1.714	1.909	2.460	NS
Cusum	7.000	9.45	10.535	12.626	9.000	10.000	12.000	NS
Cumulative deviation	0.824	1.146	1.274	1.526	1.122	1.220	1.377	NS
Worsley likelihood	1.830	2.87	3.160	3.790	3.981	5.606	6.470	NS
Rank Sum	1.323	1.645	1.960	2.576	1.722	2.018	2.669	NS
Student's t	0.675	1.672	2.001	2.662	1.593	1.816	2.110	NS
Median Crossing	0.130	1.645	1.960	2.576	1.692	1.953	2.734	NS
Turning Point	-0.207	1.645	1.960	2.576	1.762	2.073	3.006	NS
Rank Difference	-1.522	1.645	1.960	2.576	1.686	1.950	2.640	NS
Autocorrelation	0.972	1.645	1.960	2.576	1.481	1.992	3.055	NS

Note: 'NS' stands for statistically not significant at 10%; 'S' stands for significant with level inside the brackets.

Table 5.39: Trend Analysis Result of AMF series at 143015B

Test Name	Test Statistic for Each Test	Critical Values of Trend test statistics for Significance Levels at			Critical Values of Trend test Re-Sampling statistics for Significance Levels at			Result
		α=0.1	α=0.05	α=0.01	α=0.1	α=0.05	α=0.01	
Mann-Kendall	-1.802	1.645	1.960	2.576	1.638	1.922	2.508	S (0.1)
Spearman's Rho	-1.733	1.645	1.960	2.576	1.685	1.978	2.570	S (0.1)
Linear Regression	0.279	1.681	2.013	2.687	1.724	2.085	2.753	NS
Cusum	8.000	8.54	9.520	11.410	9.000	10.000	12.000	NS
Cumulative Deviation	0.839	1.139	1.269	1.518	1.138	1.276	1.479	NS
Worsley Likelihood	2.350	2.868	3.164	3.790	3.644	5.979	7.476	NS
Rank Sum	1.870	1.645	1.960	2.576	1.67	1.990	2.650	S (0.1)
Student's t	-0.011	1.681	2.012	2.685	1.66	1.923	2.265	NS
Median Crossing	0.577	1.645	1.960	2.576	1.732	2.021	2.309	NS
Turning Point	0.230	1.645	1.960	2.576	1.841	2.187	2.992	NS
Rank Difference	-1.068	1.645	1.960	2.576	1.609	1.851	2.605	NS
Autocorrelation	1.215	1.645	1.960	2.576	1.503	1.771	2.711	NS

Note: 'NS' stands for statistically not significant at 10%; 'S' stands for significant with level inside the brackets.

Table 5.40: Trend Analysis Result of AMF series at 143028A

Test Name	Test Statistic for Each Test	Critical Values of Trend test statistics for Significance Levels at			Critical Values of Trend test Re-Sampling statistics for Significance Levels at			Result
		α=0.1	α=0.05	α=0.01	α=0.1	α=0.05	α=0.01	
Mann-Kendall	0.587	1.645	1.960	2.576	1.638	2.007	2.424	NS
Spearman's Rho	0.688	1.645	1.960	2.576	1.722	2.021	2.571	NS
Linear Regression	0.900	1.682	2.017	2.694	1.628	1.967	2.424	NS
Cusum	8.000	8.274	9.224	11.055	8	9.000	10.000	S (0.1)
Cumulative Deviation	1.248	1.136	1.266	1.512	1.117	1.253	1.522	S (0.1)
Worsley Likelihood	3.308	2.862	3.176	3.790	3.433	4.151	4.885	NS
Rank Sum	0.395	1.645	1.960	2.576	1.714	2.021	2.746	NS
Student's t	-0.165	1.682	2.015	2.692	1.661	1.952	2.477	NS
Median Crossing	0.745	1.645	1.960	2.576	1.64	1.938	2.534	NS
Turning Point	-0.119	1.645	1.960	2.576	1.903	2.260	2.616	NS
Rank Difference	-1.568	1.645	1.960	2.576	1.662	1.991	2.713	NS
Autocorrelation	1.075	1.645	1.960	2.576	1.675	1.905	2.513	NS

Note: 'NS' stands for statistically not significant at 10%; 'S' stands for significant with level inside the brackets.

Table 5.41: Trend Analysis Result of AMF series at 143033A

Test Name	Test Statistic for Each Test	Critical Values of Trend test statistics for Significance Levels at			Critical Values of Trend test Re-Sampling statistics for Significance Levels at			Result
		α=0.1	α=0.05	α=0.01	α=0.1	α=0.05	α=0.01	
Mann-Kendall	0.954	1.645	1.960	2.576	1.604	1.918	2.579	NS
Spearman's Rho	0.887	1.645	1.960	2.576	1.697	2.001	2.439	NS
Linear Regression	1.928	1.684	2.021	2.704	1.749	2.022	2.572	S (0.1)
Cusum	7.000	7.907	8.814	10.564	8.000	9.000	11.000	NS
Cumulative Deviation	1.313	1.132	1.262	1.504	1.126	1.288	1.512	S (0.05)
Worsley Likelihood	3.420	2.872	3.174	3.778	2.768	3.072	3.824	S (0.05)
Rank Sum	0.906	1.645	1.960	2.576	1.66	2.063	2.767	NS
Student's t	-0.297	1.684	2.020	2.702	1.665	1.973	2.725	NS
Median Crossing	1.718	1.645	1.960	2.576	1.718	2.030	2.655	S (0.1)
Turning Point	-0.249	1.645	1.960	2.576	1.746	2.120	2.868	NS
Rank Difference	-1.797	1.645	1.960	2.576	1.665	2.031	2.734	S (0.1)
Autocorrelation	0.595	1.645	1.960	2.576	1.652	1.930	2.571	NS

Note: 'NS' stands for statistically not significant at 10%; 'S' stands for significant with level inside the brackets.

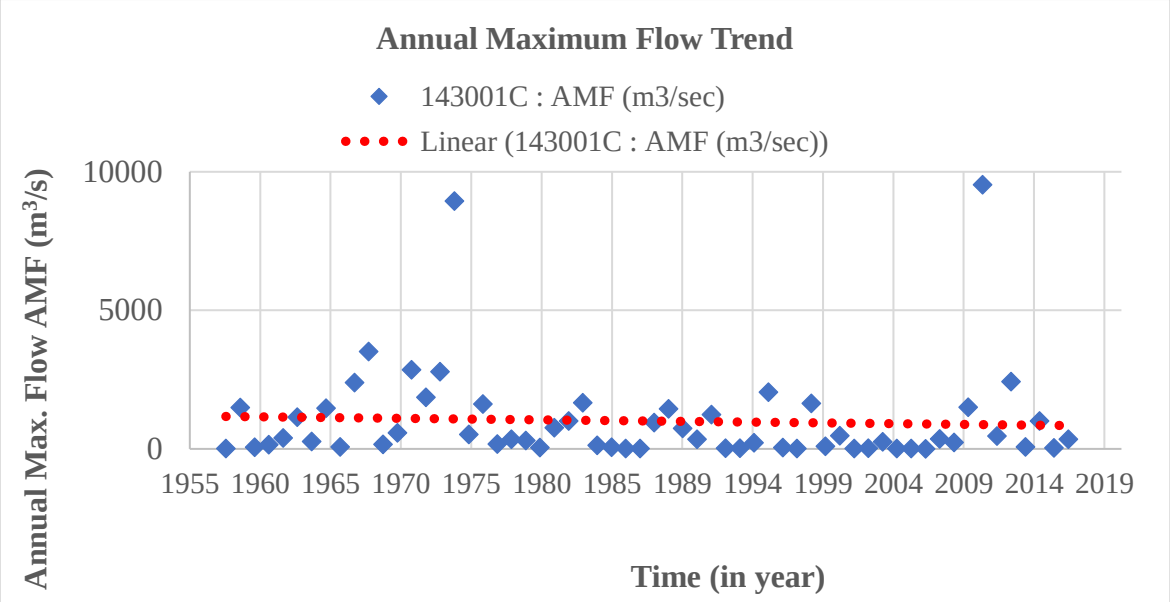

Figure 5:32: The AMF series of station 143001C and the linear trend

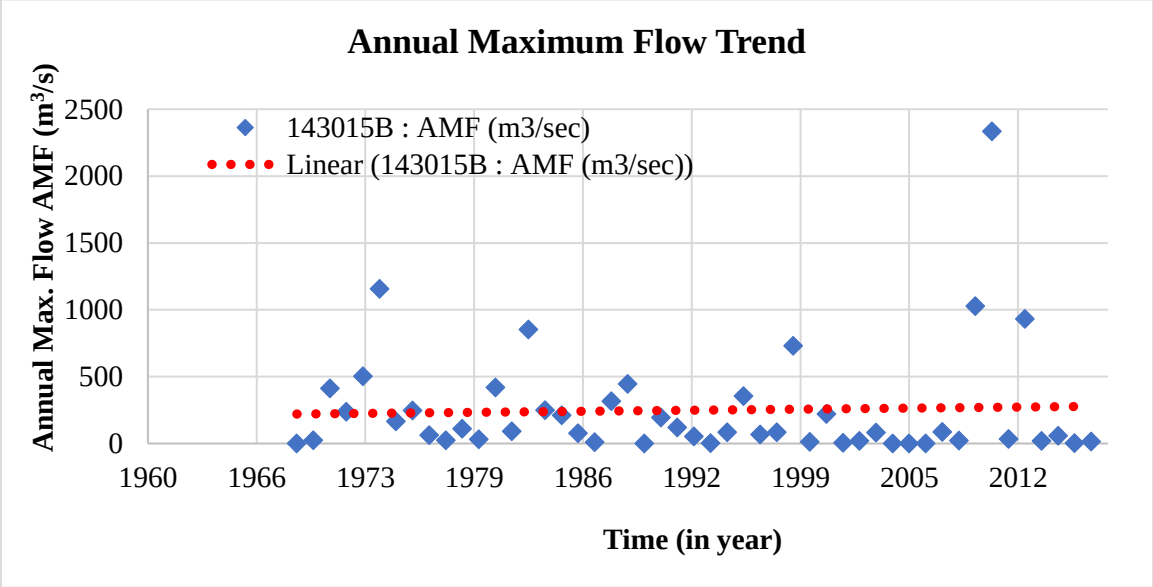

Figure 5:33: The AMF series of station 143015B and the linear trend

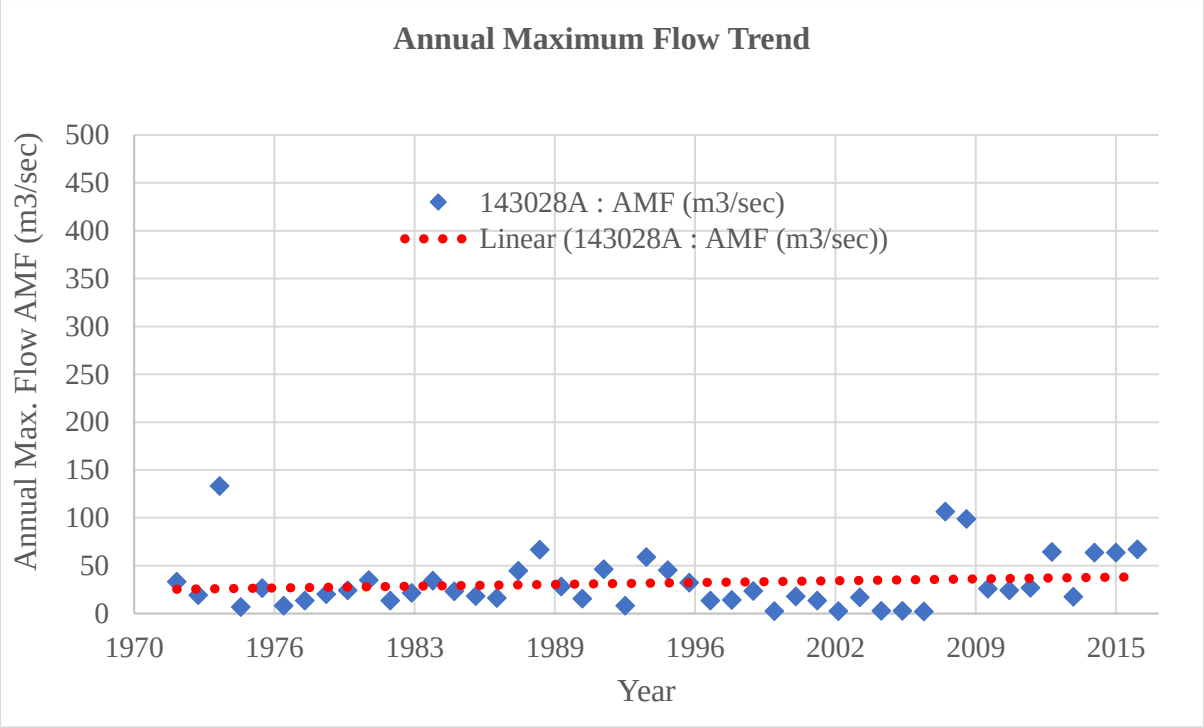

Figure 5:34: The AMF series of station 143028A and the linear trend

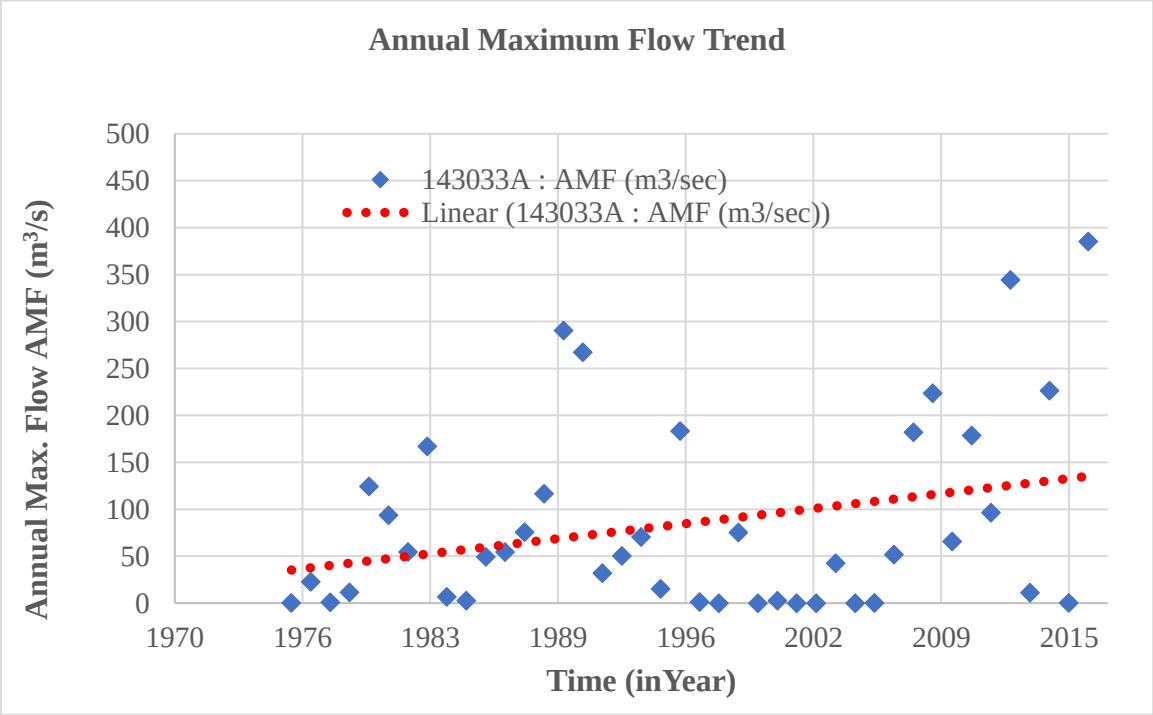

Figure 5:35: The AMF series of station 143033A and the linear trend

Figures 5.32, 5.33, 5.34 and 5.35 display the AMF series and corresponding linear regression line for stations 143001C, 143015B, 143028A and 143033A, respectively. Visual observation

of Figures 5.32 to 5.35 suggests that AMF series at these four stations do not have any sudden drop or rise. The trend analysis test statistics of MK, SR and Linear Regression tests (Table 5.38) for AMF series of station 143001C confirms that that no statistical significant trend exist in data series and test statistics of Distribution-Free CUSUM, Cumulative Deviation and Worsley Likelihood Ratio tests (Table 5.38) suggest no step jump in the mean of the data series. Rank-Sum and Student's t statistical tests statistics show "not significant (NS)" (in Table 5.38), which suggests that there is no significant difference in median values between two separate data periods within AMF time series at station 143001C. Figure 5.32 shows a mild downward slope in the regression line for the data from station 143001C.

According to MK or SR tests statistics for AMF data at 143015B in Table 5.39, no statistical trend exists. However, according to Rank-Sum test, AMF data of this station has significant difference (at 10% significant level) in median values between two data periods within the total series. Mild upward slope in the linear regression line is visible in Figure 5.33 and Figure 5.34 for AMF data at stations 143015B and 143028A, respectively. However, no significant trend is shown for these stations (Table 5.39 and Table 5.40) from Linear Regression test. Presence of step jump in data at station 143028A is suggested according to the CUSUM and Cumulative Deviation statistical tests (Table 5.40). MK or SR tests display no significant trend in the data for this station (Table 5.40, 143028A). Upward slope of linear regression line for station 143033A is visible in Figure 5.35. Although Linear Regression test statistics for 143033A show existence of trend at 10% significance level (Table 5.41), no significant trend is estimated for this station by the SR and MK tests (Table 5.41).

The summary of trend analysis tests for all selected stations are shown in Table 5.42 where some test statistics show upward (+Ve) or downward (-Ve) trend in the AMF data. The presence of step jump in the data between two sub-sets of data within the data series is evaluated using Distribution-Free CUSUM test, Cumulative Deviation test and Worsley Likelihood Ratio tests. The summary result (Table 5.42) shows that a limited number of station's AMF data have step jump at 10% significance level. It is seen in Table 5.42 that 21 station's AMF data have mild +Ve slope in their linear regression line and 5 station's data have -Ve slope. Figure 5.36 presents a layout map with statistically significant trends in AMF data at the 10% significance level for all the stations.

Table 5.42: **Trend test Summary for all station's AMF data**

Table 5.42 Summary of Trend Test for all 26 stations data

Station Number	Mann-Kendall	Spearman's Rho	Linear Regression	Cusum	Cumulative Deviation	Worsley Likelihood	Rank Sum	Student's t	Median Crossing	Turning Point	Rank Difference	Auto Correlation	Linear Regression Slope
143001C	NS	NS	NS	NS	NS	NS	NS	NS	NS	NS	NS	NS	-Ve
143007A	NS	NS	NS	NS	NS	NS	S (0.05)	NS	NS	NS	NS	NS	+Ve
143009A	NS	NS	NS	NS	NS	NS	S (0.1)	NS	NS	NS	NS	NS	-Ve
143010B	NS	NS	NS	NS	NS	NS	NS	NS	NS	NS	NS	NS	+Ve
143015B	S (0.1)	S (0.1)	NS	NS	NS	NS	S (0.1)	NS	NS	NS	NS	NS	+Ve
143028A	NS	NS	NS	S (0.1)	S (0.1)	NS	NS	NS	NS	NS	NS	NS	+Ve
143032A	NS	NS	NS	NS	NS	NS	NS	S (0.1)	NS	NS	NS	NS	-Ve
143033A	NS	NS	S (0.1)	NS	S (0.05)	S (0.05)	NS	NS	S (0.1)	NS	S (0.1)	NS	+Ve
143107A	NS	NS	NS	NS	S (0.1)	S (0.1)	NS	NS	NS	NS	NS	NS	+Ve
143108A	NS	NS	NS	NS	NS	NS	NS	NS	S (0.05)	S (0.1)	S (0.1)	NS	-Ve
143110A	NS	NS	NS	NS	NS	NS	NS	NS	NS	NS	NS	NS	+Ve
143113A	NS	NS	NS	NS	NS	NS	NS	NS	NS	NS	NS	NS	-Ve
143203C	NS	NS	S (0.1)	NS	NS	NS	NS	S (0.1)	NS	NS	NS	NS	+Ve
143207A	NS	NS	NS	NS	NS	NS	NS	NS	NS	NS	NS	NS	-Ve
143209B	NS	NS	NS	NS	NS	NS	NS	NS	NS	NS	NS	NS	-Ve
143212A	NS	NS	NS	NS	NS	NS	NS	NS	NS	NS	NS	NS	+Ve
143219A	NS	NS	NS	NS	NS	NS	NS	NS	NS	NS	NS	NS	+Ve
143229A	NS	NS	NS	NS	NS	NS	NS	NS	NS	NS	NS	NS	+Ve
143303A	NS	NS	NS	NS	NS	NS	NS	NS	NS	NS	S (0.1)	S (0.1)	-Ve
143921A	NS	NS	S (0.1)	NS	S (0.05)	NS	NS	NS	NS	NS	NS	NS	+Ve
143210B	NS	NS	NS	NS	NS	NS	NS	NS	NS	NS	NS	NS	-Ve
143306A	NS	NS	NS	NS	NS	S (0.05)	NS	NS	NS	NS	NS	NS	+Ve
143213C	NS	NS	NS	NS	NS	NS	NS	NS	NS	NS	NS	NS	+Ve
143232A	NS	NS	NS	NS	NS	NS	NS	NS	NS	NS	NS	NS	+Ve
143233A	NS	NS	NS	NS	NS	NS	NS	NS	NS	NS	NS	NS	+Ve
143307A	NS	NS	NS	NS	NS	NS	NS	NS	NS	NS	NS	NS	-Ve

NS means not significant at α = 0.1 (10%); S means statistically significant, with the significance level shown in brackets

As explained in Section 4.15; trend in the time series data is deemed to be present, if most of the trend tests detect statistically significant trend in data series at regional level. In this study, out of 12 statistical trend detection tests, most of the tests detect no trend (Table 5.42) in the AMF data series of the 26 stations.

The MK and Spearman's Rao tests for data series at 143015B shows trend at 10% significance level. As shown in Figure 5.36, this station is located at Cooyar Creek (upstream of Brisbane River). The 143015B catchment is relatively large with an area of 953 km^2. The geography of the area suggests that this catchment has not been affected by the significant human intervention. The highest AMF of 143015B was recorded in 2011 with a magnitude of 853 m^3/s. The statistically significant trend by trend test may not attribute to a real trend in AMF series for this station; however, further investigation is needed to make a firm conclusion.

Two commonly used statistical test for detecting trend in data i.e. SR and MK tests do not detect any significant trend in AMF data for Station 143033A (Table 5.42), although the Linear Regression test shows statistically significant trend at 10% significance level (Table 5.42). The plot of AMF data for site 143033A (Figure 5.35) shows that the yearly observed peak flows fluctuated year to year notably compared to that of the other gauging sites. Statistically significant test result and linear regression line slope value is shown in Figure 5.36 for station 143033A. Figure 5.36 also shows that 143033A gauging station is located at Oxley Creek, New Beith, Queensland. This creek travel from New Beith around 50 km downstream and meet with the Brisbane River at Brisbane city. In the past, major sand extraction and mitigation works were carried out along this reach of the Creek (Hossain, 2019). This has caused great impacts on geometry and configuration of the greatly mobile nature of this creek and brought several meanderings, created loops, sub-branches and oxbows along the course of the creek towards Brisbane River (Hossain, 2019; BCC, 2014). These changes due to human intervention may contribute on the flood flow magnitude and flow depth with time. Therefore, trend in AMF time series may be due to the human activities and may not be due to change of climate.

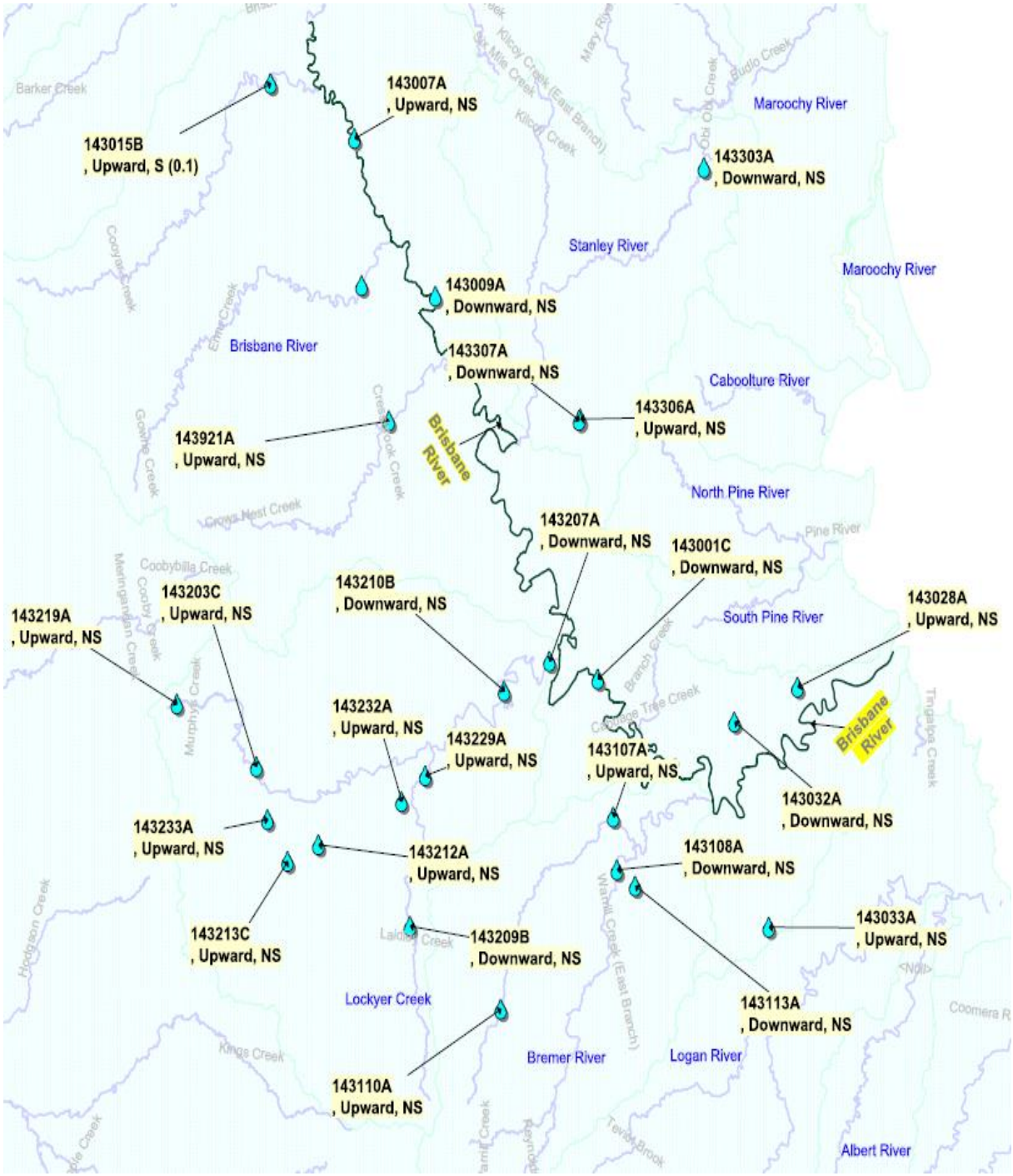

Figure 5:36: AMF series linear regression Trend (Upward/Downward) and statistical test result (S and NS at 10% significance level)

It is seen from Figure 5.36 that the slope of the regression lines for most of the stations (especially stations at upstream of catchment) are upward ((+Ve) i.e. AMF is increasing with time) indicating increasing trend. However, few stations show downstream (-Ve) or decreasing trends and these stations are located mainly at downstream of the catchment. The

Worsley Likelihood Ratio, Distribution-Free CUSUM, Cumulative Deviation statistical tests are used to detect existence of step jump in the AMF data series. All these three tests result display no significant step jump for almost all stations. Distribution-Free CUSUM test result show no significant step jump for almost all stations except 143028A. Cumulative Deviation test result shows no significant step jump for all stations except for 143028A and 143107A at 10 % significant level and Worsley Likelihood Ratio test result show no significant step jump for all stations except for 143107A at 10 % significance level. The existence of difference in the median of selected two data periods within AMF series is tested using Rank-Sum non-parametric statistical test and test results display no significant difference within data series for all stations except for 143009A and 143015B. The existence of difference in mean of selected two data periods within AMF series is tested using Student's *t* parametric statistical test and test results display no significant difference within data series for all stations except for 143032A and 143203C. The existence of randomness in data series is tested using Turning Points test, Median Crossing test, Rank Difference test and Autocorrelation test; and most of the station's AMF series show no significant result in randomness except for stations 143033A, .143108A and 143033A.

It is clear from all the statistical tests that the existence of trend or step jumps in AMF data series are not significant at regional level within Brisbane River catchment. Haddad and Rahman (2011) in their FFA study used MK test to detect trend in the AMF data at 53 stations in Tasmania, Australia and found only 3 stations having statistically downward trend at 5% significance level. Similar finding was also reported by Robson et al. (1998) in their study and they reported no significant trend in the AMF dataset from the United Kingdom.

As the trend analysis results (presented above) do not detect statistically significant trend, step jump, mean difference or median difference for the whole Brisbane River catchment at 10% significance level, non-stationary FFA is not conducted.

5.8 Chapter Summary

The results and findings of the study are presented in this chapter. The results of parameter estimation and GoF tests for the selection of the best-fit PD are discussed. Different probability plots are presented for comparison of the best-fit PD with GoF test results. The

results from quantile estimation and observed peak flow vs. ARI plots are presented for all the 5 candidate PDs.

It is clear that the LP3 distribution best fits the AMF data series for the majority of studied stations. It is also observed that GP and GEV distributions fit the data very well but are ranked second and third, respectively. Thus, a particular PD cannot be selected until the quantiles are computed and compared with the observed AMF data. To select the best-fit PD, a comparative assessment of the top three distributions at each site has been made, eventually identifying the most favourable distribution for the study area.

LP3 distribution is the rank 1 distribution in 11 cases out of the 26 stations, while GP distribution is the rank 2 distribution in 8 cases out of the 26 stations. The flood quantiles at all the sites are computed considering all the five selected PDs using FLIKE software, i.e. LN, Gumbel, GP, GEV, and LP3 distributions. The flood quantiles are computed for the aforesaid distributions and it is found that LP3 distribution yields values closer to the GP and GEV at most of the stations compared to other distributions. Analysis of the impact of outliers in data on quantile estimation show that quantile estimation is changed up to 41%, if outliers are not censored form the AMF data. Sensitivity analysis for quantile estimation on maximum recorded flow in the AMF data series show that quantile estimates change greatly and reduce up to 50% if maximum recorded flow is removed from data series. Uncertainty analysis of quantile estimation is also carried out using Monte Carlo simulation techniques. Monte Carlo simulation provides narrower confidence limits for 4 stations out of 6 compared to FLIKE. This shows that FLIKE does not provide absolute uncertainty; rather it gives an indication of possible uncertainty. The trend analysis shows that there is no statistically significant trend in the AMF data in the study region.

The next chapter presents a summary of this research and conclusions.

CHAPTER 6 : SUMMARY, CONCLUSIONS AND RECOMMENDATIONS

6.1 General

Estimation of design flood (DF) is a preliminary step in infrastructure planning, development and design process of many civil engineering works including design of flood control and drainage structures and streamflow and floodplain management. Among many DF estimation methods, at-site FFA is the most direct DF estimation method. According to the ARR 2019 guidelines (Ball et al., 2019), if record length of available streamflow data is adequate at the location of interest then at-site FFA should be used for estimation of DFs. FFA is aimed to establish a relationship between stream flow magnitude and its AEP and use the relationship to estimate the DF for different AEPs at a given location. A summary of the study, conclusions and recommendations for further study are presented in this chapter.

6.2 Summary of the Study

This study involves finding of the best-fit PD for flood quantile estimation using AMF data from 26 stream gauging stations within the Brisbane River catchment. The summary of this study are presented below.

6.2.1 Selection of Study catchments and Data Preparation

Initially more than 32 stream gauging stations are selected based on data quality, record length of streamflow data (>20-year) and catchment size. AMF time series data has been analysed for presence of missing data, quality of data and degree of regulation. Finally, a total of 26 stream gauging stations have been selected. Missing data (<2%) are infilled through regression analysis. FLIKE software is used to identify the presence of outliers in the AMF data (Section 5.4) and the outliers in data are censored as needed in FFA.

6.2.2 Selection of Probability Distribution

The selection of the most appropriate PD is a difficult task in FFA. The choice of the best-fit PD for FFA depends on the quantity and quality of recorded flood data, the goodness-of-fit (GoF) criteria used in selecting PD and visual assessment of the plotted AMF data and the fitted PD. Therefore, it is essential to evaluate several PDs by fitting with the available AMF data series to find the most appropriate PD to use for estimation of DFs. Based on a literature review, this study selects five most commonly used PDs as candidates, which are LN, Gumbel, LP3, GEV and GP to find the best-fit PD for flood estimation in the study region.

EasyFit and FLIKE software are used in this study. Both software has the option of fitting these 5 PDs with different parameter estimation methods. For Gumbel and LP3, MoM is used, for LN, MLE method is used and for GEV and GP Method of L-moments is used. Parameter estimation methods used in FLIKE are Bayesian inference and LH moments. In this study, LP3, Lognormal, GP and Gumbel distributions are fitted using the Bayesian inference method, whereas GEV distributions is fitted using the LH moments (with H = 1) method. When H = 0, the LH moments become L moments. When H > 1 is used, higher floods are given more importance in distributional fitting. Hence, for the LH moments, censoring of data is not required. It should be noted that no censoring is needed in the case of EV1, GEV and GP distributions.

6.2.3 Best-fit Probability Distribution and Quantile Estimation

In this study three different GoF tests are adopted to evaluate the appropriateness of a PD. The graphical plots from EasyFit and FLIKE software along with GoF test results are used for selection of the best-fit PD. The outcomes of GoF test and graphical plots form EasyFit are compared with the outcome of the FLIKE software. Three GoF tests (A-D, K-S and C-S) are carried out for all the five PDs for each of the 26 stations. The results of the three GoF tests show the ranking of all the five PDs, with rank 1 as the best-fit PD, rank 2 as the second best and rank 3 as the third best. The results of the GoF tests indicate that LP3 provides better fitting to the observed AMF data compared to GP, GEV, Lognormal and Gumbel distributions for most of the stream gauging stations in the study region. Results also show

that the 2-parameters Gumbel distribution is the least preferred PD in the study region. Figure 5.5 shows that for most of the rural catchments, LP3 is the best-fit PD.

The reason for LP3 distribution being selected as the best-fit distribution has little physical meaning but has few statistical justifications. The LP3 distribution is a 3-parameter distribution, and in general, a 3-parameter distribution should fit the AMF data better than a 2-parameter distribution (e.g. LN distribution) since flood data is generally skewed. The skewness coefficient measures the shape of a sampling distribution. When skewness is positive, LP3 yields slightly conservative estimates (Haktanir and Horlacher, 1993). The AMF data series of majority stations selected in this study show a positive skewness. One of the possible reasons is that the skewness of logged AMF data generally does not exceed the desirable limit of ± 1.4 (Griffis and Stedinger, 2005; Griffis and Stedinger, 2009; Rahman et al., 2016). In Australia, FFA studies conducted by Rahman et al. (2013) and Srikanthan and McMahon (1981) recommended LP3 as the most fitted distribution for FFA. Similar previous studies in the USA and in many other countries also recommended LP3 as the most suitable distribution (e.g. Vogel et al., 1993; Gunasekara and Cunnane, 1992).

Flood quantiles are estimated using FLIKE for each of the 26 stations using all the five PDs for ARIs of 2, 5, 10, 20, 50 and 100 years.

6.2.4 Sensitivity Analysis on Flood Quantile Estimation

Presence of outliers in the AMF data changes quantile estimation. It is seen from the analysis that quantile estimation can change up to 41% if outliers are not removed from the AMF data. Flood quantile estimation is also greatly affected if FFA analysis is carried out excluding maximum recorded flow data point (which is not outlier) from the AMF data series. Analysis shows that quantile estimation can reduce by 9% to 86% if FFA is repeated by removing maximum recorded flow data point form the AMF data series. This also changes the best-fit distribution selection in many cases.

6.2.4 Uncertainty Analysis on Flood Quantile Estimation

Uncertainty analysis of quantile estimation is carried out using bootstrapping and Monte Carlo simulation techniques. Uncertainty analysis with Monte Carlo simulation provides narrower confidence limits for 67% cases compared to that of by FLIKE; indicating that FLIKE gives an indication of possible uncertainty and not absolute uncertainty in FFA.

6.2.5 Trend Analysis

The detection of trend and step change in the AMF data is made using eWater's TREND software. It is found from the analysis that the trend in the AMF data is not significant for Brisbane River catchment. Haddad and Rahman (2011) found similar result in their FFA study for Tasmania; they found trends for only 3 out of 53 stations. Similar result was also found by Robson et al. (1998) in their study; they reported no significant trend in the AMF dataset of the United Kingdom. As the trend detection tests do not identify statistically significant trend in the AMF data series, non-stationary FFA is not considered in this research.

6.3 Conclusions

The following conclusions are drawn from this study:

- It is found that LP3 is the most preferred PD in the Brisbane River catchment, followed by the GP distribution. However, there are many cases where LP3 is not the best-fit PD. In many cases, the results of the goodness-of-fit tests do not agree with the outcome of the visual assessment in FLIKE plots.
- FLIKE software should be used for flood frequency analysis in Australia; however, it should be updated by incorporating GoF tests.
- The 2011 floods in the 26 stations within the Brisbane River catchment are generally smaller than a 100-year flood event.
- The selection of the best-fit PD by using three GoF statistical tests is influenced by the presence of the highest, the second highest and the third highest AMF records in

the data series; if these highest records are included, LP3 is the preferred distribution in the study region; however, the removal of the highest, the second highest and the third highest AMF data points make GP as the most preferred distribution and LP3 as the second most favourite one. It should be noted that the highest, second highest and third highest AMF values were not found as outliers. This result implies that as more and more intense flood will happen in future, the new AMF series may change the preferred distribution and GP may become the most preferred distribution in the study region. The presence of these high AMF data points affects the 100-year flood estimates significantly (by about 9 % to 86 %). This in essence indicates that if a very high flood occurs in future, the 100-year flood estimate (which are widely used in practice) could be much different than that obtained from the current AMF data series. Hence, FFA should be carried out after each big flood event to ensure that the existing hydraulic structures designed with the old AMF data do not put significant risk to the infrastructure and the community.

- The flood quantile estimates have a high level of uncertainty given that the record lengths of the AMF data are not too high; in particular, the 100-year flood has a significant level of uncertainty as found by the wider confidence intervals generated by the FLIKE and by the outcomes of the Monte Carlo simulation carried out in this study.
- There is no statistically significant trend in the AMF series within the Brisbane River catchment.

6.4 Recommendation for Future Research

The following further research tasks are recommended:

- The parent distribution should be checked by simulating AMF data from the fitted distribution at each of the sites within the study area.
- The non-stationary FFA should be conducted using the LP3, GP and GEV distributions.
- The study should be extended to other regions of Australia to confirm whether LP3 is the most preferred distribution across Australia.

- The at-site flood frequency analysis results should be compared with the ARR Regional Flood Frequency Analysis Model.
- FLIKE software should include goodness-of-fit tests in its subsequent upgrade.

REFERENCES

Abida, H., & Ellouze, M. (2008). Probability distribution of flood flows in Tunisia. *Hydrology and Earth System Sciences Discussions*, 12(3), 703-714.

Ahmad, M. I., Sinclair, C. D., & Werritty, A. (1988). Log-logistic flood frequency analysis. *Journal of Hydrology*, 98(3-4), 205-224.

Ahmad, I., Tang, D., Wang, T., Wang, M., & Wagan, B. (2015). Precipitation trends over time using Mann-Kendall and spearman's rho tests in swat river basin, Pakistan. *Advances in Meteorology*, *2015*.

Al Mamoon, A., & Rahman, A. (2014). Uncertainty in design rainfall estimation: a review. *J. Hydrol. Environ. Res*, 2(1), 65-75.

Alam, M., Emura, K., Farnham, C., & Yuan, J. (2018). Best-fit probability distributions and return periods for maximum monthly rainfall in Bangladesh. *Climate*, 6(1), 9.

Arnaud, P., Cantet, P., & Odry, J. (2017). Uncertainties of flood frequency estimation approaches based on continuous simulation using data resampling. *Journal of Hydrology*, 554, 360-369.

ARR (Australian Rainfall and Runoff) (1987). *A Guide to Flood Estimation , Vol. 1*, Editor-in-chief D.H. Pilgrim, Revised Edition 1987 (Reprinted edition 1998), Barton, ACT.

ARR (Australian Rainfall and Runoff) (2019). Ball J, Babister M, Nathan R, Weeks W, Weinmann E, Retallick M, Testoni I, (Editors) *A Guide to Flood Estimation*, Commonwealth of Australia (Geoscience Australia), 2019.

Atroosh, K. B., & Moustafa, A. T. (2012). An estimation of the probability distribution of Wadi Bana flow in the Abyan Delta of Yemen. *Journal of Agricultural Science*, 4(6), 80.

Ayre, R., Diermanse, F. L. M., Carroll, D. G., Hart, P., & Toombes, L. (2015). Reconciliation of design flood estimates for the Brisbane River catchment flood study. In *36th Hydrology and Water Resources Symposium: The art and science of water* (p. 592). Engineers Australia.

Ball, J. E., Babister, M. K., Nathan, R., Weinmann, P. E., Weeks, W., Retallick, M., & Testoni, I. (Editors) (2016). *Australian Rainfall and Runoff: A Guide to Flood estimation.* Commonwealth of Australia.

Ball, J., Babister, M., Nathan, R., Weeks, W., Weinmann, P. E., Retallick, M., & Testoni, I., (Editors), (2019). *Australian Rainfall and Runoff: A Guide to Flood Estimation,* Commonwealth of Australia.

Baghban, A. A., Younespour, S., Jambarsang, S., Yousefi, M., Zayeri, F., & Jalilian, F. A. (2013). How to test normality distribution for a variable: a real example and a simulation study. *Journal of Paramedical Sciences*, *4*(1), 73-77.

Baltussen, R. M., Hutubessy, R. C., Evans, D. B., & Murray, C. J. (2002). Uncertainty in cost-effectiveness analysis: probabilistic uncertainty analysis and stochastic league tables. *International journal of technology assessment in health care*, *18*(1), 112-119.

Bao, Y., Tung, Y. K., & Hasfurther, V. R. (1987). Evaluation of uncertainty in flood magnitude estimator on annual expected damage costs of hydraulic structures. *Water Resources Research*, 23(11), 2023-2029.

Barua, S., Muttil, N., Ng, A. W. M., & Perera, B. J. C. (2013). Rainfall trend and its implications for water resource management within the Yarra River catchment, Australia. *Hydrological Processes*, 27(12), 1727-1738.

BCC (Brisbane City Council) (2014). *Oxley Creek Flood Study Report Volume 1 of 2*, Prepared by Aurecon Australia Pty Ltd, June 2014.

Beard, L. R. (1962). *Statistical methods in hydrology*. Hydrologic Engineering Center Davis CA.

Benjamin, M. A. (2008). *Analysing urban flood risk in low-cost settlements of George, Western Cape, South Africa: Investigating physical and social dimensions* (Doctoral dissertation, University of Cape Town).

Benson, M. A. (1968). Uniform flood-frequency estimating methods for federal agencies. *Water resources research*, 4(5), 891-908.

Bethea, R. M., & Rhinehart, R. R. (1991). *Applied engineering statistics* (Vol. 121). CRC Press.

Bickel, P. J., & Doksum, K. A. (1977). *Mathematical statistics: basic ideas and selected topics*. Holden-Day. Inc. Oakland, CA.

Blazkova, S., & Beven, K. (2009). A limits of acceptability approach to model evaluation and uncertainty estimation in flood frequency estimation by continuous simulation: Skalka catchment, Czech Republic. *Water Resources Research*, 45(12).

Bobee, B. (1999). Extreme flood events valuation using frequency analysis: a critical review. *Houille Blanche*, (7), 100-105.

Bobee, B., & Rasmussen, P. F. (1995). Recent advances in flood frequency analysis. *Reviews of Geophysics*, *33*(S2), 1111-1116.

Bobee, B., Cavadias, G., Ashkar, F., Bernier, J., & Rasmussen, P. (1993). Towards a systematic approach to comparing distributions used in flood frequency analysis. *Journal of Hydrology*, 142(1-4), 121-136.

BOM (Australian Bureau of Meteorology) (2019). *Frequently Asked Questions, 2016 IFDs (new)*. Retrieved from http://www.bom.gov.au/water/designRainfalls/ifd/ifd-faq.shtml on november 2019.

Boon, H. J., Cottrell, A., & King, D. (2016). *Disasters and Social Resilience: a bioecological approach*. Routledge Explorations in Environmental Studies . Taylor & Francis, London, UK.

Boughton, W. C., & Hill, P. I. (1997). *A design flood estimation procedure using data generation and daily water balance model*. CRC for Catchment Hydrology.

Bouwer, L. M., Crompton, R. P., Faust, E., Höppe, P., & Pielke, R. A. (2007). Confronting disaster losses. *Science*, 318(5851), 753-753.

Buishand, T. A. (1982). Some methods for testing the homogeneity of rainfall records. *Journal of hydrology*, 58(1-2), 11-27.

Caballero, W. L., & Rahman, A. (2014). Development of regionalized joint probability approach to flood estimation: a case study for Eastern New South Wales, Australia. *Hydrological Processes*, *28*(13), 4001-4010.

Camici, S., Tarpanelli, A., Brocca, L., Melone, F., & Moramarco, T. (2011). Design soil moisture estimation by comparing continuous and storm-based rainfall-runoff modeling. *Water Resources Research*, 47(5).

Charalambous, J. (2004). Application of Monte Carlo Simulation Technique with URBS Runoff-Routing Model for design flood estimation in large catchments, Masters Thesis, Western Sydney University.

Charalambous, J., Rahman, A., & Carroll, D. (2005). Application of URBS-Monte Carlo simulation technique to large catchments for design flood estimation: a case study for the Johnstone River Catchment in Queensland. In *29th Hydrology and Water Resources Symposium: Water Capital, 20-23 February 2005, Rydges Lakeside, Canberra* (p. 139). Engineers Australia.

Chebana, F., Ouarda, T. B., & Duong, T. C. (2013). Testing for multivariate trends in hydrologic frequency analysis. *Journal of hydrology*, 486, 519-530.

Chiew F. (2005). Trend User Guide, CRC for Catchment Hydrology, Australia 2005.

Cohn, T. A., England, J. F., Berenbrock, C. E., Mason, R. R., Stedinger, J. R., & Lamontagne, J. R. (2013). A generalized Grubbs-Beck test statistic for detecting multiple potentially influential low outliers in flood series. *Water Resources Research*, 49(8), 5047-5058.

Cordery, I., & Pilgrim, D. H. (2000). The state of the art of flood prediction. *Floods*, 2, 185-197.

Cunderlik, J. M., & Burn, D. H. (2003). Non-stationary pooled flood frequency analysis. *Journal of Hydrology*, 276(1-4), 210-223.

Cunnane, C. (1978). Unbiased plotting positions—a review. *Journal of Hydrology*, 37(3-4), 205-222.

Cunnane, C. (1985). Factors affecting choice of distribution for flood series. *Hydrological Sciences Journal*, 30(1), 25-36.

Cunnane, C. (1989). Statistical distributions for flood frequency analysis Operational hydrology report (OHR) no. 33, WMO series no. 718. *World Meteorological Organization (WMO).*

CWC (2018). Climate Predictability of Extreme Floods, *Columbia Water Center, Earth Institute, Columbia University, USA.* Retrieved from http: ///water.columbia.edu/research-themes/global-floods-initiative/climate-predictability-of-extreme-floods/ on 15 July 2018.

Data, C. (2009). Guidelines on analysis of extremes in a changing climate in support of informed decisions for adaptation. *World Meteorological Organization (WMO).*

Debele, S. E., Strupczewski, W. G., & Bogdanowicz, E. (2017). A comparison of three approaches to non-stationary flood frequency analysis. *Acta Geophysica*, 65(4), 863-883.

Drokin, A. (2018). EasyFit Software, *MathWave Technologies* Rertieved from http://www.mathwave.c om on 9 September 2017.

DSDIP/DNRM (Department of State Development, Infrastructure and Planning/Department of Natural Resources and Mines) (2015). Document ID 238021-0000-REP-KT-0005: *Flood Frequency Analysis Report,* https://www.publications.qld.gov.au/dataset/brisbane-river-catchment-flood-study/resource/45bb1c48-2bce-4d2d-b857-294f3bb407ac on 25 August 2018

Dunne, T., & Leopold, L. B. (1978). Water in environmental planning. W. H. Freeman Co., San Francisco, 818 pp., 1978.

Efron, B., & Tibshirani, R. (1993). *An Introduction to the Bootstrap*. Boca Raton, FL Chapman & Hall/CRC.ISBN 0-412-04231-2, software.

Efron, B., & Tibshirani, R. J. (1994). *An introduction to the bootstrap*. Chapman & Hall/CRC press.

El-Kafagee, M., & Rahman, A. (2011). A study on initial and continuing losses for design flood estimation in New South Wales. *In Proceedings of the 19th International Congress on Modelling and Simulation (MODSIM2011): Sustaining our Future: Understanding and Living with Uncertainty*: Perth Convention and Exhibition Centre, Perth, Western Australia, 12-16 December 2011 (pp. 3782-3787).

eWater (2018). eWater Toolkit (Retrieved from https: //toolkit.ewater.org.au/trend) *eWater Innovation Centre*, University of Canberra, ACT 2601, www.ewater.com.au on 21 August 2017.

Feldman, A. D. (1979). *Flood Hydrograph and Peak Flow Frequency Analysis* (No. HEC-TP-62). Hydrologic Engineering Center, Davis, CA.

FLIKE, (2017) FLIKE software, *Flood estimation probability models*, Retrieved from https://flike.tuflow.com/flikehelp.htm, 3 July 2017.

Foster, H. A. (1924). Theoretical frequency curves and their application to engineering problem. *Transactions of the American Society of Civil Engineers*, 88(1), 142-173.

Franks, S. W., White, C. J., & Gensen, M. (2015). Estimating extreme flood events–assumptions, uncertainty and error. *Proceedings of the International Association of Hydrological Sciences*, 369, 31-36.

Frisby, S. R., Yan, Y., Niven, D., & Yu, B. (2018). Efficient flood estimation using ARR 2016 temporal patterns in South East Queensland. In *Hydrology and Water Resources Symposium (HWRS 2018): Water and Communities* (p. 252). Engineers Australia.

Gabriele, S., & Arnell, N. (1991). A hierarchical approach to regional flood frequency analysis. *Water Resources Research*, 27(6), 1281-1289.

Ghasemi, A., & Zahediasl, S. (2012). Normality tests for statistical analysis: a guide for non-statisticians. *International journal of Endocrinology and Metabolism*, 10(2), 486.

Gilroy, K. L., & McCuen, R. H. (2012). A nonstationary flood frequency analysis method to adjust for future climate change and urbanization. *Journal of Hydrology*, 414, 40-48.

Green, J. H., Johnson, F. M., & The, C. (2011). Revision of the Short Duration Intensity-Frequency-Duration (IFD) Design Rainfall Estimates for Australia. In: Valentine, EM (Editor); Apelt, CJ (Editor); Ball, J (Editor); Chanson, H (Editor); Cox, R (Editor); Ettema, R (Editor); Kuczera, G (Editor); Lambert, M (Editor); Melville, BW (Editor); Sargison, JE (Editor). *Proceedings of the 34th World Congress of the International Association for Hydro-Environment Research and Engineering: 33rd Hydrology and Water Resources Symposium and 10th Conference on Hydraulics in Water Engineering.* Barton, A.C.T.: Engineers Australia, 2011: 147-153.

Griffis, V. W., & Stedinger, J. R. (2005). The LP3 distribution and its use for flood frequency analysis. *In Impacts of Global Climate Change* (pp. 1-12).

Griffis, V. W., & Stedinger, J. R. (2007). Log-Pearson Type 3 distribution and its application in flood frequency analysis. I: Distribution characteristics. *Journal of Hydrologic Engineering*, 12(5), 482-491.

Griffis, V. W., & Stedinger, J. R. (2009). Log-Pearson Type 3 distribution and its application in flood frequency analysis. III: Sample skew and weighted skew estimators. *Journal of Hydrologic Engineering*, 14(2), 121-130.

Grimaldi, S., Petroselli, A., & Serinaldi, F. (2012). Design hydrograph estimation in small and ungauged watersheds: continuous simulation method versus event-based approach. *Hydrological Processes*, 26(20), 3124-3134.

Grubbs, F. E. (1969). Procedures for detecting outlying observations in samples. *Technometrics*, 11(1), 1-21.

Grubbs, F. E., & Beck, G. (1972). Extension of sample sizes and percentage points for significance tests of outlying observations. *Technometrics*, 14(4), 847-854.

Gubareva, T. S. (2011). Types of probability distributions in the evaluation of extreme floods. *Water Resources*, 38(7), 962-971.

Gumbel, E. J. (1941). Probability-interpretation of the observed return-periods of floods. *Eos, Transactions American Geophysical Union*, 22(3), 836-850.

Gunasekara, T. A. G., & Cunnane, C. (1992). Split sampling technique for selecting a flood frequency analysis procedure. *Journal of Hydrology*, 130(1-4), 189-200.

Guru, N., & Jha, R. (2015). Flood frequency analysis of Tel Basin of Mahanadi river system, India using annual maximum and POT flood data. *Aquatic Procedia*, 4, 427-434.

Gyau-Boakye, P., & Schultz, G. A. (1994). Filling gaps in runoff time series in West Africa. *Hydrological Sciences Journal*, 39(6), 621-636.

Haddad, K. (2008). *Design flood estimation for ungauged catchments in Victoria: ordinary and generalised least squares methods compared.* M.Eng.(Hons) Thesis, Western Sidney University, Australia.

Haddad, K. (2013). *Regional flood frequency analysis in the range of small to large floods: development and testing of Bayesian regression-based approaches*. Doctor of Philosophy Thesis, Western Sidney University, Australia.

Haddad, K., & Rahman, A. (2008). Investigation on at-site flood frequency analysis in south-east Australia. IEM Journal, *The Journal of The Institution of Engineers*, Malaysia, 69(3), 59-64.

Haddad, K., & Rahman, A. (2011). Selection of the best fit flood frequency distribution and parameter estimation procedure: a case study for Tasmania in Australia. *Stochastic Environmental Research and Risk Assessment*, 25(3), 415-428.

Haddad, K., & Rahman, A. (2012). Regional flood frequency analysis in eastern Australia: Bayesian GLS regression-based methods within fixed region and ROI framework–Quantile Regression vs. Parameter Regression Technique. *Journal of Hydrology*, 430, 142-161.

Haddad, K., Rahman, A., Zaman, M., & Shrestha, S. (2013). Applicability of Monte Carlo cross validation technique for model development and validation in hydrologic regression analysis using ordinary and generalised least squares regression. *Journal of Hydrology*, 482, 119-128.

Haddad, K., Rahman, A., Weinmann, P. E., Kuczera, G., & Ball, J. (2010). Streamflow data preparation for regional flood frequency analysis: Lessons from southeast Australia. *Australasian Journal of Water Resources*, 14(1), 17-32.

Hajani, E., & Rahman, A. (2017). [In Press] Characterising changes in rainfall: a case study for New South Wales State, Australia. *International Journal of Climatology.* 38(3), 1452-1462.

Hajani, E., & Rahman, A. (2018). Characterizing changes in rainfall: a case study for New South Wales, Australia. *International Journal of Climatology*, 38(3), 1452-1462.

Hajani, E., Rahman, A., & Ishak, E. (2017). Trends in extreme rainfall in the state of New South Wales, Australia. *Hydrological Sciences Journal*, 62(13), 2160-2174.

Haktanir, T. (1992). Comparison of various flood frequency distributions using annual flood peaks data of rivers in Anatolia. *Journal of Hydrology*, 136(1-4), 1-31.

Haktanir, T., & Horlacher, H. B. (1993). Evaluation of various distributions for flood frequency analysis. *Hydrological Sciences Journal*, 38(1), 15-32.

Harlin, J., & Kung, C. S. (1992). Parameter uncertainty and simulation of design floods in Sweden. *Journal of Hydrology*, 137(1-4), 209-230.

Hazen, A., (1914). Discussion on 'Flood flows' by W. E. Fuller, *Transaction of American Society of Civil Engineer*, 77, 626-632.

Hirsch, R. M. (1979). An evaluation of some record reconstruction techniques. *Water Resources Research*, 15(6), 1781-1790.

Hossain, A., Rahman, M. M., & Rahman, A. (2017). Queensland Flood in 2010-11: Will This Type of Flood Occur Soon? In *Proceedings of the 1st International Conference on Engineering Research and Practice, 4-5 February 2017, Dhaka, Bangladesh* (pp. 102-108).

Hossain, S. A., & Rahman, A. (2019, January). Trend Analysis in Flood Data in the Brisbane River Catchment, Australia. In *2nd International Conference on Water and Environmental Engineering (iCWEE-2019, Dhaka*.

Hossain, S. M. A. (2019). Selection of the best-fit probability distribution for Brisbane River Catchment. *International Journal of Engineering, Construction and Computing, pp90-103 Volume 1 Issue 1, 2019.*

Houghton, J. C., (1977). Robust estimations of the frequency of extreme events in a flood frequency context, Ph.D. dissertation, *Harvard University, Cambridge, Mass.*

Houghton, J. C., (1978). Birth of a parent: The Wakeby distribution for modeling flood flows, *Water Resour. Research*, 14(6), 1105-1110.

Hounkpe, J., Diekkrüger, B., Badou, D., & Afouda, A. (2015). Non-stationary flood frequency analysis in the Oueme River Basin, Benin Republic. *Hydrology*, 2(4), 210-229.

Huntington, T. G. (2006). Evidence for intensification of the global water cycle: review and synthesis. *Journal of Hydrology*, 319(1-4), 83-95.

IACWD (Interagency Advisory Committee on Water Data.) (1982). Guidelines for determining flood flow frequency: Bulletin 17B of the Hydrology Subcommittee. *Office of Water Data Coordination, US Geological Survey*.

I. E. Aust. (Institute of Engineers Australia) (2014). ARR Project 13, *Rational Method Developments for Estimation of the peak flow on a small to medium sized rural catchment*, P13/S3/001, February 2014, Barton ACT, Australia.

I. E. Aust. (Institution of Engineers Australia) (1987). *Australian Rainfall and Runoff A Guide to Flood Estimation, Vol. 1*, I. E. Aust., Canberra, 1987.

IFM (Integrated Flood Management), (2018). *Approach to Flood Estimation*, Flood Manager eLearning. Retrieved from http://daad.wb.tu-harburg.de/tutorial/flood-probability-assessment/hydrology-of-floods/flood-frequencies-and-design-flood/design-flood/approaches-to-flood-estimation/, on 3 Feb 2018.

IFMRC (Interagency Floodplain Management Review Committee) (US), Interagency Floodplain Management Review Committee (US)., & United States. Federal Interagency Floodplain Management Task Force. (1994). *Sharing the Challenge: Floodplain Management into the 21st Century: Report of the Interagency Floodplain Management Review Committee* to the Administration Floodplain Management Task Force, Washington DC, USA.

IPCC (Intergovernmental Panel on Climate Change) (2007). *Summary for Policymakers. In Climate Change 2007 The Physical Science Basis*. Contribution of Working Group I to the Fourth Assessment Report of the Intergovernmental Panel on Climate Change [Solomon, S., D. Qin, M. Manning, Z. Chen, M. Marquis, K.B. Averyt, M. Tignor and H.L. Miller (eds.)], Cambridge University Press Cambridge, UK and New York, USA.

IPCC (Intergovernmental Panel on Climate Change) (2014). *Climate change 2014; assessment synthesis report [online]*. Retrieved from http://www.ipcc.ch/report/ar5/syr on 19 January 2018.

Ishak, E. H., Rahman, A., Westra, S., Sharma, A., & Kuczera, G. (2010). Preliminary analysis of trends in Australian flood data. *In World Environmental and Water Resources Congress 2010: Challenges of Change* (pp. 115-124).

Ishak, E. H., Rahman, A., Westra, S., Sharma, A., & Kuczera, G. (2013). Evaluating the non-stationarity of Australian annual maximum flood. *Journal of Hydrology*, 494, 134-145.

Jackson, D. R. (1981). WRC standard flood frequency guidelines. *Journal of the Water Resources Planning and Management Division*, 107(1), 211-224.

James, W., & Robinson, M. (1986). Continuous deterministic urban runoff modelling. In Urban Drainage Modeling, *Proc., International Symp. on Comparison of Urban Drainage Models with Real Catchments Data, UDM'86* (pp. 347-378). Pergamon, New York.

Javari, M. (2016). Trend and Homogeneity Analysis of Precipitation in Iran. *Climate*, 4(3), 44.

Jenkinson, A. F. (1955). The frequency distribution of the annual maximum (or minimum) values of meteorological elements. *Quarterly Journal of the Royal Meteorological Society*, 81(348), 158-171.

Jordan, P., Seed, A., Nathan, R., Hill, P., Kordomenidi, E., Pierce, C., & Leonard, M. (2014). Stochastic simulation of inflow hydrographs for Wivenhoe and Somerset dams. *Ancold* 2014, 1-8.

Kamal, V., Mukherjee, S., Singh, P., Sen, R., Vishwakarma, C. A., Sajadi, P., ... & Rena, V. (2017). Flood frequency analysis of Ganga river at Haridwar and Garhmukteshwar. *Applied Water Science*, 7(4), 1979-1986.

Karim, M. A., & Chowdhury, J. U. (1995). A comparison of four distributions used in flood frequency analysis in Bangladesh. *Hydrological Sciences Journal*, 40(1), 55-66.

Karmakar, S., Simonovic, S. P., Peck, A., & Black, J. (2010). An information system for risk-vulnerability assessment to flood. *Journal of Geographic Information System*, 2(03), 129.

Kendall, M.G. (1975). Rank correlation methods. Vol. 202. London Griffin Publishers.

Khaliq, M. N., Ouarda, T. B., Gachon, P., Sushama, L., & St-Hilaire, A. (2009). Identification of hydrological trends in the presence of serial and cross correlations: A review of selected methods and their application to annual flow regimes of Canadian rivers. *Journal of Hydrology*, 368(1-4), 117-130.

Khaliq, M. N., Ouarda, T. B. M. J., Ondo, J. C., Gachon, P., & Bobée, B. (2006). Frequency analysis of a sequence of dependent and/or non-stationary hydro-meteorological observations: A review. *Journal of Hydrology*, 329(3-4), 534-552.

Kidson, R., & Richards, K. S. (2005). Flood frequency analysis: assumptions and alternatives. *Progress in Physical Geography*, 29(3), 392-410.

Kim, S., Kho, Y., Shin, H., & Heo, J.H. (2008). Derivation of the probability plot correlation coefficient test statistics for the generalized logistic and the generalized Pareto distributions. *In World Environmental and Water Resources Congress 2008*: Ahupua'A (pp. 1-10).

Klemes, V. (1988). The improbable probabilities of extreme floods and droughts. *In Hydrology of Disasters: Proceedings of the World Meteorological Organization Technical Conference* Held in Geneva.

Kopittke, R. A., Stewart, B. J., & K. S. Tickle, K. S. (1976). Frequency analysis of flood data in Queensland. In *Hydrological Symposium, Institution of Engineers Australia, National Conference, Publication*, no. 76/2, p. 20. 1976.

Kuczera, G., & Franks, S. (2016). At-site flood frequency analysis. *Australian Rainfall and Runoff: A Guide to Flood Estimation*; Ball, JE, Babister, M., Nathan, R., Weeks, W., Weinmann, E., Retallick, M., Testoni, I., Eds.

Kuczera, G., Kavetski, D., Franks, S., & Thyer, M. (2005). *Characterizing model error in conceptual rainfall-runoff models using storm-dependent parameters*. 16th International Congress on Modelling and Simulation (Melbourne, Victoria) Modelling and Simulation Society of Australia and New Zealand, December 2005 / Andre Zerger and Robert M. Argent (eds.): pp. 2925-293.

Kuczera, G. (1983). A Bayesian surrogate for regional skew in flood frequency analysis. *Water Resources Research* 19(3), 821–832.

Kuczera, G. (1999). Comprehensive at-site flood frequency analysis using Monte Carlo Bayesian inference. *Water Resources Research*, 35(5), 1551-1557.

Kunkel, K. E. (2003). North American trends in extreme precipitation. *Natural Hazards*, 29(2), 291-305.

Laio, F., Di Baldassarre, G., & Montanari, A. (2009). Model selection techniques for the frequency analysis of hydrological extremes. *Water Resources Research*, 45(7).

Lamontagne, J. R., Stedinger, J. R., Cohn, T. A., & Barth, N. A. (2013). Robust national flood frequency guidelines: What is an outlier? In *World Environmental and Water Resources Congress 2013: Showcasing the Future* (pp. 2454-2466).

Laz, O. U., Rahman, A., Yilmaz, A., & Haddad, K. (2014). Trends in sub-hourly, sub-daily and daily extreme rainfall events in eastern Australia. *Journal of Water and Climate Change*, 5(4), 667-675.

Li, Z., Shao, Q., Xu, Z., & Cai, X. (2010). Analysis of parameter uncertainty in semi-distributed hydrological models using bootstrap method: A case study of SWAT model applied to Yingluoxia watershed in northwest China. *Journal of Hydrology*, 385(1-4), 76-83.

Liang, Z., Chang, W., & Li, B. (2012). Bayesian flood frequency analysis in the light of model and parameter uncertainties. *Stochastic Environmental Research and Risk Assessment*, 26(5), 721-730.

Lim, Y. H., & Lye, L. M. (2003). Regional flood estimation for ungauged basins in Sarawak, Malaysia. *Hydrological Sciences Journal*, 48(1), 79-94.

Liu, X., Liu, C., Luo, Y., Zhang, M., & Xia, J. (2012). Dramatic decrease in streamflow from the headwater source in the central route of China's water diversion project: Climatic variation or human influence? *Journal of Geophysical Research: Atmospheres*, 117(D6).

Lumb, A. M., & James, L. D. (1976). Runoff files for flood hydrograph simulation. *Journal of the Hydraulics Division*, 102(ASCE# 12499).

Machiwal, D., & Jha, M. K. (2009). Time series analysis of hydrologic data for water resources planning and management: a review. *Journal of Hydrology and Hydromechanics*, 54(3), 237-257.

Mamoon, A. A., & Rahman, A. (2017). Selection of the best fit probability distribution in rainfall frequency analysis for Qatar, *Natural Hazards*, 86(1), 281-296.

Mamoon, A. A., & Rahman, A. (2019). Uncertainty analysis in design rainfall estimation due to limited data length: A case study in Qatar. *In Extreme Hydrology and Climate Variability* (pp. 37-45). Elsevier.

Mann, H. B. (1945). Nonparametric tests against trend. Econometrica: *Journal of the Econometric Society*, 245-259.

Mathwave (2017). MathWave Technologies, *EasyFit version 6.5*, Retrieved from http:////www.mathwave.com, on 11 Feb 2017.

Mazumder, T. (2005). Application of the joint probability approach to ungauged catchments for design flood estimation, MPhil Thesis, Western Sydney University, Australia.

McMahon, T. A., & Srikanthan, R. (1981). Log Pearson III distribution—is it applicable to flood frequency analysis of Australian streams? *Journal of Hydrology*, 52(1-2), 139-147.

McMahon, G. M., & Kiem, A. S. (2018). Large floods in South East Queensland, Australia: Is it valid to assume they occur randomly? *Australasian Journal of Water Resources*, *22*(1), 4-14.

Melching, C. S. (1995). Reliability estimation. In: *Computer Models of Watershed Hydrology*, Water Resource Publications.

Merz, B., & Thieken, A. H. (2005). Separating natural and epistemic uncertainty in flood frequency analysis. *Journal of Hydrology*, 309(1-4), 114-132.

Millington, N., Das, S., & Simonovic, S. P. (2011). The comparison of GEV, log-Pearson type 3 and Gumbel distributions in the Upper Thames River watershed under global climate models. Department of Civil and Environmental Engineering, The University of Western Ontario.

Mirfenderesk, H., Carroll, D., Chong, E., Rahman, M., Kabir, M., Van Doorn, R., & Vis, S. (2013). Comparison between design event and joint probability hydrological modelling. *In Flood Management Association National Conference*, Tweed Heads (pp. 1-9).

Mishra, B. K., Takara, K., Yamashiki, Y., & Tachikawa, Y. (2010). An assessment of predictive accuracy for two regional flood-frequency estimation methods. *Annual Journal of Hydraulic Engineering*, 54, 7-12.

Muzik, I. (2002). A first-order analysis of the climate change effect on flood frequencies in a subalpine watershed by means of a hydrological rainfall–runoff model. *Journal of Hydrology*, 267(1-2), 65-73.

NERC (National Environment Research Council) (1975). *Flood Studies Report*, I, Hydro. Studies, London, England, UK.

NERC (National Environment Research Council) (1999). *Flood Studies Report, (in five volumes)*, London, England, UK.

Nortje, J. H. (2010). Estimation of extreme flood peaks by selective statistical analyses of relevant flood peak data within similar hydrological regions. *Journal of the South African Institution of Civil Engineering*, 52(2), 48-57.

NRC (National Research Council) (1988). Committee on techniques for estimating probabilities of extreme floods. *Estimating probabilities of extreme floods, methods and recommended research*, National Academies Press.

O'Brien, N. L., & Burn, D. H. (2014). A nonstationary index-flood technique for estimating extreme quantiles for annual maximum streamflow. *Journal of Hydrology*, 519, 2040-2048.

OQCS (2016). *Understanding Flood*, Office of the Queensland Chief Scientist, Australia 2016. Retrieved from www.chiefscientist.qld.gov.au/publications/understanding-loods/flood-consequences on 27 June 2018.

Palmen, L. B., & Weeks, W. D. (2011). Regional flood frequency for Queensland using the quantile regression technique. *Australasian Journal of Water Resources*, *15*(1), 47-57.

Pandey, H. K., Dwivedi, S., & Kumar, K. (2018). Flood Frequency Analysis of Betwa River, Madhya Pradesh India. *Journal of the Geological Society of India*, 92(3), 286-290.

Pekarova, P., Miklanek, P., & Pekar, J. (2003). Spatial and temporal runoff oscillation analysis of the main rivers of the world during the 19th–20th centuries. *Journal of Hydrology*, 274(1-4), 62-79.

Petrow, T., & Merz, B. (2009). Trends in flood magnitude, frequency and seasonality in Germany in the period 1951–2002. *Journal of Hydrology*, 371(1-4), 129-141.

Pilgrim, D. H., & McDermott, G. E. (1982). Design Floods for small rural catchments in eastern New South Wales. Civil Engineering Transactions Institution of Engineers Australia, CE24(3), 226–234.

Platt, R.H. (1995). Sharing the Challenge: Floodplain Management into the 21st Century: Interagency Floodplain Management Review Committee of the Floodplain Management Task Force. *Environment: Science and Policy for Sustainable Development*, *37*(1), pp.25-28.

QLD Gov. (Queensland State Government) (2017). *Brisbane River Catchment Flood Study Technical Summary Report.* Retrived from https://www.publications.qld.gov.au/dataset/brisbane-river-catchment-flood-study/resource/f8f0f20f-60cc-4233-b282-6b6d85f65817, on 6 Feb 2018.

Rahman, A., Bates, B. C., Mein, R. G., & Weinmann, E. (1997). Towards a new regional flood frequency analysis procedure for South-East Australia. *In Hydrology and Water Resources Symposium 1997 (pp. 179-184).* New Zealand Hydrological Society.

Rahman, A., Hoang, T. M. T., Weinmann, P. E., & Laurenson, E. M. (1998). Joint probability approaches to design flood estimation: A review. Report 98, 8, Monash University, Australia.

Rahman, A., Rima, K., & Weeks, W. (2008). Development of regional flood estimation methods using quantile regression technique: A case study for North-eastern part of Queensland. *Proceedings of Water Down Under 2008*, 329.

Rahman, A. S., Rahman, A., Zaman, M. A., Haddad, K., Ahsan, A., & Imteaz, M. (2013). A study on selection of probability distributions for at-site flood frequency analysis in Australia. *Natural Hazards*, 69(3), 1803-1813.

Rahman, A., Charron, C., Ouarda, T. B., & Chebana, F. (2018). Development of regional flood frequency analysis techniques using generalized additive models for Australia. *Stochastic Environmental Research and Risk Assessment*, 32(1), 123-139.

Rahman, A., Haddad, K., Ishak, E., Weinmann, E., & Kuczera, G. (2010). Regional flood estimation in Australia: An overview of the study in relation to the upgrade of Australian rainfall and runoff. *Flood Management Association Conference, Australia*.

Rahman A., Haddad K., Kuczera G., Weinmann P.E. (2016). *Regional flood methods*. In Australian Rainfall & Runoff, Chapter 3, Book 3, edited by Ball et al., Commonwealth of Australia.

Rahman, A., Haddad, K., Kuczera, G., & Weinmann, E. (2019). *Regional flood methods*. Australian Rainfall and Runoff: A Guide to Flood Estimation. Book 3, Peak Flow Estimation, 105-146.

Rahman, A., Haddad, K., Zaman, M., Kuczera, G., Weinmann, E., & Weeks, W. (2012). Regional flood estimation in Australia: an overview of the study for the upgrade of'Australian Rainfall and Runoff'. *In Hydrology and Water Resources Symposium* 2012 (p. 1441). Engineers Australia.

Rahman, A., Haque, M.M., Haddad, K., Rahman, A.S., Kuczera, G., Weinmann, P.E. (2013). Assessment of the Impacts of Rating Curve Uncertainty on At-Site Flood Frequency Analysis: A Case Study for New South Wales, Australia, 35th *Hydrology and Water Resources Symposium*, Perth, Engineers Australia, 24-27 February 2014, 962-969.

Rahman, A., Haddad, K., & Eslamian, S. (2014a). Regional flood frequency analysis. Handbook of Engineering Hydrology: Modeling, *Climate Change and Variability*, 451-469.

Rahman, A. S., Haddad, K., & Rahman, A. (2014b). Impacts of outliers in flood frequency analysis: A case study for Eastern Australia. *Journal of Hydrology and Environment Research*, 2(1), 17-13.

Rahman, A., Weinmann, P. E., Hoang, T. M. T., & Laurenson, E. M. (2002). Monte Carlo simulation of flood frequency curves from rainfall. *Journal of Hydrology*, 256(3-4), 196-210.

Rahman, A., Zaman, M. A., Haddad, K., El Adlouni, S., & Zhang, C. (2015). Applicability of Wakeby distribution in flood frequency analysis: a case study for eastern *Australia. Hydrological processes*, 29(4), 602-614.

Rao, R.A., & Hamed, K. (2000). *Flood Frequency Analysis*. CRC Press LCC, (2000) NW Corporate Blvd., Boca Ranton, Florida.

Renard, B., Kavetski, D., Kuczera, G., Thyer, M., & Franks, S. W. (2010). Understanding predictive uncertainty in hydrologic modeling: The challenge of identifying input and structural errors. *Water Resources Research*, 46(5).

Robson, A. J., Jones, T. K., Reed, D. W., & Bayliss, A. C. (1998). A study of national trend and variation in UK floods. *International Journal of Climatology: A Journal of the Royal Meteorological Society*, 18(2), 165-182.

Rogger, M., Kohl, B., Pirkl, H., Viglione, A., Komma, J., Kirnbauer, R., & Blöschl, G. (2012). Runoff models and flood frequency statistics for design flood estimation in Austria–Do they tell a consistent story? *Journal of Hydrology*, 456, 30-43.

Rosner, B. (1975). On the detection of many outliers. *Technometrics*, 17(2), 221-227.

Rosner, B. (1983). Percentage points for a generalized ESD many-outlier procedure. *Technometrics*, 25(2), 165-172.

Rossi, F., Fiorentino, M., & Versace, P. (1984). Two-component extreme value distribution for flood frequency analysis. *Water Resources Research*, 20(7), 847-856.

Sadeghi, S. H. R., & Hazbavi, Z. (2015). Trend analysis of the rainfall erosivity index at different time scales in Iran. *Natural Hazards*, 77(1), 383-404.

Salas, J. D. (1993). Chapter 19: Analysis and modeling of hydrologic time series. *Handbook of Hydrology. McGraw-Hill Inc, New York.*

Sarauskiene, D., & Kriauciuniene, J. (2011). Flood frequency analysis of Lithuanian rivers. In *Environmental Engineering. Proceedings of the International Conference on Environmental Engineering. ICEE* (Vol. 8, p. 666). Vilnius Gediminas Technical University.

Seckin, N., Haktanir, T., & Yurtal, R. (2011). Flood frequency analysis of Turkey using L-moments method. *Hydrological Processes*, 25(22), 3499-3505.

Sharma, P.J., Patel, P.L., & Jothiprakash, V. (2016). At-site flood frequency analysis for upper Tapi Basin, India, *ISH - HYDRO 2016 International*.

Singo, L. R., Kundu, P. M., Odiyo, J. O., Mathivha, F. I., & Nkuna, T. R. (2012). Flood frequency analysis of annual maximum stream flows for Luvuvhu River Catchment, Limpopo Province, South Africa.

Smithers, J. C. (2012). Methods for design flood estimation in South Africa. *Water SA*, 38(4), 633-646.

Srikanthan, R., & McMahon, T. A. (1981). Log Pearson III distribution—An empirically-derived plotting position. *Journal of Hydrology*, 52(1-2), 161-163.

Solaiman, T. A. (2011). Uncertainty estimation of extreme precipitations under climate change: A non-parametric approach, PhD Thesis, The University of Western Ontario.

SoQ (State of Queensland) (2017). *Brisbane River Catchment Flood Study (BRCFS) Technical Summary Report, Hydrologic and Hydraulic Assessments*. Retrieved from https://cabinet.qld.gov.au/documents/2017/Apr/FloodStudies/Attachments/TechnicalSummary.PDF, on 12 Feb 2018.

Stedinger, J. R., & Cohn, T. A. (1986). Flood frequency analysis with historical and paleoflood information. *Water Resources Research*, 22(5), 785-793.

Stedinger, J. R., Vogel, R. M & Foufoula-Georgiou, E. (1993). Frequency analysis of extreme events. In *Handbook of Hydrology*, edited by D.R Maidment, McGraw-Hill, N.Y., Chap.18.

Tao, D. Q., Nguyen, V. T., & Bourque, A. (2002). On selection of probability distributions for representing extreme precipitations in Southern Quebec. *In Annual conference of the Canadian society for civil engineering* (Vol. 5, pp. 1-8).

Tencaliec, P., Favre, A. C., Prieur, C., & Mathevet, T. (2015). Reconstruction of missing daily streamflow data using dynamic regression models. *Water Resources Research*, 51(12), 9447-9463.

Thompson R.D., & Perry, A. (Eds.) (1998). *Applied Climatology, Principles and Practice*, Routledge, London, p. 352.

Tung, Y. K., & Wong, C. L. (2014). Assessment of design rainfall uncertainty for hydrologic engineering applications in Hong Kong. *Stochastic Environmental Research and Risk Assessment*, 28(3), 583-592.

USDIGS (U.S. Department of the Interior Geological Syrvey) (1981). *Guidelines for determining flood flow frequency*, *Bulletin #17* of the Hydrology Sub Committee, Office of Water Data Coordination, U.S. Dep of the Int. Geol. Surv., Reston, Virginia.

USWRC (United States Water Resources Council) (1967). *A Uniform Technique for Determining Flood Flow Frequencies, Bulletin 15*, USWRC, Washington DC, USA.

van den Honert, R. C., & McAneney, J. (2011). The 2011 Brisbane floods: causes, impacts and implications. *Water*, 3(4), 1149-1173.

Van Herk, S. (2014). Delivering integrated flood risk management: Governance for collaboration, learning and adaptation. *IHE Delft Institute for Water Education*.

Viglione, A., Merz, R., & Blöschl, G. (2009). On the role of the runoff coefficient in the mapping of rainfall to flood return periods. *Hydrology and Earth System Sciences*, 13(5), 577-593.

Viglione, A., Merz, R., Salinas, J. L., & Blöschl, G. (2013). Flood frequency hydrology: 3. A Bayesian analysis. *Water Resources Research*, 49(2), 675-692.

Vogel, R. M., McMahon, T. A., & Chiew, F. H. (1993). Floodflow frequency model selection in Australia. *Journal of Hydrology*, 146, 421-449.

Villarini, G., Smith, J. A., Serinaldi, F., Bales, J., Bates, P. D., & Krajewski, W. F. (2009). Flood frequency analysis for nonstationary annual peak records in an urban drainage basin. *Advances in Water Resources*, 32(8), 1255-1266.

Vogel, R. M., & Kroll, C. N. (1989). Low-flow frequency analysis using probability-plot correlation coefficients. *Journal of Water Resources Planning and Management*, 115(3), 338-357.

Vogel, R. M., McMahon, T. A., & Chiew, F. H. (1993). Floodflow frequency model selection in Australia. *Journal of Hydrology*, 146, 421-449.

Weber, T. (2018). *Focus Catchment Coordinator (Brisbane River Catchment* -eWater , CRC for Catchment Hydrolog Retrieved from https://ewater.org.au/archive/crcch/focus_catchments/brisriver.html on 11 November 2018.

Wallis, J. R., Lettenmaier, D. P., & Wood, E. F. (1991). A daily hydroclimatological data set for the continental United States. *Water Resources Research*, 27(7), 1657-1663.

Weeks, W. D. (1991). Design floods for small rural catchments in Queensland. *Transactions of the Institution of Engineers, Australia. Civil Engineering*, *33*(4), 249-261.

Wijesekera, N.T.S. & Perera, L.R.H. (2012). Key Issues of Data and Data Checking for Hydrological Analyses-Case Study of Rainfall Data in the Attanagalu Oya Basin of Sri Lanka. Engineer: *Journal of the Institution of Engineers*, Sri Lanka, 45(2).

Woodhouse, C. A., Gray, S. T., & Meko, D. M. (2006). Updated streamflow reconstructions for the Upper Colorado River basin. *Water Resources Research*, 42(5).

Xu, Y. P., Booij, M. J., & Tong, Y. B. (2010). Uncertainty analysis in statistical modeling of extreme hydrological events. *Stochastic Environmental Research and Risk Assessment*, 24(5), 567-578.

Yevjevich, V. M., & Jeng, R. I. S. (1969). Properties of non-homogeneous hydrologic time series. *Hydrology papers (Colorado State University)*, No. 32.

Zaman, M. A., Rahman, A., Haddad, K., & Hagare, D. (2012). Identification of the best-fit probability distributions in at-site flood frequency analysis: A case study for Australia using 127 stations. *In Hydrology and Water Resources Symposium 2012* (p. 939). Engineers Australia.

Zevenbergen, C., van Herk, S., Rijke, J., Kabat, P., Bloemen, P., Ashley, R., ..., & Veerbeek, W. (2013). Taming global flood disasters. Lessons learned from Dutch experience. *Natural Hazards*, 65(3), 1217-1225.

APPENDIX - A

PARAMETER ESTIMATION

Table A.1: Parameter estimation for stream gauging sites (continued)

Station ID	Lognormal	Log Pearson Type III	Gumbel	Generalised Pareto	Generalised Extreme Value
143001C	σ=1.1018, μ=6.6497	α=129.87, β=0.09786, γ=−6.0592	σ=1534.9, μ=539.89	κ=0.33611, σ=906.41, μ=60.561	κ=0.45938, σ=611.88, μ=569.44
143007A	σ=1.8747, μ=4.8721	α=135.02, β=−0.16285, γ=26.86	σ=699.94, μ=121.97	κ=0.49192, σ=293.06, μ=−50.824	κ=0.57188, σ=217.25, μ=119.61
143009A	σ=1.809, μ=5.5886	α=916.39, β=−0.0603, γ=60.845	σ=1402.5, μ=235.84	κ=0.50966, σ=557.23, μ=−91.044	κ=0.58517, σ=417.39, μ=234.27
143010B	σ=1.2579, μ=4.792	α=51.857, β=0.17685, γ=−4.3788	σ=324.39, μ=82.992	κ=0.47107, σ=141.61, μ=2.509	κ=0.55639, σ=103.69, μ=84.493
143015B	σ=1.3766, μ=4.8268	α=1013.0, β=0.04379, γ=−39.533	σ=344.2, μ=98.83	κ=0.39069, σ=188.6, μ=−12.03	κ=0.49796, σ=131.62, μ=95.21
143028A	σ=0.70423, μ=3.3097	α=49.305, β=0.10154, γ=−1.6967	σ=22.112, μ=22.646	κ=0.11359, σ=23.892, μ=8.4558	κ=0.31059, σ=14.047, μ=21.156
143032A	σ=0.68113, μ=4.1836	α=7.4035, β=0.2551, γ=2.295	σ=57.318, μ=52.123	κ=0.27019, σ=44.986, μ=23.567	κ=0.41394, σ=29.162, μ=48.428
143033A	σ=0.70979, μ=4.6949	α=171.21,β=0.05536, γ=−4.7841	σ=78.691, μ=94.691	κ=−0.08655, σ=126.13, μ=24.033	κ=0.18707, σ=65.363, μ=87.697

Table A.1: Parameter estimation for stream gauging sites (continued).					
143107A	σ=0.57327, μ=6.0638	α=16.735, β=0.14212, γ=3.6853	σ=283.46, μ=350.28	κ=0.07299, σ=313.65, μ=175.54	κ=0.2848, σ=179.77, μ=340.55
143108A	σ=0.62102, μ=5.9675	α=4.3399, β=0.3032, γ=4.6516	σ=324.46, μ=302.91	κ=0.3266, σ=216.42, μ=168.82	κ=0.45275, σ=145.25, μ=290.05
143110A	σ=0.44065, μ=5.0792	α=12.797, β=0.12464, γ=3.4842	σ=68.2, μ=138.72	κ=−0.0604, σ=101.97, μ=81.923	κ=0.20271, σ=53.727, μ=133.75
143113A	σ=0.55816, μ=4.6851	α=386.22, β=0.02894, γ=−6.493	σ=60.594, μ=91.74	κ=−0.2178, σ=108.25, μ=37.828	κ=0.11072, σ=51.634, μ=90.606
143203C	σ=0.94131, μ=5.0343	α=10.405, β=0.29392, γ=1.976	σ=359.08, μ=56.559	κ=0.4383, σ=129.61, μ=33.087	κ=0.53232, σ=93.07, μ=107.58
143207A	σ=1.2339, μ=5.7545	α=8039.6, β=−0.01389, γ=117.39	σ=582.41, μ=291.26	κ=0.24046, σ=490.47, μ=−18.314	κ=0.39383, σ=312.15, μ=250.79
143209B	σ=0.41863, μ=5.2312	α=455.7, β=−0.01997, γ=14.332	σ=64.525, μ=166.31	κ=−0.64646, σ=209.11, μ=76.548	κ=−0.11691, σ=76.297, μ=167.5
143210B	σ=0.9498, μ=5.3512	α=391.27, β=−0.04905, γ=24.543	σ=247.52, μ=178.19	κ=0.16363, σ=241.76, μ=31.998	κ=0.34293, σ=146.67, μ=162.14
143212A	σ=1.8643, μ=4.0861	α=89.53, β=−0.19916, γ=21.917	σ=273.84, μ=67.35	κ=0.43071, σ=142.98, μ=−25.748	κ=0.5268, σ=102.21, μ=56.294

Table A.1. Parameter estimation for stream gauging sites (continued).					
143213C	σ=1.7181, μ=3.4407	α=162.55, β=−0.13891, γ=26.02	σ=118.56, μ=33.446	κ=0.45447, σ=61.265, μ=−10.422	κ=0.54416, σ=44.42, μ=24.918
143219A	σ=1.7174, μ=1.6268	α=1118.5, β=−0.05202, γ=59.812	σ=45.54, μ=−5.2243	κ=0.69301, σ=6.5771, μ=−0.36228	κ=0.7289, σ=5.4611, μ=3.6184
143229A	σ=1.2477, μ=4.7086	α=112.82, β=0.12037, γ=−8.8719	σ=274.4, μ=81.008	κ=0.47297, σ=124.34, μ=3.4628	κ=0.55779, σ=91.151, μ=75.482
143232A	σ=0.37395, μ=3.0578	α=18.017, β=0.09119, γ=1.4148	σ=7.3649, μ=18.633	κ=−0.04658, σ=10.921, μ=12.449	κ=0.21103, σ=5.8043, μ=18.02
143233A	σ=0.99703, μ=4.1201	α=12.204, β=0.29476, γ=0.52281	σ=101.76, μ=46.64	κ=0.4162, σ=56.508, μ=8.5861	κ=0.51628, σ=40.045, μ=40.904
143303A	σ=0.34518, μ=5.8019	α=77.703, β=0.03962, γ=2.7231	σ=100.22, μ=293.79	κ=−0.29861, σ=211.49, μ=188.78	κ=0.06537, σ=95.869, μ=289.7
143306A	σ=0.68592, μ=4.1585	α=60.677, β=−0.09023, γ=9.6334	σ=39.066, μ=56.751	κ=−0.36972, σ=93.211, μ=11.25	κ=0.02646, σ=40.405, μ=54.895
143921A	σ=2.2125, μ=2.4998	α=27.893, β=−0.42633, γ=14.392	σ=114.68, μ=4.8255	κ=0.62279, σ=28.969, μ=−5.7746	κ=0.67242, σ=23.148, μ=11.531
143307A	σ=0.82367, μ=4.6424	α=210.89, β=0.05794, γ=−7.5764	σ=95.422, μ=89.457	κ=0.04507, σ=122.17, μ=16.6	κ=0.26728, σ=68.799, μ=80.414

APPENDIX - B

GOODNESS OF FIT TEST STATISTICS

Table B.1. GoF test statistics for candidate distributions fitting AMF data of Station 143001C

Distribution	Kolmogorov Smirnov (K-S) test		Anderson Darling (A-D) test		Chi-Squared (C-S) test		Avg. Rank
	Statistics	Rank	Statistics	Rank	Statistics	Rank	
Log Pearson type III	0.1004	3	0.3797	2	4.2757	3	2.7
Lognormal	0.0959	2	0.3936	3	2.6442	1	2.0
Generalised. Pareto	**0.0893**	**1**	**0.3372**	**1**	**3.0459**	**2**	**1.3**
Gen. Extreme Value	0.1004	4	0.5760	4	4.7671	4	4.0
Gumbel	0.2626	5	3.3359	5	6.1503	5	5.0

Table B.2. GoF test statistics for candidate distributions fitting AMF data of Station 143010B

Distribution	Kolmogorov (K-S) test		Anderson (A-D) test		Chi-Squared (C-S) test		Avg. Rank
	Statistics	Rank	Statistics	Rank	Statistics	Rank	
Log Pearson type III	**0.0932**	**2**	**0.2548**	**1**	**1.8224**	**2**	**1.7**
Lognormal	0.0990	4	0.3105	2	5.7295	4	3.3
Generalised Pareto	0.0836	1	0.3839	3	2.6960	3	2.3
Gen. Extreme Value	0.0948	3	0.5281	4	1.2491	1	2.7
Gumbel	0.2859	5	4.2470	5	11.8940	5	5.0

Table B.3. GoF test statistics for candidate distributions fitting AMF data of Station 143028a

Distribution	Kolmogorov (K-S) test		Anderson (A-D) test		Chi-Squared (C-S) test		Avg. Rank
	Statistics	Rank	Statistics	Rank	Statistics	Rank	
Log Pearson type III	**0.0908**	**1**	**0.3276**	**1**	**0.4349**	**1**	**1.0**
Lognormal	0.0938	3	0.4415	3	1.2236	3	3.0
Generalised Pareto	0.1198	4	11.3280	5	-	5	4.7
Gen. Extreme Value	0.0929	2	0.3973	2	0.6476	2	2.0
Gumbel	0.1494	5	1.4505	4	9.1637	4	4.3

Table B.4. GoF test statistics for candidate distributions fitting AMF data of Station 143032A

Distribution	Kolmogorov (K-S) test		Anderson (A-D) test		Chi-Squared (C-S) test		Avg. Rank
	Statistics	Rank	Statistics	Rank	Statistics	Rank	
Log Pearson type III	0.0818	2	0.2550	2	0.4758	3	2.3
Lognormal	0.1307	4	0.5800	4	1.8315	4	4.0
Generalised Pareto	**0.0876**	**3**	**0.2201**	**1**	**0.2044**	**1**	**1.7**
Gen. Extreme Value	0.0766	1	0.3063	3	0.2656	2	2.0
Gumbel	0.2027	5	1.5291	5	4.6322	5	5.0

Table B.5. GoF test statistics for candidate distributions fitting AMF data of Station 143033A

Distribution	Kolmogorov (K-S) test		Anderson (A-D) test		Chi-Squared (C-S) test		Avg. Rank
	Statistics	Rank	Statistics	Rank	Statistics	Rank	
Log Pearson type III	0.1268	2	0.4578	2	0.5162	3	2.3
Lognormal	0.1371	3	0.5145	3	0.4859	2	2.7
Generalised Pareto	**0.1040**	**1**	**0.3554**	**1**	**0.2665**	**1**	**1.0**
Gen. Extreme Value	0.1397	4	0.5676	4	1.4662	4	4.0
Gumbel	0.1594	5	0.7128	5	4.3549	5	5.0

Table B.6. GoF test statistics for candidate distributions fitting AMF data of Station 143107A

Distribution	Kolmogorov (K-S) test		Anderson (A-D) test		Chi-Squared (C-S) test		Avg. Rank
	Statistics	Rank	Statistics	Rank	Statistics	Rank	
Log Pearson type III	0.0804	2	0.2071	1	0.1753	2	1.7
Lognormal	0.1092	4	0.2892	3	0.6088	3	3.3
Generalised Pareto	0.0846	3	4.2359	5	-	5	4.3
Gen. Extreme Value	**0.0768**	**1**	**0.2118**	**2**	**0.0955**	**1**	**1.3**
Gumbel	0.1557	5	1.0610	4	5.7386	4	4.3

Table B.7. GoF test statistics for candidate distributions fitting AMF data of Station 143108A

Distribution	Kolmogorov (K-S) test		Anderson (A-D) test		Chi-Squared (C-S) test		Avg. Rank
	Statistics	Rank	Statistics	Rank	Statistics	Rank	
Log Pearson type III	0.0858	2	0.2336	1	0.6744	2	1.7
Lognormal	0.1242	4	0.7670	3	1.4165	3	3.3
Generalised Pareto	0.0902	3	3.9690	5	-	5	4.3
Gen. Extreme Value	**0.0858**	**1**	**0.2637**	**2**	**0.5508**	**1**	**1.3**
Gumbel	0.2202	5	1.8846	4	3.6801	4	4.3

Table B.8. GoF test statistics for candidate distributions fitting AMF data of Station 143110A

Distribution	Kolmogorov (K-S) test		Anderson (A-D) test		Chi-Squared (C-S) test		Avg. Rank
	Statistics	Rank	Statistics	Rank	Statistics	Rank	
Log Pearson type III	0.1132	2	0.6684	1	1.2564	1	1.3
Lognormal	0.1427	4	1.2216	3	1.9886	3	3.3
Generalised Pareto	**0.1064**	**1**	**4.3741**	**5**	-	**5**	**3.7**
Gen. Extreme Value	0.1160	3	0.7277	2	1.2825	2	2.3
Gumbel	0.1626	5	1.4466	4	9.6872	4	4.3

Table B.9. GoF test statistics for candidate distributions fitting AMF data of Station 143113A

Distribution	Kolmogorov (K-S) test		Anderson (A-D) test		Chi-Squared (C-S) test		Avg. Rank
	Statistics	Rank	Statistics	Rank	Statistics	Rank	
Log Pearson type III	0.1350	5	0.3710	1	0.3565	3	3.0
Lognormal	0.1323	4	0.3843	2	0.4493	4	3.3
Generalised Pareto	0.1162	2	4.0949	5	-	5	4.0
Gen. Extreme Value	**0.1230**	**3**	**0.3847**	**3**	**0.2763**	**1**	**2.3**
Gumbel	0.1070	1	0.4652	4	0.2976	2	2.3

Table B.10. GoF test statistics for candidate distributions fitting AMF data of Station 143203C

Distribution	Kolmogorov (K-S) test		Anderson (A-D) test		Chi-Squared (C-S) test		Avg. Rank
	Statistics	Rank	Statistics	Rank	Statistics	Rank	
Log Pearson type III	**0.0821**	**2**	**0.4608**	**1**	**2.8625**	**1**	**1.3**
Lognormal	0.0889	4	0.6304	3	4.9568	2	3.0
Generalised Pareto	0.0609	1	4.2051	4	-	5	3.3
Gen. Extreme Value	0.0841	3	0.6106	2	6.0260	3	2.7
Gumbel	0.3438	5	9.1429	5	17.6010	4	4.7

Table B.11. GoF test statistics for candidate distributions fitting AMF data of Station 143207A

Distribution	Kolmogorov (K-S) test		Anderson (A-D) test		Chi-Squared (C-S) test		Avg. Rank
	Statistics	Rank	Statistics	Rank	Statistics	Rank	
Log Pearson type III	**0.0671**	**1**	**0.3036**	**1**	**3.6297**	**3**	**1.7**
Lognormal	0.0696	2	0.3193	2	3.6335	4	2.7
Generalised Pareto	0.0906	3	0.7151	3	3.1422	2	2.7
Gen. Extreme Value	0.1105	4	1.0746	4	2.9709	1	3.0
Gumbel	0.2069	5	3.2960	5	5.6219	5	5.0

Table B.12. GoF test statistics for candidate distributions fitting AMF data of Station 143209B

Distribution	Kolmogorov (K-S) test		Anderson (A-D) test		Chi-Squared (C-S) test		Avg. Rank
	Statistics	Rank	Statistics	Rank	Statistics	Rank	
Log Pearson type III	0.1549	2	0.8160	3	6.3167	3	2.7
Lognormal	0.1565	3	0.8850	4	6.6048	4	3.7
Generalised Pareto	**0.1128**	**1**	**0.4134**	**1**	**0.9727**	**1**	**1.0**
Gen. Extreme Value	0.1586	4	0.7101	2	4.0892	2	2.7
Gumbel	0.1784	5	1.0941	5	7.0879	5	5.0

Table B.13. GoF test statistics for candidate distributions fitting AMF data of Station 143210B

Distribution	Kolmogorov (K-S) test		Anderson (A-D) test		Chi-Squared (C-S) test		Avg. Rank
	Statistics	Rank	Statistics	Rank	Statistics	Rank	
Log Pearson type III	0.1806	3	0.4264	3	0.0679	2	2.7
Lognormal	0.1857	4	0.4674	4	0.0992	3	3.7
Generalised Pareto	0.1937	5	0.4126	1	0.1476	4	3.3
Gen. Extreme Value	**0.1636**	**1**	**0.4135**	**2**	**0.0113**	**1**	**1.3**
Gumbel	0.1728	2	0.9433	5	7.7914	5	4.0

Table B.14. GoF test statistics for candidate distributions fitting AMF data of Station 143212A

Distribution	Kolmogorov (K-S) test		Anderson (A-D) test		Chi-Squared (C-S) test		Avg. Rank
	Statistics	Rank	Statistics	Rank	Statistics	Rank	
Log Pearson type III	**0.0583**	**1**	**0.1989**	**1**	**1.5158**	**2**	**1.3**
Lognormal	0.0639	2	0.2412	2	0.1330	1	1.7
Generalised Pareto	0.1656	4	1.3676	3	1.7702	3	3.3
Gen. Extreme Value	0.1517	3	1.6306	4	2.4725	4	3.7
Gumbel	0.2799	5	4.6635	5	9.6672	5	5.0

Table B.15. GoF test statistics for candidate distributions fitting AMF data of Station 143213C

Distribution	Kolmogorov (K-S) test		Anderson (A-D) test		Chi-Squared (C-S) test		Avg. Rank
	Statistics	Rank	Statistics	Rank	Statistics	Rank	
Log Pearson type III	**0.1091**	**2**	**0.1776**	**1**	**1.3834**	**2**	**1.7**
Lognormal	0.0974	1	0.1937	2	1.3420	1	1.3
Generalised Pareto	0.1630	3	0.5636	3	2.2576	3	3.0
Gen. Extreme Value	0.1752	4	0.6257	4	2.7429	4	4.0
Gumbel	0.2683	5	1.6164	5	3.9090	5	5.0

Table B.16. GoF test statistics for candidate distributions fitting AMF data of Station 143219A

Distribution	Kolmogorov (K-S) test		Anderson (A-D) test		Chi-Squared (C-S) test		Avg. Rank
	Statistics	Rank	Statistics	Rank	Statistics	Rank	
Log Pearson type III	**0.0815**	**2**	**0.2361**	**1**	**0.8389**	**1**	**1.3**
Lognormal	0.0820	3	0.2536	2	1.8653	4	3.0
Generalised Pareto	0.0756	1	0.2810	3	1.1543	2	2.0
Gen. Extreme Value	0.0934	4	0.4137	4	1.2510	3	3.7
Gumbel	0.4110	5	7.6925	5	15.2790	5	5.0

Distribution	Kolmogorov (K-S) test		Anderson (A-D) test		Chi-Squared (C-S) test		Avg. Rank
	Statistics	Rank	Statistics	Rank	Statistics	Rank	
Log Pearson type III	**0.1124**	**3**	**0.2517**	**1**	**0.0036**	**2**	**2.0**
Lognormal	0.1125	4	0.2575	2	0.0006	1	2.3
Generalised Pareto	0.1073	2	0.2667	3	0.0256	3	2.7
Gen. Extreme Value	0.1032	1	0.2754	4	0.6107	4	3.0
Gumbel	0.2809	5	2.0294	5	0.8732	5	5.0

Table B.18. GoF test statistics for candidate distributions fitting AMF data of Station 143232A

Distribution	Kolmogorov (K-S) test		Anderson (A-D) test		Chi-Squared (C-S) test		Avg. Rank
	Statistics	Rank	Statistics	Rank	Statistics	Rank	
Log Pearson type III	**0.2490**	**3**	**0.9722**	**1**	**0.3086**	**1**	**1.7**
Lognormal	0.2776	5	1.1119	4	4.6840	4	4.3
Generalised Pareto	0.2325	1	4.6210	5	-	5	3.7
Gen. Extreme Value	0.2391	2	1.0163	2	0.4079	2	2.0
Gumbel	0.2682	4	1.0288	3	4.0081	3	3.3

Table B.19. GoF test statistics for candidate distributions fitting AMF data of Station 143233A

Distribution	Kolmogorov (K-S) test		Anderson (A-D) test		Chi-Squared (C-S) test		Avg. Rank
	Statistics	Rank	Statistics	Rank	Statistics	Rank	
Log Pearson type III	**0.1479**	**2**	**0.2572**	**1**	**0.3618**	**3**	**2.0**
Lognormal	0.1808	4	0.4035	4	0.9800	4	4.0
Generalised Pareto	0.1194	1	0.3341	2	0.1470	2	1.7
Gen. Extreme Value	0.1542	3	0.4031	3	0.1184	1	2.3
Gumbel	0.2550	5	1.2594	5	1.7135	5	5.0

Table B.20. GoF test statistics for candidate distributions fitting AMF data of Station 143303A

Distribution	Kolmogorov (K-S) test		Anderson (A-D) test		Chi-Squared (C-S) test		Avg. Rank
	Statistics	Rank	Statistics	Rank	Statistics	Rank	
Log Pearson type III	0.1003	2	0.3103	2	0.7195	1	1.7
Lognormal	0.1147	4	0.3574	4	2.5747	4	4.0
Generalised Pareto	0.1209	5	8.1037	5	-	5	5.0
Gen. Extreme Value	**0.0961**	**1**	**0.3054**	**1**	**0.7272**	**2**	**1.3**
Gumbel	0.1121	3	0.3394	3	2.5477	3	3.0

Table B.21. GoF test statistics for five candidate distributions used to fit AMF data for Station 143306A

Distribution	Kolmogorov (K-S) test		Anderson (A-D) test		Chi-Squared (C-S) test		Avg. Rank
	Statistics	Rank	Statistics	Rank	Statistics	Rank	
Log Pearson type III	0.1117	2	0.3000	2	0.3840	3	2.3
Lognormal	0.1183	4	0.3687	4	0.6838	5	4.3
Generalised Pareto	**0.0887**	**1**	**0.2348**	**1**	**0.3914**	**4**	**2.0**
Gen. Extreme Value	0.1144	3	0.3164	3	0.0699	1	2.3
Gumbel	0.1218	5	0.3809	5	0.1331	2	4.0

Table B.22. GoF test statistics for candidate distributions fitting AMF data of Station 143307A

Distribution	Kolmogorov (K-S) test		Anderson (A-D) test		Chi-Squared (C-S) test		Avg. Rank
	Statistics	Rank	Statistics	Rank	Statistics	Rank	
Log Pearson type III	0.1025	2	0.2954	2	1.5598	3	2.3
Lognormal	0.1123	3	0.3346	3	1.6010	4	3.3
Generalised Pareto	**0.0933**	**1**	**0.2779**	**1**	**1.0383**	**1**	**1.0**
Gen. Extreme Value	0.1171	4	0.4096	4	2.0534	5	4.3
Gumbel	0.1668	5	0.7242	5	1.2659	2	4.0

Table B.23. GoF test statistics for candidate distributions fitting AMF data of Station 143921A

Distribution	Kolmogorov (K-S) test		Anderson (A-D) test		Chi-Squared (C-S) test		Avg. Rank
	Statistics	Rank	Statistics	Rank	Statistics	Rank	
Log Pearson type III	**0.0764**	**1**	**0.1644**	**1**	**0.9861**	**4**	**2.0**
Lognormal	0.0870	2	0.2458	2	0.6970	3	2.3
Generalised Pareto	0.1726	4	0.7262	3	0.2627	1	2.7
Gen. Extreme Value	0.1607	3	0.7939	4	0.3849	2	3.0
Gumbel	0.3526	5	4.2857	5	5.0657	5	5.0

Table B.24. Number of time-series records show Rank-2 in GoF test

Probability Distribution	Number of Time-series station AMF record with Rank-2 in A-D Test	Number of Time-series station AMF record with Rank-2 in K-S Test	Number of Time-series station AMF record with Rank-2 in C-S Test	Average
Log Pearson type III	6	14	8	9.33
Lognormal	11	7	3	7.00
Gumbel	0	1	3	1.33
General Pareto	1	2	5	2.67
General Extreme Value	8	2	7	5.67

Table B.25. Number of time-series records show Rank-3 in GoF test

Probability Distribution	Number of Time-series station AMF record with Rank-3 in A-D Test	Number of Time-series station AMF record with Rank-3 in K-S Test	Number of Time-series station AMF record with Rank-3 in C-S Test	Average
Log Pearson type III	2	4	10	5.33
Lognormal	8	5	6	6.33
Gumbel	2	1	2	1.67
General Pareto	10	6	5	7.00
General Extreme Value	4	10	3	5.67

APPENDIX - C

VISUAL DISTRIBUTION FITTING

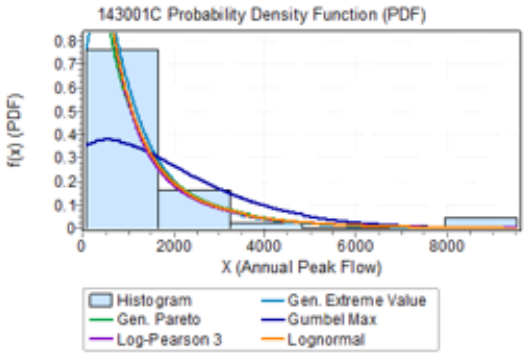
143001C Probability Density Function (PDF)
f(x) (PDF)
X (Annual Peak Flow)
Histogram
Gen. Extreme Value
Gen. Pareto
Gumbel Max
Log-Pearson 3
Lognormal

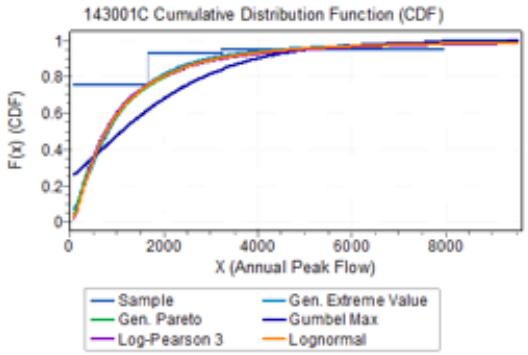
143001C Cumulative Distribution Function (CDF)
F(x) (CDF)
X (Annual Peak Flow)
Sample
Gen. Extreme Value
Gen. Pareto
Gumbel Max
Log-Pearson 3
Lognormal

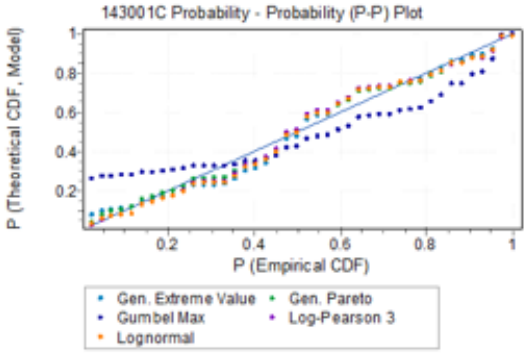
143001C Probability - Probability (P-P) Plot
P (Theoretical CDF, Model)
P (Empirical CDF)
Gen. Extreme Value
Gen. Pareto
Gumbel Max
Log-Pearson 3
Lognormal

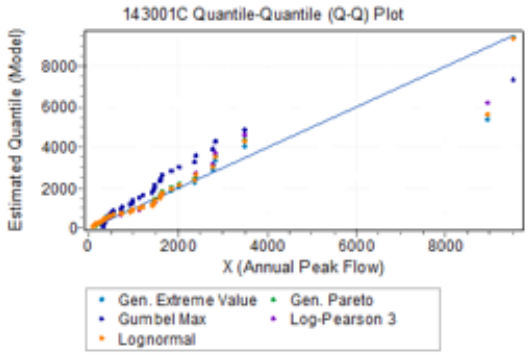
143001C Quantile-Quantile (Q-Q) Plot
Estimated Quantile (Model)
X (Annual Peak Flow)
Gen. Extreme Value
Gen. Pareto
Gumbel Max
Log-Pearson 3
Lognormal

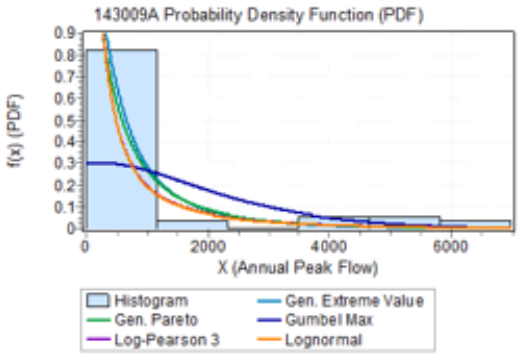
143009A Probability Density Function (PDF)
f(x) (PDF)
X (Annual Peak Flow)
Histogram
Gen. Extreme Value
Gen. Pareto
Gumbel Max
Log-Pearson 3
Lognormal

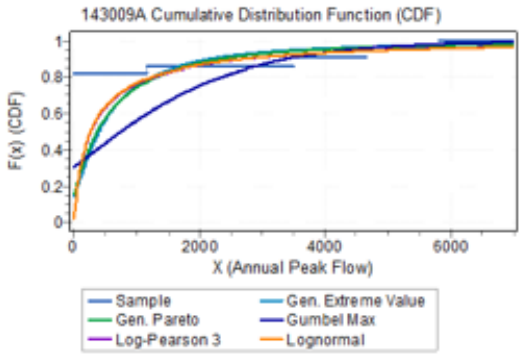
143009A Cumulative Distribution Function (CDF)
F(x) (CDF)
X (Annual Peak Flow)
Sample
Gen. Extreme Value
Gen. Pareto
Gumbel Max
Log-Pearson 3
Lognormal

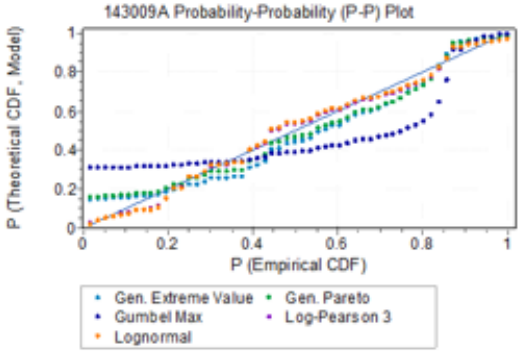
143009A Probability-Probability (P-P) Plot
P (Theoretical CDF, Model)
P (Empirical CDF)
Gen. Extreme Value
Gen. Pareto
Gumbel Max
Log-Pearson 3
Lognormal

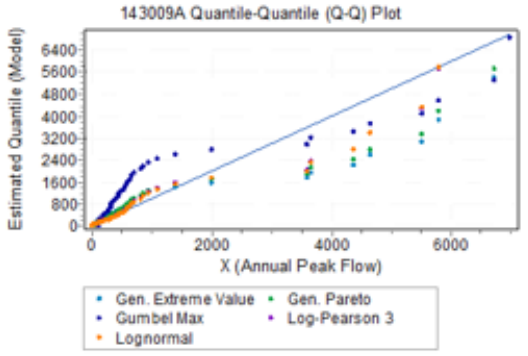
143009A Quantile-Quantile (Q-Q) Plot
Estimated Quantile (Model)
X (Annual Peak Flow)
Gen. Extreme Value
Gen. Pareto
Gumbel Max
Log-Pearson 3
Lognormal

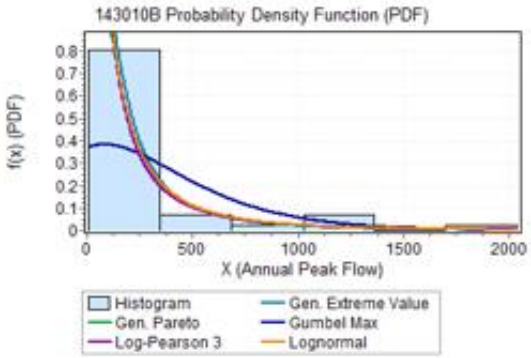
143010B Probability Density Function (PDF)
f(x) (PDF)
X (Annual Peak Flow)
Histogram
Gen. Extreme Value
Gen. Pareto
Gumbel Max
Log-Pearson 3
Lognormal

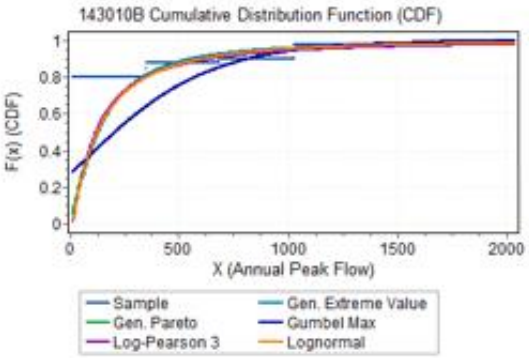
143010B Cumulative Distribution Function (CDF)
F(x) (CDF)
X (Annual Peak Flow)
Sample
Gen. Extreme Value
Gen. Pareto
Gumbel Max
Log-Pearson 3
Lognormal

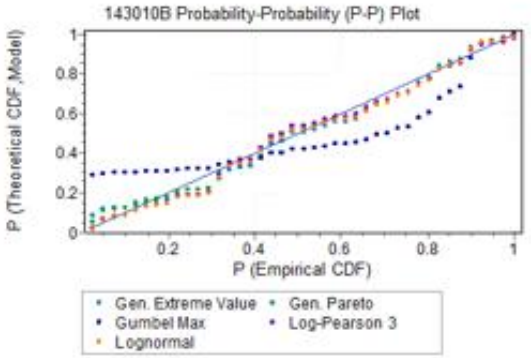
143010B Probability-Probability (P-P) Plot
P (Theoretical CDF,Model)
P (Empirical CDF)
Gen. Extreme Value
Gen. Pareto
Gumbel Max
Log-Pearson 3
Lognormal

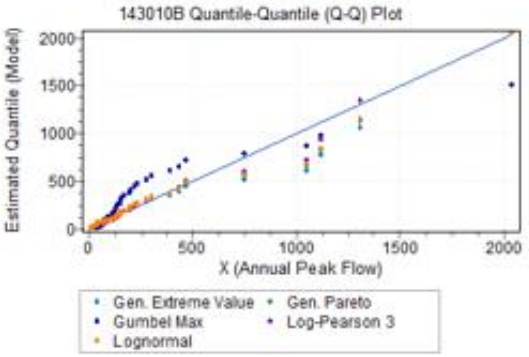
143010B Quantile-Quantile (Q-Q) Plot
Estimated Quantile (Model)
X (Annual Peak Flow)
Gen. Extreme Value
Gen. Pareto
Gumbel Max
Log-Pearson 3
Lognormal

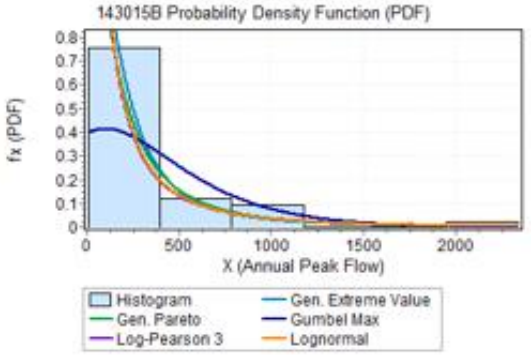
143015B Probability Density Function (PDF)
fx (PDF)
X (Annual Peak Flow)
Histogram
Gen. Extreme Value
Gen. Pareto
Gumbel Max
Log-Pearson 3
Lognormal

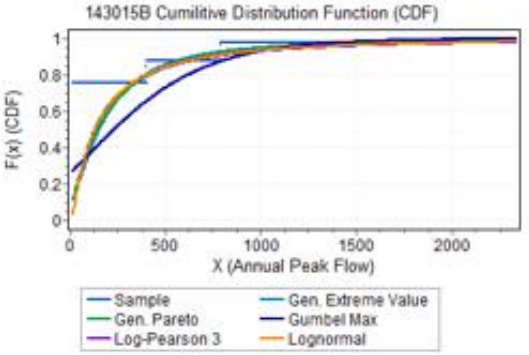
143015B Cumilitive Distribution Function (CDF)
F(x) (CDF)
X (Annual Peak Flow)
Sample
Gen. Extreme Value
Gen. Pareto
Gumbel Max
Log-Pearson 3
Lognormal

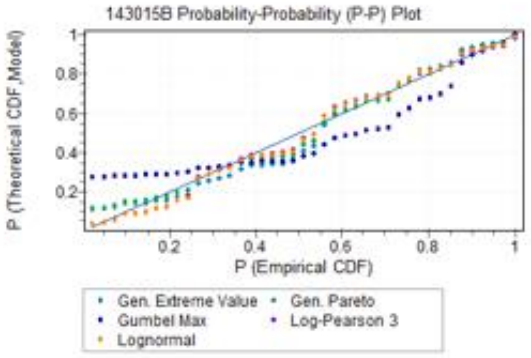
143015B Probability-Probability (P-P) Plot
P (Theoretical CDF,Model)
P (Empirical CDF)
Gen. Extreme Value
Gen. Pareto
Gumbel Max
Log-Pearson 3
Lognormal

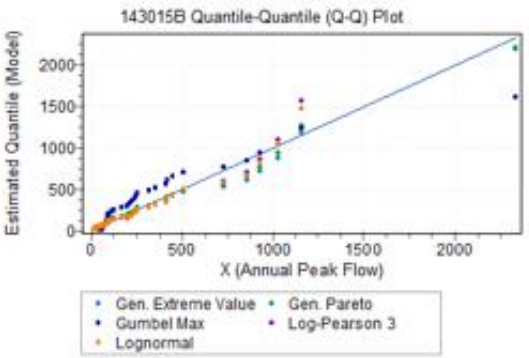
143015B Quantile-Quantile (Q-Q) Plot
Estimated Quantile (Model)
X (Annual Peak Flow)
Gen. Extreme Value
Gen. Pareto
Gumbel Max
Log-Pearson 3
Lognormal

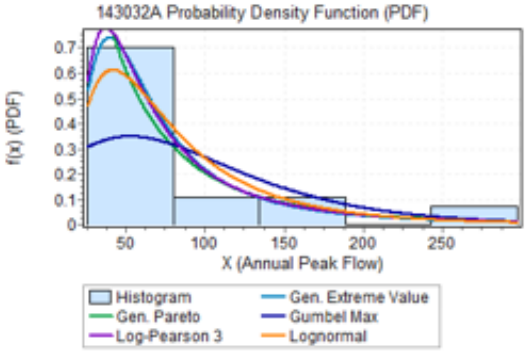
143032A Probability Density Function (PDF)
f(x) (PDF)
X (Annual Peak Flow)
Histogram
Gen. Extreme Value
Gen. Pareto
Gumbel Max
Log-Pearson 3
Lognormal

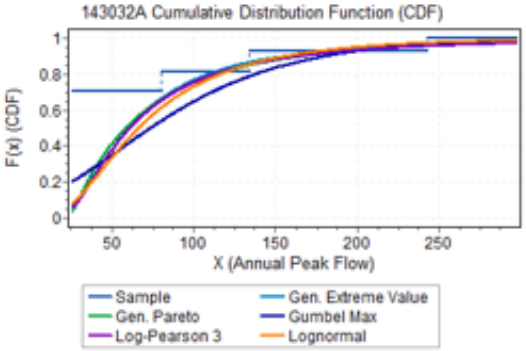
143032A Cumulative Distribution Function (CDF)
F(x) (CDF)
X (Annual Peak Flow)
Sample
Gen. Extreme Value
Gen. Pareto
Gumbel Max
Log-Pearson 3
Lognormal

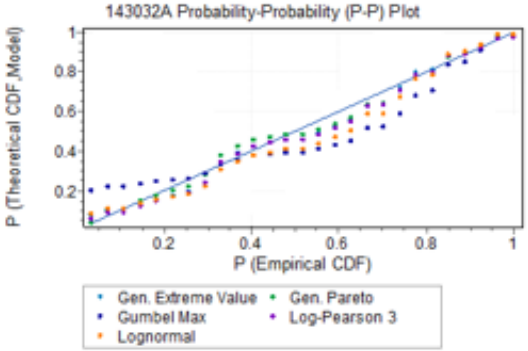
143032A Probability-Probability (P-P) Plot
P (Theoretical CDF,Model)
P (Empirical CDF)
Gen. Extreme Value
Gen. Pareto
Gumbel Max
Log-Pearson 3
Lognormal

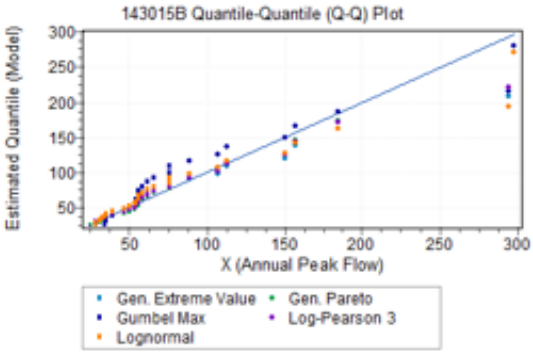
143015B Quantile-Quantile (Q-Q) Plot
Estimated Quantile (Model)
X (Annual Peak Flow)
Gen. Extreme Value
Gen. Pareto
Gumbel Max
Log-Pearson 3
Lognormal

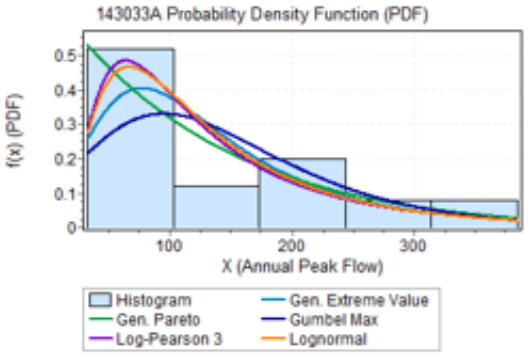
143033A Probability Density Function (PDF)
f(x) (PDF)
X (Annual Peak Flow)
Histogram
Gen. Extreme Value
Gen. Pareto
Gumbel Max
Log-Pearson 3
Lognormal

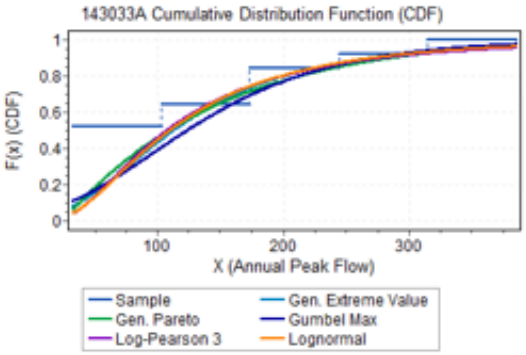
143033A Cumulative Distribution Function (CDF)
F(x) (CDF)
X (Annual Peak Flow)
Sample
Gen. Extreme Value
Gen. Pareto
Gumbel Max
Log-Pearson 3
Lognormal

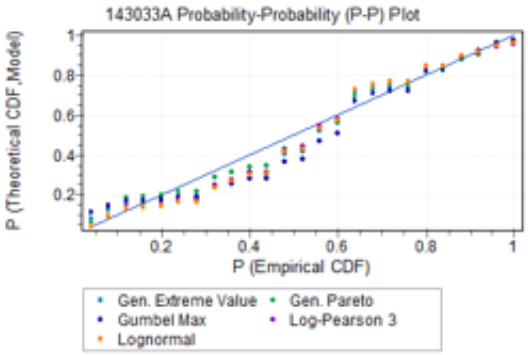
143033A Probability-Probability (P-P) Plot
P (Theoretical CDF,Model)
P (Empirical CDF)
Gen. Extreme Value
Gen. Pareto
Gumbel Max
Log-Pearson 3
Lognormal

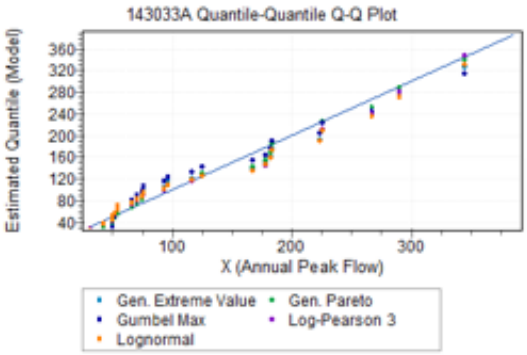
143033A Quantile-Quantile Q-Q Plot
Estimated Quantile (Model)
X (Annual Peak Flow)
Gen. Extreme Value
Gen. Pareto
Gumbel Max
Log-Pearson 3
Lognormal

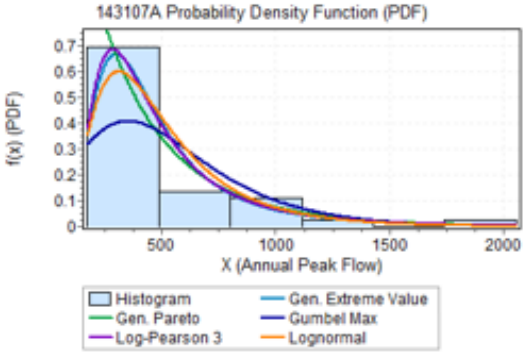
143107A Probability Density Function (PDF)
f(x) (PDF)
X (Annual Peak Flow)
Histogram
Gen. Extreme Value
Gen. Pareto
Gumbel Max
Log-Pearson 3
Lognormal

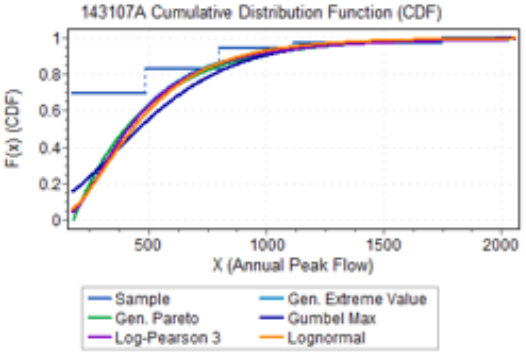
143107A Cumulative Distribution Function (CDF)
F(x) (CDF)
X (Annual Peak Flow)
Sample
Gen. Extreme Value
Gen. Pareto
Gumbel Max
Log-Pearson 3
Lognormal

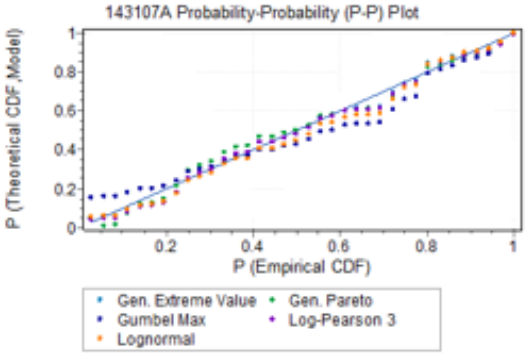
143107A Probability-Probability (P-P) Plot
P (Theoretical CDF,Model)
P (Empirical CDF)
Gen. Extreme Value
Gen. Pareto
Gumbel Max
Log-Pearson 3
Lognormal

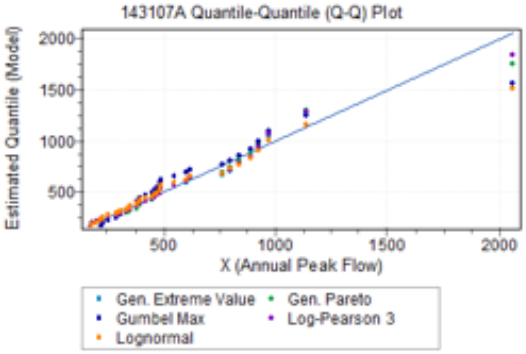
143107A Quantile-Quantile (Q-Q) Plot
Estimated Quantile (Model)
X (Annual Peak Flow)
Gen. Extreme Value
Gen. Pareto
Gumbel Max
Log-Pearson 3
Lognormal

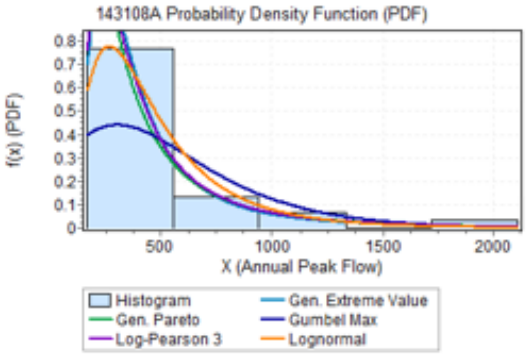
143108A Probability Density Function (PDF)
f(x) (PDF)
X (Annual Peak Flow)
Histogram
Gen. Extreme Value
Gen. Pareto
Gumbel Max
Log-Pearson 3
Lognormal

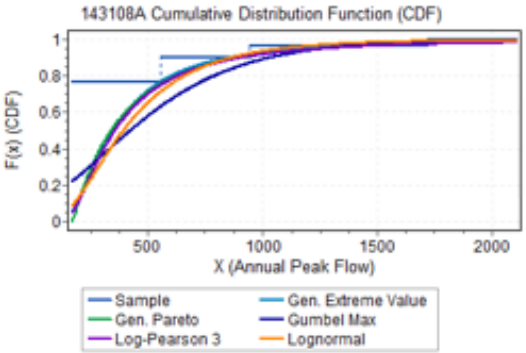
143108A Cumulative Distribution Function (CDF)
F(x) (CDF)
X (Annual Peak Flow)
Sample
Gen. Extreme Value
Gen. Pareto
Gumbel Max
Log-Pearson 3
Lognormal

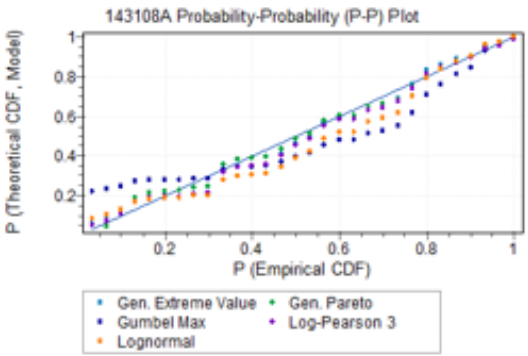
143108A Probability-Probability (P-P) Plot
P (Theoretical CDF, Model)
P (Empirical CDF)
Gen. Extreme Value
Gen. Pareto
Gumbel Max
Log-Pearson 3
Lognormal

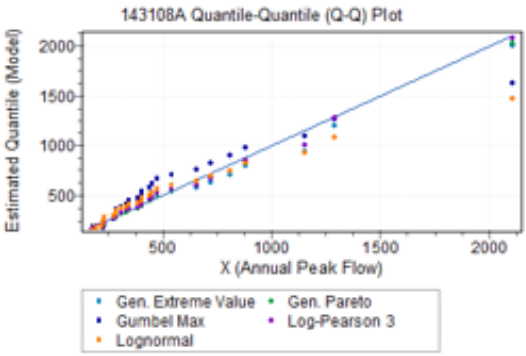
143108A Quantile-Quantile (Q-Q) Plot
Estimated Quantile (Model)
X (Annual Peak Flow)
Gen. Extreme Value
Gen. Pareto
Gumbel Max
Log-Pearson 3
Lognormal

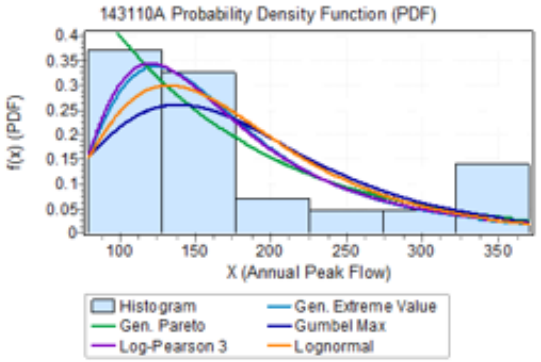
143110A Probability Density Function (PDF)
f(x) (PDF)
X (Annual Peak Flow)
Histogram
Gen. Extreme Value
Gen. Pareto
Gumbel Max
Log-Pearson 3
Lognormal

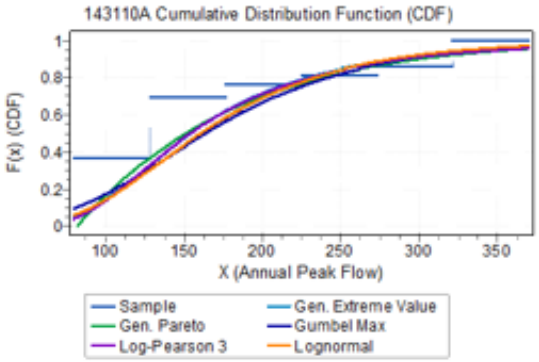
143110A Cumulative Distribution Function (CDF)
F(x) (CDF)
X (Annual Peak Flow)
Sample
Gen. Extreme Value
Gen. Pareto
Gumbel Max
Log-Pearson 3
Lognormal

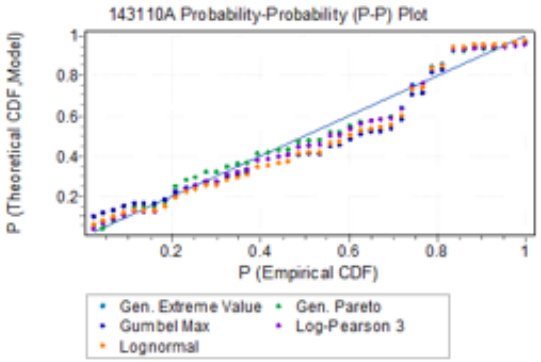
143110A Probability-Probability (P-P) Plot
P (Theoretical CDF ,Model)
P (Empirical CDF)
Gen. Extreme Value
Gen. Pareto
Gumbel Max
Log-Pearson 3
Lognormal

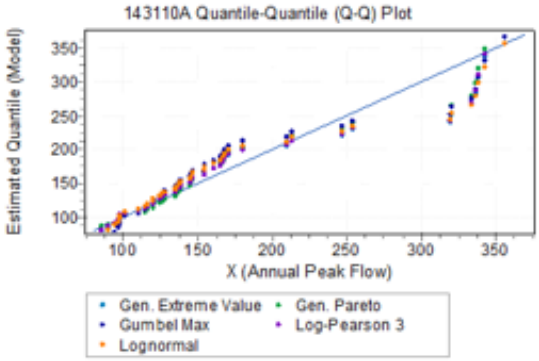
143110A Quantile-Quantile (Q-Q) Plot
Estimated Quantile (Model)
X (Annual Peak Flow)
Gen. Extreme Value
Gen. Pareto
Gumbel Max
Log-Pearson 3
Lognormal

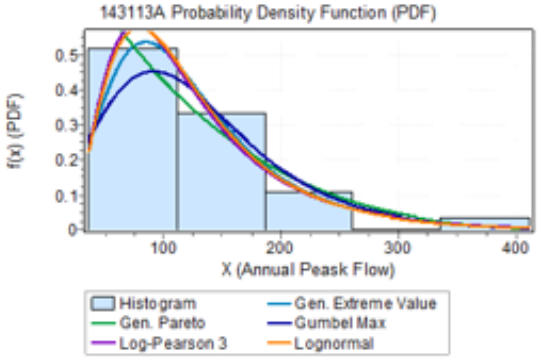
143113A Probability Density Function (PDF)
f(x) (PDF)
X (Annual Peask Flow)
Histogram
Gen. Extreme Value
Gen. Pareto
Gumbel Max
Log-Pearson 3
Lognormal

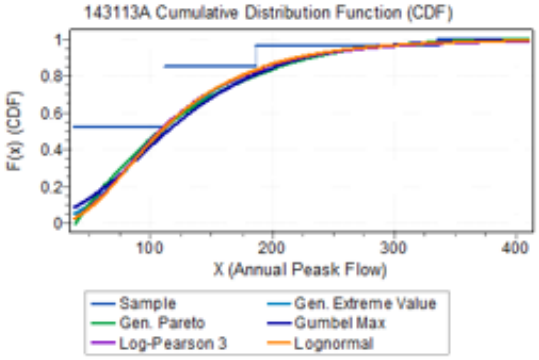
143113A Cumulative Distribution Function (CDF)
F(x) (CDF)
X (Annual Peask Flow)
Sample
Gen. Extreme Value
Gen. Pareto
Gumbel Max
Log-Pearson 3
Lognormal

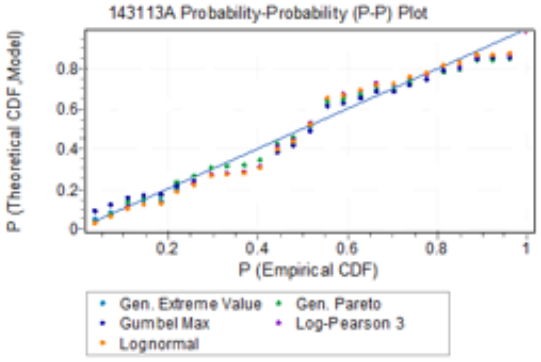
143113A Probability-Probability (P-P) Plot
P (Theoretical CDF ,Model)
P (Empirical CDF)
Gen. Extreme Value
Gen. Pareto
Gumbel Max
Log-Pearson 3
Lognormal

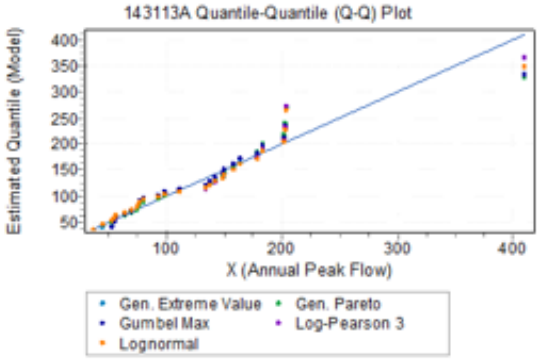
143113A Quantile-Quantile (Q-Q) Plot
Estimated Quantile (Model)
X (Annual Peak Flow)
Gen. Extreme Value
Gen. Pareto
Gumbel Max
Log-Pearson 3
Lognormal

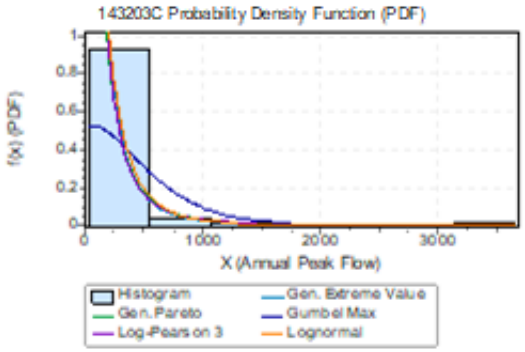
143203C Probability Density Function (PDF)
f(x) (PDF)
X (Annual Peak Flow)
Histogram
Gen. Extreme Value
Gen. Pareto
Gumbel Max
Log-Pearson 3
Lognormal

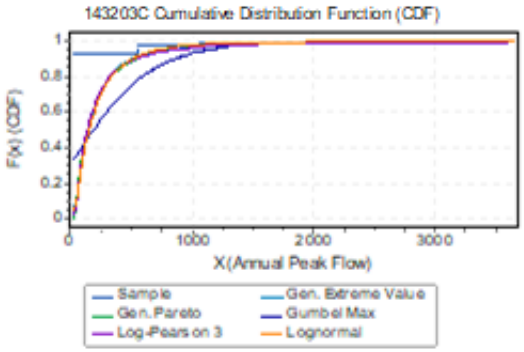
143203C Cumulative Distribution Function (CDF)
F(x) (CDF)
X (Annual Peak Flow)
Sample
Gen. Extreme Value
Gen. Pareto
Gumbel Max
Log-Pearson 3
Lognormal

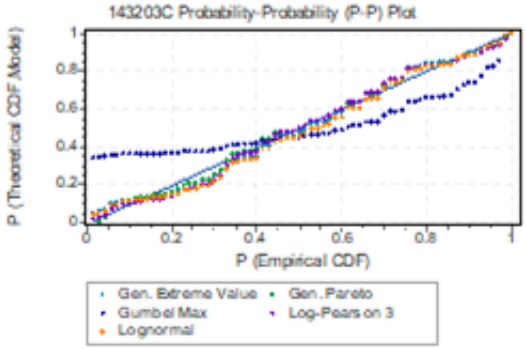
143203C Probability-Probability (P-P) Plot
P (Theoretical CDF Model)
P (Empirical CDF)
Gen. Extreme Value
Gen. Pareto
Gumbel Max
Log-Pearson 3
Lognormal

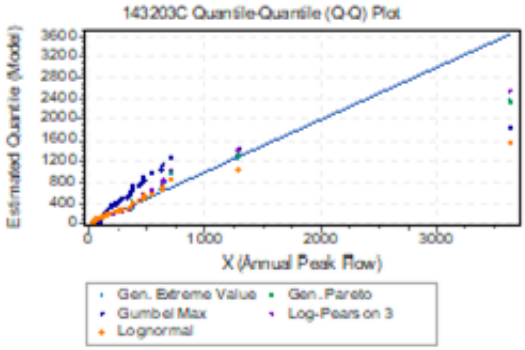
143203C Quantile-Quantile (Q-Q) Plot
Estimated Quantile (Model)
X (Annual Peak Flow)
Gen. Extreme Value
Gen. Pareto
Gumbel Max
Log-Pearson 3
Lognormal

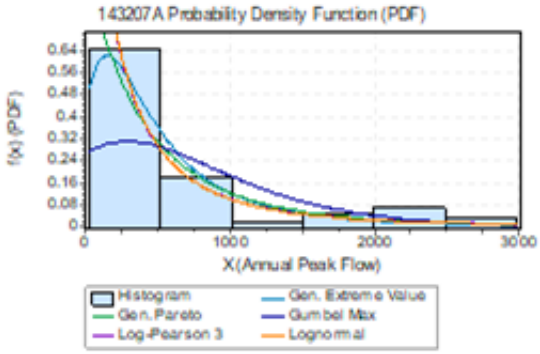
143207A Probability Density Function (PDF)
f(x) (PDF)
X (Annual Peak Flow)
Histogram
Gen. Extreme Value
Gen. Pareto
Gumbel Max
Log-Pearson 3
Lognormal

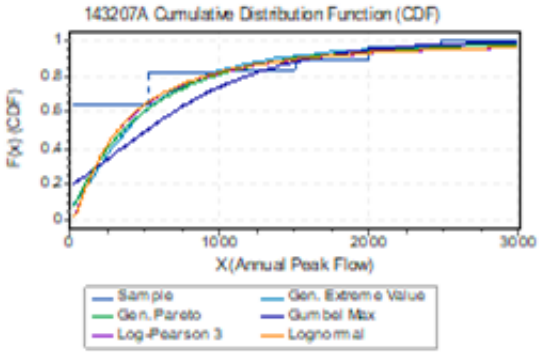
143207A Cumulative Distribution Function (CDF)
F(x) (CDF)
X (Annual Peak Flow)
Sample
Gen. Extreme Value
Gen. Pareto
Gumbel Max
Log-Pearson 3
Lognormal

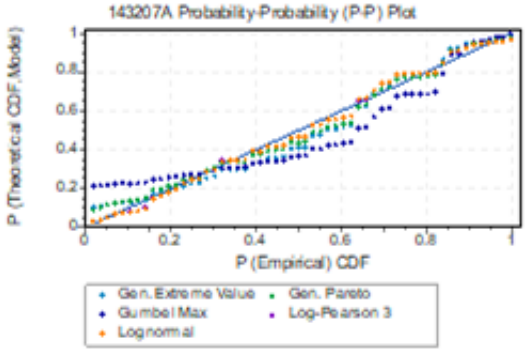
143207A Probability-Probability (P-P) Plot
P (Theoretical CDF Model)
P (Empirical) CDF
Gen. Extreme Value
Gen. Pareto
Gumbel Max
Log-Pearson 3
Lognormal

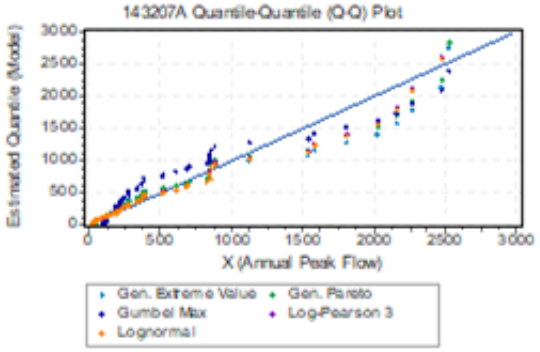
143207A Quantile-Quantile (Q-Q) Plot
Estimated Quantile (Model)
X (Annual Peak Flow)
Gen. Extreme Value
Gen. Pareto
Gumbel Max
Log-Pearson 3
Lognormal

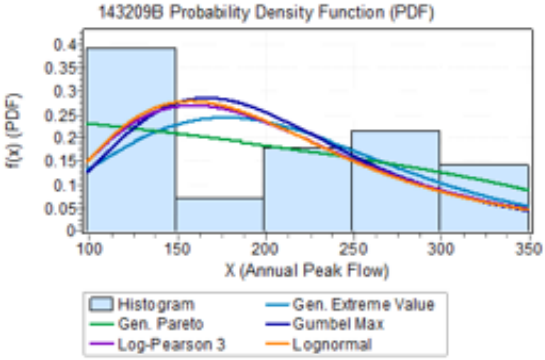
143209B Probability Density Function (PDF)
f(x) (PDF)
X (Annual Peak Flow)
Histogram
Gen. Extreme Value
Gen. Pareto
Gumbel Max
Log-Pearson 3
Lognormal

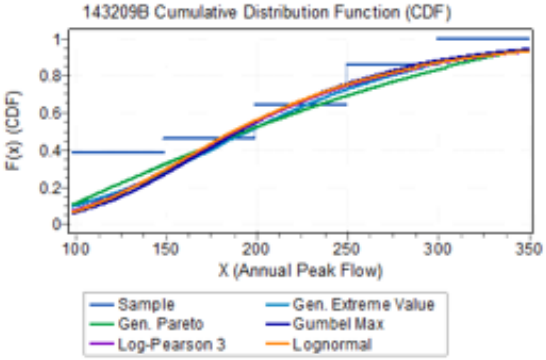
143209B Cumulative Distribution Function (CDF)
F(x) (CDF)
X (Annual Peak Flow)
Sample
Gen. Extreme Value
Gen. Pareto
Gumbel Max
Log-Pearson 3
Lognormal

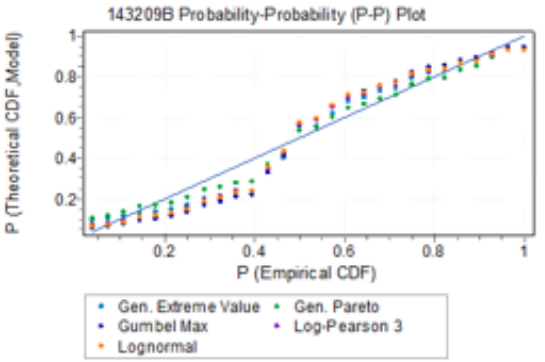
143209B Probability-Probability (P-P) Plot
P (Theoretical CDF_Model)
P (Empirical CDF)
Gen. Extreme Value
Gen. Pareto
Gumbel Max
Log-Pearson 3
Lognormal

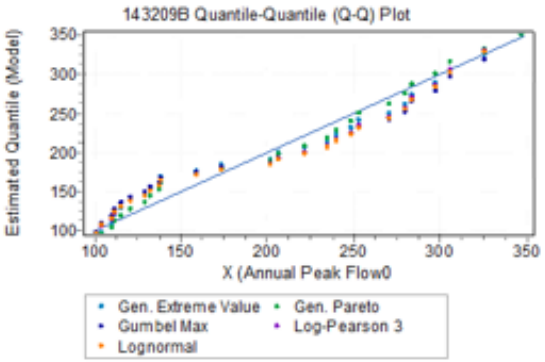
143209B Quantile-Quantile (Q-Q) Plot
Estimated Quantile (Model)
X (Annual Peak Flow0
Gen. Extreme Value
Gen. Pareto
Gumbel Max
Log-Pearson 3
Lognormal

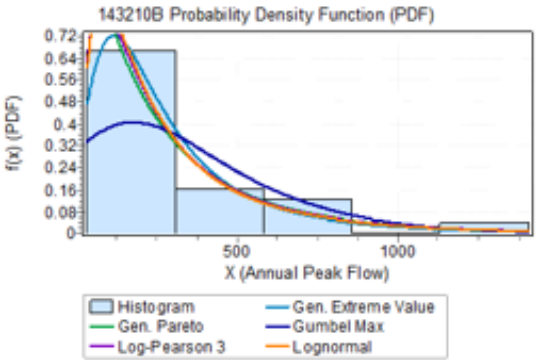
143210B Probability Density Function (PDF)
f(x) (PDF)
X (Annual Peak Flow)
Histogram
Gen. Extreme Value
Gen. Pareto
Gumbel Max
Log-Pearson 3
Lognormal

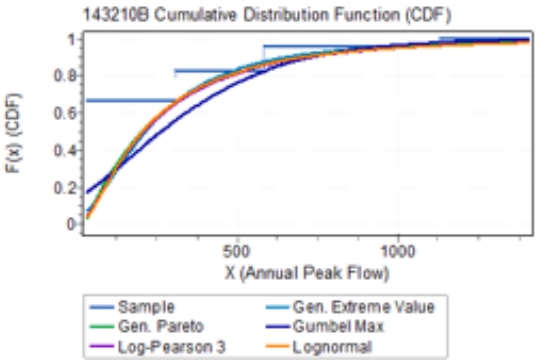
143210B Cumulative Distribution Function (CDF)
F(x) (CDF)
X (Annual Peak Flow)
Sample
Gen. Extreme Value
Gen. Pareto
Gumbel Max
Log-Pearson 3
Lognormal

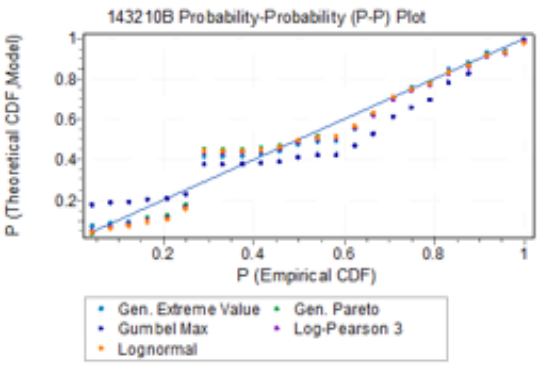
143210B Probability-Probability (P-P) Plot
P (Theoretical CDF_Model)
P (Empirical CDF)
Gen. Extreme Value
Gen. Pareto
Gumbel Max
Log-Pearson 3
Lognormal

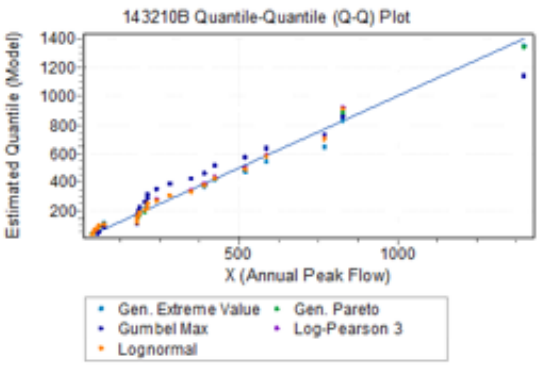
143210B Quantile-Quantile (Q-Q) Plot
Estimated Quantile (Model)
X (Annual Peak Flow)
Gen. Extreme Value
Gen. Pareto
Gumbel Max
Log-Pearson 3
Lognormal

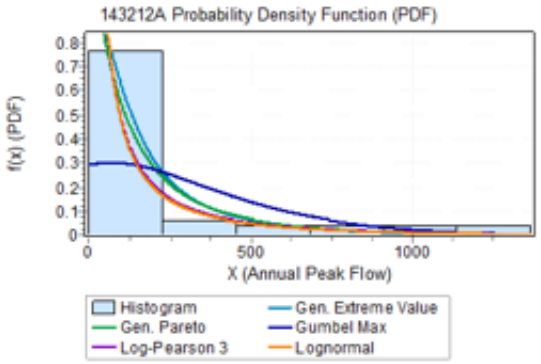
143212A Probability Density Function (PDF)
f(x) (PDF)
X (Annual Peak Flow)
Histogram
Gen. Extreme Value
Gen. Pareto
Gumbel Max
Log-Pearson 3
Lognormal

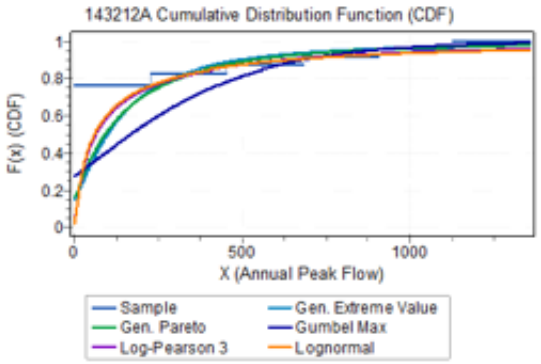
143212A Cumulative Distribution Function (CDF)
F(x) (CDF)
X (Annual Peak Flow)
Sample
Gen. Extreme Value
Gen. Pareto
Gumbel Max
Log-Pearson 3
Lognormal

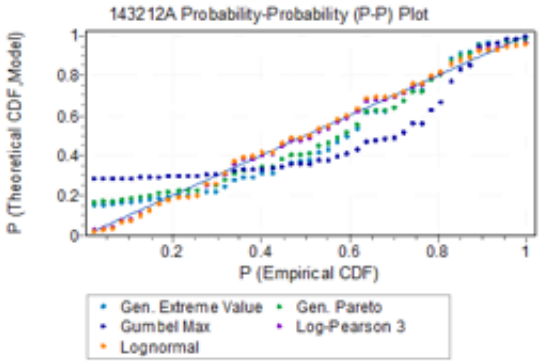
143212A Probability-Probability (P-P) Plot
P (Theoretical CDF_Model)
P (Empirical CDF)
Gen. Extreme Value
Gen. Pareto
Gumbel Max
Log-Pearson 3
Lognormal

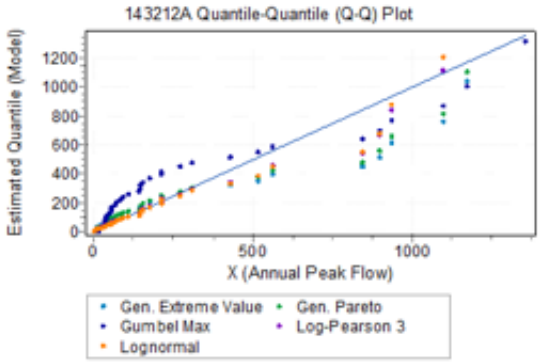
143212A Quantile-Quantile (Q-Q) Plot
Estimated Quantile (Model)
X (Annual Peak Flow)
Gen. Extreme Value
Gen. Pareto
Gumbel Max
Log-Pearson 3
Lognormal

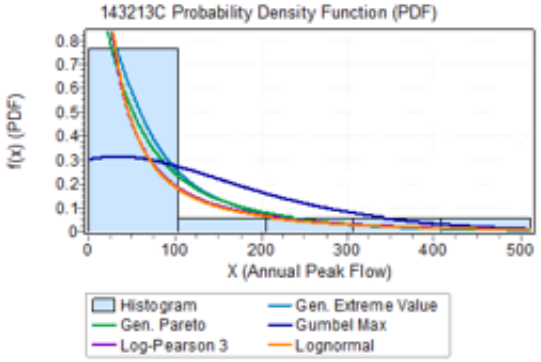
143213C Probability Density Function (PDF)
f(x) (PDF)
X (Annual Peak Flow)
Histogram
Gen. Extreme Value
Gen. Pareto
Gumbel Max
Log-Pearson 3
Lognormal

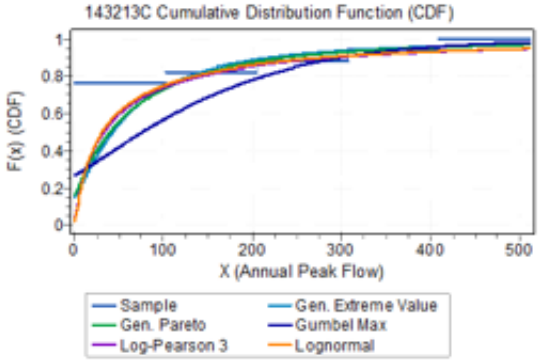
143213C Cumulative Distribution Function (CDF)
F(x) (CDF)
X (Annual Peak Flow)
Sample
Gen. Extreme Value
Gen. Pareto
Gumbel Max
Log-Pearson 3
Lognormal

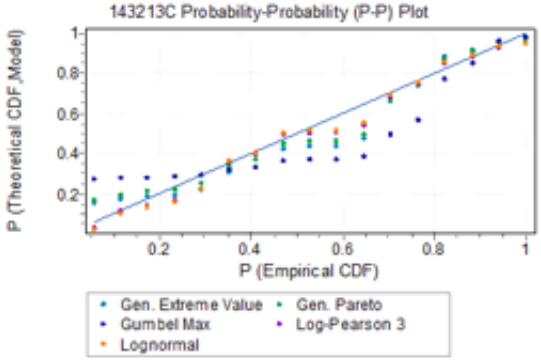
143213C Probability-Probability (P-P) Plot
P (Theoretical CDF_Model)
P (Empirical CDF)
Gen. Extreme Value
Gen. Pareto
Gumbel Max
Log-Pearson 3
Lognormal

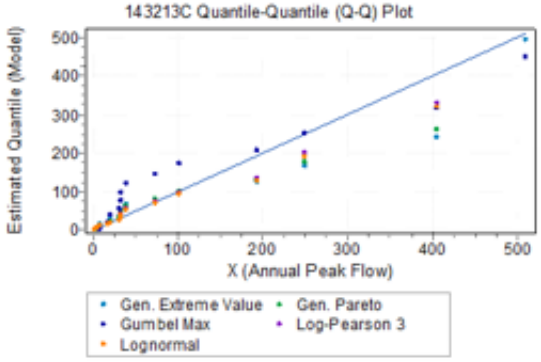
143213C Quantile-Quantile (Q-Q) Plot
Estimated Quantile (Model)
X (Annual Peak Flow)
Gen. Extreme Value
Gen. Pareto
Gumbel Max
Log-Pearson 3
Lognormal

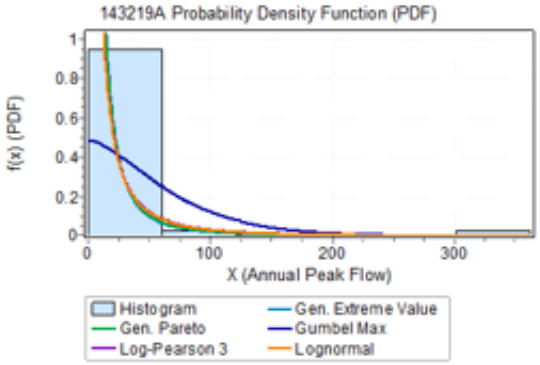
143219A Probability Density Function (PDF)
f(x) (PDF)
X (Annual Peak Flow)
Histogram
Gen. Extreme Value
Gen. Pareto
Gumbel Max
Log-Pearson 3
Lognormal

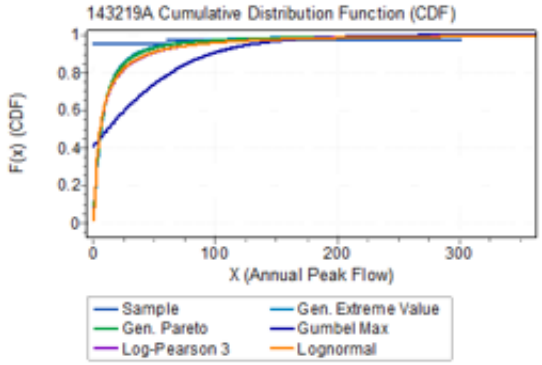
143219A Cumulative Distribution Function (CDF)
F(x) (CDF)
X (Annual Peak Flow)
Sample
Gen. Extreme Value
Gen. Pareto
Gumbel Max
Log-Pearson 3
Lognormal

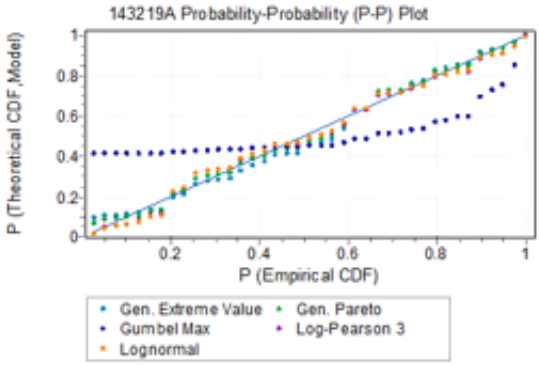
143219A Probability-Probability (P-P) Plot
P (Theoretical CDF,Model)
P (Empirical CDF)
Gen. Extreme Value
Gen. Pareto
Gumbel Max
Log-Pearson 3
Lognormal

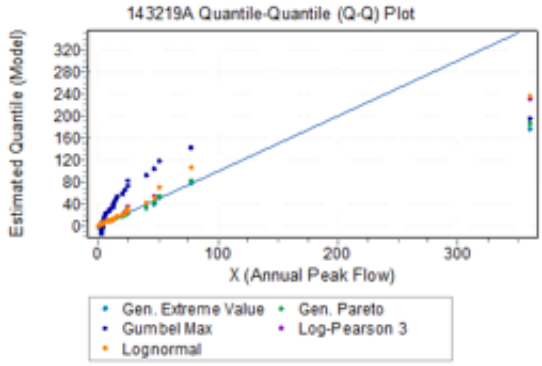
143219A Quantile-Quantile (Q-Q) Plot
Estimated Quantile (Model)
X (Annual Peak Flow)
Gen. Extreme Value
Gen. Pareto
Gumbel Max
Log-Pearson 3
Lognormal

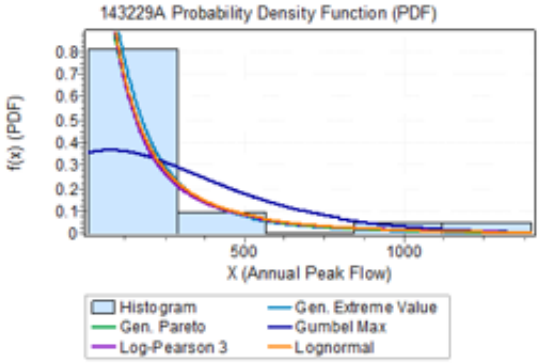
143229A Probability Density Function (PDF)
f(x) (PDF)
X (Annual Peak Flow)
Histogram
Gen. Extreme Value
Gen. Pareto
Gumbel Max
Log-Pearson 3
Lognormal

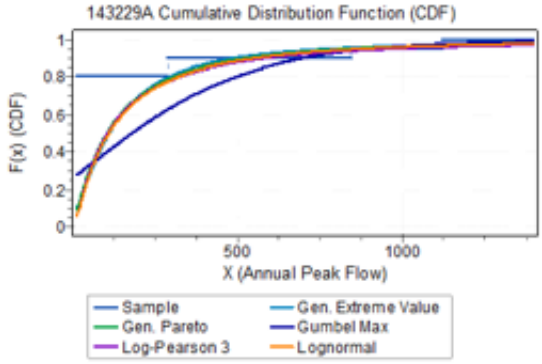
143229A Cumulative Distribution Function (CDF)
F(x) (CDF)
X (Annual Peak Flow)
Sample
Gen. Extreme Value
Gen. Pareto
Gumbel Max
Log-Pearson 3
Lognormal

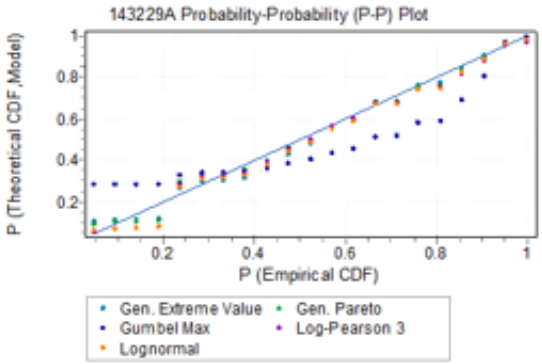
143229A Probability-Probability (P-P) Plot
P (Theoretical CDF,Model)
P (Empirical CDF)
Gen. Extreme Value
Gen. Pareto
Gumbel Max
Log-Pearson 3
Lognormal

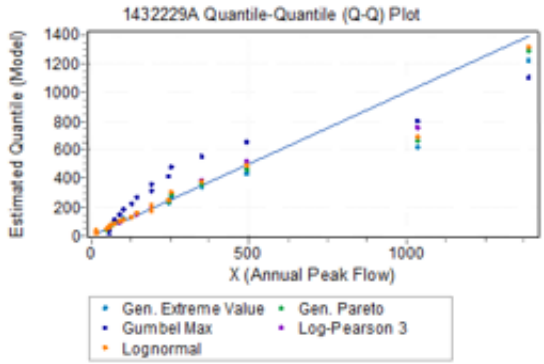
1432229A Quantile-Quantile (Q-Q) Plot
Estimated Quantile (Model)
X (Annual Peak Flow)
Gen. Extreme Value
Gen. Pareto
Gumbel Max
Log-Pearson 3
Lognormal

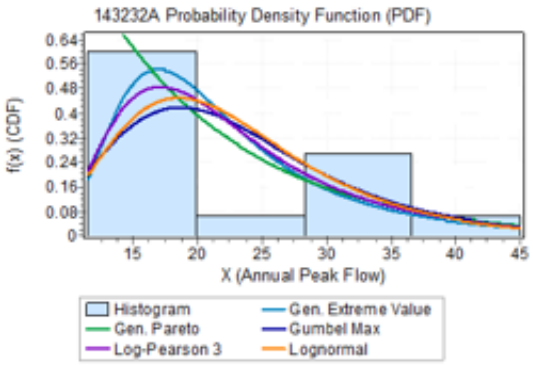
143232A Probability Density Function (PDF)
f(x) (CDF)
X (Annual Peak Flow)
Histogram
Gen. Extreme Value
Gen. Pareto
Gumbel Max
Log-Pearson 3
Lognormal

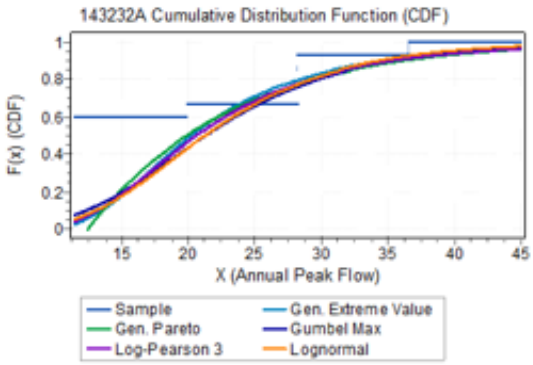
143232A Cumulative Distribution Function (CDF)
F(x) (CDF)
X (Annual Peak Flow)
Sample
Gen. Extreme Value
Gen. Pareto
Gumbel Max
Log-Pearson 3
Lognormal

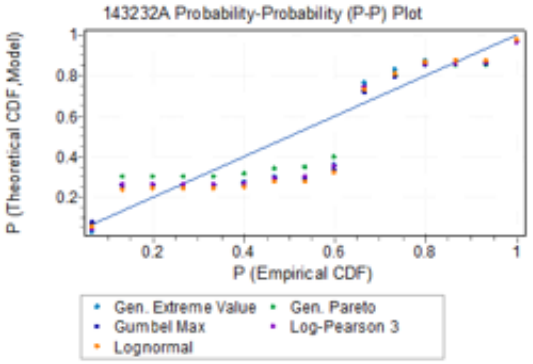
143232A Probability-Probability (P-P) Plot
P (Theoretical CDF ,Model)
P (Empirical CDF)
Gen. Extreme Value
Gen. Pareto
Gumbel Max
Log-Pearson 3
Lognormal

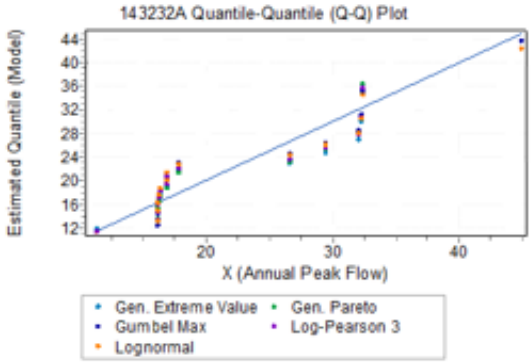
143232A Quantile-Quantile (Q-Q) Plot
Estimated Quantile (Model)
X (Annual Peak Flow)
Gen. Extreme Value
Gen. Pareto
Gumbel Max
Log-Pearson 3
Lognormal

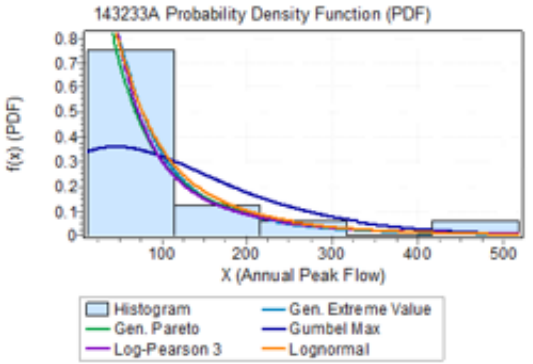
143233A Probability Density Function (PDF)
f(x) (PDF)
X (Annual Peak Flow)
Histogram
Gen. Extreme Value
Gen. Pareto
Gumbel Max
Log-Pearson 3
Lognormal

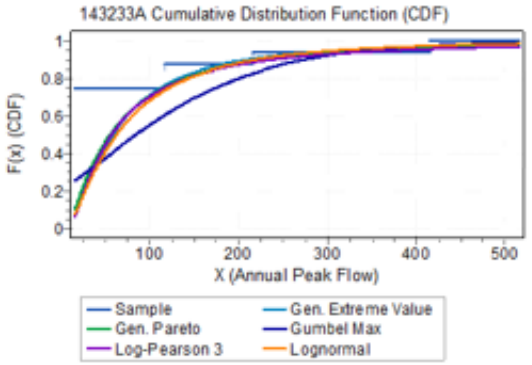
143233A Cumulative Distribution Function (CDF)
F(x) (CDF)
X (Annual Peak Flow)
Sample
Gen. Extreme Value
Gen. Pareto
Gumbel Max
Log-Pearson 3
Lognormal

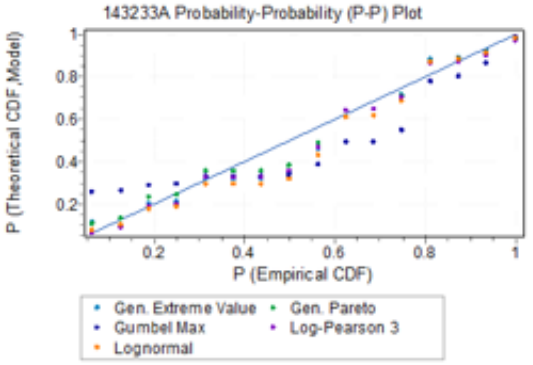
143233A Probability-Probability (P-P) Plot
P (Theoretical CDF ,Model)
P (Empirical CDF)
Gen. Extreme Value
Gen. Pareto
Gumbel Max
Log-Pearson 3
Lognormal

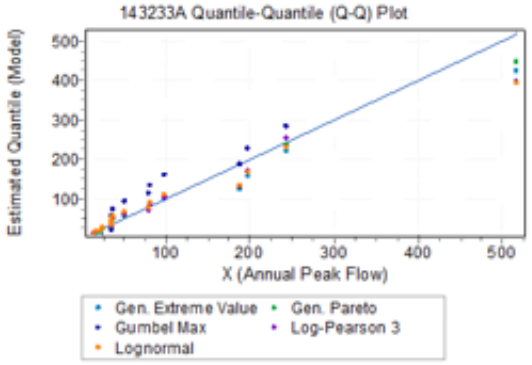
143233A Quantile-Quantile (Q-Q) Plot
Estimated Quantile (Model)
X (Annual Peak Flow)
Gen. Extreme Value
Gen. Pareto
Gumbel Max
Log-Pearson 3
Lognormal

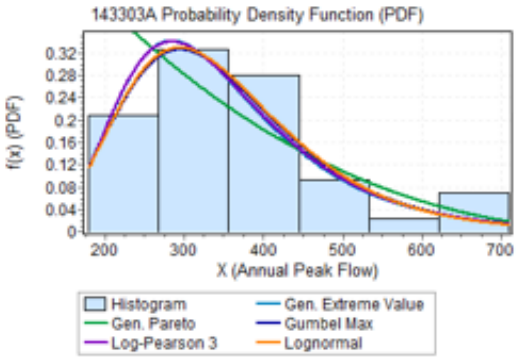
143303A Probability Density Function (PDF)
f(x) (PDF)
X (Annual Peak Flow)
Histogram
Gen. Extreme Value
Gen. Pareto
Gumbel Max
Log-Pearson 3
Lognormal

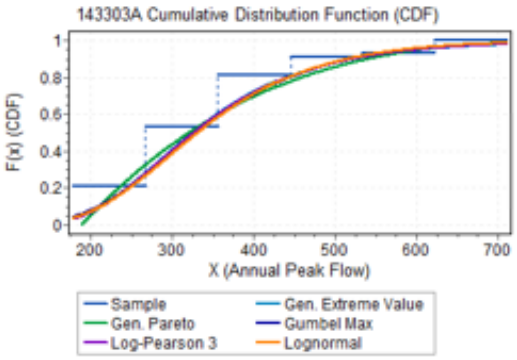
143303A Cumulative Distribution Function (CDF)
F(x) (CDF)
X (Annual Peak Flow)
Sample
Gen. Extreme Value
Gen. Pareto
Gumbel Max
Log-Pearson 3
Lognormal

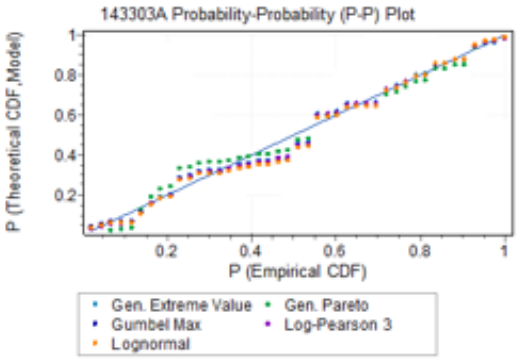
143303A Probability-Probability (P-P) Plot
P (Theoretical CDF,Model)
P (Empirical CDF)
Gen. Extreme Value
Gen. Pareto
Gumbel Max
Log-Pearson 3
Lognormal

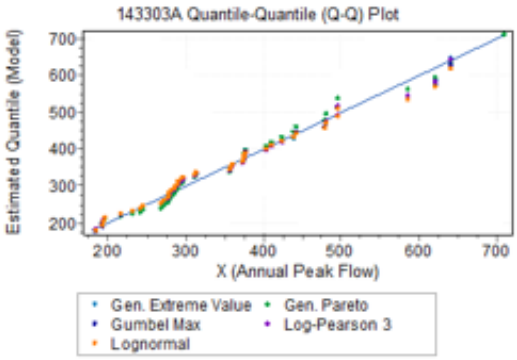
143303A Quantile-Quantile (Q-Q) Plot
Estimated Quantile (Model)
X (Annual Peak Flow)
Gen. Extreme Value
Gen. Pareto
Gumbel Max
Log-Pearson 3
Lognormal

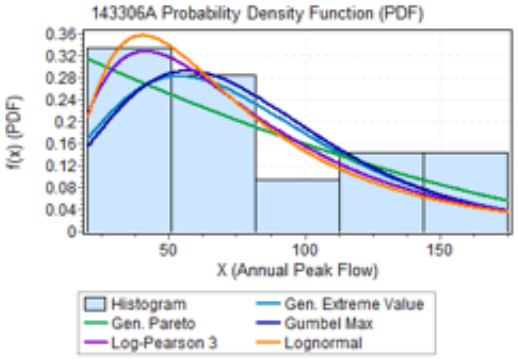
143306A Probability Density Function (PDF)
f(x) (PDF)
X (Annual Peak Flow)
Histogram
Gen. Extreme Value
Gen. Pareto
Gumbel Max
Log-Pearson 3
Lognormal

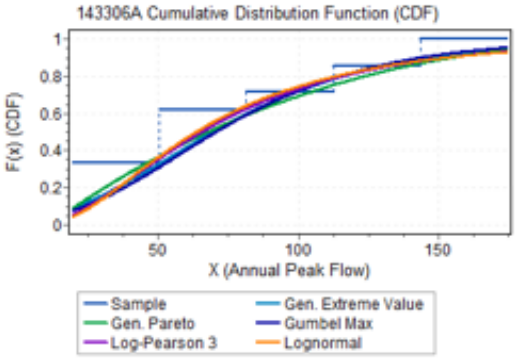
143306A Cumulative Distribution Function (CDF)
F(x) (CDF)
X (Annual Peak Flow)
Sample
Gen. Extreme Value
Gen. Pareto
Gumbel Max
Log-Pearson 3
Lognormal

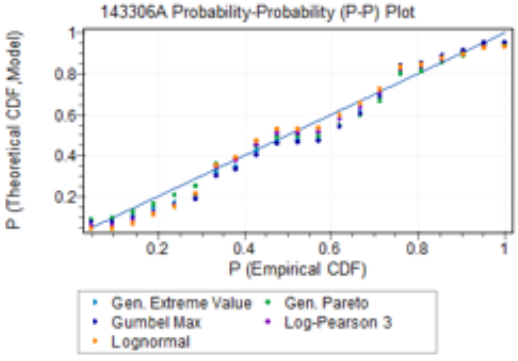
143306A Probability-Probability (P-P) Plot
P (Theoretical CDF,Model)
P (Empirical CDF)
Gen. Extreme Value
Gen. Pareto
Gumbel Max
Log-Pearson 3
Lognormal

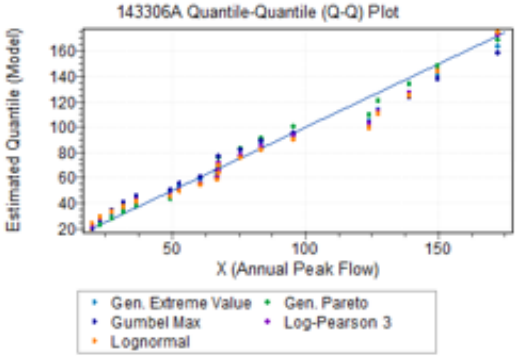
143306A Quantile-Quantile (Q-Q) Plot
Estimated Quantile (Model)
X (Annual Peak Flow)
Gen. Extreme Value
Gen. Pareto
Gumbel Max
Log-Pearson 3
Lognormal

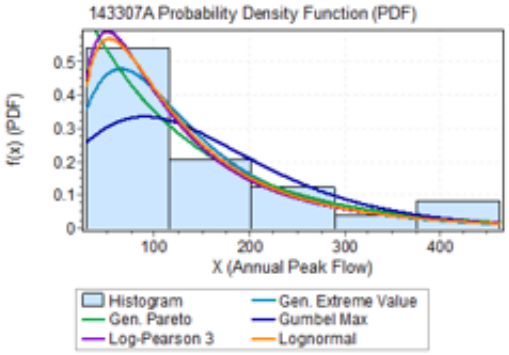
143307A Probability Density Function (PDF)
f(x) (PDF)
X (Annual Peak Flow)
Histogram
Gen. Extreme Value
Gen. Pareto
Gumbel Max
Log-Pearson 3
Lognormal

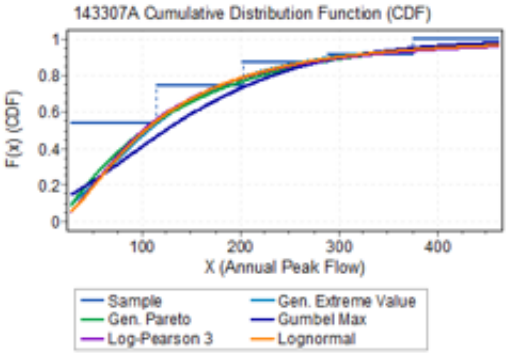
143307A Cumulative Distribution Function (CDF)
F(x) (CDF)
X (Annual Peak Flow)
Sample
Gen. Extreme Value
Gen. Pareto
Gumbel Max
Log-Pearson 3
Lognormal

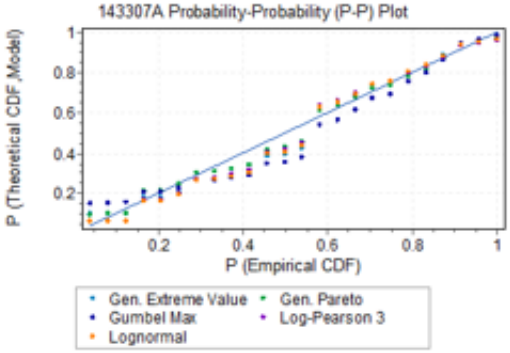
143307A Probability-Probability (P-P) Plot
P (Theoretical CDF,Model)
P (Empirical CDF)
Gen. Extreme Value
Gen. Pareto
Gumbel Max
Log-Pearson 3
Lognormal

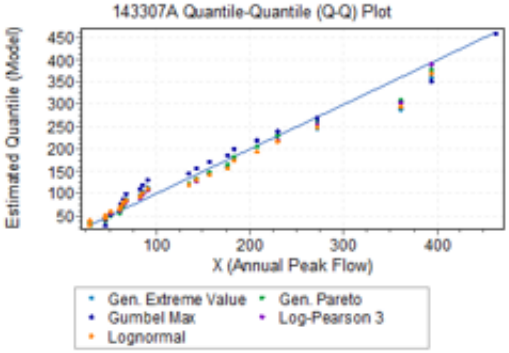
143307A Quantile-Quantile (Q-Q) Plot
Estimated Quantile (Model)
X (Annual Peak Flow)
Gen. Extreme Value
Gen. Pareto
Gumbel Max
Log-Pearson 3
Lognormal

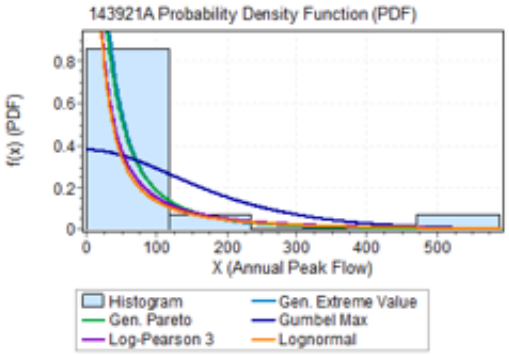
143921A Probability Density Function (PDF)
f(x) (PDF)
X (Annual Peak Flow)
Histogram
Gen. Extreme Value
Gen. Pareto
Gumbel Max
Log-Pearson 3
Lognormal

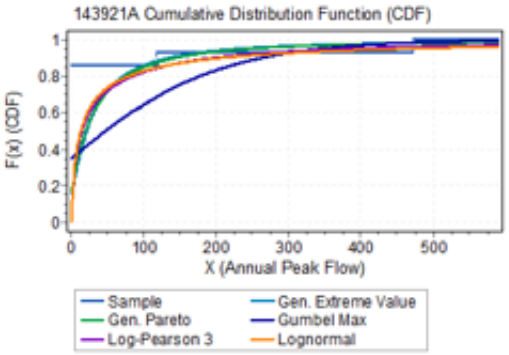
143921A Cumulative Distribution Function (CDF)
F(x) (CDF)
X (Annual Peak Flow)
Sample
Gen. Extreme Value
Gen. Pareto
Gumbel Max
Log-Pearson 3
Lognormal

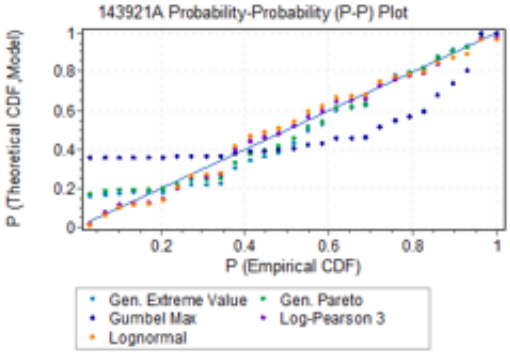
143921A Probability-Probability (P-P) Plot
P (Theoretical CDF,Model)
P (Empirical CDF)
Gen. Extreme Value
Gen. Pareto
Gumbel Max
Log-Pearson 3
Lognormal

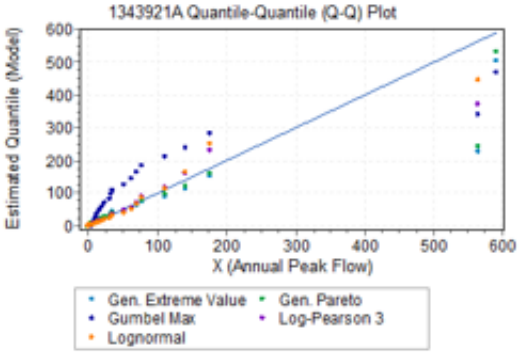
1343921A Quantile-Quantile (Q-Q) Plot
Estimated Quantile (Model)
X (Annual Peak Flow)
Gen. Extreme Value
Gen. Pareto
Gumbel Max
Log-Pearson 3
Lognormal

APPENDIX - D

PROBABILITY PLOT

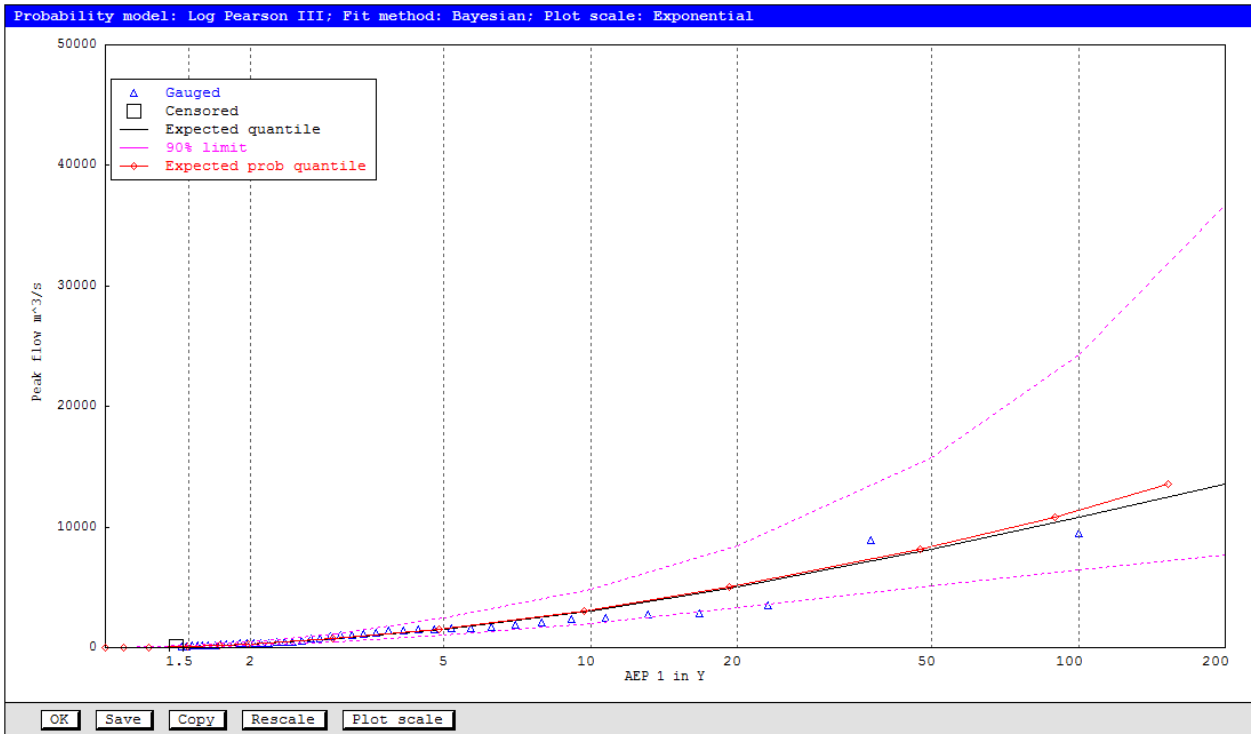

Figure D.1: LP3 Probability Plot Visual Fitting: AMF, Estimated Quantile for 143001C

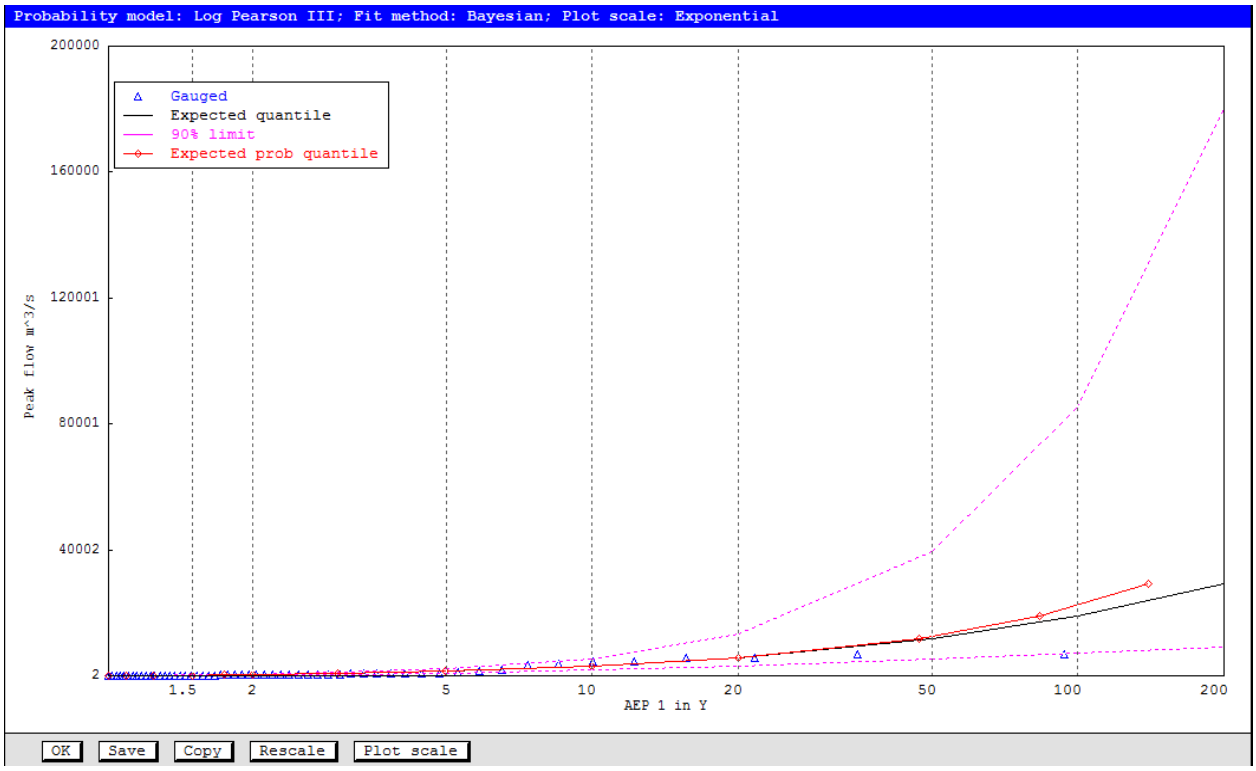

Figure D.2: LP3 Probability Plot Visual Fitting: AMF, Estimated Quantile for 143009A

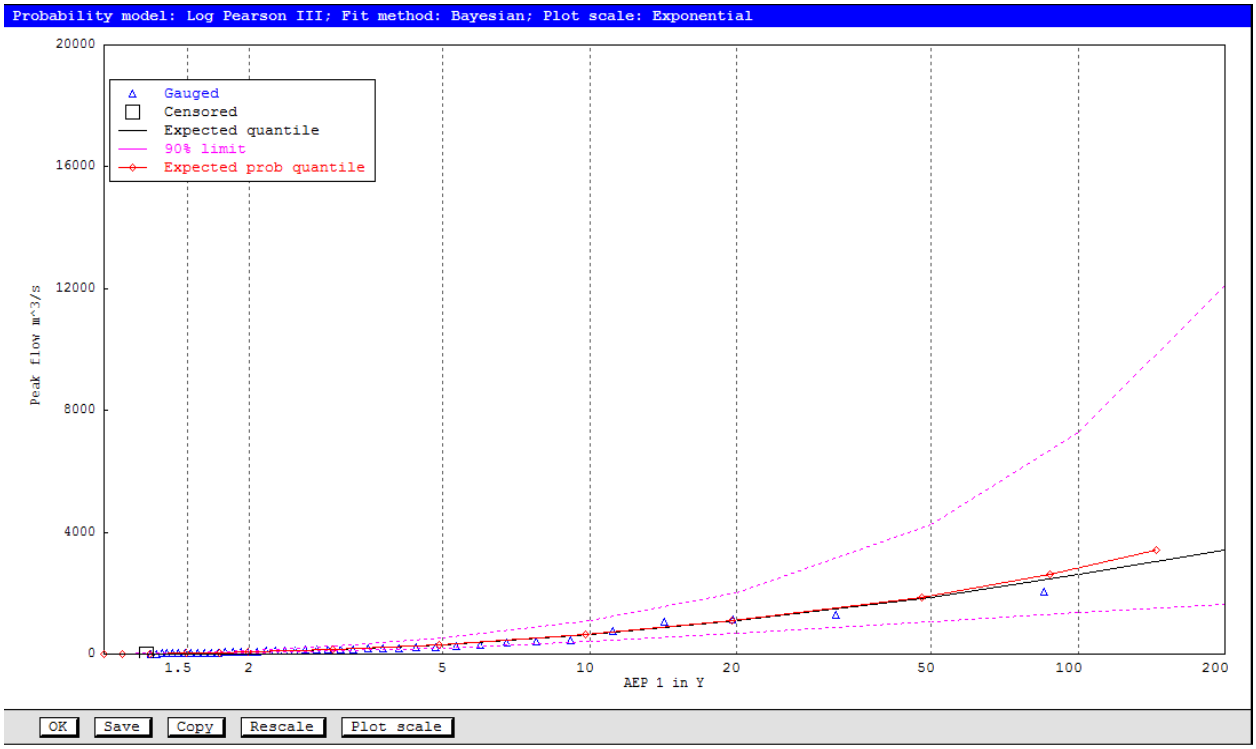

Figure D.3: LP3 Probability Plot Visual Fitting: AMF, Estimated Quantile for 143010B

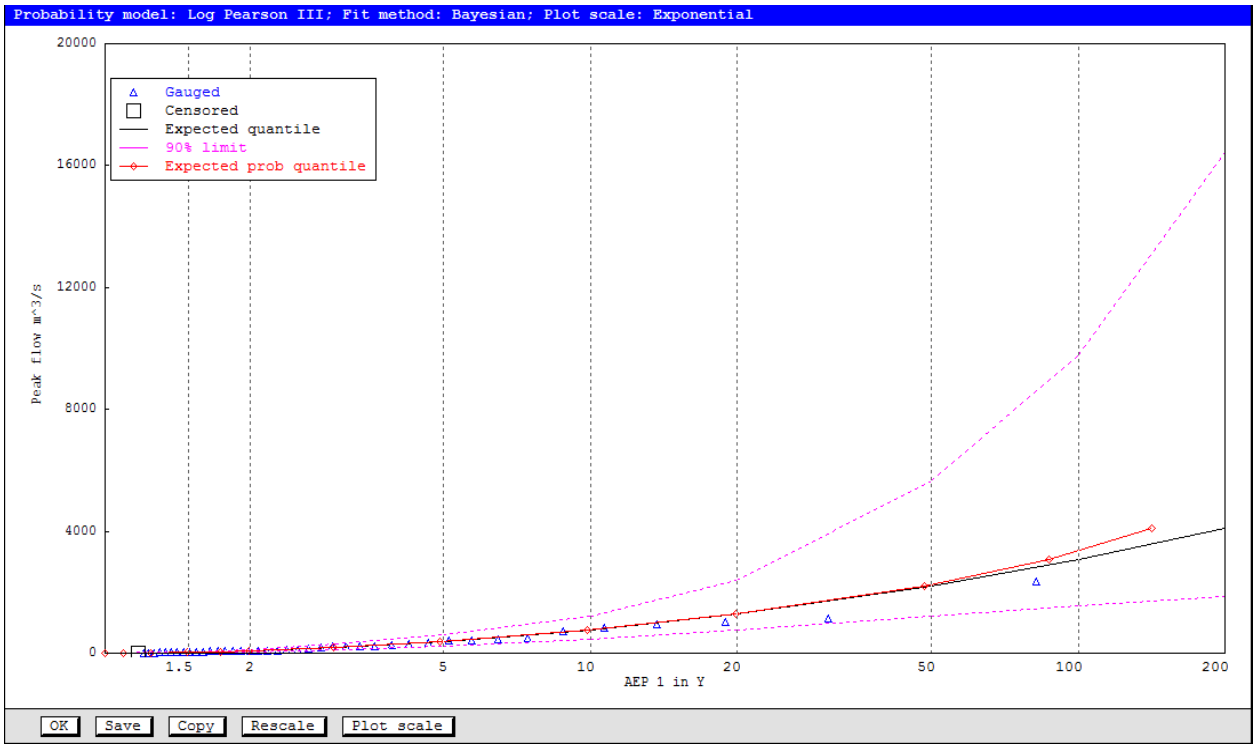

Figure D.4: LP3 Probability Plot Visual Fitting: AMF, Estimated Quantile for 143015B

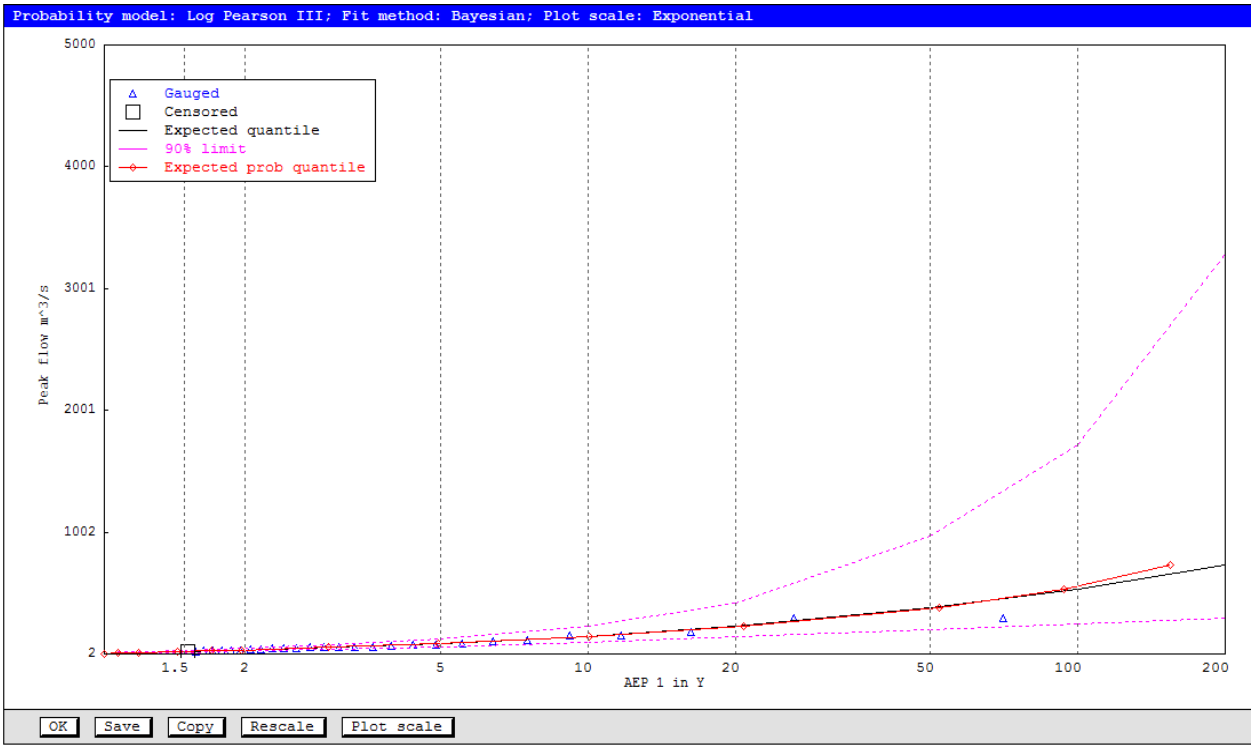

Figure D.5: LP3 Probability Plot Visual Fitting: AMF, Estimated Quantile for 143032A

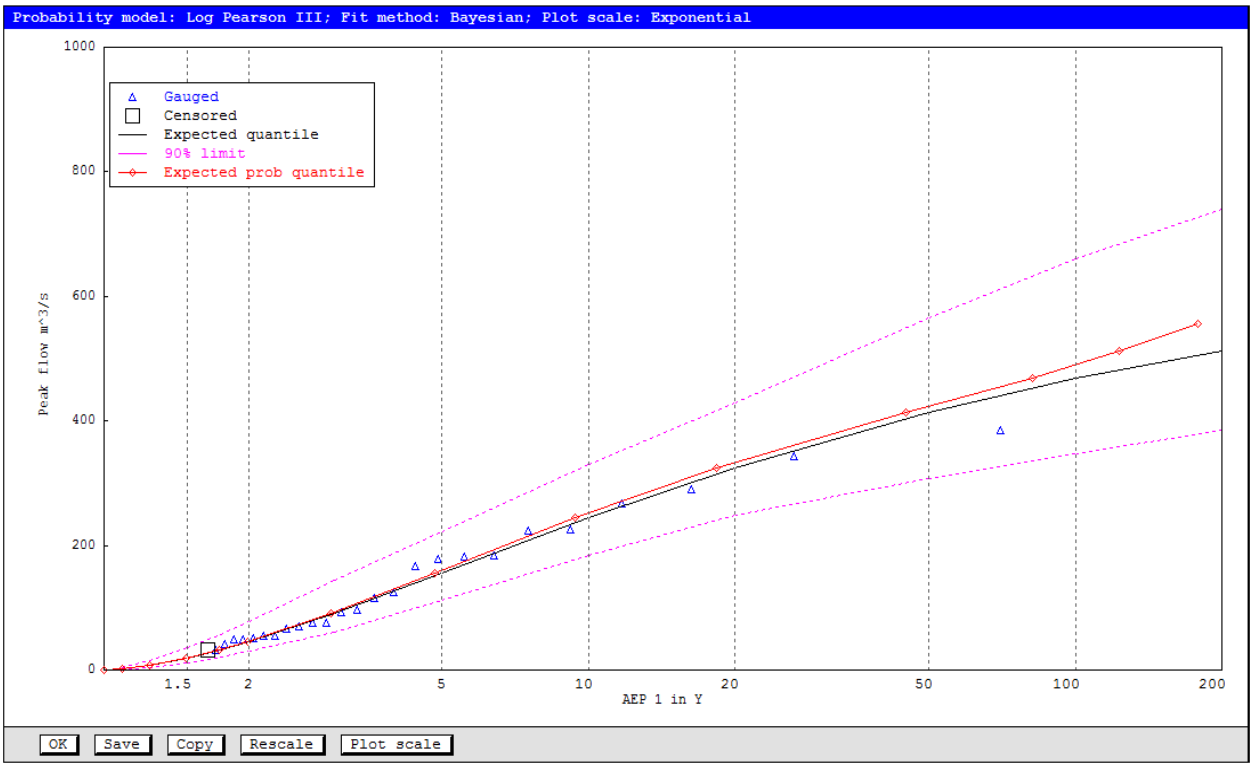

Figure D.6: LP3 Probability Plot Visual Fitting: AMF, Estimated Quantile for 143033A

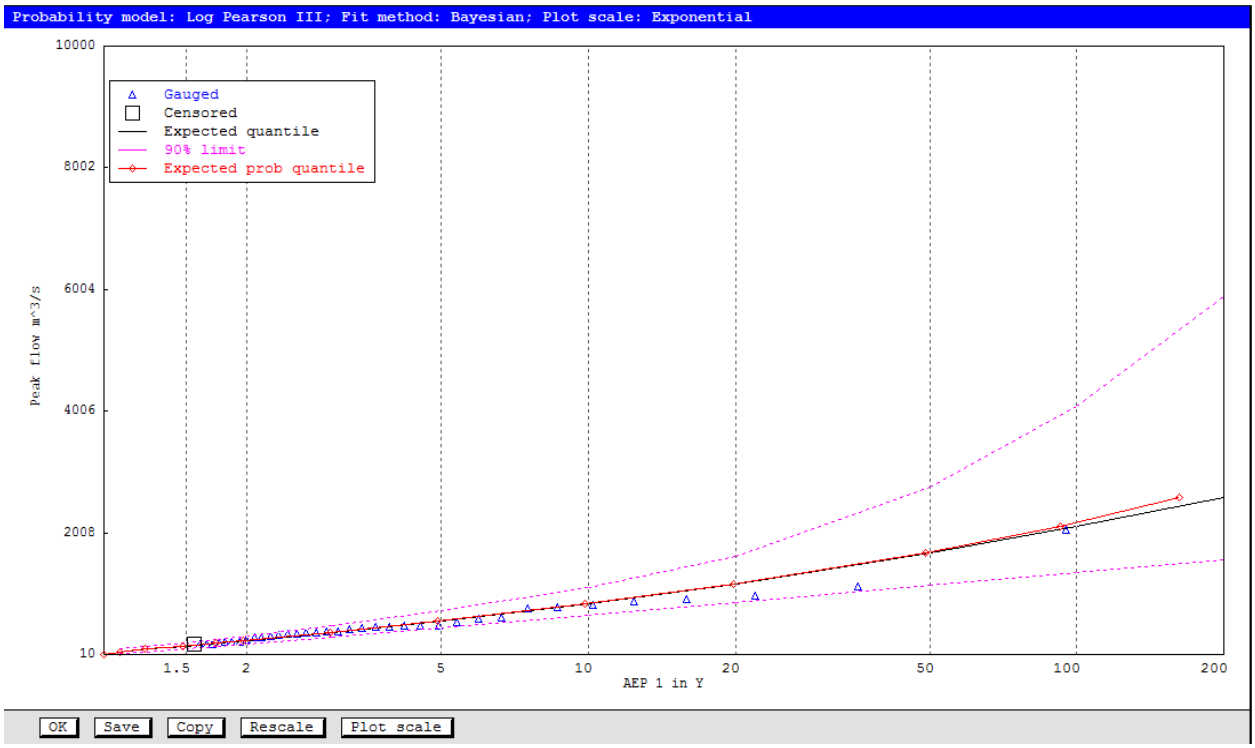

Figure D.7: LP3 Probability Plot Visual Fitting: AMF, Estimated Quantile for 143107A

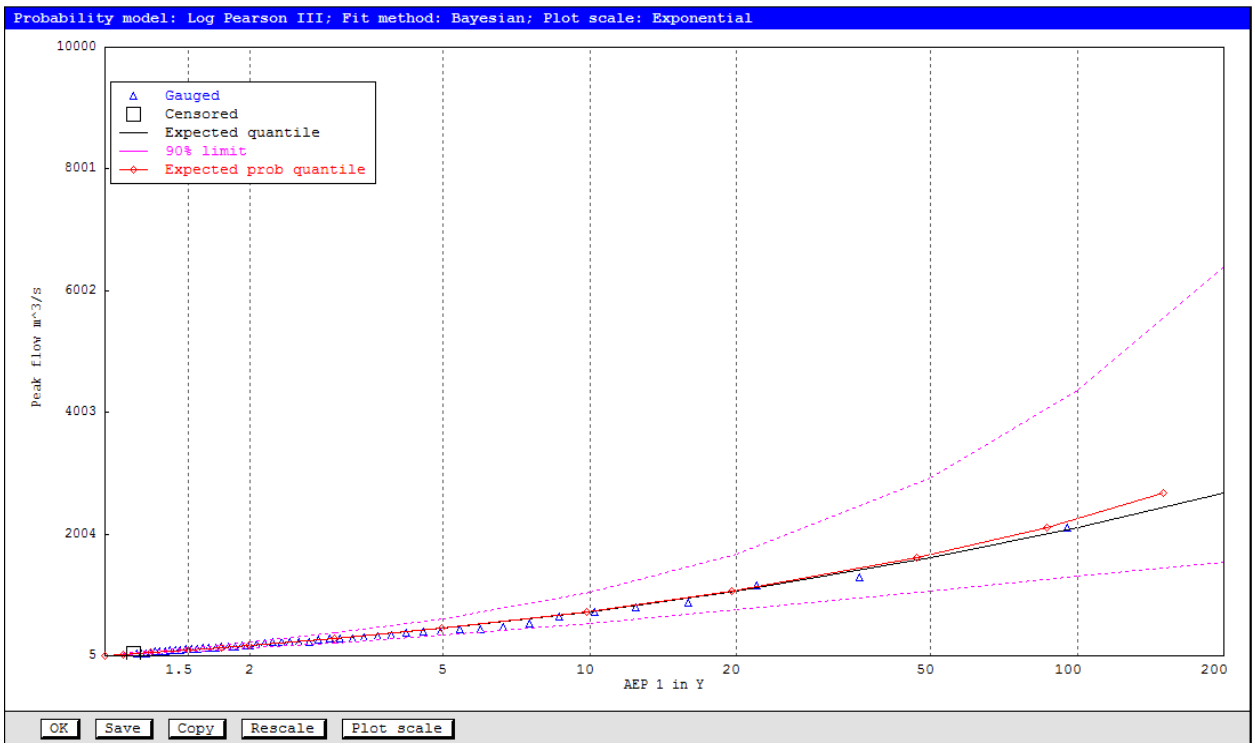

Figure D.8: LP3 Probability Plot Visual Fitting: AMF, Estimated Quantile for 143108A

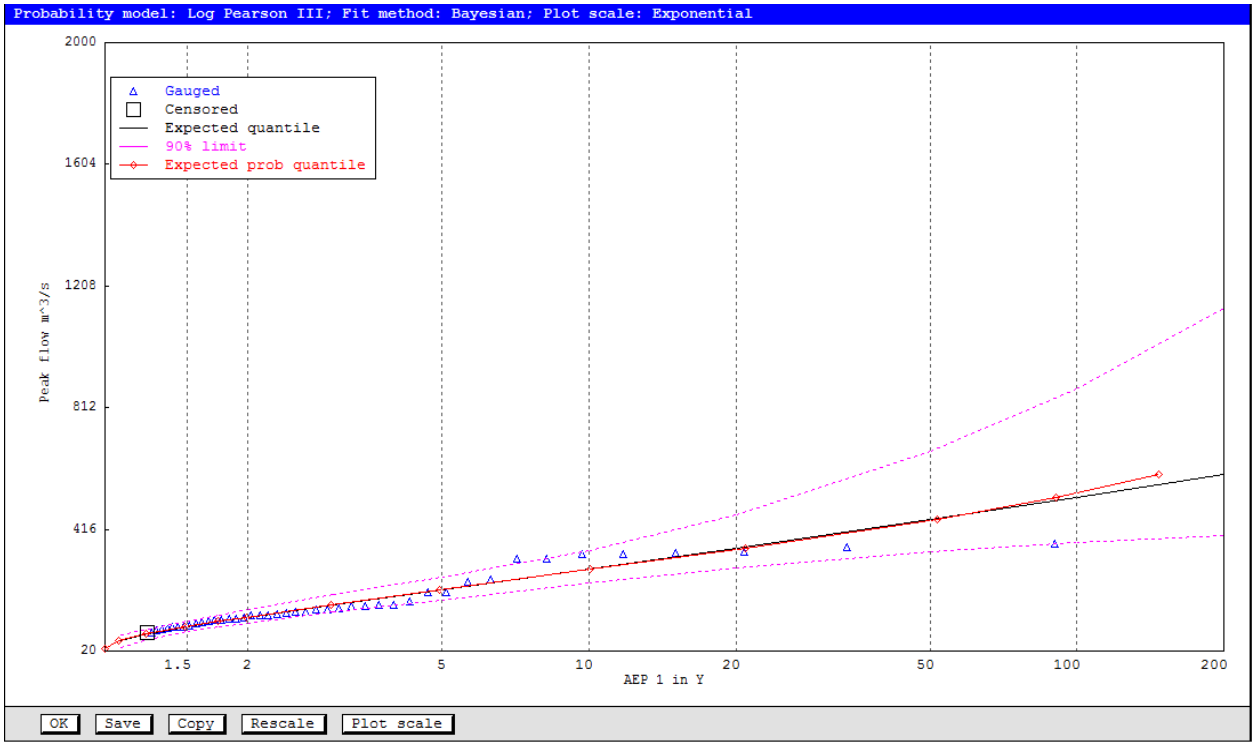

Figure D.9: LP3 Probability Plot Visual Fitting: AMF, Estimated Quantile for 143110A

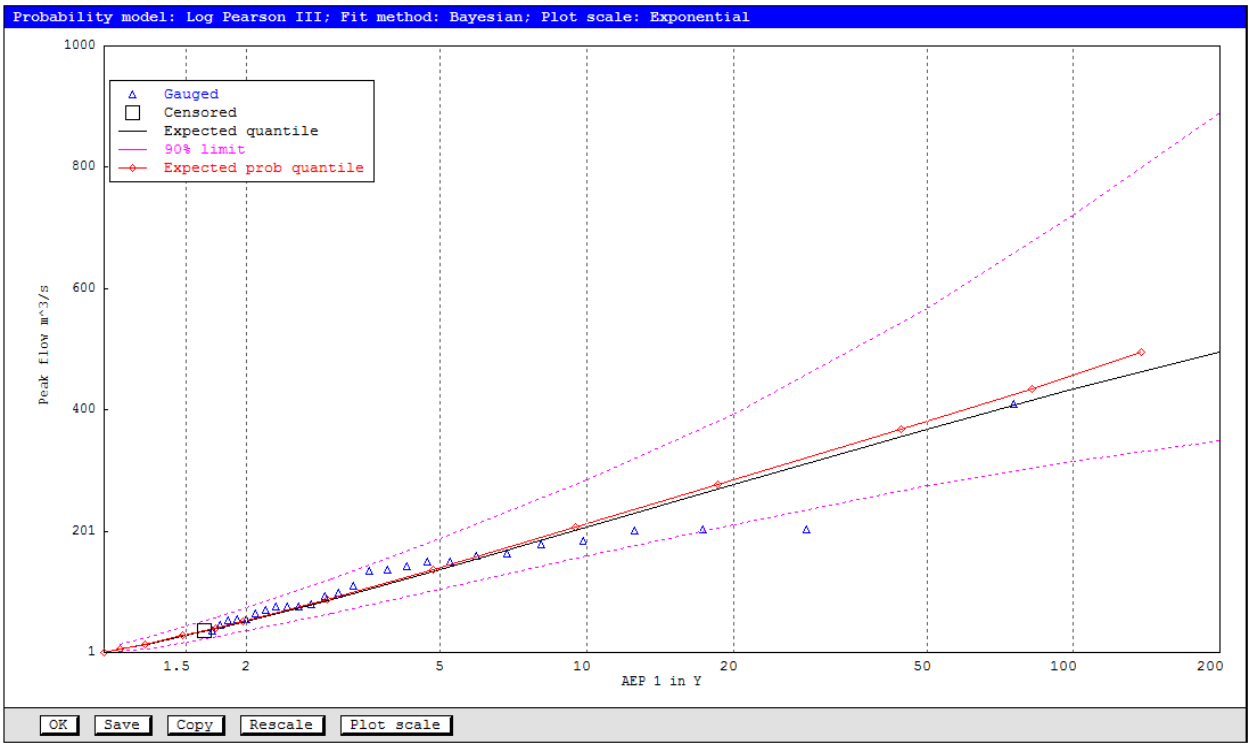

Figure D.10: LP3 Probability Plot Visual Fitting: AMF, Estimated Quantile for 143113A

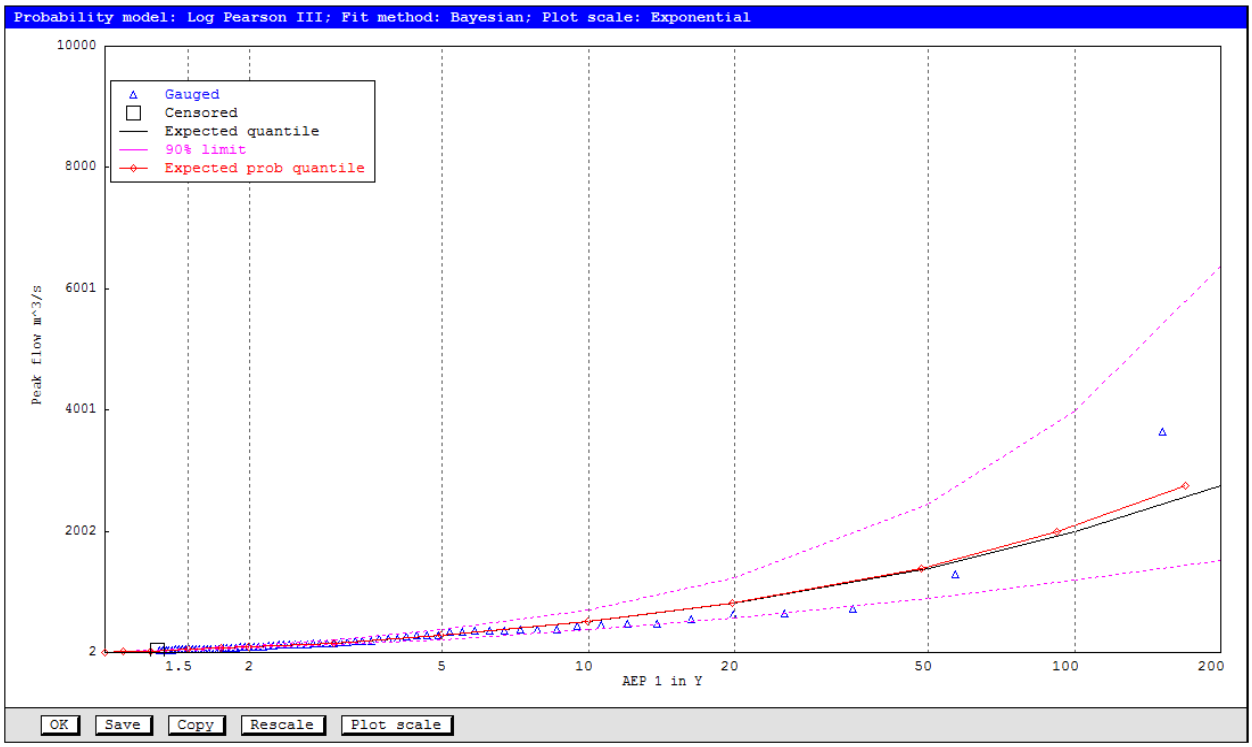

Figure D.11: LP3 Probability Plot Visual Fitting: AMF, Estimated Quantile for 143203C

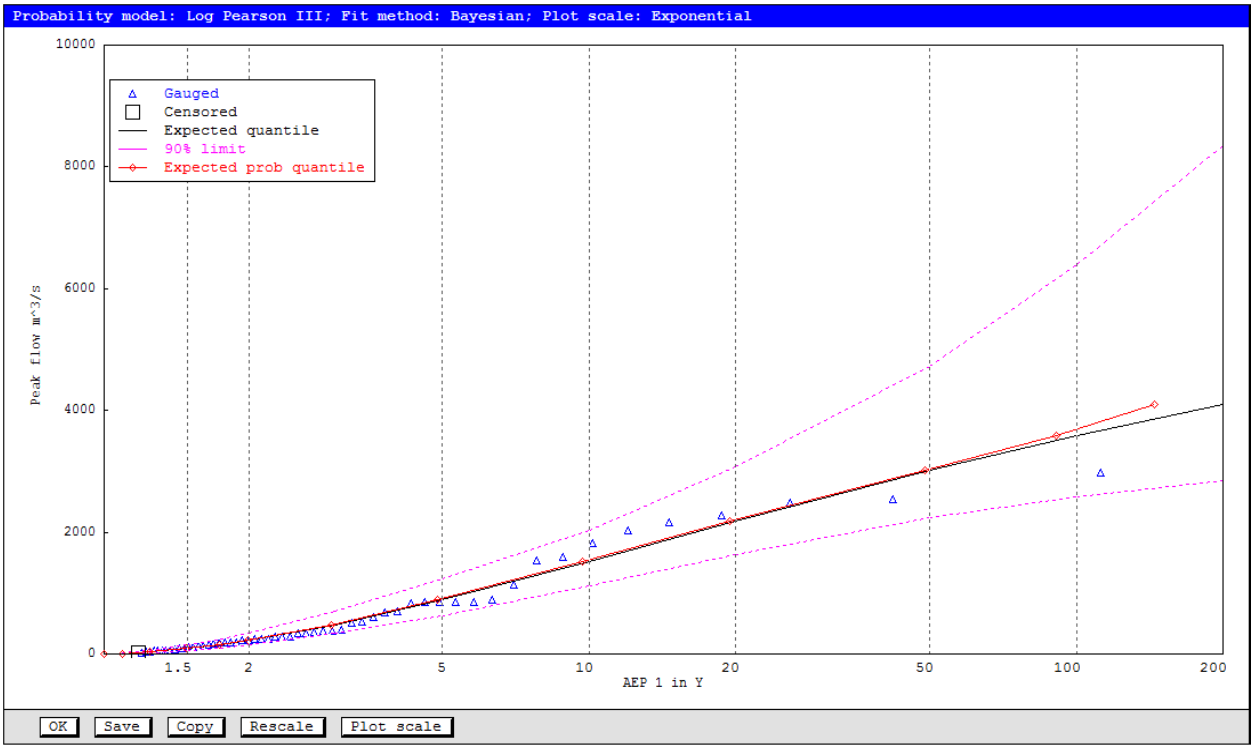

Figure D.12: LP3 Probability Plot Visual Fitting: AMF, Estimated Quantile for 143207A

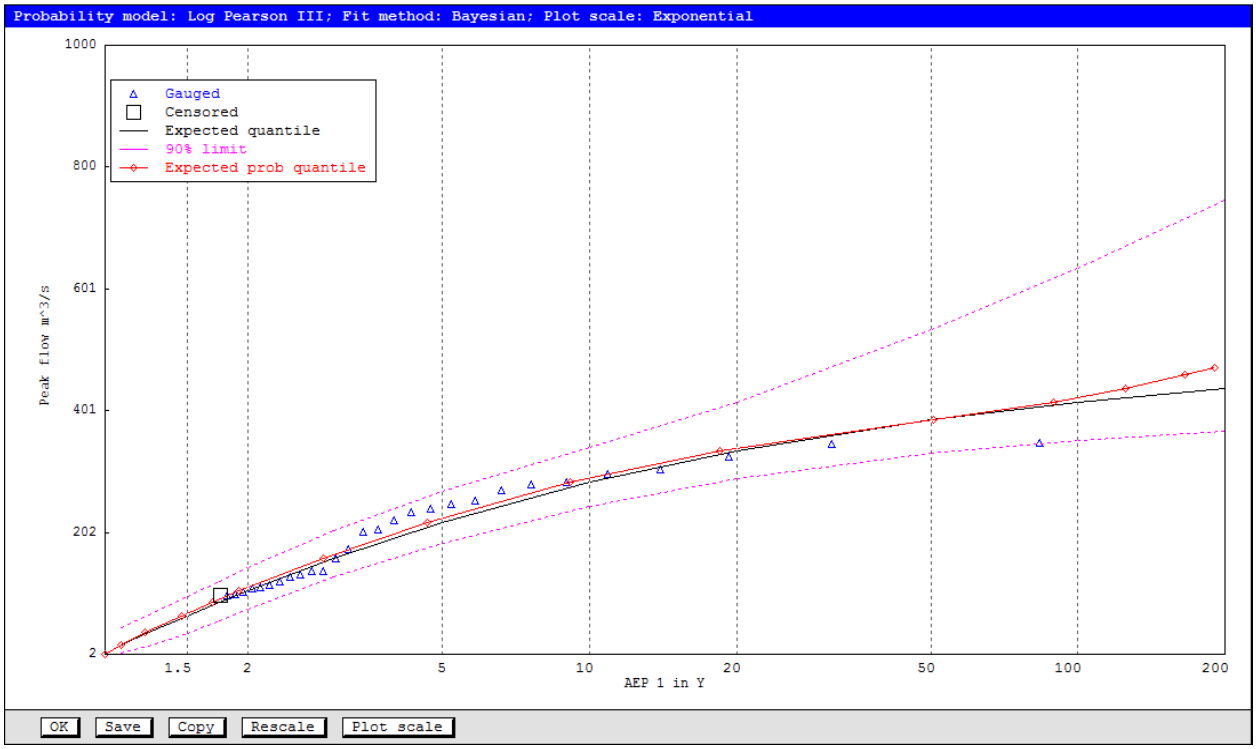

Figure D.13: LP3 Probability Plot Visual Fitting: AMF, Estimated Quantile for 143209B

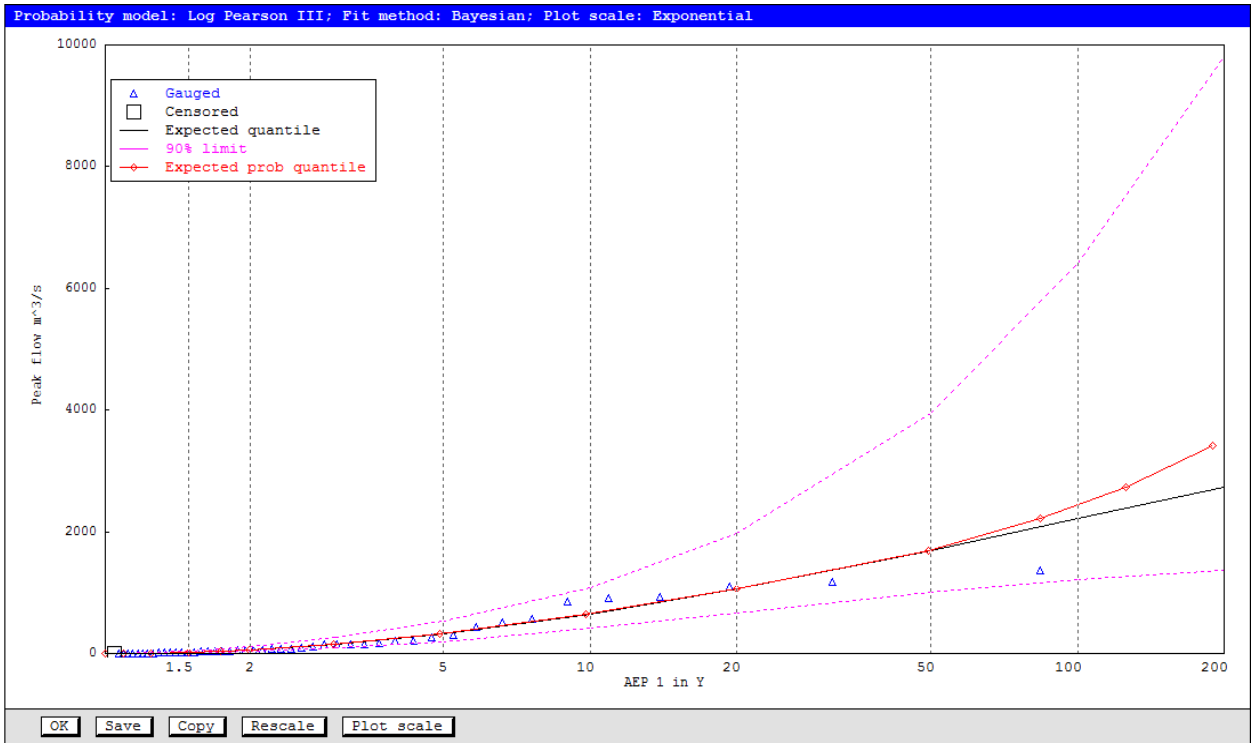

Figure D.14: LP3 Probability Plot Visual Fitting: AMF, Estimated Quantile for 143212A

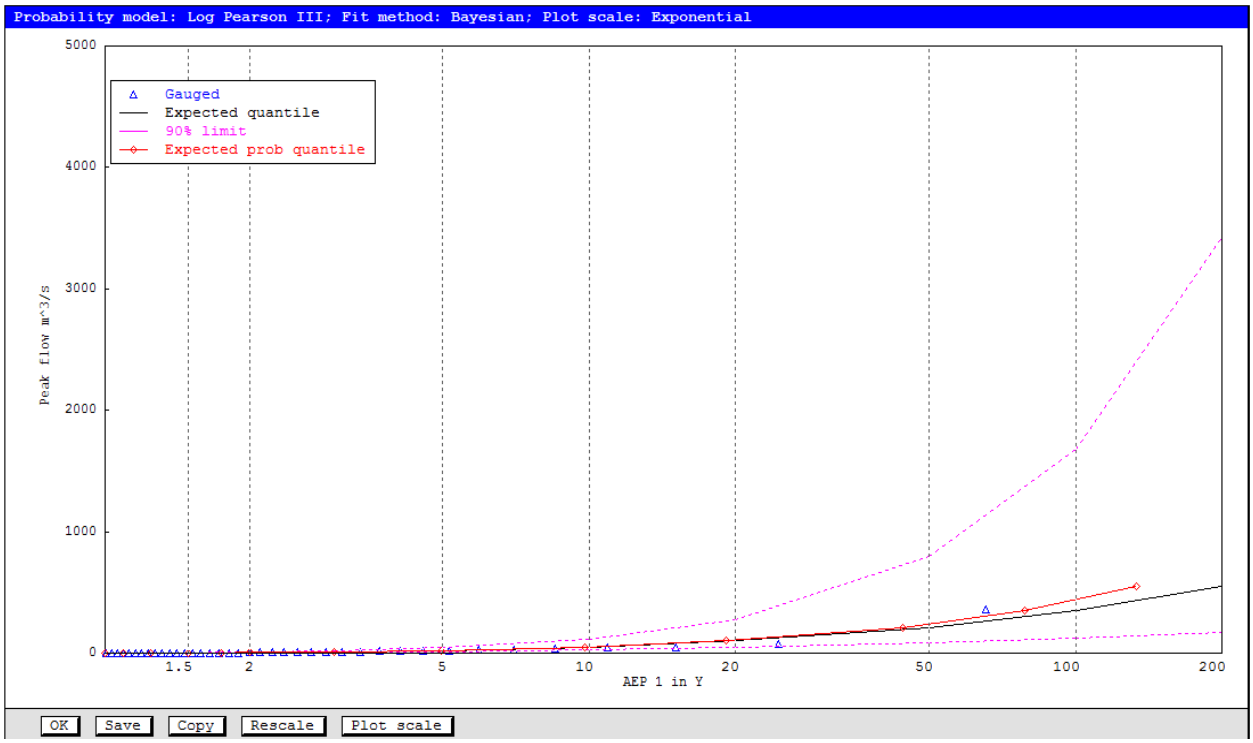

Figure D.15: LP3 Probability Plot Visual Fitting: AMF, Estimated Quantile for 143219A

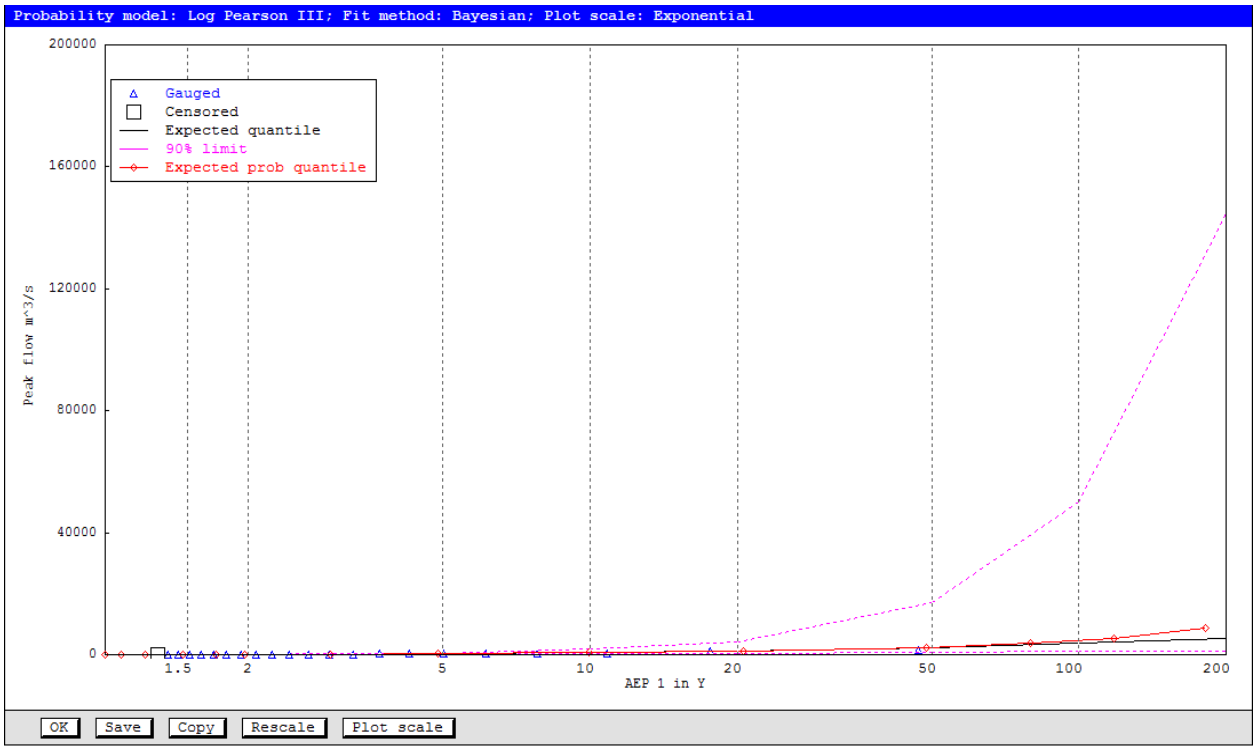

Figure D.16: LP3 Probability Plot Visual Fitting: AMF, Estimated Quantile for 143229A

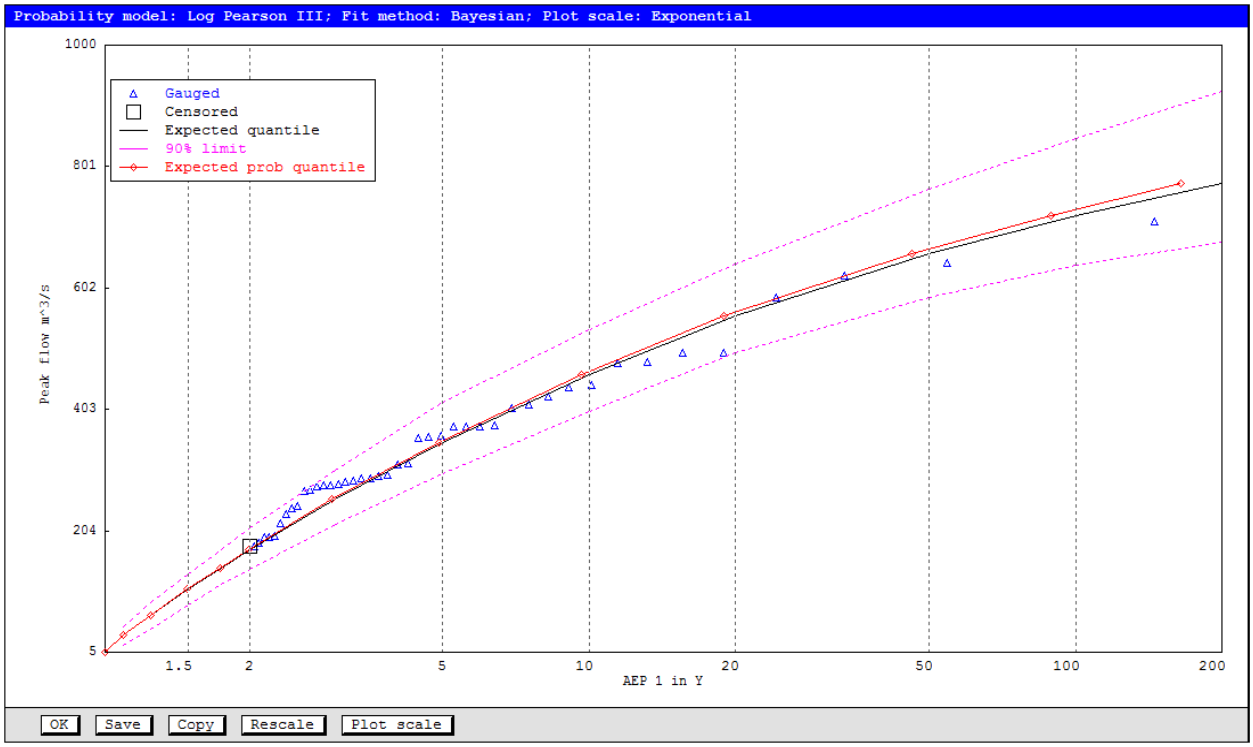

Figure D.17: LP3 Probability Plot Visual Fitting: AMF, Estimated Quantile for 143303A

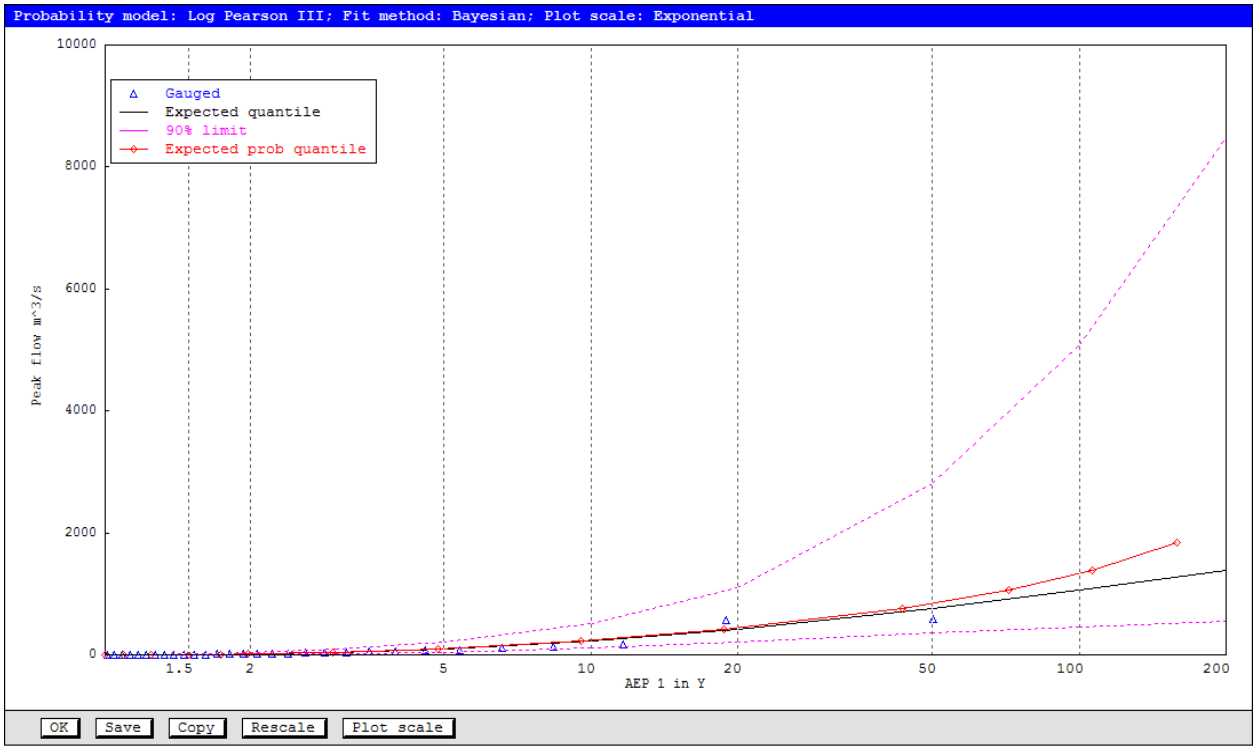

Figure D.18: LP3 Probability Plot Visual Fitting: AMF, Estimated Quantile for 1433921A

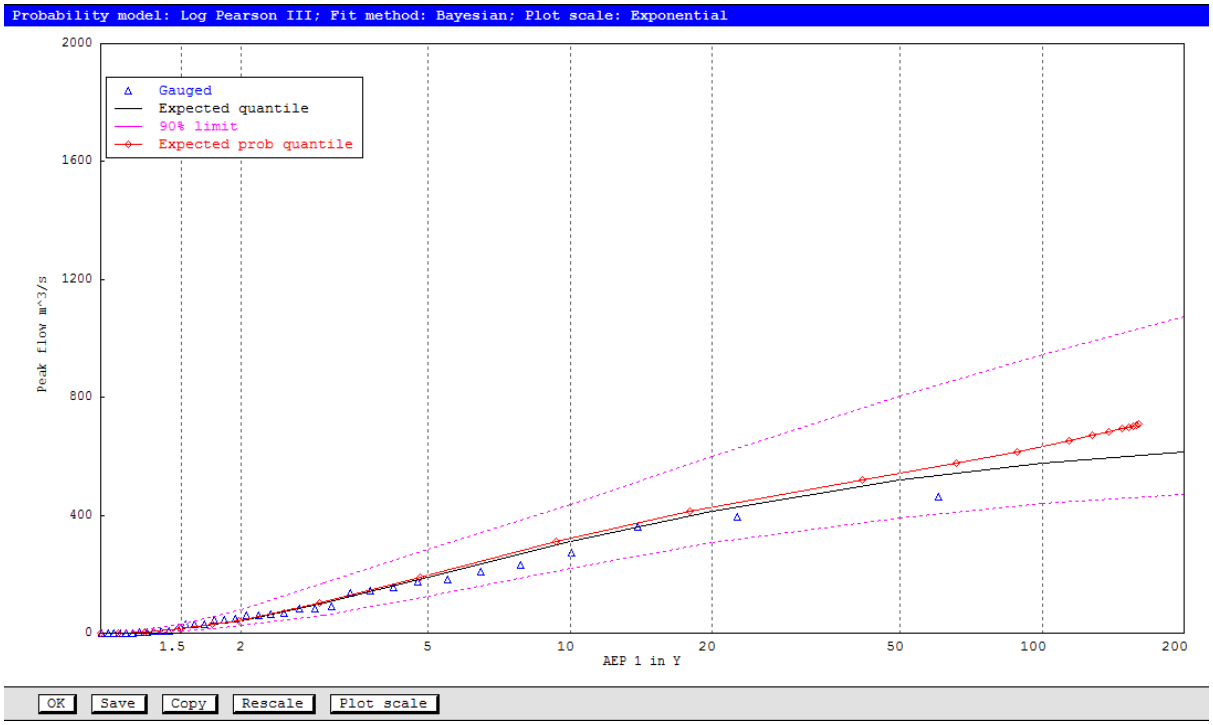

Figure D.19: LP3 Probability Plot Visual Fitting: AMF, Estimated Quantile for 143307A

APPENDIX – E
QUANTILE ESTIMAITON

Table E.1: Quantile estimation for 143001C with LP3 distribution			
	Estimated Annual Max Flow Quantile (qY)	Monte Carlo 90% quantile probability limits	
ARI (AEP 1 in Y)	Estimated AMF (m3/sec) - LP3	Lower Limit	Upper Limit
2	315	194	513
5	1549	1026	2426
10	3067	2031	4886
20	5020	3278	8472
50	8134	5087	15784
100	10784	6439	24327
200	13598	7675	36695
500	17451	9068	59015

Table E.2: Quantile estimation for 143007A with LP3 distribution			
	Estimated Annual Max Flow Quantile (qY)	Monte Carlo 90% quantile probability limits	
ARI (AEP 1 in Y)	Estimated AMF (m3/sec) - LP3	Lower Limit	Upper Limit
2	142	88	232
5	694	433	1126
10	1506	916	2677
20	2781	1567	5951
50	5389	2597	15413
100	8240	3390	30195
200	12014	4166	56789
500	18704	5138	127248

Table E.3: Quantile estimation for 143009A with LP3 distribution			
	Estimated Annual Max Flow Quantile (qY)	Monte Carlo 90% quantile probability limits	
ARI (AEP 1 in Y)	Estimated AMF (m3/sec) – LP3	Lower Limit	Upper Limit
2	277	173	446
5	1336	832	2185
10	2983	1769	5455
20	5734	3085	13208
50	11842	5230	39389
100	19085	7041	85287
200	29411	8930	180196
500	49401	11500	449266

Table E.4: Quantile estimation for 143010B with LP3 distribution			
	Estimated Annual Max Flow Quantile (qY)	Monte Carlo 90% quantile probability limits	
ARI (AEP 1 in Y)	Estimated AMF (m3/sec) – LP3	Lower Limit	Upper Limit
2	67	41	111
5	321	205	524
10	649	408	1085
20	1099	670	1998
50	1878	1064	4237
100	2600	1370	7297
200	3427	1649	12125
500	4665	1962	22701

Table E.5: Quantile estimation for 143015B with LP3 distribution			
	Estimated Annual Max Flow Quantile (qY)	Monte Carlo 90% quantile probability limits	
ARI (AEP 1 in Y)	Estimated AMF (m3/sec) – LP3	Lower Limit	Upper Limit
2	79	48	133
5	371	234	598
10	751	472	1232
20	1277	768	2400
50	2205	1209	5645
100	3080	1542	9799
200	4099	1851	16421
500	5655	2204	32776

Table E.6: Quantile estimation for 143028A with LP3 distribution			
	Estimated Annual Max Flow Quantile (qY)	Monte Carlo 90% quantile probability limits	
ARI (AEP 1 in Y)	Estimated AMF (m3/sec) – LP3	Lower Limit	Upper Limit
2	23	18	30
5	50	39	64
10	72	56	97
20	96	72	140
50	131	93	217
100	159	107	295
200	189	119	396
500	230	133	567

Table E.7: Quantile estimation for 143032A with LP3 distribution			
	Estimated Annual Max Flow Quantile (qY)	Monte Carlo 90% quantile probability limits	
ARI (AEP 1 in Y)	Estimated AMF (m3/sec) - LP3	Lower Limit	Upper Limit
2	34	26	48
5	89	63	129
10	148	100	228
20	229	143	420
50	379	205	970
100	533	250	1721
200	732	292	3281
500	1082	336	7181

Table E.8: Quantile estimation for 143033A with LP3 distribution			
	Estimated Annual Max Flow Quantile (qY)	Monte Carlo 90% quantile probability limits	
ARI (AEP 1 in Y)	Estimated AMF (m3/sec) - LP3	Lower Limit	Upper Limit
2	45	30	79
5	156	111	222
10	244	185	330
20	325	248	429
50	415	308	566
100	469	347	660
200	512	386	740
500	555	417	896

Table E.9: Quantile estimation for 143107A with LP3 distribution			
	Estimated Annual Max Flow Quantile (qY)	Monte Carlo 90% quantile probability limits	
ARI (AEP 1 in Y)	Estimated AMF (m3/sec) - LP3	Lower Limit	Upper Limit
2	238	184	309
5	552	437	721
10	837	645	1107
20	1166	864	1627
50	1671	1152	2751
100	2107	1364	4092
200	2593	1564	5888
500	3311	1796	9531

Table E.10: Quantile estimation for 143108A with LP3 distribution			
	Estimated Annual Max Flow Quantile (qY)	Monte Carlo 90% quantile probability limits	
ARI (AEP 1 in Y)	Estimated AMF (m3/sec) - LP3	Lower Limit	Upper Limit
2	173	132	229
5	456	345	613
10	735	541	1044
20	1074	758	1670
50	1622	1068	2918
100	2117	1306	4372
200	2683	1539	6397
500	3549	1829	10237

Table E.11: Quantile estimation for 143110A with LP3 distribution			
	Estimated Annual Max Flow Quantile (qY)	Monte Carlo 90% quantile probability limits	
ARI (AEP 1 in Y)	Estimated AMF (m3/sec) - LP3	Lower Limit	Upper Limit
2	130	112	155
5	221	187	262
10	287	240	346
20	355	289	462
50	447	344	669
100	520	373	872
200	595	396	1135
500	699	417	1584

Table E.12: Quantile estimation for 143113A with LP3 distribution			
	Estimated Annual Max Flow Quantile (qY)	Monte Carlo 90% quantile probability limits	
ARI (AEP 1 in Y)	Estimated AMF (m3/sec) - LP3	Lower Limit	Upper Limit
2	52	36	74
5	138	105	189
10	208	160	285
20	278	212	394
50	369	275	567
100	434	315	721
200	496	350	890
500	571	388	1123

Table E.13: Quantile estimation for 143203C with LP3 distribution			
	Estimated Annual Max Flow Quantile (qY)	Monte Carlo 90% quantile probability limits	
ARI (AEP 1 in Y)	Estimated AMF (m3/sec) - LP3	Lower Limit	Upper Limit
2	90	70	116
5	281	216	373
10	505	374	704
20	816	574	1229
50	1395	901	2440
100	1989	1192	3992
200	2748	1512	6373
500	4055	1975	11638

Table E.14: Quantile estimation for 143207A with LP3 distribution			
	Estimated Annual Max Flow Quantile (qY)	Monte Carlo 90% quantile probability limits	
ARI (AEP 1 in Y)	Estimated AMF (m3/sec) - LP3	Lower Limit	Upper Limit
2	224	149	340
5	887	631	1239
10	1518	1129	2039
20	2175	1639	3073
50	3009	2233	4717
100	3582	2587	6402
200	4092	2853	8343
500	4668	3093	11236

Table E.15: Quantile estimation for 143209B with LP3 distribution			
	Estimated Annual Max Flow Quantile (qY)	Monte Carlo 90% quantile probability limits	
ARI (AEP 1 in Y)	Estimated AMF (m3/sec) - LP3	Lower Limit	Upper Limit
2	106	77	144
5	218	184	269
10	283	244	340
20	335	290	414
50	387	332	534
100	416	352	634
200	438	367	746
500	460	378	912

Table E.16: Quantile estimation for 143210B with LP3 distribution			
	Estimated Annual Max Flow Quantile (qY)	Monte Carlo 90% quantile probability limits	
ARI (AEP 1 in Y)	Estimated AMF (m3/sec) - LP3	Lower Limit	Upper Limit
2	139	86	224
5	438	284	685
10	730	474	1209
20	1065	679	1971
50	1558	936	3520
100	1958	1109	5112
200	2373	1255	7683
500	2935	1411	12717

Table E.17: Quantile estimation for 143212A with LP3 distribution			
	Estimated Annual Max Flow Quantile (qY)	Monte Carlo 90% quantile probability limits	
ARI (AEP 1 in Y)	Estimated AMF (m3/sec) - LP3	Lower Limit	Upper Limit
2	60	34	107
5	323	198	523
10	650	411	1083
20	1062	666	1964
50	1696	1002	3941
100	2213	1209	6411
200	2738	1360	9807
500	3422	1502	16679

Table E.18: Quantile estimation for 143213C with LP3 distribution			
	Estimated Annual Max Flow Quantile (qY)	Monte Carlo 90% quantile probability limits	
ARI (AEP 1 in Y)	Estimated AMF (m3/sec) - LP3	Lower Limit	Upper Limit
2	6	2	26
5	115	45	345
10	296	131	759
20	511	221	1602
50	772	343	4398
100	927	427	6850
200	1043	499	9825
500	1148	577	14126

Table E.19: Quantile estimation for 143219A with LP3 distribution			
	Estimated Annual Max Flow Quantile (qY)	Monte Carlo 90% quantile probability limits	
ARI (AEP 1 in Y)	Estimated AMF (m3/sec) - LP3	Lower Limit	Upper Limit
2	5	3	9
5	23	14	43
10	52	28	114
20	101	50	275
50	212	89	798
100	348	128	1679
200	547	173	3429
500	945	242	8768

Table E.20: Quantile estimation for 143229A with LP3 distribution			
	Estimated Annual Max Flow Quantile (qY)	Monte Carlo 90% quantile probability limits	
ARI (AEP 1 in Y)	Estimated AMF (m3/sec) - LP3	Lower Limit	Upper Limit
2	51	26	104
5	267	136	546
10	603	289	1768
20	1149	500	4252
50	2305	826	16902
100	3606	1080	50133
200	5368	1306	144555
500	8567	1523	436502

Table E.21: Quantile estimation for 143232A with LP3 distribution			
	Estimated Annual Max Flow Quantile (qY)	Monte Carlo 90% quantile probability limits	
ARI (AEP 1 in Y)	Estimated AMF (m3/sec) - LP3	Lower Limit	Upper Limit
2	17	13	22
5	28	22	36
10	36	27	48
20	44	33	65
50	55	38	93
100	63	42	120
200	72	45	159
500	84	48	231

Table E.22: Quantile estimation for 143233A with LP3 distribution			
	Estimated Annual Max Flow Quantile (qY)	Monte Carlo 90% quantile probability limits	
ARI (AEP 1 in Y)	Estimated AMF (m3/sec) - LP3	Lower Limit	Upper Limit
2	28	15	55
5	115	58	240
10	247	111	649
20	472	183	1678
50	993	299	6793
100	1645	394	18118
200	2629	479	50790
500	4677	568	195647

Table E.23: Quantile estimation for 143303A with LP3 distribution			
	Estimated Annual Max Flow Quantile (qY)	Monte Carlo 90% quantile probability limits	
ARI (AEP 1 in Y)	Estimated AMF (m3/sec) - LP3	Lower Limit	Upper Limit
2	173	140	209
5	349	298	415
10	461	399	535
20	555	496	641
50	658	586	764
100	721	640	847
200	774	677	925
500	830	715	1016

Table E.24: Quantile estimation for 143306A with LP3 distribution			
	Estimated Annual Max Flow Quantile (qY)	Monte Carlo 90% quantile probability limits	
ARI (AEP 1 in Y)	Estimated AMF (m3/sec) - LP3	Lower Limit	Upper Limit
2	24	12	43
5	83	60	127
10	129	97	183
20	168	130	254
50	208	161	390
100	231	176	517
200	247	185	662
500	263	191	902

Table E.25: Quantile estimation for 143307A with LP3 distribution			
	Estimated Annual Max Flow Quantile (qY)	Monte Carlo 90% quantile probability limits	
ARI (AEP 1 in Y)	Estimated AMF (m3/sec) - LP3	Lower Limit	Upper Limit
2	50	31	84
5	161	108	253
10	263	180	392
20	372	262	540
50	517	357	858
100	624	414	1124
200	726	456	1456
500	850	493	2349

Table E.26: Quantile estimation for 143921A with LP3 distribution			
	Estimated Annual Max Flow Quantile (qY)	Monte Carlo 90% quantile probability limits	
ARI (AEP 1 in Y)	Estimated AMF (m3/sec) - LP3	Lower Limit	Upper Limit
2	13	5	31
5	98	47	214
10	231	115	516
20	424	209	1092
50	758	354	2815
100	1058	464	5088
200	1384	555	8477
500	1838	644	16106

APPENDIX - F

STATISTICAL TREND TEST SUMMARY

Table F.1: Trend analysis test result for 143007A

Test Name	Test Statistic for Each Test	Critical Values of Trend test Statistics for Significance Levels at			Critical Values of Trend test Re-Sampling Statistics for Significance Levels at			Result
		a=0.1	a=0.05	a=0.01	a=0.1	a=0.05	a=0.01	
Mann-Kendall	-1.611	1.645	1.960	2.576	1.626	1.940	2.380	NS
Spearman's Rho	-1.658	1.645	1.960	2.576	1.711	2.060	2.619	NS
Linear regression	0.222	1.678	2.008	2.676	1.647	1.956	2.546	NS
Cusum	7.000	8.965	9.994	11.978	9.0000	10.000	12.000	NS
Cumulative deviation	0.604	1.142	1.272	1.522	1.108	1.261	1.576	NS
Worsley likelihood	1.715	2.87	3.160	3.790	3.53	4.935	5.514	NS
Rank Sum	1.903	1.645	1.960	2.576	1.661	1.886	2.647	S (0.05)
Student's t	0.197	1.677	2.007	2.674	1.76	2.051	2.549	NS
Median Crossing	0.412	1.645	1.960	2.576	1.786	2.060	2.610	NS
Turning Point	1.094	1.645	1.960	2.576	1.86	2.189	2.845	NS
Rank Difference	-0.634	1.645	1.960	2.576	1.665	1.996	2.740	NS
Auto Correlation	0.521	1.645	1.960	2.576	1.583	1.910	2.819	NS

Table F.2: Trend analysis test result for 143009A

Test Name	Test Statistic for Each Test	Critical Values of Trend test Statistics for Significance Levels at			Critical Values of Trend test Re-Sampling Statistics for Significance Levels at			Result
		a=0.1	a=0.05	a=0.01	a=0.1	a=0.05	a=0.01	
Mann-Kendall	-1.548	1.645	1.960	2.576	1.654	2.028	2.728	NS
Spearman's Rho	-1.564	1.645	1.960	2.576	1.661	1.924	2.525	NS
Linear regression	-0.082	1.676	2.006	2.672	1.693	2.030	2.542	NS
Cusum	7.000	9.13	10.177	12.198	9.0000	10.000	11.000	NS
Cumulative deviation	0.428	1.144	1.272	1.524	1.126	1.274	1.480	NS
Worsley likelihood	1.158	2.87	3.160	3.790	3.444	3.806	4.879	NS
Rank Sum	1.893	1.645	1.960	2.576	1.647	1.975	2.548	S (0.1)
Student's t	0.627	1.676	2.005	2.670	1.598	1.872	2.392	NS
Median Crossing	0.135	1.645	1.960	2.576	1.753	2.023	2.562	NS
Turning Point	0.644	1.645	1.960	2.576	1.933	2.255	2.900	NS
Rank Difference	-0.557	1.645	1.960	2.576	1.672	2.008	2.647	NS
Auto Correlation	0.164	1.645	1.960	2.576	1.551	1.845	2.814	NS

Table F.3: Trend analysis test result for 143032A

Test Name	Test Statistic for Each Test	Critical Values of Trend test Statistics for Significance Levels at			Critical Values of Trend test Re-Sampling Statistics for Significance Levels at			Result
		a=0.1	a=0.05	a=0.01	a=0.1	a=0.05	a=0.01	
Mann-Kendall	0.141	1.645	1.960	2.576	1.658	1.983	2.764	NS
Spearman's Rho	0.224	1.645	1.960	2.576	1.636	1.916	2.533	NS
Linear regression	-0.307	1.684	2.021	2.704	1.649	1.980	2.708	NS
Cusum	4.000	7.907	8.814	10.564	8.0000	9.000	11.000	NS
Cumulative deviation	0.843	1.132	1.262	1.504	1.115	1.225	1.480	NS
Worsley likelihood	1.738	2.872	3.174	3.778	3.715	4.010	5.179	NS
Rank Sum	1.157	1.645	1.960	2.576	1.736	1.962	2.566	NS
Student's t	1.655	1.684	2.020	2.702	1.636	1.956	2.408	S (0.1)
Median Crossing	1.406	1.645	1.960	2.576	1.718	2.030	2.343	NS
Turning Point	0.125	1.645	1.960	2.576	1.746	2.120	2.868	NS
Rank Difference	-0.066	1.645	1.960	2.576	1.58	1.917	2.590	NS
Auto Correlation	1.474	1.645	1.960	2.576	1.541	1.890	2.417	NS

Table F.4: Trend analysis test result for 143107A

Test Name	Test Statistic for Each Test	Critical Values of Trend test Statistics for Significance Levels at			Critical Values of Trend test Re-Sampling Statistics for Significance Levels at			Result
		a=0.1	a=0.05	a=0.01	a=0.1	a=0.05	a=0.01	
Mann-Kendall	-0.145	1.645	1.960	2.576	1.563	1.934	2.423	NS
Spearman's Rho	-0.178	1.645	1.960	2.576	1.708	2.004	2.632	NS
Linear regression	1.336	1.676	2.005	2.670	1.663	1.919	2.563	NS
Cusum	5.000	9.211	10.268	12.306	9.0000	10.000	12.000	NS
Cumulative deviation	1.218	1.144	1.273	1.524	1.112	1.234	1.476	S (0.1)
Worsley likelihood	3.475	2.87	3.160	3.790	3.341	4.569	6.378	S (0.1)
Rank Sum	0.375	1.645	1.960	2.576	1.604	1.860	2.466	NS
Student's t	-0.797	1.675	2.004	2.668	1.632	1.921	2.468	NS
Median Crossing	0.802	1.645	1.960	2.576	1.604	1.871	2.673	NS
Turning Point	-1.171	1.645	1.960	2.576	1.809	2.128	2.767	NS
Rank Difference	-1.070	1.645	1.960	2.576	1.631	1.906	2.471	NS
Auto Correlation	0.396	1.645	1.960	2.576	1.469	1.886	2.571	NS

Table F.5: Trend analysis test result for 143108A

Test Name	Test Statistic for Each Test	Critical Values of Trend test Statistics for Significance Levels at			Critical Values of Trend test Re-Sampling Statistics for Significance Levels at			Result
		a=0.1	a=0.05	a=0.01	a=0.1	a=0.05	a=0.01	
	-0.757	1.645	1.960	2.576	1.652	1.955	2.492	NS
Spearman's Rho	-0.706	1.645	1.960	2.576	1.648	2.016	2.581	NS
Linear regression	-0.555	1.676	2.005	2.670	1.638	1.954	2.500	NS
Cusum	7.000	9.211	10.268	12.306	9.0000	10.000	13.000	NS
Cumulative deviation	0.903	1.144	1.273	1.524	1.104	1.244	1.556	NS
Worsley likelihood	2.048	2.87	3.160	3.790	3.564	5.297	7.128	NS
Rank Sum	1.046	1.645	1.960	2.576	1.588	1.923	2.530	NS
Student's t	0.938	1.675	2.004	2.668	1.608	1.971	2.535	NS
Median Crossing	2.138	1.645	1.960	2.576	1.604	1.871	2.405	S (0.05)
Turning Point	-1.809	1.645	1.960	2.576	1.809	2.128	2.767	S (0.1)
Rank Difference	-1.951	1.645	1.960	2.576	1.597	1.981	2.670	S (0.1)
Auto Correlation	0.311	1.645	1.960	2.576	1.387	1.679	2.405	NS

Table F.6: Trend analysis test result for 143110A

Test Name	Test Statistic for Each Test	Critical Values of Trend test Statistics for Significance Levels at			Critical Values of Trend test Re-Sampling Statistics for Significance Levels at			Result
		a=0.1	a=0.05	a=0.01	a=0.1	a=0.05	a=0.01	
Mann-Kendall	-0.127	1.645	1.960	2.576	1.694	2.059	2.581	NS
Spearman's Rho	-0.185	1.645	1.960	2.576	1.651	1.877	2.463	NS
Linear regression	0.008	1.678	2.008	2.676	1.669	1.977	2.561	NS
Cusum	5.000	8.965	9.994	11.978	9.0000	10.000	12.000	NS
Cumulative deviation	0.647	1.142	1.272	1.522	1.165	1.309	1.596	NS
Worsley likelihood	2.103	2.87	3.160	3.790	2.942	3.341	4.073	NS
Rank Sum	0.381	1.645	1.960	2.576	1.643	1.989	2.647	NS
Student's t	0.264	1.677	2.007	2.674	1.644	2.023	2.583	NS
Median Crossing	0.137	1.645	1.960	2.576	1.786	2.060	2.610	NS
Turning Point	0.109	1.645	1.960	2.576	1.86	2.408	2.845	NS
Rank Difference	0.090	1.645	1.960	2.576	1.603	1.861	2.581	NS
Auto Correlation	0.380	1.645	1.960	2.576	1.671	1.977	2.534	NS

Table F.7: Trend analysis test result for 143113A

Test Name	Test Statistic for Each Test	Critical Values of Trend test Statistics for Significance Levels at			Critical Values of Trend test Re-Sampling Statistics for Significance Levels at			Result
		a=0.1	a=0.05	a=0.01	a=0.1	a=0.05	a=0.01	
Mann-Kendall	-0.186	1.645	1.960	2.576	1.634	1.966	2.671	NS
Spearman's Rho	-0.096	1.645	1.960	2.576	1.676	2.035	2.491	NS
Linear regression	-0.557	1.683	2.018	2.697	1.765	2.036	2.500	NS
Cusum	7.000	8.184	9.123	10.934	9.0000	10.000	11.000	NS
Cumulative deviation	0.719	1.135	1.265	1.510	1.126	1.248	1.462	NS
Worsley likelihood	2.315	2.86	3.180	3.790	3.077	4.062	5.055	NS
Rank Sum	0.738	1.645	1.960	2.576	1.692	1.987	2.577	NS
Student's t	0.753	1.682	2.017	2.694	1.668	2.004	2.459	NS
Median Crossing	0.905	1.645	1.960	2.576	1.508	1.809	2.412	NS
Turning Point	0.481	1.645	1.960	2.576	1.925	2.286	2.767	NS
Rank Difference	-1.389	1.645	1.960	2.576	1.714	2.016	2.638	NS
Auto Correlation	0.390	1.645	1.960	2.576	1.574	1.847	2.365	NS

Table F.8: Trend analysis test result for 143203C

Test Name	Test Statistic for Each Test	Critical Values of Trend test Statistics for Significance Levels at			Critical Values of Trend test Re-Sampling Statistics for Significance Levels at			Result
		a=0.1	a=0.05	a=0.01	a=0.1	a=0.05	a=0.01	
Mann-Kendall	-0.555	1.645	1.960	2.576	1.68	1.964	2.544	NS
Spearman's Rho	-0.536	1.645	1.960	2.576	1.675	2.035	2.705	NS
Linear regression	1.610	1.665	1.990	2.639	1.59	1.906	2.353	S (0.1)
Cusum	5.000	11.64	12.974	15.549	12.00	14.000	17.000	NS
Cumulative deviation	0.852	1.165	1.286	1.545	1.096	1.197	1.433	NS
Worsley likelihood	2.843	2.87	3.159	3.790	4.356	6.486	16.068	NS
Rank Sum	-0.020	1.645	1.960	2.576	1.655	1.949	2.528	NS
Student's t	-1.612	1.664	1.990	2.638	1.608	1.835	2.223	S (0.1)
Median Crossing	0.843	1.645	1.960	2.576	1.687	1.897	2.741	NS
Turning Point	-1.088	1.645	1.960	2.576	1.842	2.093	2.679	NS
Rank Difference	0.050	1.645	1.960	2.576	1.615	1.870	2.536	NS
Auto Correlation	0.223	1.645	1.960	2.576	1.236	1.702	2.710	NS

Table F.9: Trend analysis test result for 143207A

Test Name	Test Statistic for Each Test	Critical Values of Trend test Statistics for Significance Levels at			Critical Values of Trend test Re-Sampling Statistics for Significance Levels at			Result
		a=0.1	a=0.05	a=0.01	a=0.1	a=0.05	a=0.01	
Mann-Kendall	-0.801	1.645	1.960	2.576	1.596	1.937	2.581	NS
Spearman's Rho	-0.652	1.645	1.960	2.576	1.613	2.008	2.723	NS
Linear regression	-0.221	1.67	1.998	2.656	1.759	2.028	2.627	NS
Cusum	7.000	9.986	11.132	13.342	10.00	11.000	14.000	NS
Cumulative deviation	0.891	1.15	1.277	1.530	1.162	1.287	1.476	NS
Worsley likelihood	2.355	2.87	3.160	3.790	3.137	3.618	4.694	NS
Rank Sum	1.173	1.645	1.960	2.576	1.699	1.950	2.540	NS
Student's t	1.137	1.67	1.998	2.656	1.662	1.954	2.547	NS
Median Crossing	0.739	1.645	1.960	2.576	1.723	1.969	2.462	NS
Turning Point	-0.098	1.645	1.960	2.576	1.86	2.154	3.035	NS
Rank Difference	-0.760	1.645	1.960	2.576	1.643	1.961	2.508	NS
Auto Correlation	0.386	1.645	1.960	2.576	1.52	1.792	2.741	NS

Table F.10: Trend analysis test result for 143209B

Test Name	Test Statistic for Each Test	Critical Values of Trend test Statistics for Significance Levels at			Critical Values of Trend test Re-Sampling Statistics for Significance Levels at			Result
		a=0.1	a=0.05	a=0.01	a=0.1	a=0.05	a=0.01	
Mann-Kendall	-0.510	1.645	1.960	2.576	1.681	2.024	2.501	NS
Spearman's Rho	-0.674	1.645	1.960	2.576	1.657	2.005	2.571	NS
Linear regression	-0.798	1.681	2.012	2.685	1.646	1.946	2.770	NS
Cusum	6.000	8.627	9.617	11.526	9.0000	9.000	11.000	NS
Cumulative deviation	0.772	1.14	1.270	1.520	1.167	1.281	1.543	NS
Worsley likelihood	1.551	2.87	3.160	3.790	2.792	3.218	3.698	NS
Rank Sum	1.067	1.645	1.960	2.576	1.572	1.940	2.619	NS
Student's t	1.117	1.68	2.011	2.682	1.677	2.008	2.543	NS
Median Crossing	0.429	1.645	1.960	2.576	1.571	2.143	2.714	NS
Turning Point	-0.342	1.645	1.960	2.576	1.708	2.392	3.075	NS
Rank Difference	-0.290	1.645	1.960	2.576	1.615	1.905	2.443	NS
Auto Correlation	-0.085	1.645	1.960	2.576	1.611	1.862	2.623	NS

Table F.11: Trend analysis test result for 143212A

Test Name	Test Statistic for Each Test	Critical Values of Trend test Statistics for Significance Levels at			Critical Values of Trend test Re-Sampling Statistics for Significance Levels at			Result
		a=0.1	a=0.05	a=0.01	a=0.1	a=0.05	a=0.01	
Mann-Kendall	0.468	1.645	1.960	2.576	1.606	1.916	2.476	NS
Spearman's Rho	0.536	1.645	1.960	2.576	1.687	1.917	2.624	NS
Linear regression	1.492	1.681	2.012	2.685	1.658	1.935	2.711	NS
Cusum	5.000	8.627	9.617	11.526	9.0000	10.000	11.000	NS
Cumulative deviation	1.067	1.14	1.270	1.520	1.138	1.288	1.490	NS
Worsley likelihood	3.129	2.87	3.160	3.790	3.372	3.932	5.192	NS
Rank Sum	0.116	1.645	1.960	2.576	1.688	2.018	2.697	NS
Student's t	-0.895	1.68	2.011	2.682	1.559	1.922	2.400	NS
Median Crossing	0.429	1.645	1.960	2.576	1.571	1.857	2.429	NS
Turning Point	-0.683	1.645	1.960	2.576	1.708	2.050	2.733	NS
Rank Difference	0.497	1.645	1.960	2.576	1.642	1.932	2.471	NS
Auto Correlation	0.016	1.645	1.960	2.576	1.593	1.944	2.945	NS

Table F.12: Trend analysis test result for 143219A

Test Name	Test Statistic for Each Test	Critical Values of Trend test Statistics for Significance Levels at			Critical Values of Trend test Re-Sampling Statistics for Significance Levels at			Result
		a=0.1	a=0.05	a=0.01	a=0.1	a=0.05	a=0.01	
Mann-Kendall	-0.944	1.645	1.960	2.576	1.669	2.008	2.734	NS
Spearman's Rho	-0.747	1.645	1.960	2.576	1.773	2.129	2.734	NS
Linear regression	0.802	1.688	2.027	2.718	1.701	1.926	2.296	NS
Cusum	4.000	7.619	8.493	10.179	8.0000	9.000	11.000	NS
Cumulative deviation	0.813	1.129	1.258	1.496	1.052	1.175	1.466	NS
Worsley likelihood	2.071	2.88	3.178	3.790	4.603	12.230	21.595	NS
Rank Sum	0.295	1.645	1.960	2.576	1.672	1.953	2.543	NS
Student's t	-0.691	1.687	2.025	2.713	1.544	1.744	2.339	NS
Median Crossing	1.298	1.645	1.960	2.576	1.622	1.947	2.596	NS
Turning Point	1.296	1.645	1.960	2.576	1.815	2.204	2.982	NS
Rank Difference	0.027	1.645	1.960	2.576	1.731	2.013	2.660	NS
Auto Correlation	0.371	1.645	1.960	2.576	1.21	1.600	2.924	NS

Table F.13: Trend analysis test result for 143229A

Test Name	Test Statistic for Each Test	Critical Values of Trend test Statistics for Significance Levels at			Critical Values of Trend test Re-Sampling Statistics for Significance Levels at			Result
		a=0.1	a=0.05	a=0.01	a=0.1	a=0.05	a=0.01	
Mann-Kendall	0.652	1.645	1.960	2.576	1.719	2.015	2.726	NS
Spearman's Rho	0.853	1.645	1.960	2.576	1.76	2.105	2.599	NS
Linear regression	1.374	1.706	2.056	2.779	1.605	1.914	2.556	NS
Cusum	2.000	6.456	7.196	8.625	6.0000	7.000	9.000	NS
Cumulative deviation	1.042	1.116	1.236	1.452	1.076	1.171	1.418	NS
Worsley likelihood	2.470	2.872	3.206	3.892	4.685	5.516	8.338	NS
Rank Sum	-0.758	1.645	1.960	2.576	1.631	1.907	2.550	NS
Student's t	-1.277	1.703	2.052	2.771	1.652	1.854	2.340	NS
Median Crossing	1.347	1.645	1.960	2.576	1.732	2.117	2.502	NS
Turning Point	0.309	1.645	1.960	2.576	2.008	2.472	2.935	NS
Rank Difference	0.877	1.645	1.960	2.576	1.686	1.989	2.697	NS
Auto Correlation	0.101	1.645	1.960	2.576	1.329	1.638	2.529	NS

Table F.14: Trend analysis test result for 143303A

Test Name	Test Statistic for Each Test	Critical Values of Trend test Statistics for Significance Levels at			Critical Values of Trend test Re-Sampling Statistics for Significance Levels at			Result
		a=0.1	a=0.05	a=0.01	a=0.1	a=0.05	a=0.01	
Mann-Kendall	-0.103	1.645	1.960	2.576	1.639	1.965	2.577	NS
Spearman's Rho	-0.179	1.645	1.960	2.576	1.623	1.907	2.309	NS
Linear regression	-0.122	1.666	1.992	2.642	1.689	2.055	2.737	NS
Cusum	6.000	11.38	12.685	15.204	11.00	13.000	16.000	NS
Cumulative deviation	0.570	1.162	1.285	1.542	1.179	1.298	1.552	NS
Worsley likelihood	1.744	2.87	3.159	3.790	2.958	3.230	3.736	NS
Rank Sum	0.225	1.645	1.960	2.576	1.583	1.906	2.364	NS
Student's t	0.233	1.665	1.991	2.641	1.674	1.992	2.598	NS
Median Crossing	1.294	1.645	1.960	2.576	1.725	1.941	2.588	NS
Turning Point	-1.199	1.645	1.960	2.576	1.713	1.970	2.484	NS
Rank Difference	-1.703	1.645	1.960	2.576	1.626	1.992	2.651	S (0.1)
Auto Correlation	1.671	1.645	1.960	2.576	1.634	1.908	2.470	S (0.1)

Table F.15: Trend analysis test result for 143921A

Test Name	Test Statistic for Each Test	Critical Values of Trend test Statistics for Significance Levels at			Critical Values of Trend test Re-Sampling Statistics for Significance Levels at			Result
		a=0.1	a=0.05	a=0.01	a=0.1	a=0.05	a=0.01	
Mann-Kendall	0.856	1.645	1.960	2.576	1.588	1.927	2.569	NS
Spearman's Rho	0.878	1.645	1.960	2.576	1.604	1.913	2.591	NS
Linear regression	1.785	1.701	2.048	2.763	1.726	2.025	2.631	S (0.1)
Cusum	4.000	6.682	7.449	8.928	7.0000	7.000	9.000	NS
Cumulative deviation	1.235	1.12	1.240	1.460	1.075	1.168	1.358	S (0.05)
Worsley likelihood	4.022	2.86	3.190	3.860	4.461	4.876	8.089	NS
Rank Sum	-0.083	1.645	1.960	2.576	1.742	1.949	2.613	NS
Student's t	-1.113	1.699	2.045	2.756	1.609	1.801	2.135	NS
Median Crossing	0.186	1.645	1.960	2.576	1.671	2.043	2.785	NS
Turning Point	-0.745	1.645	1.960	2.576	1.936	2.085	2.978	NS
Rank Difference	-0.111	1.645	1.960	2.576	1.646	1.959	2.433	NS
Auto Correlation	0.120	1.645	1.960	2.576	1.294	1.697	2.869	NS

Table F.16: Trend analysis test result for 143210B

Test Name	Test Statistic for Each Test	Critical Values of Trend test Statistics for Significance Levels at			Critical Values of Trend test Re-Sampling Statistics for Significance Levels at			Result
		a=0.1	a=0.05	a=0.01	a=0.1	a=0.05	a=0.01	
Mann-Kendall	-0.571	1.645	1.960	2.576	1.641	1.998	2.676	NS
Spearman's Rho	-0.483	1.645	1.960	2.576	1.633	1.930	2.414	NS
Linear regression	-0.304	1.701	2.048	2.763	1.769	2.125	2.695	NS
Cusum	5.000	6.682	7.449	8.928	7.0000	7.000	9.000	NS
Cumulative deviation	0.489	1.12	1.240	1.460	1.093	1.193	1.452	NS
Worsley likelihood	1.172	2.86	3.190	3.860	3.394	4.611	5.776	NS
Rank Sum	-0.166	1.645	1.960	2.576	1.659	1.949	2.489	NS
Student's t	0.111	1.699	2.045	2.756	1.631	1.911	2.220	NS
Median Crossing	0.557	1.645	1.960	2.576	1.671	2.043	2.414	NS
Turning Point	0.149	1.645	1.960	2.576	2.085	2.531	2.978	NS
Rank Difference	0.343	1.645	1.960	2.576	1.646	1.898	2.494	NS
Auto Correlation	-0.215	1.645	1.960	2.576	1.627	1.899	2.435	NS

Table F.17: Trend analysis test result for 143306A

Test Name	Test Statistic for Each Test	Critical Values of Trend test Statistics for Significance Levels at			Critical Values of Trend test Re-Sampling Statistics for Significance Levels at			Result
		a=0.1	a=0.05	a=0.01	a=0.1	a=0.05	a=0.01	
Mann-Kendall	0.929	1.645	1.960	2.576	1.661	2.027	2.668	NS
Spearman's Rho	1.081	1.645	1.960	2.576	1.706	2.092	2.700	NS
Linear regression	1.722	1.69	2.031	2.727	1.75	2.133	3.102	NS
Cusum	6.000	7.421	8.273	9.915	8.0000	9.000	10.000	NS
Cumulative deviation	0.949	1.127	1.254	1.488	1.143	1.305	1.533	NS
Worsley likelihood	3.997	2.88	3.194	3.830	2.913	3.322	4.200	S (0.05)
Rank Sum	-0.046	1.645	1.960	2.576	1.595	1.930	2.568	NS
Student's t	-0.666	1.689	2.029	2.722	1.634	1.960	2.423	NS
Median Crossing	0.333	1.645	1.960	2.576	1.667	2.000	2.667	NS
Turning Point	-1.333	1.645	1.960	2.576	1.733	2.132	3.332	NS
Rank Difference	-1.139	1.645	1.960	2.576	1.621	1.884	2.497	NS
Auto Correlation	1.314	1.645	1.960	2.576	1.528	1.847	2.477	NS

Table F.18: Trend analysis test result for 143213C

Test Name	Test Statistic for Each Test	Critical Values of Trend test Statistics for Significance Levels at			Critical Values of Trend test Re-Sampling Statistics for Significance Levels at			Result
		a=0.1	a=0.05	a=0.01	a=0.1	a=0.05	a=0.01	
Mann-Kendall	0.053	1.645	1.960	2.576	1.611	1.902	2.403	NS
Spearman's Rho	0.199	1.645	1.960	2.576	1.784	2.100	2.540	NS
Linear regression	0.988	1.721	2.080	2.831	1.725	2.020	2.774	NS
Cusum	4.000	5.851	6.522	7.817	6.0000	7.000	9.000	NS
Cumulative deviation	0.903	1.106	1.226	1.432	1.094	1.205	1.387	NS
Worsley likelihood	1.974	2.894	3.250	4.016	3.722	4.500	8.099	NS
Rank Sum	-0.462	1.645	1.960	2.576	1.693	2.000	2.554	NS
Student's t	-1.278	1.717	2.740	2.819	1.616	1.858	2.327	NS
Median Crossing	0.426	1.645	1.960	2.576	1.706	1.706	2.558	NS
Turning Point	1.546	1.645	1.960	2.576	2.061	2.576	3.092	NS
Rank Difference	0.504	1.645	1.960	2.576	1.65	1.879	2.567	NS
Auto Correlation	1.091	1.645	1.960	2.576	1.431	1.705	2.317	NS

Table F.19: Trend analysis test result for 143232A

Test Name	Test Statistic for Each Test	Critical Values of Trend test Statistics for Significance Levels at			Critical Values of Trend test Re-Sampling Statistics for Significance Levels at			Result
		a=0.1	a=0.05	a=0.01	a=0.1	a=0.05	a=0.01	
Mann-Kendall	0.487	1.563	1.862	2.447	1.622	1.849	2.433	NS
Spearman's Rho	0.596	1.563	1.862	2.447	1.737	2.025	2.576	NS
Linear regression	0.448	1.734	2.101	2.878	1.82	2.168	2.984	NS
Cusum	3.000	5.456	6.082	7.290	6.0000	7.000	8.000	NS
Cumulative deviation	0.587	1.1	1.220	1.420	1.104	1.231	1.460	NS
Worsley likelihood	1.661	2.9	3.280	4.130	2.853	3.288	4.887	NS
Rank Sum	-0.491	1.563	1.862	2.447	1.776	2.079	2.684	NS
Student's t	-0.631	1.729	2.093	2.861	1.659	1.906	2.536	NS
Median Crossing	0.688	1.563	1.862	2.447	1.606	2.065	2.524	NS
Turning Point	-1.112	1.563	1.862	2.447	2.225	2.225	3.337	NS
Rank Difference	0.057	1.563	1.862	2.447	1.599	1.942	2.513	NS
Auto Correlation	-0.444	1.563	1.862	2.447	1.666	1.978	2.501	NS

Table F.20: Trend analysis test result for 143233A

Test Name	Test Statistic for Each Test	Critical Values of Trend test Statistics for Significance Levels at			Critical Values of Trend test Re-Sampling Statistics for Significance Levels at			Result
		a=0.1	a=0.05	a=0.01	a=0.1	a=0.05	a=0.01	
Mann-Kendall	-0.423	1.645	1.960	2.576	1.611	1.902	2.377	NS
Spearman's Rho	-0.510	1.645	1.960	2.576	1.784	2.104	2.674	NS
Linear regression	0.104	1.721	2.080	2.831	1.663	2.041	2.621	NS
Cusum	3.000	5.851	6.522	7.817	7.0000	7.000	10.000	NS
Cumulative deviation	0.589	1.106	1.226	1.432	1.078	1.172	1.392	NS
Worsley likelihood	1.222	2.894	3.250	4.016	4.583	5.671	7.277	NS
Rank Sum	0.154	1.645	1.960	2.576	1.693	2.000	2.677	NS
Student's t	-0.544	1.717	2.740	2.819	1.645	1.923	2.326	NS
Median Crossing	1.279	1.645	1.960	2.576	1.706	1.706	2.558	NS
Turning Point	-0.515	1.645	1.960	2.576	2.061	2.576	3.092	NS
Rank Difference	0.367	1.645	1.960	2.576	1.65	1.925	2.383	NS
Auto Correlation	0.838	1.645	1.960	2.576	1.36	1.709	2.559	NS

Table F.21: Trend analysis test result for 143307A

Test Name	Test Statistic for Each Test	Critical Values of Trend test Statistics for Significance Levels at			Critical Values of Trend test Re-Sampling Statistics for Significance Levels at			Result
		a=0.1	a=0.05	a=0.01	a=0.1	a=0.05	a=0.01	
Mann-Kendall	-0.204	1.645	1.960	2.576	1.689	2.002	2.602	NS
Spearman's Rho	-0.492	1.645	1.960	2.576	1.713	2.094	2.752	NS
Linear regression	-0.039	1.692	2.034	2.732	1.738	2.054	2.788	NS
Cusum	4.000	7.32	8.160	9.780	7.0000	8.000	9.000	NS
Cumulative deviation	0.625	1.126	1.252	1.484	1.152	1.252	1.488	NS
Worsley likelihood	1.594	2.88	3.202	3.850	3.22	3.727	4.805	NS
Rank Sum	1.566	1.645	1.960	2.576	1.629	1.914	2.547	NS
Student's t	1.025	1.69	2.031	2.727	1.678	1.962	2.661	NS
Median Crossing	0.507	1.645	1.960	2.576	1.521	1.859	2.535	NS
Turning Point	-0.676	1.645	1.960	2.576	1.893	2.299	2.704	NS
Rank Difference	0.008	1.645	1.960	2.576	1.592	1.866	2.384	NS
Auto Correlation	0.393	1.645	1.960	2.576	1.592	1.919	2.654	NS

Table F.22: Trend analysis test result for 14010B

Test Name	Test Statistic for Each Test	Critical Values of Trend test Statistics for Significance Levels at			Critical Values of Trend test Re-Sampling Statistics for Significance Levels at			Result
		a=0.1	a=0.05	a=0.01	a=0.1	a=0.05	a=0.01	
Mann-Kendall	-1.072	1.645	1.960	2.576	1.616	1.876	2.526	NS
Spearman's Rho	-1.088	1.645	1.960	2.576	1.656	2.046	2.633	NS
Linear regression	1.005	1.68	2.011	2.682	1.626	2.008	2.659	NS
Cusum	5.000	8.713	9.712	11.641	9.0000	10.000	13.000	NS
Cumulative deviation	0.703	1.141	1.270	1.521	1.113	1.238	1.486	NS
Worsley likelihood	1.969	2.87	3.160	3.790	3.465	4.891	7.015	NS
Rank Sum	0.838	1.645	1.960	2.576	1.63	1.969	2.628	NS
Student's t	-0.720	1.68	2.010	2.680	1.681	1.893	2.360	NS
Median Crossing	1.131	1.645	1.960	2.576	1.697	1.980	2.546	NS
Turning Point	-0.564	1.645	1.960	2.576	1.916	2.254	2.931	NS
Rank Difference	-1.656	1.645	1.960	2.576	1.718	1.991	2.607	NS
Auto Correlation	-0.021	1.645	1.960	2.576	1.35	1.728	2.503	NS